https://theses.gla.ac.uk/

Theses Digitisation:

https://www.gla.ac.uk/myglasgow/research/enlighten/theses/digitisation/

This is a digitised version of the original print thesis.

Copyright and moral rights for this work are retained by the author

A copy can be downloaded for personal non-commercial research or study, without prior permission or charge

This work cannot be reproduced or quoted extensively from without first obtaining permission in writing from the author

The content must not be changed in any way or sold commercially in any format or medium without the formal permission of the author

When referring to this work, full bibliographic details including the author, title, awarding institution and date of the thesis must be given

Enlighten: Theses
https://theses.gla.ac.uk/
research-enlighten@glasgow.ac.uk

PASSIVE WAVEGUIDE COMPONENTS FOR INTEGRATED OPTICS

A THESIS

submitted to the Faculty of Engineering

of the University of Glasgow

for the degree of

Doctor of Philosophy

by

Charles Stewart Wilson.

September 1979.

ProQuest Number: 10984232

All rights reserved

INFORMATION TO ALL USERS
The quality of this reproduction is dependent upon the quality of the copy submitted.

In the unlikely event that the author did not send a complete manuscript
and there are missing pages, these will be noted. Also, if material had to be removed,
a note will indicate the deletion.

ProQuest 10984232

Published by ProQuest LLC (2018). Copyright of the Dissertation is held by the Author.

All rights reserved.
This work is protected against unauthorized copying under Title 17, United States Code
Microform Edition © ProQuest LLC.

ProQuest LLC.
789 East Eisenhower Parkway
P.O. Box 1346
Ann Arbor, MI 48106 – 1346

FOR MY PARENTS

They say Wilson has blundered.
Perhaps he has but I notice that he usually
blunders forward.

Thomas Edison

If the door's of perception were cleansed,
everything would appear to man as it is, infinite.

William Blake

I N D E X

ABSTRACT

This thesis incorporates studies of optical waveguiding in both planar and two dimensional (quasi-rectangular) waveguides of thin film Corning type 7059 glass. Single mode propagation in trapezoidal waveguide devices has been achieved throughout this investigation.

He - Ne laser light of wavelength 0.6328 μm is guided in thin-film, planar, 7059 glass waveguides sputtered onto microscope slide substrates. Measurements indicate that these thin film planar waveguides may have losses which are typically 0.5 dB/cm and which may be as low as 0.1 dB/cm. These losses are mainly attributable to scattering from substrate imperfections at the thin film/substrate interface. The refractive index, deposition rate and waveguide loss are determined by the use of prism coupling techniques.

The fabrication of stripe 7059 glass waveguides by ion-beam etching is discussed. Experimental modal propagation characteristics are related to a simple theoretical analysis which accurately predicts the modal propagation constants and has been verified by an independent numerical method. Waveguide losses of these two dimensional dielectric waveguides were typically 4 - 6 dB/cm, the relatively large loss is due to scatter induced by the rough waveguide walls formed in the ion etching process.

Single mode passive waveguide devices formed in ion etched 7059 glass waveguides are considered both theoretically and experimentally. Transmission loss measurement have been carried out on waveguide tilts, Y-junctions and waveguide power splitters. Measured transmission data on waveguide tilts are compared with

predicted values. Useful tilt angles to an upper limit of around 5^{o} have been observed. A modification introduced into the Y-junction analysis of Anderson has allowed both the power transmission of Ti diffused $LiNbO_3$ and ion-etched 7059 glass stripe Y-junctions to be predicted accurately. The design of a waveguide power splitter based on a further modification of the Y-junction analysis has led to the successful fabrication of a stripe waveguide power splitter. Measurements have shown that a device exhibiting a 10:1 power ratio between the output waveguides may be fabricated, although its practical usefulness may be limited due to the high device transmission loss of 50%, attributable to junction defect effects.

A comparison between exact and approximate solutions for the launching of a surface wave on a grounded dielectric sheet has been undertaken. Results indicate that neglecting radiation in the backward direction from a waveguide discontinuity of this type, is valid. This assumption allows an approximate analytical solution to problems which otherwise could only be solved numerically (c.f. Y-junction etc).

As an example of the application of the above results, a design study of a novel type of waveguide coupler, utilising two curved touching 7059 glass stripe waveguides, is undertaken.

ACKNOWLEDGEMENTS

I wish to express my thanks to Professor J. Lamb for the provision of research facilities in the Department of Electronics and Electrical Engineering, and for his interest during the course of this research.

I wish to express my sincere gratitude to my supervisor Dr. I. Anderson and latterly Dr. R. Dunsmuir for helpful guidance and assistance throughout this work and in the preparation of the thesis. I should especially like to thank Dr. R. Dunsmuir for painstakingly reading and offering suggestions on the penultimate draft of the thesis.

I wish to thank Mr. R.G. Walker and Dr. C.D.W. Wilkinson for carrying out the computer analysis of the trapezoidal waveguides presented in Chapter 4.

I should also like to thank the staff, technical staff, and my fellow research students for their help and suggestions at various stages during this work. In particular I wish to thank Mr. R.H. Hutchins for his constant enthusiasm, interest and encouragement, and for looking after my personal well-being.

The technical assistance of G. Boyle, K. Piechowiak, L. Hobbs, B. Miller, J. Crichton, S. Brownlie and J. Clark is gratefully acknowledged, and thanks are due to Ms. I. Adams who typed the thesis.

This work was supported by a grant from the U.K. Science Research Council.

CHAPTER 1.

CHAPTER 1. INTRODUCTION

1.1. General.

Just over a decade has elapsed since S.E.Miller (1) first coined the term "integrated optics". During this period much human endeavour has been directed towards the development of a sound and reliable technology for optical communications purposes.

The idea of using optical frequencies as the carrier for an ultra high data transmission rate communications system has been considered for many years but it was only with the advent of the laser (2) in the early 1960's that interest in optical communications began to expand rapidly. Miller envisaged integrated optical devices as being in direct analogy with integrated electronic circuit counterparts and proposed a similar technology whereby complete signal processing techniques could take place on a single active substrate containing lasers, modulators, logic circuits and waveguides. The potential benefits of such a technology are an improved reduction in size and weight, rigidity, ease of alignment, freedom from external environmental effects and eventually, low cost, when compared to current technologies, (e.g. strowger switching telephone exchanges).

Prior to Miller's proposals many researchers had studied thick dielectric waveguides usually at microwave frequencies. In 1964 Osterberg and Smith (3) achieved probably the first recorded case of optical waveguide information transmission using glass sheets and prisms to couple images formed in incoherent visible light into and out of thick glass sheet dielectric waveguides. It was not until the development of the prism film coupler (4), which permitted efficient excitation of discrete modes in thin film waveguides, that "integrated optics" began to

expand rapidly. Integrated optics depends mainly on a thin film fabrication technology and has rapidly progressed from the initial development of relatively lossy passive planar waveguides to that of low loss active waveguides incorporating devices such as modulators and switches (5,6,7) often in two dimensional (quasi-rectangular) dielectric waveguide form. Lately low loss semiconductor thin film optical waveguides grown by Molecular Beam Epitaxy (M.B.E.) in gallium arsenide have been reported (8). These have the potential advantage of integrating a complete communication system consisting of lasers, switches, modulators, waveguides and detectors as well as the associated electronics on the same substrate. Gallium arsenide and its associated isomorphs are well suited to this task, as it allows the fabrication of near-infrared solid state lasers emitting in the 1.3μm wavelength region (9). As 1.3μm corresponds to the minimum loss point, and is close to the minimum dispersion point of the latest low loss single mode optical fibres (10), the future of the III - V semiconductor compounds (and M.B.E.) is promising. Already extensive development of the III - V semiconductor compounds is under-way at several laboratories throughout the world, and notably at the British Post Office Research Centre in England.

The basic requirement of any thin film optical waveguide device is a high quality film, and in the field of integrated optics this means the fabrication of dielectric waveguides with low attenuation and uniform film thickness. The level of technology required for this is extremely exacting with approximately four orders of magnitude improvement in film loss required compared to the dielectric layers used in optical filters. In optical fibre technology the waveguide may be drawn from high purity bulk material and losses of less than 2 dB/km have been reported (11).

However, planar technology by its very nature does not permit the use of a similar technique and the dielectric waveguides must be formed directly onto a substrate in either planar form (Fig. 1.1a) or rectangular form (Fig. 1.1b). Many waveguide devices have been fabricated in planar form, but comparatively few have been made in single mode rectangular waveguides due to the advanced photolithographic procedures necessary to produce waveguides with small widths and acceptable waveguide losses. The development of single-mode, two-dimensional dielectric waveguides and associated devices presents a much greater technological challenge than that of planar waveguide devices, due to the additional scatter loss from the sides of the waveguide.

Most methods of thin film deposition have been used including evaporation (14), sputtering (15), ion exchange (16), proton implantation (17), diffusion (18,19) and chemical vapour deposition (20). Initially waveguides were fabricated in passive noncrystalline materials such as glasses (12) and organosilicones (13). However, the need for active devices quickly led to investigations of crystalline films which require more stringent fabrication technologies (e.g. M.B.E.), than do their amorphous counterparts.

For most device applications rectangular waveguides, with their lateral confinement of the guided light, provide lower cross-talk interference and allow larger packing densities of devices on a single substrate. For these reasons waveguide fabrication has most recently been diverted toward the production of low loss rectangular waveguides in both passive and active media (21,22,23).

It is not the purpose of this brief introduction to give a complete review of the field of integrated optics. Extensive reviews have been given in the literature and those interested should consult (24,25,26,27,28).

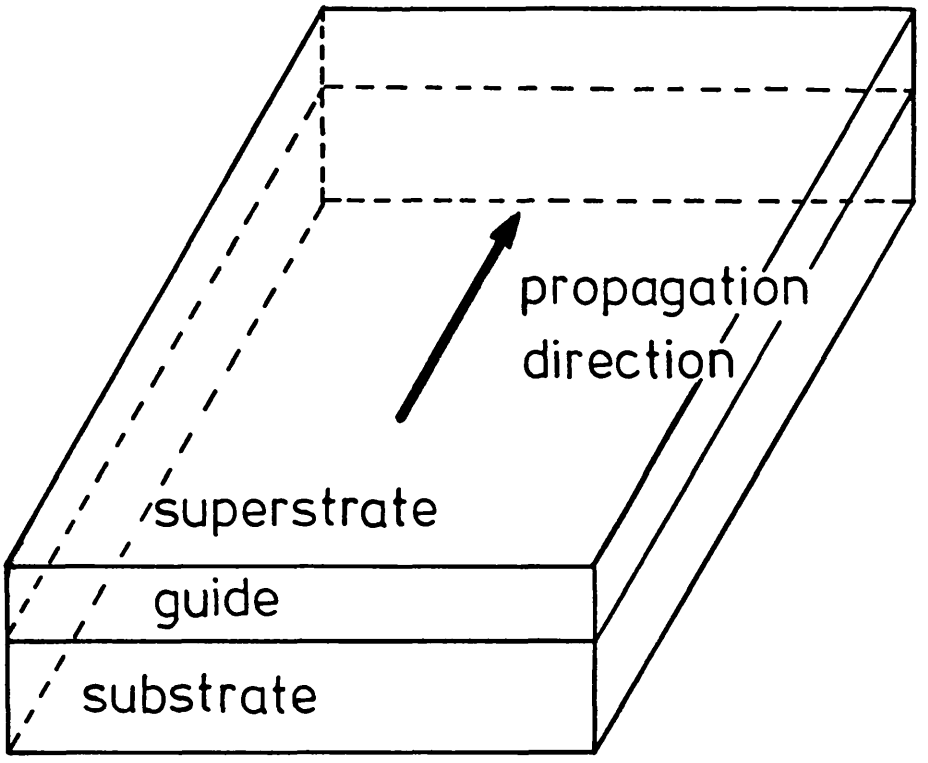

(a) slab waveguide

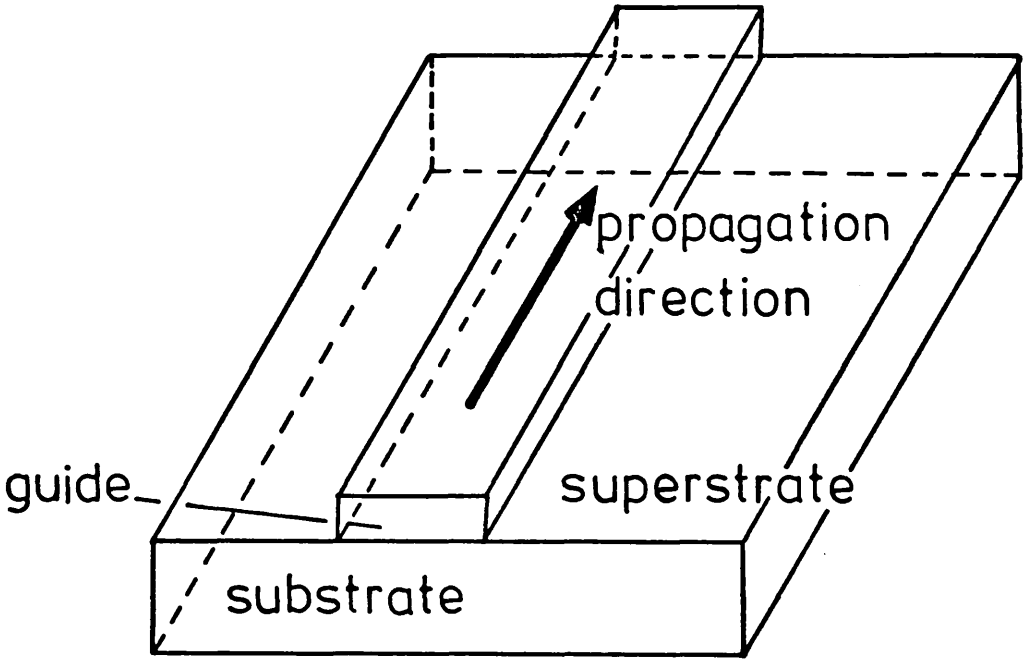

(b) rectangular waveguide

Fig.1.1 Waveguide structures

1.2. Aims of the Research Work Described in this Thesis.

The aims of the research were essentially threefold:-

(1) To fabricate and characterise planar dielectric optical waveguides formed by R.F. sputtering "Corning" 7059 glass onto microscope slide substrates and to determine the thin film deposition rate and refractive index.

(2) To manufacture two-dimensional (stripe), trapezoidal, R.F. sputtered 7059 glass waveguides formed by ion beam etching (micro-machining) the above planar waveguides and to find a theoretical description of propagation in these trapezoidal waveguides and compare with the measured behaviour.

(3) To fabricate stripe, single mode, passive, optical waveguide devices such as Y-junctions, power splitters etc, and to find a theoretical description of power transmission in these single mode devices and compare with measured behaviour.

Having given an account of the aims of this thesis a short description will now be made on R.F. Sputtering technique, which is central to the work described in this thesis.

1.3. R.F. Sputtering.

It has been found that R.F. sputtering of Corning 7059 glass provides low loss durable optical films (12), which grow at a slow rate (approximately 70 Å/min). If the discharge is kept stable the growth rate is linear with time and films of a specific thickness may be grown to great accuracy. Extensive and detailed descriptions of R.F. Sputtering may be found in Jackson (29) and other review articles (30). However, to explain the major properties of sputtered films some of the more pertinent points are given below.

Sputtering is a process in which material is removed from a surface as a result of bombardment with atoms or ions. Since it is easier to accelerate charged particles, ions are normally used. The particles that are removed from the target surface can be collected on a conveniently located substrate, accumulating with time, to form a thin film.

The bombarding particles penetrate the surface of the target material, transferring their momentum to the lattice of the target, thereby knocking one or more target atoms out of their equilibrium positions. If these target atoms are close to the surface they may emerge, but more probably they will hit surface atoms from below and cause them to fly off. Since the energy needed to move a lattice atom from its equilibrium position is much greater than that required to remove an atom from the surface of the target the thin film on the substrate is built up by the slow accumulation of atoms with appreciable energy (29). This is possibly the reason for the low loss properties and durability of the majority of sputtered thin films (29).

The rate at which a material is sputtered is proportional to the product of the sputtering yield, i.e. the number of sputtered atoms per incident ion, and the number of ions striking the target. As the number of ions striking the target is proportional to the current in the discharge, the sputtering yield increases with voltage and the sputtering rate increases with the power in the discharge.

The sputtering yield varies with target materials and gases. Light gases, such as hydrogen and helium, have a very low sputtering yield (i.e. very little target material is sputtered due to the small kinetic energies of such ionised gases). Moreover, because they can carry a disproportionately large share of the discharge current, small amounts of these gases in a plasma can alter the sputtering rate significantly. Hence the purity of the plasma is important.

In addition the sputtering yield for a given type of atom in a compound target depends on the probability that the incident ion will cause that kind of target atom to be dislodged from the surface. In a compound target, the sputtering yields for different types of atoms depend on the composition of the target material. As a result it is possible that some atoms in the target are sputtered more easily than others, thus causing a layer of different composition on the surface of the substrate. This compositional change continues until an equilibrium is reached between the ratio of the different atoms in the target and the rate at which they are sputtered.

Even if the target does not change composition, a film deposited by sputtering does not in general have the same composition as the target material. This is due to the fact that some types

of atoms stick to the surface better than others. Moreover, the sticking coefficients are temperature dependent. Consequently the temperature of the substrate may well be higher than that of the substrate holder and may change with substrate materials due to different thermal conductivities. Experiments carried out in the department show that the refractive index of R.F. sputtered "Corning" 7059 glass is higher than that of the bulk material (approximately 1.561 as opposed to 1.528), and, further, that the refractive index of the sputtered film may be varied by altering the input power (31,32).

Most of the effects mentioned in this discussion have been observed in work carried out in the department (31). However, due to the homogeneous nature of the thin films produced (see Chapter 3), no evidence was recorded of change in the sputtering layer refractive index with increasing film thickness (29). We may conclude, therefore, that R.F. sputtering in general provides durable low loss films whose thickness may be controlled to great accuracy.

1.4. Synopsis of Thesis.

This thesis is organised into three parts. Part I is concerned with the growth and optical waveguiding of R.F. sputtered 7059 glass thin films on microscope slide substrates. In Chapter 2, the basic properties of planar thin film dielectric waveguides are summarised and they are then related to the specific case of R.F. sputtered 7059 glass. Chapter 3 describes the experimental method for the growth of the R.F. sputtered thin films, and presents the physical parameters of refractive index, deposition rate and attenuation, associated with them.

Part II contains the bulk of the thesis and is devoted to the fabrication and characterisation of two-dimensional trapezoidal 7059 glass passive waveguide devices formed by ion beam etching. Chapter 4 contains a brief review of rectangular dielectric waveguide analyses and presents a theoretical and experimental comparison for trapezoidal 7059 glass stripe waveguides. Particular emphasis is placed on the routine production of single mode waveguides. Chapters 5 through 7 consider three single mode stripe waveguide devices that may find applications in future integrated optical communications systems and compares the experimentally derived power transmission with that of a theoretical model.

Part III contains the concluding discussion on the work carried out for this thesis and the results obtained. It includes some proposals for future work and alternative devices.

Appendices A-E contain theory relevant to the main body of the thesis and as such are included and referenced from parts I - III.

PART I

R.F. SPUTTERED 7059 GLASS FILM WAVEGUIDES

CHAPTER 2.

CHAPTER 2. THEORY OF PLANAR DIELECTRIC OPTICAL WAVEGUIDES.

The theory of the propagation of light in thin film dielectric waveguides is well known (25,26,33,100) and is of fundamental importance to the understanding of R.F. sputtered 7059 glass "stripe" or "two dimensional", waveguides and associated devices, as considered in later chapters. There are two well established approaches in the evaluation of thin film dielectric waveguide propagation; both have been extensively reported in the literature and hence will only be briefly summarised here. The first is the "ray optics" approach (33), and the second involves a solution through electromagnetic field theory (26).

In this chapter a simple three layer planar waveguide is considered, as shown in Fig. 2.1. The waveguide consists of a thin film with substrates of lower but not identical refractive index on either side (see Fig. 2.1). All the media are assumed to be homogeneous and isotropic and to extend infinitely in the y direction. The theory is then extended to the specific case of R.F. sputtered 7059 glass (43) optical waveguides. Methods of beam-to-film coupling are also discussed.

2.1. Propagation in Homogeneous Isotropic Media.

The ray optics approach considers a waveguide mode to consist of rays of light which propagate along a zig-zag path, (Fig. 2.2) with the reflections at the guide-substrate/superstrate interfaces occuring due to total internal reflection. In order to satisfy the criteria for guided modes the refractive index of the guide n_1 must be larger than those of the substrate and the superstrate i.e. $n_0 < n_1 > n_2$. When the wave is totally reflected there is a phase change which can be represented as a lateral

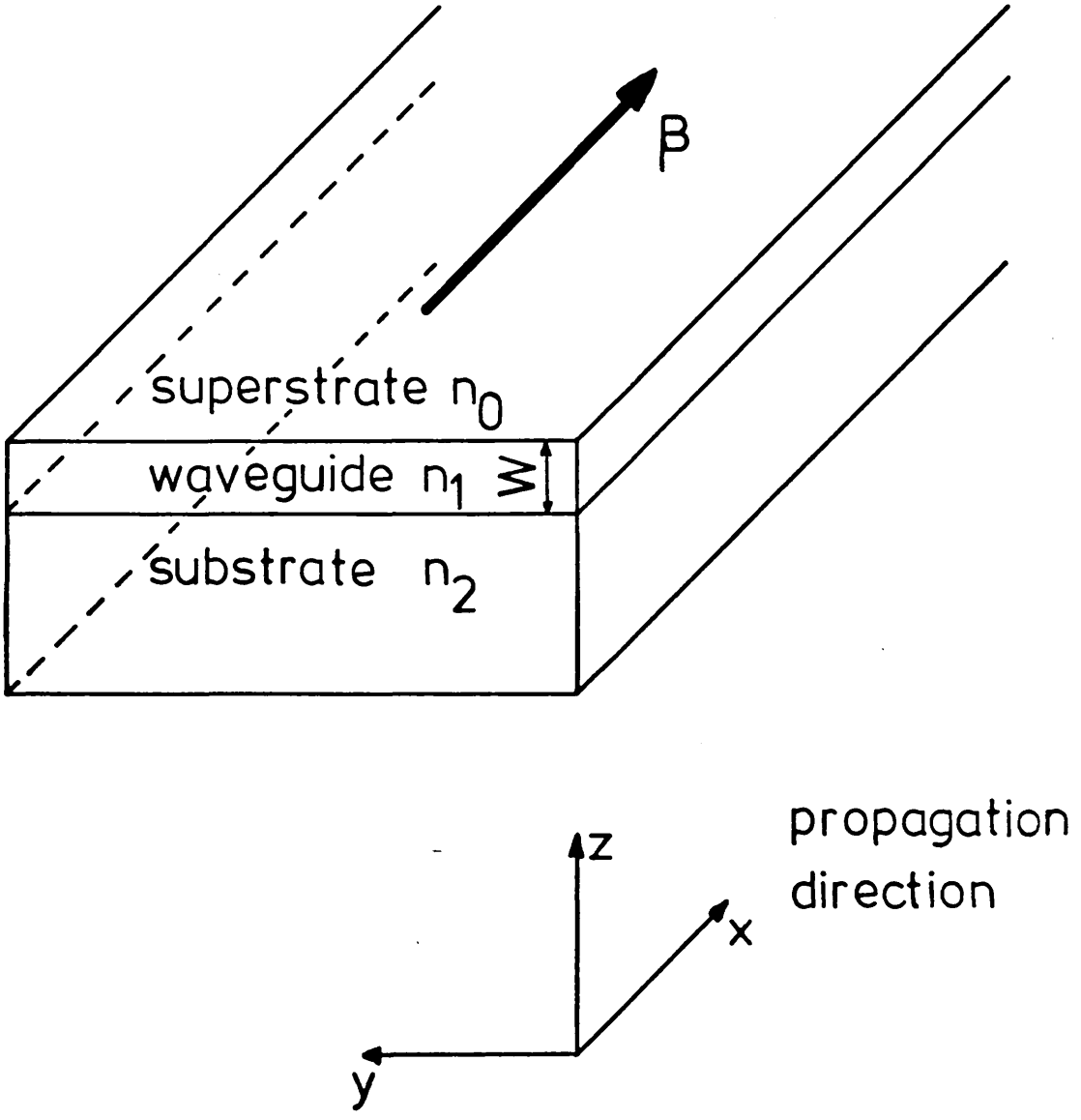

Fig. 2.1 Planar homogeneous isotropic waveguide geometry

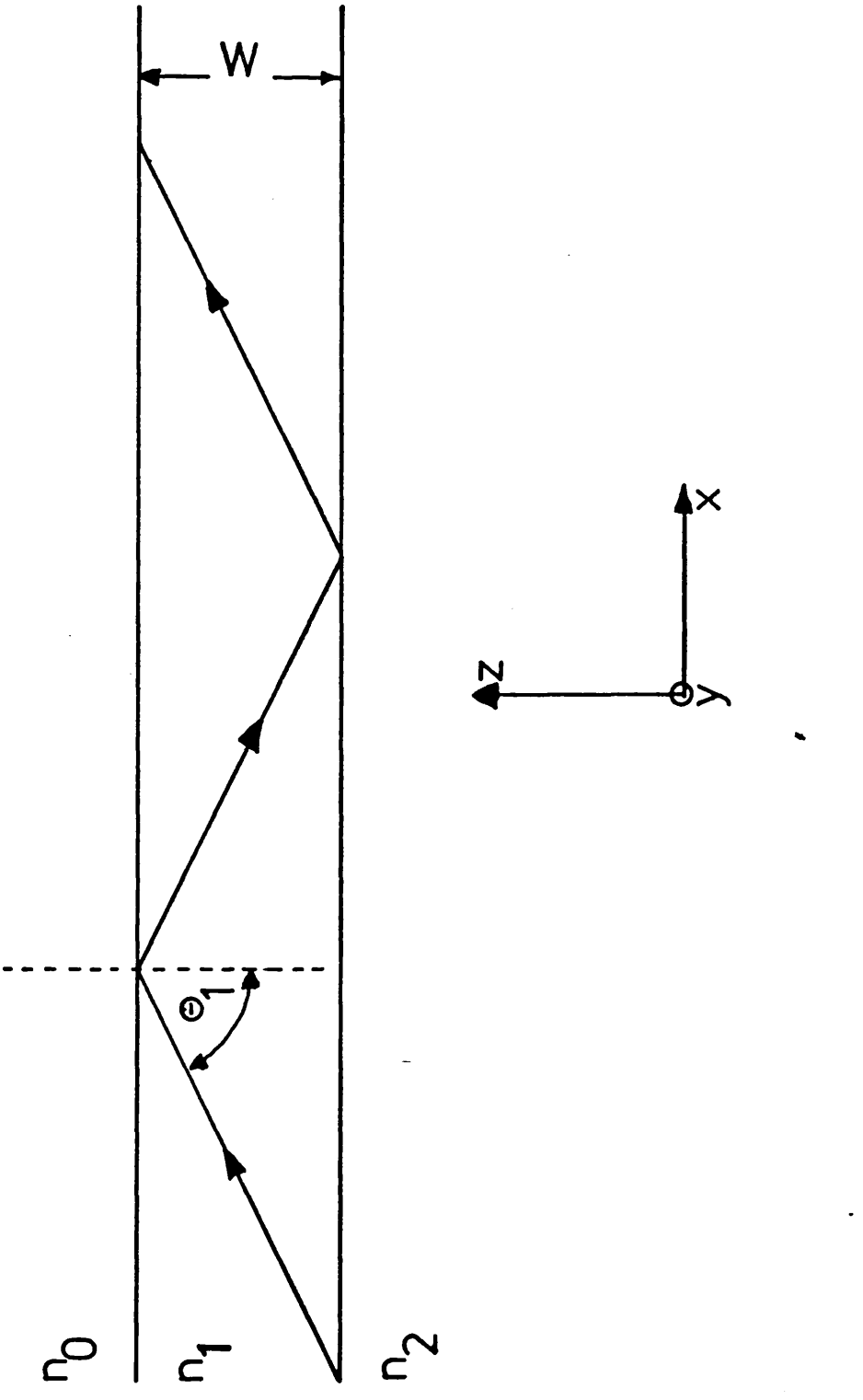

Fig. 2.2 A ray optics representation of a guided wave

shift on reflection, known as the Goos-Haenchen lateral shift (34) (Fig. 2.3). For any guided mode the waves should interfere constructively; that is, for any one round trip within the waveguide, the total phase change should be an integral multiple of 2π. These criteria yield the equation,

$$2\, k_o n_1 W \cos\theta_1 - 2\phi_{10} - 2\phi_{12} = 2M\pi \qquad (2.1)$$

which provides the condition for guided modes, where $k_o = 2\pi/\lambda$ the wave number, ϕ_{10} and ϕ_{12} are the phase changes on reflection at the guide/superstrate and guide/substrate junctions respectively, and M is an integer = 0,1,2, ..., known as the mode number. From (33) the phase changes on total internal reflection are,

$$\phi_{12} = \tan^{-1}\left[(n_1^2 \sin^2\theta_1 - n_2^2)^{\frac{1}{2}}/n_1 \cos\theta_1 \right] \qquad (2.2)$$

$$\phi_{10} = \tan^{-1}\left[(n_1^2 \sin^2\theta_1 - n_o^2)^{\frac{1}{2}}/n_1 \cos\theta_1 \right] \qquad (2.3)$$

for T.E. modes, and

$$\phi_{12} = \tan^{-1}\left[n_1^2(n_1^2 \sin^2\theta_1 - n_2^2)^{\frac{1}{2}}/n_2^2\, n_1 \cos\theta_1 \right] \qquad (2.4)$$

$$\phi_{10} = \tan^{-1}\left[n_1^2(n_1^2 \sin^2\theta_1 - n_o^2)^{\frac{1}{2}}/n_o^2\, n_1 \cos\theta_1 \right] \qquad (2.5)$$

for T.M. modes.

The propagation constant β is defined as,

$$\beta = k_o n_1 \sin\theta_1 \qquad (2.6)$$

and the wave velocity V as,

$$V = C(k_o/\beta) \qquad (2.7)$$

Defining the effective waveguide index n_e to be:

$$n_e = \beta/k_o = n_1 \sin\theta_1 \ , \qquad (2.8)$$

we may rewrite the above equations.

$$k_o W (n_1^2 - n_e^2)^{\frac{1}{2}} = M\pi + \tan^{-1}\frac{(n_e^2 - n_2^2)^{\frac{1}{2}}}{(n_1^2 - n_e^2)^{\frac{1}{2}}} + \tan^{-1}\frac{(n_e^2 - n_o^2)^{\frac{1}{2}}}{(n_1^2 - n_e^2)^{\frac{1}{2}}} \qquad (2.9)$$

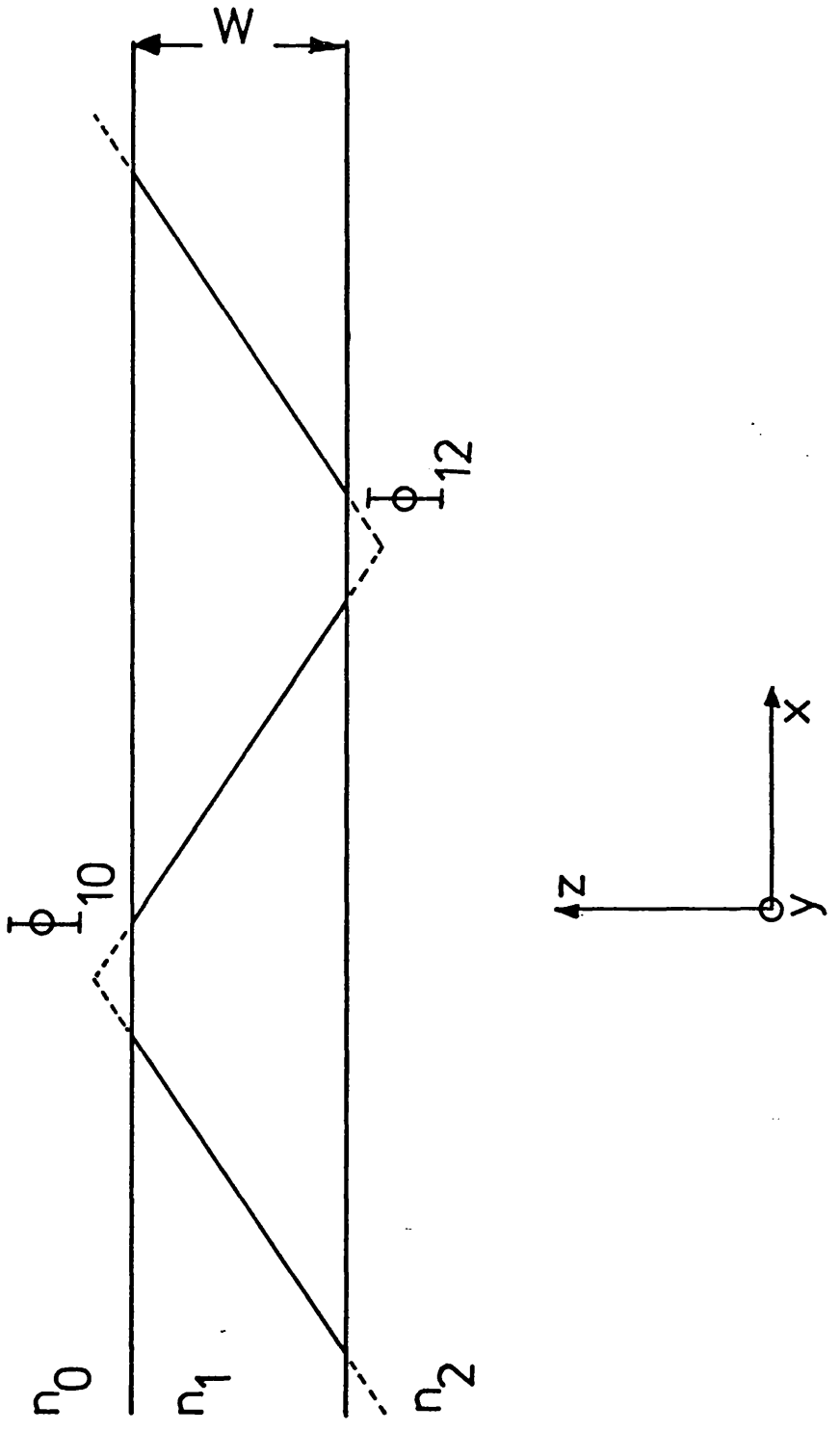

Fig. 2.3 Phase change on reflection represented by the GOOS – HAENCHEN shift

for T.E. modes, and

$$k_o W(n_1^2-n_e^2)^{\frac{1}{2}} = M\pi + \tan^{-1}\frac{n_1^2}{n_2^2}\frac{(n_e^2-n_2^2)^{\frac{1}{2}}}{(n_1^2-n_e^2)^{\frac{1}{2}}} + \tan^{-1}\frac{n_1^2}{n_o^2}\frac{(n_e^2-n_o^2)^{\frac{1}{2}}}{(n_1^2-n_e^2)^{\frac{1}{2}}} \qquad (2.10)$$

for T.M. waves.

Equations (2.9) and (2.10) are the waveguide characteristic equations and may be used to determine β for any three-layer isotropic, homogeneous, planar, dielectric waveguide.

Equations (2.9) and (2.10) can alternatively be derived from electromagnetic field theory (26,100,101). For a time-harmonic field in non-gyrotropic, isotropic, homogeneous, charge free media, Maxwell's equations may be expressed as,

$$\underline{\nabla} \times \underline{E} = -\mu_o \frac{\partial \underline{H}}{\partial t} \qquad (2.11a)$$

$$\underline{\nabla} \times \underline{H} = \varepsilon_o n^2 \frac{\partial \underline{E}}{\partial t} \qquad (2.11b)$$

$$\underline{\nabla} \cdot \underline{E} = 0 \qquad (2.11c)$$

$$\underline{\nabla} \cdot \underline{H} = 0 \qquad (2.11d)$$

which yields the wave equation,

$$\underline{\nabla}^2 \underline{E} = \mu_o \varepsilon_o n^2 \frac{\partial^2 \underline{E}}{\partial t^2} \qquad (2.12)$$

for the rectangular coordinate system of Fig. 2.1. By applying the appropriate boundary conditions to equation (2.12) equations (2.9) and (2.10) may be derived. T.E. waves have field components E_y, H_x, and H_z, while T.M.waves have H_y, E_x and E_z. A boundary matching problem of this type is given in the rectangular (stripe) waveguide analysis of Appendix B1, in which futher details will be found.

Inside the waveguide there is a cosinusoidal field variation

for even modes (m = 0,2,4,....) and a sinusoidal field variation for odd modes (m = 1,3,5,....). Outside the waveguide the field decays exponentially with distance and is termed the evanescent field. The proportion of power carried in these evanescent fields is critically dependent on waveguide thickness and on the refractive index difference between the waveguide and its surrounding media. The proportion of power carried by the evanescent fields is of particular importance when active waveguide devices employing metal electrode structures are being considered due to the high intrinsic loss of metal boundaries at optical frequencies.

Both the "ray optics", and the electromagnetic field theory methods of solution have been outlined here, because each is individually useful as a means of analysis, depending on the nature of the problem to be solved. Further use of each method will be made in later chapters.

Equations (2.9) and (2.10) cannot be solved directly to yield β. Accurate specific solutions of β are most readily obtained by numerical interpolation using a high speed digital computer.

However, by choosing values of effective guide index n_e, and by knowing the various refractive indices, wavelength of operation and mode number, the waveguide thickness may be calculated directly. A computer program was written to calculate waveguide effective index (n_e) for TE and TM modes for changes in waveguide thickness (W). Figure 2.4 shows n_e plotted against W for a number of TE and TM modes in an air-7059 glass-glass substrate system at a wavelength (λ) of 0.6328 μm. It can be seen that there is a minimum thickness that will support a particular guided mode; known as the cut-off thickness. This occurs when $n_e = n$, where n is the larger of n_0 and n_2.

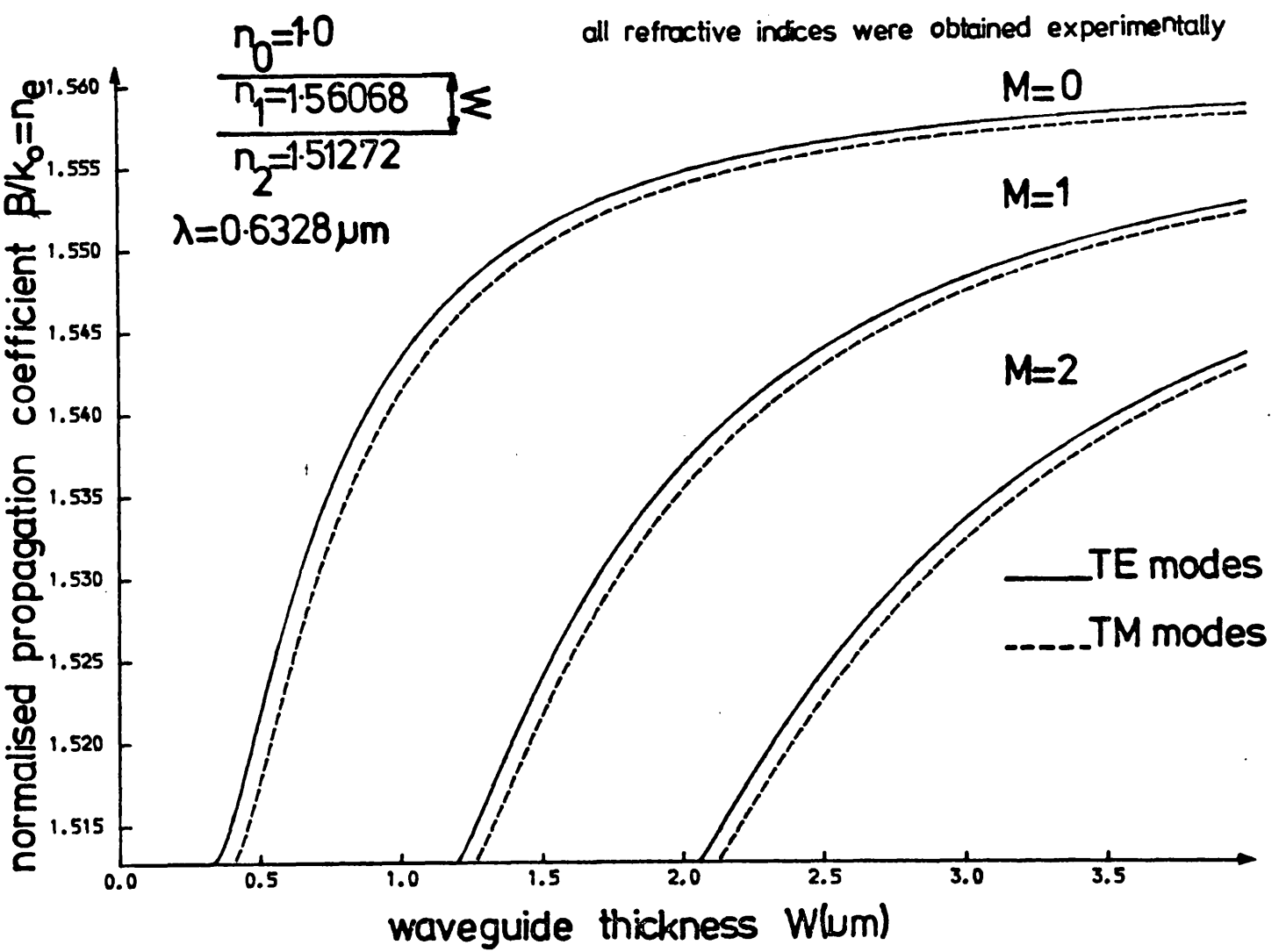

Fig.2.4 Normalised propagation coefficient versus waveguide thickness

$$W_{\text{CUT-OFF TE}} = \left[m\pi + \tan^{-1}\left[(n_2^2 - n_o^2)^{\frac{1}{2}}/(n_1^2-n_2^2)^{\frac{1}{2}}\right]\right]/k_o(n_1^2-n_2^2)^{\frac{1}{2}} \quad (2.13)$$

$$W_{\text{CUT-OFF TM}} = \left[m\pi + \tan^{-1}\left[n_1^2(n_2^2-n_o^2)^{\frac{1}{2}}/n_o^2(n_1^2-n_2^2)^{\frac{1}{2}}\right]\right]/k_o(n_1^2-n_2^2)^{\frac{1}{2}} \quad (2.14)$$

For the above example of the air-7059 glass-glass system the cut-off thickness of the TE_o mode is 0.3265 μm. When the film thickness approaches this value the evanescent fields penetrate deeper into the substrate.

As the waveguide thickness increases the number of possible modes also increases and the n_e value of each tends to the guide refractive index n_1. In very wide guides the effective indices of the modes and plane waves become indistinguishable, i.e. $n_e \rightarrow n_1$. Under these conditions the proportion of power which is carried in the evanescent fields is very small and most of the energy travels in the waveguide.

2.2. Waveguide Propagation in the Case of R.F. Sputtered 7059 Glass.

Effective index measurements (n_e) carried out on R.F. sputtered 7059 glass planar waveguides (see Chapter 3), revealed that the physical properties of the waveguides are very close to those of the ideal guides described in the previous section. We may deduce therefore, that 7059 glass thin film waveguides are essentially homogeneous (having an extremely low loss of $\sim$0.5 dB/cm, see Chapter 3), and exhibit no anisotropic or gyrotropic properties. Hence, for the purposes of analysis all planar thin film 7059 glass waveguides will be treated as if they were ideal.

2.3. Beam Coupling to Thin Film Waveguides.

There are many methods of coupling free-space-propagating-light into thin film waveguides, some more efficient than others and some easier to effect than others. These include edge focusing (end firing)(35), tapered film coupling (38), grating coupling (39) and prism coupling (4). All have been the subject of extensive theoretical and experimental studies. Only a brief description of the prism coupler will be given since it forms an integral part of all the experimental work carried out, for which the efficient excitation of discrete modes in a multimode waveguide is essential.

2.3.1. The Prism Coupler.

Prism couplers permit accurate measurements of modal propagation constants; the launching of light at any chosen point on the film, and have a theoretical maximum input efficiency of 81% (40).

In this type of coupler, represented in Figure 2.5 coupling takes place through the surface of the film. The evanescent field associated with the total internal reflection of light at the boundary between the prism base and the air gap allows the light to "tunnel" into the waveguide (Fig. 2.5). Coupling to a guided mode occurs when the angle of incidence on the lower prism face is such that the evanescent field in the region of the gap travels with the same phase velocity along the film direction as the guided mode. The coupler is a reciprocal device and the prism is truncated after the maximum light energy has been transferred to the film to prevent light coupling back out of the waveguide.

The propagation constants of the modes can be obtained by measuring the coupling angles associated with the modes. The measurements of two or more mode angles permits the film refractive

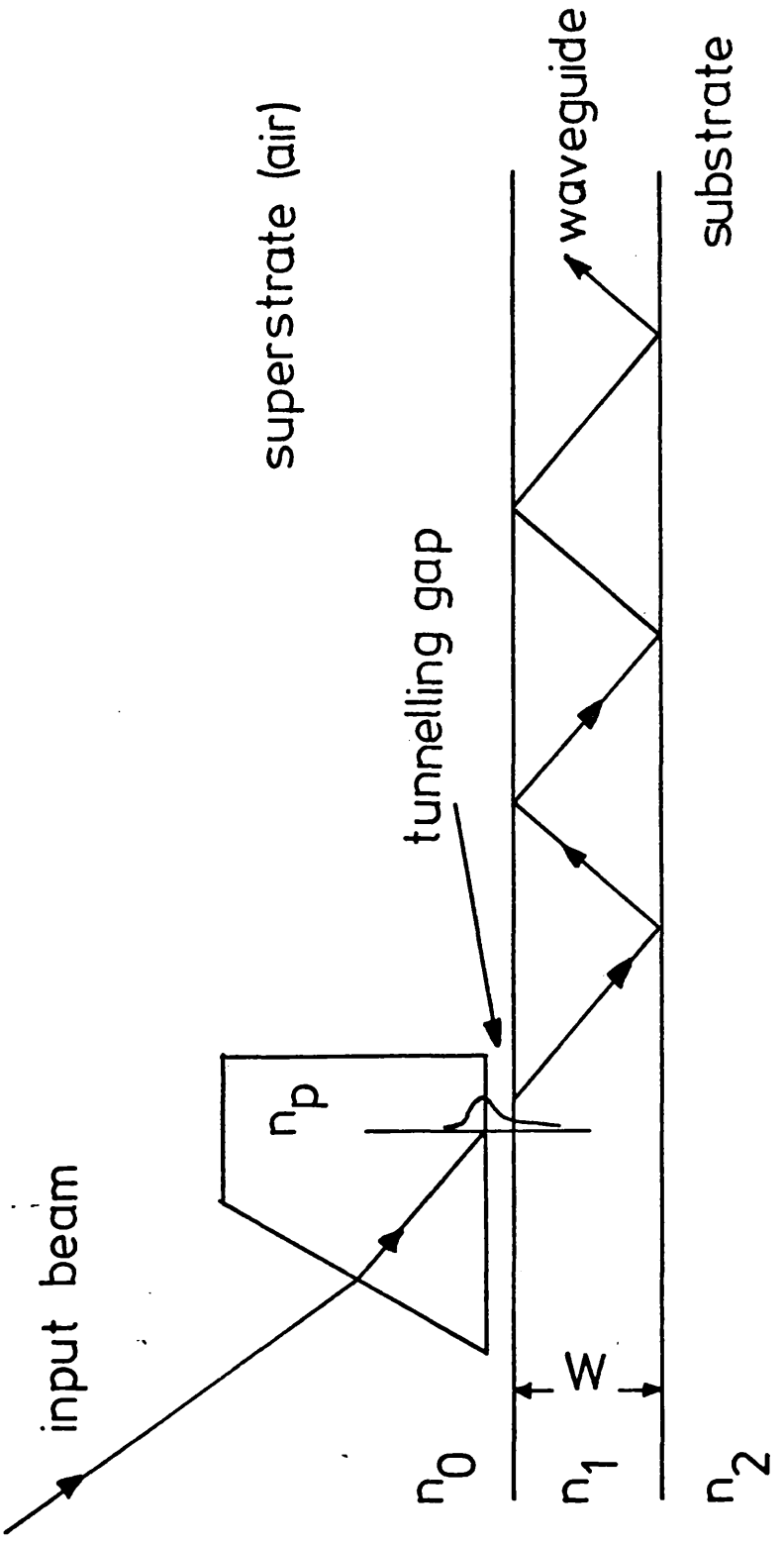

Fig. 2.5 Prism thin-film coupler

index and thickness to be calculated from the mode equation provided that the surrounding indices and wavelength of operation are known (41,42). A numerical method is used to solve the equations. A flow diagram for the computer program is given in Appendix A1. A more complete description of this method which was used almost exclusively in the evaluation of thin film 7059 glass waveguides is given in the next chapter.

Most of the prism couplers used in the launching of light into thin film 7059 glass waveguides were cut from Schott SF15 glass with a refractive index of approximately 1.694. As the prism refractive index is reasonably close to that of the waveguide (R.F. sputtered 7059 glass index $\simeq$ 1.561), coupling into the waveguides was relatively straight-forward (25) and enabled the thin film parameters to be determined accurately because of the relatively large angular separation between the modes.

CHAPTER 3.

CHAPTER 3. GROWTH OF R.F. SPUTTERED 7059 GLASS OPTICAL WAVEGUIDES.

The preparation of R.F. sputtered 7059 glass (43,44) optical waveguides has been extensively reported by many researchers investigating the properties of light guiding in thin film dielectric optical waveguides. Ramaswamy (45) has demonstrated controlled directional guiding in strip loaded thin film planar 7059 glass waveguides, while Goell and Standley (12) have demonstrated multimode guidance in raised 7059 glass stripe waveguides. Clearly R.F. sputtered 7059 glass would appear to be a suitable material for the fabrication of passive integrated optical components in both planar and two dimensional (rectangular) form.

There exists in this department, an 'in house' built R.F. sputtering rig designed exclusively for the fabrication of low loss thin film 7059 glass optical waveguides (82). It was decided to investigate the nature of these films, with a view to using them to fabricate single mode stripe waveguide devices.

This chapter mainly considers the growth of 7059 glass sputtered films on soda-lime glass microscope slide substrates. Mention is made of the design of the sputtering system (including a novel in-process optical thickness monitor system), and the conditions under which the sputtering takes place. Evaluation of the thin films is also discussed.

3.1. Deposition of Thin Film 7059 Glass Optical Waveguides.

3.1.1. Substrate Preparation.

Throughout the course of the project precleaned, polished "Fisher" (46) soda-lime glass microscope slide substrates were used exclusively. This choice is due to the consistent quality, relatively stable refractive index variation within a batch, and moderate cost.

To achieve extremely low loss thin film dielectric optical waveguides, it is essential that the substrates are scrupulously cleaned prior to sputtering; to this end the following substrate cleaning procedure is used.

Cleaning consists of thoroughly degreasing the substrates by placing them in "electronic grade", trichloroethylene and ultrasonically cleaning them for twenty minutes followed by a further twenty minutes of ultrasonic cleaning in "electronic grade" acetone. This is followed immediately by an individual wash in filtered deionised water using a soft sponge and detergent. The substrates are then allowed to rinse in deionised water for twenty minutes before each is individually blown dry using a high pressure filtered dry nitrogen line. Each sample is then individually inspected before being placed in a glass "slide bath", and stored in a dessicator. Samples are then transferred straight from the dessicator to the sputtering rig using the "slide bath", thus minimising contamination due to the relatively non clean atmosphere surrounding the sputtering unit.

3.1.2. Sputtering Equipment.

Thin films of 7059 glass are grown in an "in house" designed R.F. sputtering unit. As this is the subject of a departmental internal report (47), and also of Dalgoutte's thesis (82), only a brief mention of the salient points is given here.

3.1.2.1. Vacuum system.

The vacuum plant consists of a standard "Edwards" 6" silicone oil diffusion pump, backed out with a rotary pump. To avoid contaminating the sputtering chambers with "backstreaming" diffusion pump oil, a liquid nitrogen cold trap is fitted. This also has the advantage of raising the ultimate vacuum available

by freezing out some of the unwanted slow pumping background species. Figure 3.1 shows a general schematic of the pumping system.

3.1.2.2. Sputtering chamber design.

The sputtering unit consists of a "Double Chamber", system with two sputtering heads, fed from a balanced, crystal controlled, 13.56 MHz 1 KW (into 50Ω) R.F. generator. Impedance matching to the heads is achieved by the use of a π matching network (82). A magnetic field of ∿7mT situated round each sputtering head is used to help confine the plasma and increase the plasma density. All-aluminium construction of the sputtering heads instead of stainless steel, results in low loss, undoped sputtered films (15,32), whilst still maintaining acceptable system vacuum performance.

Figure 3.2 shows the general layout of the sputtering system; note the use of the R.F. cage to help contain the high power radiated R.F. signal.

3.1.2.3. Laser film thickness monitor.

Included in the sputtering unit is a novel film thickness monitor, developed in the department. As it is the subject of a departmental internal report (48), only a brief mention of the operating principle will be given.

The thickness of thin transparent films on substrates of different refractive index may be monitored by observing the periodic change in reflectivity as the film thickness increases. This change in reflectivity is due to the increasing path length difference between the interfering beams of light reflected at the upper film surface and the film/substrate interface.

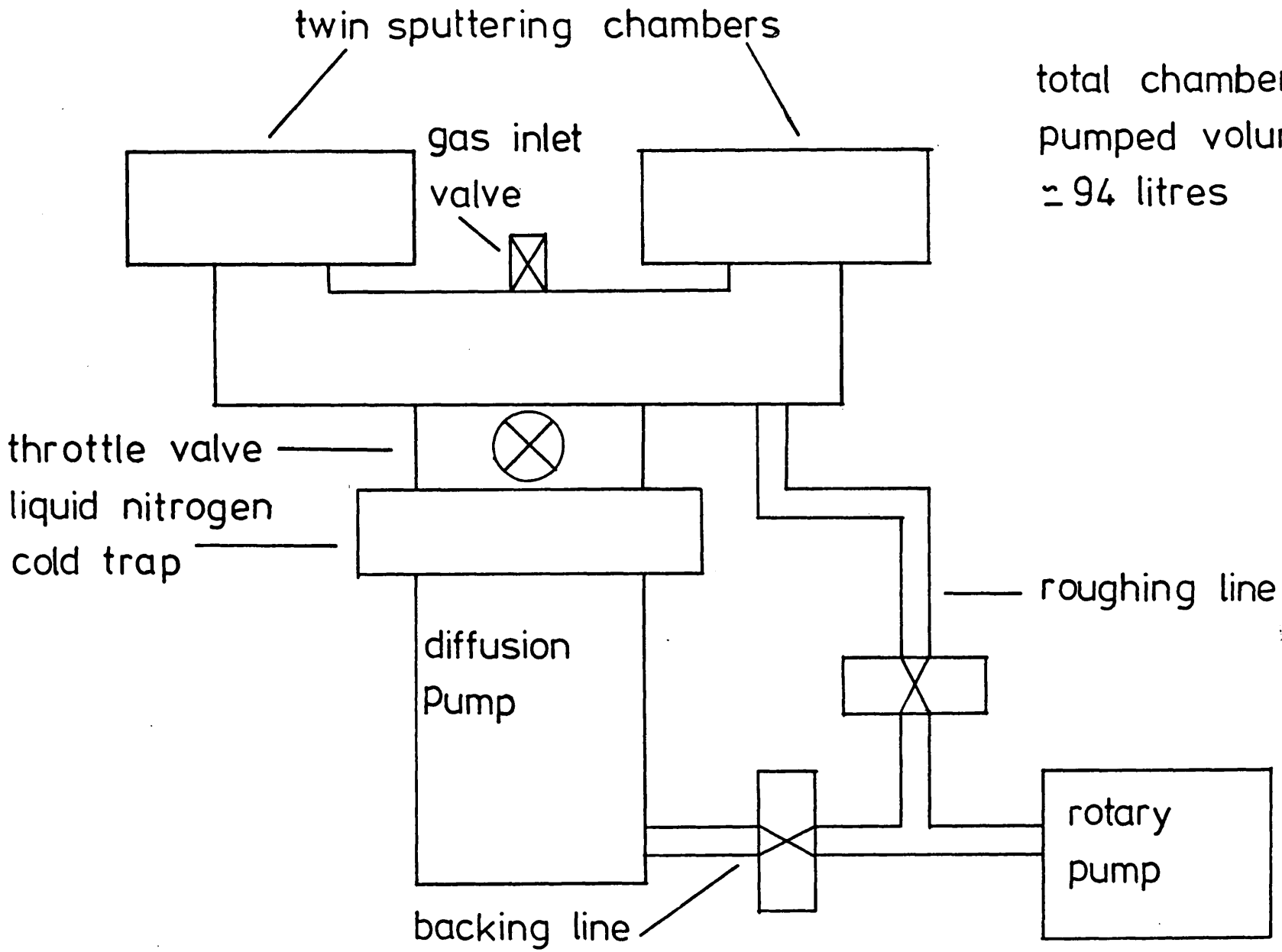

Fig.3.1 Schematic diagram of the R.F. sputtering unit

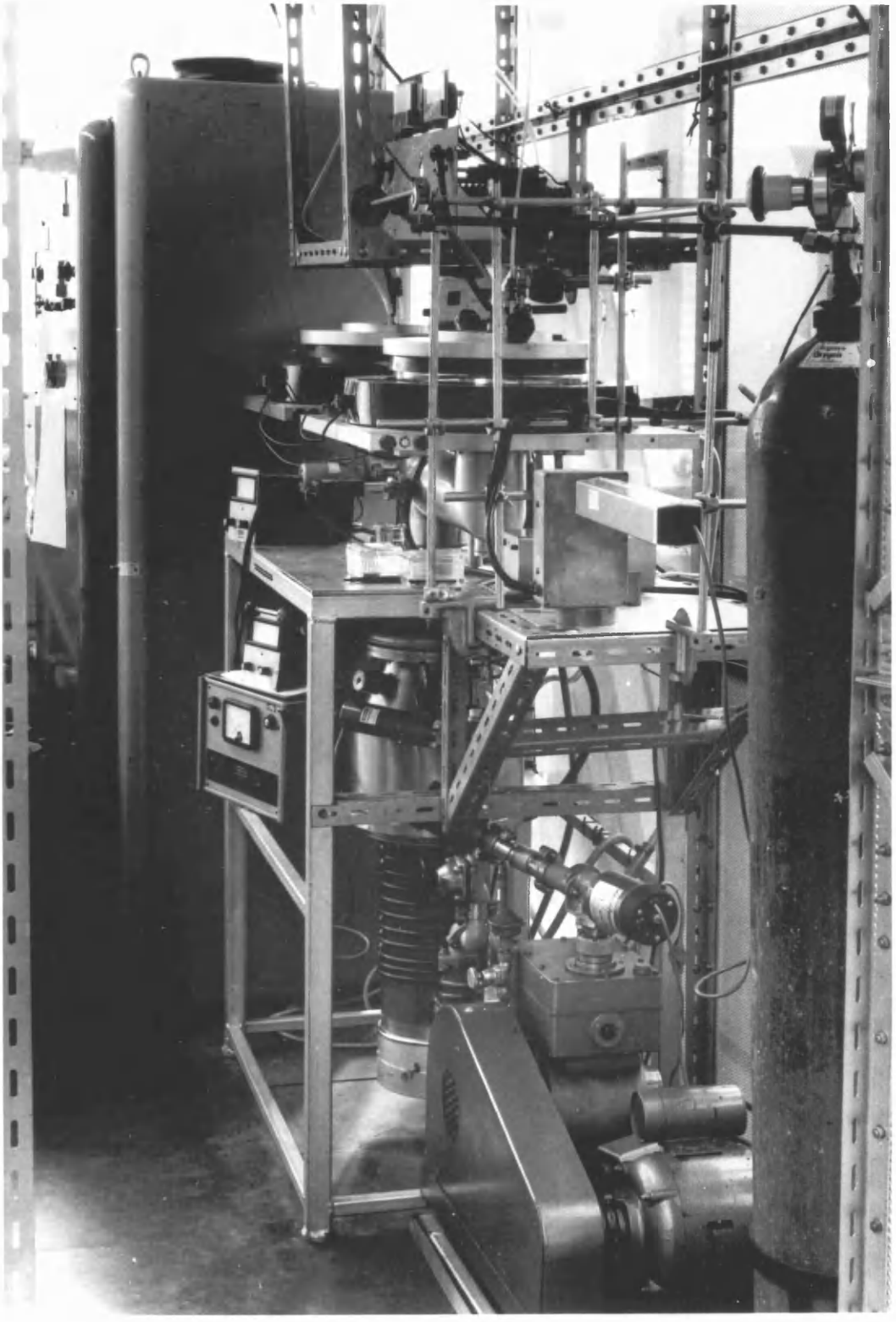

Fig. 3.2 R.F. Sputtering plant

Basically the monitor system comprises of a polarised, "chopped", 0.6328 μm wavelength He - Ne laser beam impinging at a known angle onto a test specimen. The rear surface of the specimen is ground finished to prevent spurious changes in reflectivity due to thermally induced thickness changes in the substrate. The reflected light is detected using a narrow band pass optical filter and photo-diode. The modulation due to chopping is then removed by use of a tuned amplifier, after which the signal undergoes amplification. This rectified signal is used to drive a chart recorder giving a display of reflected light intensity against time. Knowing the film refractive index, (measured using the method outlined in Sections 2.3.1 and 3.2.1) the change in film thickness corresponding to a complete cycle in reflectivity can be calculated. Use of this film thickness monitor allows continual display of film thickness during growth, whilst offering complete immunity to R.F. interference that would upset many alternative instruments, e.g. a quartz crystal monitor.

The above system allows precise thicknesses of thin film 7059 glass to be grown, with an estimated maximum error of ±0.02μm (82). It is thus possible to produce 7059 glass waveguides with precise thin film thicknesses, a criterion that proves essential in later chapters.

3.1.3. Growth Conditions.

Growth of R.F. sputtered 7059 glass optical waveguides are carried out under the following carefully controlled conditions.

Initial Vacuum	$< 2 \times 10^{-6}$ torr
Gas pressure 80% Ar/20%O_2	$= 2 \times 10^{-3}$ torr
R.F. current in each target electrode	= 6 Amperes
Forward power (arbitary units)	= 6.0

Reverse power (arbitary units) = 0.2

Magnet supply current = 3 Amperes

All sputtering runs are constantly supervised and adjusted during the first hour of any run, to compensate for equipment "warm up". This mainly involves the R.F. oscillator, as all other associated electrical equipment is switched on some 3 - 4 hours in advance.

Constant level R.F. power is essential for the production of homogeneous, isotropic, thin films. Pitt (32) has shown that the refractive index of R.F. sputtered 7059 glass varies considerably with the R.F. power density of the plasma. Constant supervision of the R.F. power level is thus essential. 80%/20% Ar/O_2 gas mixture is used to ensure good low loss optical films at moderate sputtering rates. Higher sputtering rates can be obtained by the use of pure Ar gas, but this results in films with unacceptable losses. From the literature, it would appear that the presence of oxygen in the sputtering chamber helps to repair any stoichiometric damage induced by the plasma and results in good low loss films. Further details of this phenomenon may be found in an excellent review article by Pitt et al (15).

3.2. R.F. Sputtered Thin Film 7059 Glass Optical Waveguide Evaluation.

3.2.1. Measurement of Refractive Index and Thickness.

The refractive index and thickness of the sputtered thin film waveguides are determined simultaneously by use of purely optical techniques, as developed by Ulrich and Torge (42). This is the same method as described in Section 2.3.1, further details of the (necessary) mode angle measurements will be found in Section 3.2.2. A flow diagram of the computer program used to calculate the waveguide refractive index and thickness for minimum variance in waveguide thickness is given in Appendix A1. This technique of

obtaining the waveguide refractive index and thickness has been extensively used and reported by other researchers (15,41,49,82), and its accuracy verified (41,82); as such it will only be briefly mentioned here.

As stated in Section 2.3.1, knowledge of at least two mode coupling angles allows accurate calculation of both waveguide refractive index and thickness. In practice, knowledge of more than two mode angles makes it possible, in the case of films supporting several modes, to obtain highly accurate averaged values of refractive index and improved estimates for film thickness. Film thickness measurements become more accurate as the refractive index difference between the thin film and the substrate becomes greater. This is due to the propagation coefficient (β) becoming a more rapidly varying function of film thickness with increasing refractive index difference, resulting in a more accurate measurement of film thickness. For films of refractive index $\sim$1.57 on soda-lime glass substrates of index $\sim$1.51, the estimated accuracy in thickness measurement for films supporting three or more modes is $\pm$5% (82). When making prism coupler mode angle measurements, care must be taken to ensure that the coupler does not affect the propagation coefficients (β's) of the modes. This involves reducing the clamping pressure as far as possible without losing the mode. The reason for this is that a high pressure, i.e. strong coupling, broadens the modes and may shift them (42). Thus in all experiments only very lightly clamped prisms were used. To carry out the necessary calculations a computer program has been used, which solves film refractive index and thickness for every available pair of mode coupling angles and which also averages over all the

solutions to give a mean square error in both the thickness and refractive index. Further details and a flow diagram of this program will be found in Appendix A1. Details of the necessary mode angle measurements are given in the next section.

3.2.1.1. Mode angle measurements and results.

Lightly clamped Schott SF15 glass prisms of known refractive index and angle were used to couple light from a 0.6328μm wavelength He - Ne laser into and out of relatively thick film (3-5μm) sputtered 7059 glass waveguides. Table 3.1 lists some of the SF15 glass prism refractive indices and major angles used in determining the mode angles. Mode angle measurements were made at the input prism without the use of a focussing lens. The small aperture laser iris and large sample to laser iris distance, resulted in a large effective length "optical lever", which allowed the prism normal to be accurately defined. Figure 3.3 shows a general schematic diagram of the experimental apparatus used in measuring the mode angles. By observing the far field radiation pattern of the reflected light from the region of the "coupling spot" (42), the synchronous mode coupling angles can be measured on a precise rotating table using the prism normal as a reference angle. To check the accuracy of this technique, mode-coupling measurements were also made at the output prism, (further details of which will be found in Section 4.6). Normalised propagation coefficients (β/k_o) obtained in this way were determined to an estimated accuracy of 0.0004, corresponding to an angular variation of approximately ±2 minutes of arc.

Synchronous mode coupling angles of several thin film waveguides, all grown under the same sputtering conditions, were measured. All the waveguides were of 3 - 4 μm in thickness and

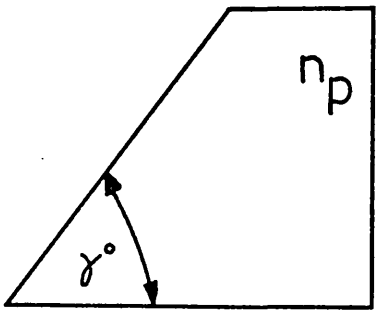

PRISM NO.	MAJOR ANGLE γ ° (DEGREES)	REFRACTIVE INDEX n_p
1	59.658	1.69400
2	60.258	1.69400
3	60.042	1.69415
4	60.008	1.69560
5	60.033	1.69392
6	60.050	1.69395
7	59.683	1.69400
A3	60.016	1.69294

TABLE 3.1. SOME MEASURED SF15 GLASS PRISM PARAMETERS USED IN THE CHARACTERISATION OF RF SPUTTERED 7059 THIN FILM GLASS.

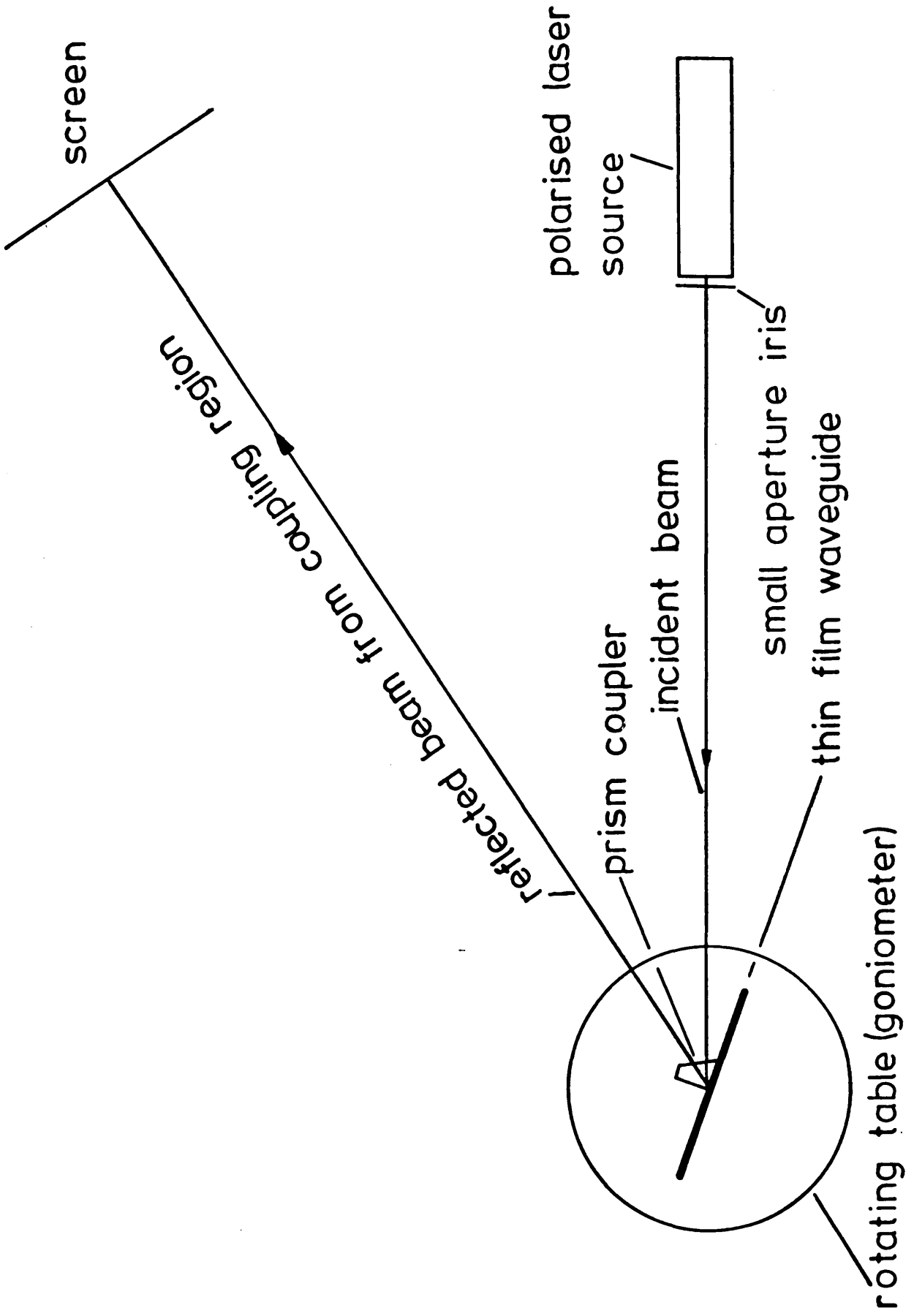

Fig. 3.3 Schematic diagram of the apparatus used in determining the mode coupling angles of thin film 7059 glass waveguides

capable of supporting 4 - 5 TE or TM modes. Using the mode angle measurements and the computer program of Appendix A1, the thin film 7059 glass waveguide refractive index and thickness was determined. Typical results are presented in Table 3.2 for a sputtered 7059 glass film of approximately 3μm thickness. The sputtered thin film 7059 glass waveguides were found to have an average refractive index of n_g = 1.56287±∿0.0001, with all values of waveguide thickness displaying a variance considerably less than the quoted ±5% (82). It is interesting to note that the computer calculated mean square error (variance) of ∿±0.0001 in refractive index is considerably less than the estimated maximum error of ±0.0004 in the measurement of the normalised propagation coefficients. This indicates that the mode angle measurements are probably more accurate than may at first appear and that the sputtered thin film is truly homogeneous in nature. Small mean square errors can only result from homogeneous waveguides (15,42). Inserting the synchronous coupling mode angles obtained from non-homogeneous silver ion exchange waveguides (83) into the computer program results in ill-defined waveguide refractive index values displaying a large mean square error.

Periodic tests on sputtered 7059 glass waveguides revealed no change in thin film refractive index or deposition rate, indicating that the sputtering system was consistently producing thin film 7059 glass waveguides of known refractive index and thickness. During the course of the project new Corning 7059 glass targets were installed and the thin film refractive index fell to a new value of n_g = 1.56068. Again no significant change in waveguide refractive index was noted for many runs carried out over a period of six months, and the deposition rate remained the

N = 4
N0 = 1.00000
N2 = 1.51269
N3 = 1.69392

GAMMA = 60.03300
WAVELENGTH = 0.63280

TE MODES

ALPHA	MODE	NORM.BETA
18.02	0	1.55987
19.33	1	1.55093
21.41	2	1.53612
23.98	3	1.51678

ARITHMETIC MEAN AND MEAN DEVIATION

REFRACTIVE INDEX OF FILM

1.56283 0.00008

THICKNESS OF FILM

2.92956 0.00555

INDIVIDUAL RESULTS FOR REFR. INDEX AND THICKNESS

1.56286	2.93110
1.56287	2.92405
1.56286	2.93131
1.56294	2.91986
1.56286	2.93136
1.56261	2.93968

TABLE 3.2. TYPICAL PRISM-FILM COUPLER THIN FILM MEASUREMENTS MADE ON AN R.F. SPUTTERED 7059 GLASS WAVEGUIDE.

same as before (0.420μm/hour). The reasons for this drop in refractive index are not clear, but it is thought that the new targets came from a different production batch and may have a slightly different composition.

As well as providing an accurate means of measuring the thin film waveguide refractive index, the above method also allows the film thickness to be calculated, the computer program also indicating the mean square error (see Table 3.2). Comparison between the computed and laser monitor values of thickness revealed that the monitor system was over-reading by a constant 4%. The reason for this is thought to arise from the laser beam not impinging on the substrate at the correct angle of 60° to the normal of the film, thus introducing a small error into the calibration of the instrument. As it was difficult to measure accurately the angle between the substrate and the incoming laser beam, it was thought best to leave the thickness monitor over-reading by this small amount. This however is not a problem as the sputtering is extremely linear with time and it is possible to time an accurate thin film thickness whilst using the monitor as a check. By applying a 4% correction factor to the laser monitor, thin films of precise thickness were grown. This was to prove essential for the fabrication of single mode quasi-rectangular waveguide devices as considered in later chapters. The deposition rate of sputtered 7059 glass was time averaged over many long sputtering runs and was found to be 0.420μm/hour.

To ensure that the above measurements of film refractive index and thickness were accurate, it was essential to have accurate knowledge of the prism and substrate refractive indices. To this end an Abbé Refractometer (84) accurate to ±0.0002 was employed.

Tables 3.1 and 3.3 list some of the experimentally measured values of prism and substrate refractive indices used in evaluating the thin films. Accurate knowledge of the prism major angle is also required. This was obtained by placing the prism on a high accuracy rotating table and locating the prism face normals in the same manner as when measuring the synchronous mode coupling angles (see Figure 3.3). A knowledge of these enables all the relevant angles of a prism film coupler to be found. An accuracy of ±1 minute of arc is estimated when using this method. Table 3.1 lists some experimentally obtained values of prism major angles measured using the above method.

3.2.2. Waveguide Loss Measurements.

Loss measurements were carried out using prism film couplers in a manner similar to the loss measurements of Tien et al (13). The output "m lines", obtained from a prism coupler were focussed using a large convex lens onto the detector head of a U.D.T. laser power meter (50). To eliminate the possible effect of damaging the guides through prism contact, care was taken to ensure that all initial power readings were obtained as far away from the input prism as was possible. Subsequent power readings were then taken by moving the output prism closer to the input prism in steps of approximately 1cm. An average 2.54 x 7.62cm soda-lime glass microscope slide substrate usually allowed 3 to 4 of such measurements to be made. At each power measuring point the distance between the input and output prisms was measured using a micrometer. By comparing the different power readings and by noting the difference in micrometer readings, the guide attenuation could be calculated. This method of measuring waveguide attenuation is based on the assumption that the output prism consistently couples out all, or a fixed proportion of, the power propagating in the

ALL SUBSTRATES CONSIST OF PRE-CLEANED "FISHER" BRAND SODA-LIME GLASS MICROSCOPE SLIDES.

SLIDE NO.	EXPERIMENTALLY DETERMINED REFRACTIVE INDEX
N 48b	1.51269
N 48c	1.51269
N 48d	1.51266
N 48f	1.51268
N 66b	1.51277
N 66c	1.51271
N 66d	1.51273
N 66f	1.51274

TABLE 3.3. TYPICAL VALUES OF SUBSTRATE REFRACTIVE INDEX.

waveguide. This would appear to be a valid assumption, as no power was observed in the thin film waveguides after passing below the output coupling prism. From the literature it would appear that a prism coupler may be used to couple out all the power from a thin film waveguide (4,13,33,40).

The results showed that single mode waveguides can have losses as low as 0.1dB/cm, although 0.5dB/cm is closer to the norm. Close examination of the guiding film with a microscope revealed that most of the guide attenuation could be attributed to random scatter points, thought to arise from the presence of small substrate imperfections. Figure 3.4 shows light guiding in a single mode planar waveguide of 0.5μm thickness. The scattering points appear as random bright dots.

In general waveguide losses were seen to decrease with increasing guide thickness although not by any significant amount. This supports the theory that the waveguides themselves are basically low loss with most of the attenuation being attributable to substrate imperfections, thus making substrate preparation a vital issue in the fabrication of low loss planar waveguides. Tien et al (13) have also reported the same effect with low loss V.T.M.S. organosilicon films.

3.3. Discussion of Results.

The results of Section 3.2 have shown that it is possible to fabricate low loss thin film R.F. sputtered 7059 glass optical waveguides with precise knowledge of refractive index and thickness. This facility is essential to the production of single mode quasi-rectangular stripe waveguide devices as considered in later chapters where the lateral confinement of the guided light imposes stringent

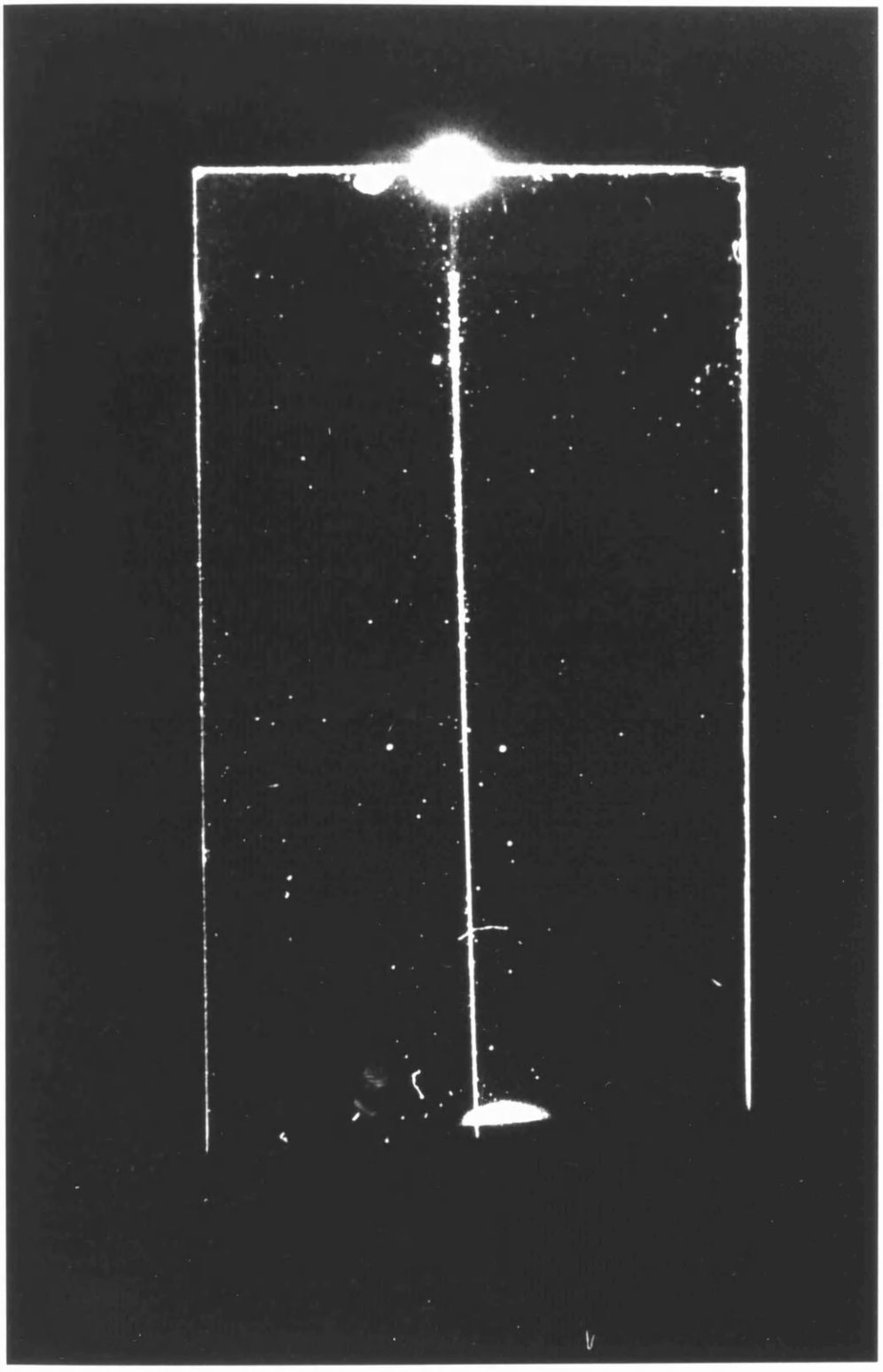

Fig. 3.4 He–Ne Laser light guiding in a planar 7059 glass waveguide

tolerance requirements on the various waveguide fabrication parameters. These requirements, coupled with other factors, make stripe single mode 7059 glass waveguides much more difficult to fabricate than the planar waveguides.

As all the stripe waveguides and devices considered in later chapters are based on single mode (TE_o and TM_o) thin film 7059 glass waveguides the mode angle measurement technique of Section (3.2.1.1) could not be used to compute the single mode waveguide refractive index and thickness. However, as mode angle measurements on multimode waveguides (3-5 TE or TM modes) revealed that the thin films were homogeneous (i.e. all of the same refractive index, see Section 3.2.1.1), it was concluded that single mode waveguides would also have the same thin film refractive index. The homogeneous nature of the thin films suggests that the initial lower index sputtered region at the substrate thin film interface, as observed by other researchers (15,29,32), was not being produced. Thus all the single mode waveguides were assumed to have the same refractive index as the multimode waveguides of Section 3.2. This was checked by measuring the single mode waveguide normalised propagation coefficient (β/k_o), (using the method of Section 3.2.1.1.) and comparing it with the expected value computed from a knowledge of the waveguide structure refractive indices and thickness, using the mode equations of Section 2.1. Agreement was within the experimental error. Thus from the above observations it was concluded that the thin film single mode waveguides were of known refractive index and thickness.

As the object of the project was to fabricate single mode stripe waveguide devices from planar waveguides, no purely planar

devices were considered. However, many interesting and useful devices have been made in thin film form, and due to the planar waveguide nature they are generally much easier to analyse. McMurray (51) has fabricated an electro-optic cadmium sulphide planar waveguide modulator using sputtered 7059 glass as a lower index buffer region, while Wilson and Teh (52) have demonstrated a tapered directional coupler using sputtered films of different refractive indices. Clearly there is still much work to be carried out on passive planar waveguide devices.

An interesting fact to emerge is that the sputtered 7059 glass thin films have a much higher refractive index than that of the bulk material, 1.57 as compared to 1.53. This is thought to occur through preferential sputtering of some of the constituent target compounds, and is dependent upon the R.F. power in the plasma as well as the substrate material. This effect has been used in (52) and it is certain to find many other applications in the fabrication of integrated optical components in both planar and stripe waveguide form. Further details of this phenomenon may be found in the excellent review articles by Jackson(29) and Pitt (15).

3.4. Conclusions.

Useful low loss thin film 7059 glass waveguides of accurately known refractive index and thickness have been fabricated with excellent repeatability. Knowledge of and precise control of these waveguide parameters were essential for the manufacture of single mode quasi-rectangular stripe waveguide devices as considered in the remainder of this thesis.

P A R T I I

TWO DIMENSIONAL TRAPEZOIDAL (QUASI-RECTANGULAR) ION ETCHED STRIPE WAVEGUIDES AND DEVICES

SYNOPSIS

A planar waveguide provides no lateral confinement of the guided light. For some devices this confinement is not necessary and in others not even desirable. However, with the requirement of high device packing densities on the same substrate, crosstalk isolation demands the use of rectangular waveguides. In active integrated optical devices such as lasers and modulators, the use of rectangular rather than planar waveguides leads to a reduction in drive power requirements and hence to an increase in efficiency. If optical damage is to be avoided, power densities in stripe waveguide devices may be limited by the choice of waveguide material. However, sputtered 7059 glass, although not an active material, is well suited for the fabrication of passive integrated optical devices, combining reasonably low loss waveguides with large power handling capacity. With two further waveguide boundaries in rectangular waveguides one of the major problems is in fabricating devices with acceptable losses. To overcome this problem two dimensional waveguides are often prepared by diffusion processes, e.g. of titanium into lithium niobate (53) or silver ion exchange in soda lime glass (22). However, these methods yield waveguides which are inhomogeneous thus making them difficult to analyse.

The advantages of thin-film 7059 glass planar waveguides have been described in Part I, but to fully exploit the benefits thereof, this technology must be applicable to situations where lateral confinement of the guided wave can be induced, i.e. stripe waveguides. This part of the thesis is divided into four chapters: the first describes the fabrication and characterisation of ion-etched trapezoidal 7059 glass waveguides while the other

three consider single mode (E^{x}_{11}) stripe waveguide devices designed on the basis of the theories presented in chapter four.

CHAPTER 4.

CHAPTER 4. RECTANGULAR DIELECTRIC WAVEGUIDES.

To achieve the extremely high data transmission rates obtainable at optical frequencies (now being realised with graded index optical fibres (54)), the associated signal processing circuitry should possess the same large bandwidth. This, together with low drive power requirements coupled with large device packing densitites, necessitates the use of single mode low-loss rectangular dielectric optical waveguides.

Section 4.1 of this chapter outlines the theory of rectangular dielectric waveguides and compares different methods of analysis.

4.1. Theoretical Analysis of Rectangular Dielectric Waveguides.

The analysis of a rectangular dielectric waveguide is much more complex than that of the planar waveguide discussed in Chapter 2. Unlike the latter case or that of a hollow rectangular metal waveguide, the electric and magnetic fields of a rectangular dielectric waveguide cannot be expressed exactly by separable functions of the rectangular coordinates. Rigorous solutions can only be found through detailed numerical analysis. Many workers (55-59) have exerted considerable effort to finding a means by which the properties of the modes of a rectangular dielectric waveguide can be characterised.

This section mainly summarises the various theories and considers in detail the approach of Marcatili (56), and that of Knox and Toulious (57). The validity of these theories for modes close to cut-off is discussed, and investigated by the use of numerical examples. A result identical to that of Marcatili

is derived in Appendix B1 where the fields of a rectangular dielectric waveguide are obtained using a separation of variables technique. Section 4.2 considers the fabrication of quasi-rectangular (trapezoidal) stripe waveguides. Section 4.3 introduces a modification into Marcatili's analysis which allows the propagation coefficients of the quasi-rectangular waveguides to be determined. Use of this modified theory is made in Section 4.4 in which a theoretical and experimental comparison is undertaken. Section 4.4 also compares the above results with those obtained from an independent numerical solution as well as presenting loss measurements on the stripe waveguides.

4.1.1. Summary of Published Analyses.

There are two basic ways of analysing a rectangular dielectric waveguide. One method is to opt for a numerical solution with its attendant extensive computer programming effort and time. This was the method adopted by Goell (55) who used a circular-harmonic field expansion and by Pelosi et al (60) who used a finite element technique. The other method is to try for an analytical close approximation to the problem, and ensure that it provides solutions valid over the range of interest. This was the method chosen by Marcatili (56) and by Knox and Toulious (57).

Gallagher (61) has applied the "effective index" method as proposed by Knox and Toulious to trapezoidal (quasi-rectangular) waveguides with reasonable results. Millar (62) has found good agreement with Marcatili's theory when measuring high aspect ratio sandwich ribbon fibres.

Early during the project it was decided to concentrate on an analytical solution mainly due to the evidence presented

by Gallagher (61) and Millar (62), but also due to the complexity of implementing a numerical solution. The two methods of Marcatili and Knox and Toulious are presented briefly below.

4.1.1.1. Marcatili's Analytical Solution.

Marcatili has described an approximate analytical solution in closed form using simple sinusoidal and exponential functions. The waveguide geometry considered is illustrated in Figure 4.1. In this analysis the fields in the shaded regions are neglected due to the difficulties of matching the tangential fields over the boundaries.

The analysis assumes that for well guided modes the fields decay exponentially in regions 2,3,4 and 5 with most of the power travelling in region 1, with very little in regions 2,3,4 and 5, and with even less in the shaded areas. Consequently only a small error should be introduced into the solution for modes reasonably far away from cut-off. The field matching along the four sides of region 1 may be achieved by assuming simple field distributions. The largest field components are found to be perpendicular to the axis of propagation, with the guided modes of essentially the T.E.M. type, which may be grouped into two families E^x_{pq} and E^y_{pq}. The main field components of the members of the first family are E_x and H_y, while those in the second are E_y and H_x. The subindices p and q represent the number of nodes in the x and y directions respectively. Marcatili has shown that the longitudinal propagation coefficient β_z may be written as,

$$k_z = \beta_z = (k_1^2 - k_x^2 - k_y^2)^{\frac{1}{2}} \qquad (4.1)$$

with $k_1 = n_1 k_o = n_1 2\pi/\lambda$, and where k_x and k_y are the propagation coefficients in the x and y directions respectively, and are the solutions of the following transcendental equations.

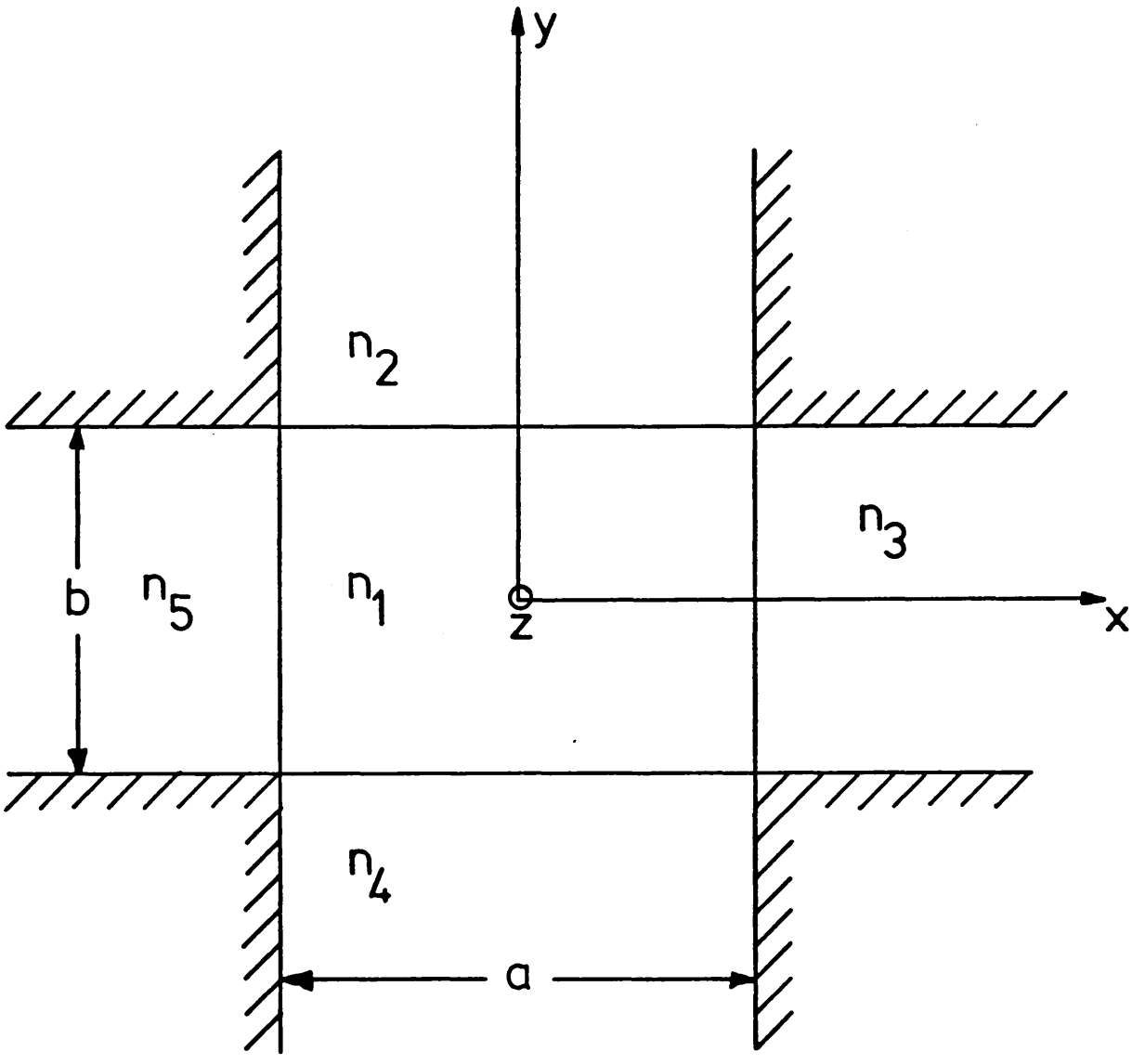

Fig. 4.1 Rectangular waveguide geometry

$$k_x.a = p\pi - \tan^{-1} k_x\xi_3 - \tan^{-1} k_x\xi_5 \qquad (4.2)$$

$$k_y.b = q\pi - \tan^{-1} \frac{n_2^2}{n_1^2}.k_y\zeta_2 - \tan^{-1} \frac{n_4^2}{n_1^2} k_y\zeta_4 \qquad (4.3)$$

for E^y_{pq} modes, and

$$k_x.a = p\pi - \tan^{-1} \frac{n_3^2}{n_1^2} k_x\xi_3 - \tan^{-1} \frac{n_5^2}{n_1^2} k_x\xi_5 \qquad (4.4)$$

$$k_y.b = q\pi - \tan^{-1} k_y\zeta_2 - \tan^{-1} k_y\zeta_4 \qquad (4.5)$$

for E^x_{pq} modes, where

$$\xi_i = \frac{1}{|k_{xi}|} = \frac{1}{\left[(\pi/A_i)^2 - k_x^2\right]^{\frac{1}{2}}} \qquad i = 3,5 \qquad (4.6)$$

$$\zeta_i = \frac{1}{|k_{yi}|} = \frac{1}{\left[(\pi/A_i)^2 - k_y^2\right]^{\frac{1}{2}}} \qquad i = 2,4 \qquad (4.7)$$

$$A_i = \frac{\lambda}{2(n_1^2 - n_i^2)^{\frac{1}{2}}} \qquad i = 2,3,4,5 \qquad (4.8)$$

$$k_i = \frac{2\pi}{\lambda} n_i = k_o n_i \qquad i = 1,2,3,4,5 \qquad (4.9)$$

As the field components in regions 2,3,4 and 5 decay exponentially the constants ξ_i and ζ_i are inverse measures of the distance the evanescent field penetrates into each region. Marcatili has shown that as the mode tends towards cut-off, the discrepancy between his analytical solutions and Goell's computer solutions becomes greater due to the fields in the shaded regions becoming more significant and carrying more power. Thus the above equations apply only to the case of guided modes reasonably far away from cut-off. As we shall see in Section 4.4 this is not a stringent condition as Marcatili's theory will be shown to be valid over all areas of practical interest when considering ion-etched 7059 glass waveguides. In this case in which the refractive index difference between the waveguide and the

surrounding media is large and the waveguide has a large aspect ratio (i.e. a>>b), the E^x_{pq} and E^y_{pq} modes tend to those of the TE_m and TM_m modes of a planar waveguide with m = q-1. In fact if $a \to \infty$, then $k_x \to 0$ and the two eigenvalue equations (4.5) and (4.3) reduce to those of the planar waveguide supporting TE and TM modes, as considered in Chapter 2.

An alternative derivation of Marcatili's solutions is presented in Appendix B1 where a separation of variables technique is employed. This method is much simpler to understand than Marcatili's and is used extensively in future chapters in the design of passive single mode stripe waveguide components.

4.1.1.2. The Knox and Toulious Solution.

In 1970 Knox and Toulious (57) proposed an alternative analysis to that of Marcatili which gave somewhat better agreement with the circular harmonic computer analysis of Goell (55) when considering modes close to cut-off. This "effective index" method, as it has come to be known, has been used extensively by many investigators (45, 59, 73, 85-87), giving in most cases reasonable results.

Basically the effective index method proceeds by deriving an effective waveguide dielectric constant which serves to couple the two planar waveguides that approximate the original rectangular waveguide (see Figure 4.2). From the literature there would appear to be no real mathematical or physical justification for this method, other than the fact that it predicts propagation constants which are closer to those found by Goell, than those of Marcatili for modes closer to cut-off.

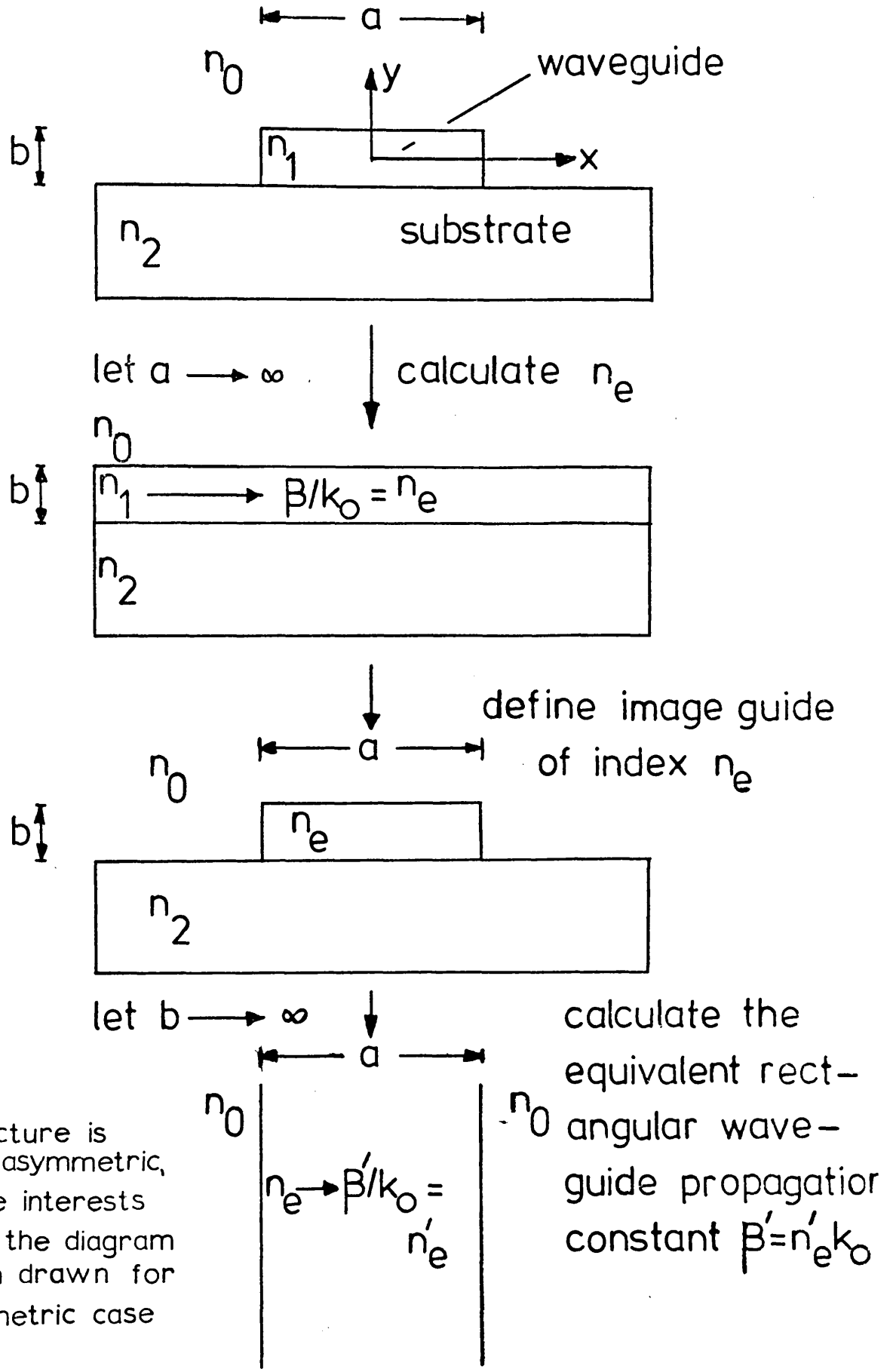

note :-

this structure is generally asymmetric, but in the interests of clarity the diagram has been drawn for the symmetric case

calculate the equivalent rectangular waveguide propagation constant $\beta' = n'_e k_0$

Fig. 4.2 Calculation of rectagular waveguide propagation constant using the effective index method

Referring to Figure 4.2, Knox and Toulious first consider that the waveguide width $a \to \infty$, reducing the structure to an asymmetrical planar waveguide of thickness b, for which a normalised propagation coefficient $n_e = \beta/k_o$ can be calculated. This value of n_e is then used to define a second asymmetrical planar waveguide of width a for which a new value of propagation coefficient $n_e' = \beta'/k_o$ is calculated. n_e' is then taken as the normalised propagation coefficient $= \beta_z/k_o$ for the rectangular waveguide structure of width a and thickness b. When using this method care must be exercise to ensure polarisation continuity. For example, if considering an E^x_{pq} mode (quasi planar TE_{q-1} mode), then the asymmetric planar waveguide of thickness b must support a TE_{q-1} mode, while the asymmetric planar waveguide of width a must propagate a TM_{p-1} mode. The above TE and TM mode conventions are reversed when considering E^y_{pq} modes; in this case we have TM_{q-1} and TE_{p-1} modes instead.

From the results presented by other researchers (45, 59, 73, 85-87) this method of Knox and Toulious seems to give reasonable agreement. However, there would appear to be no explanation in the literature as to why the problem should not be approached the other way round, i.e. by considering the asymmetrical planar waveguide of width a first, and then considering the asymmetrical planar waveguide of thickness b. Referring to Figure 4.3 we first let $b \to \infty$ and calculate n_e for the asymmetrical planar waveguide of width a. This value of n_e is then used to define an asymmetrical planar waveguide of thickness b for which the equivalent rectangular waveguide normalised propagation coefficient $\beta_z/k_o = n_e'$ may

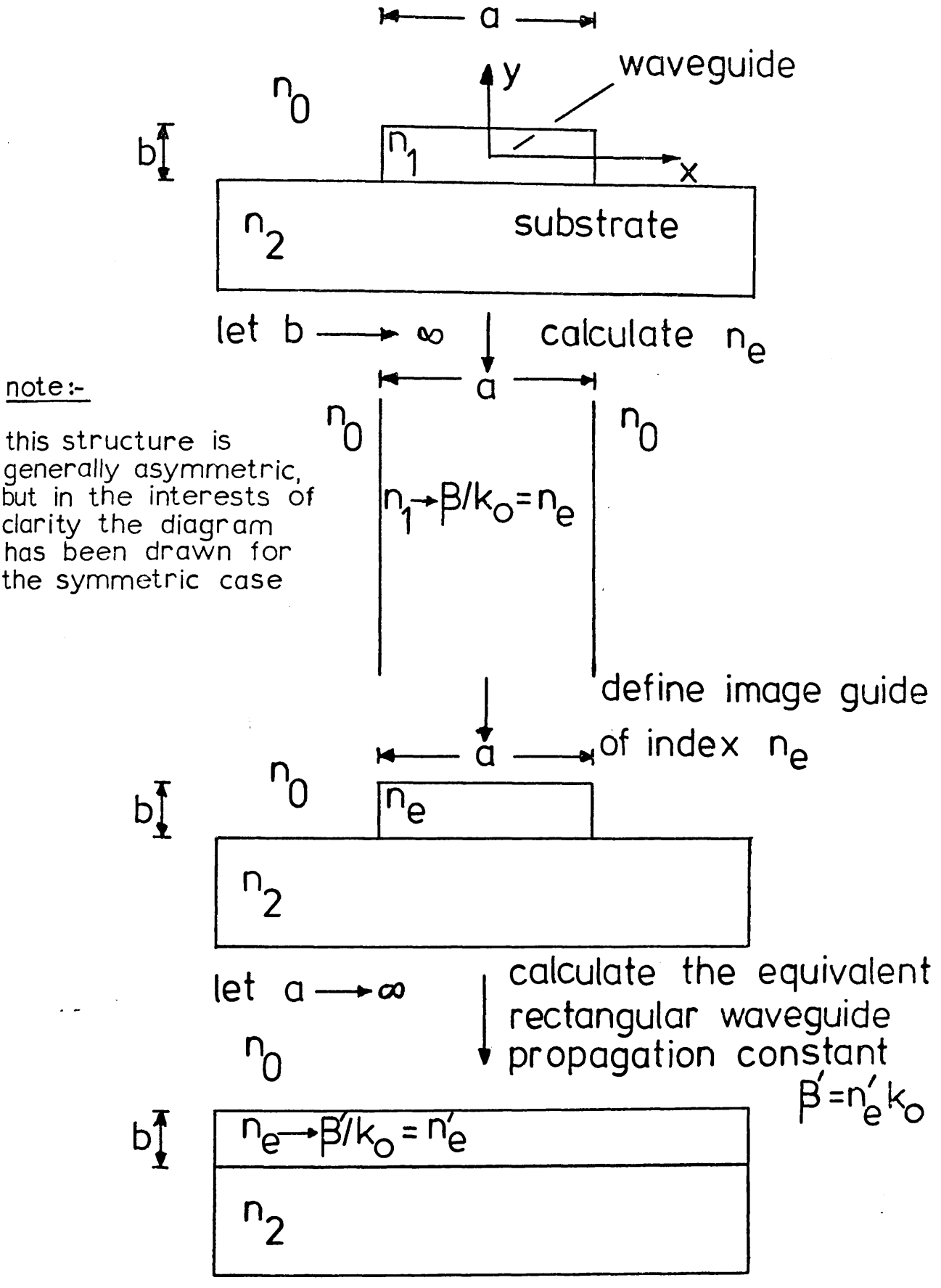

Fig. 4.3 Calculation of rectangular waveguide propagation constant using the effective index method

be calculated. Both ways of calculating the effective index would appear to be equally valid as no evidence can be found to support choosing one in preference to the other. However, both methods cannot be correct as they return different values for effective index when considering the same waveguide problem.

Figure 4.4 shows a plot of normalised propagation coefficient v.s. waveguide width for a rectangular waveguide operating close to cut-off. From the curves it is apparent that the effective index calculated in the conventional manner is identical to that of Marcatili (varying only in the sixth decimal place), whereas the effective index calculated from the opposite approach is markedly higher. This would tend to indicate an inconsistency in the method and for some specific waveguide configurations may give an inaccurate value of propagation coefficient, e.g. in the case of a waveguide when $b>>a$ and $a\simeq\lambda$. In this specific case the second effective index method would give a value of β_z closer to the expected value, than would the conventional effective index method, see Figure 4.5

Comparison between the effective index method as considered by Knox and Toulious and Marcatili, reveals that for the specific case of ion-etched stripe 7059 glass waveguides there is little difference ($<10^{-5}$) in the computed values of propagation ceofficient. It would appear, therefore, common sense to choose the theory of Marcatili which has analytical justification, and offers details of the waveguide fields, in preference to the effective index method which does not. For the above reasons and for others given in Section 4.3 and Appendix B1 it was decided not to use the effective index method.

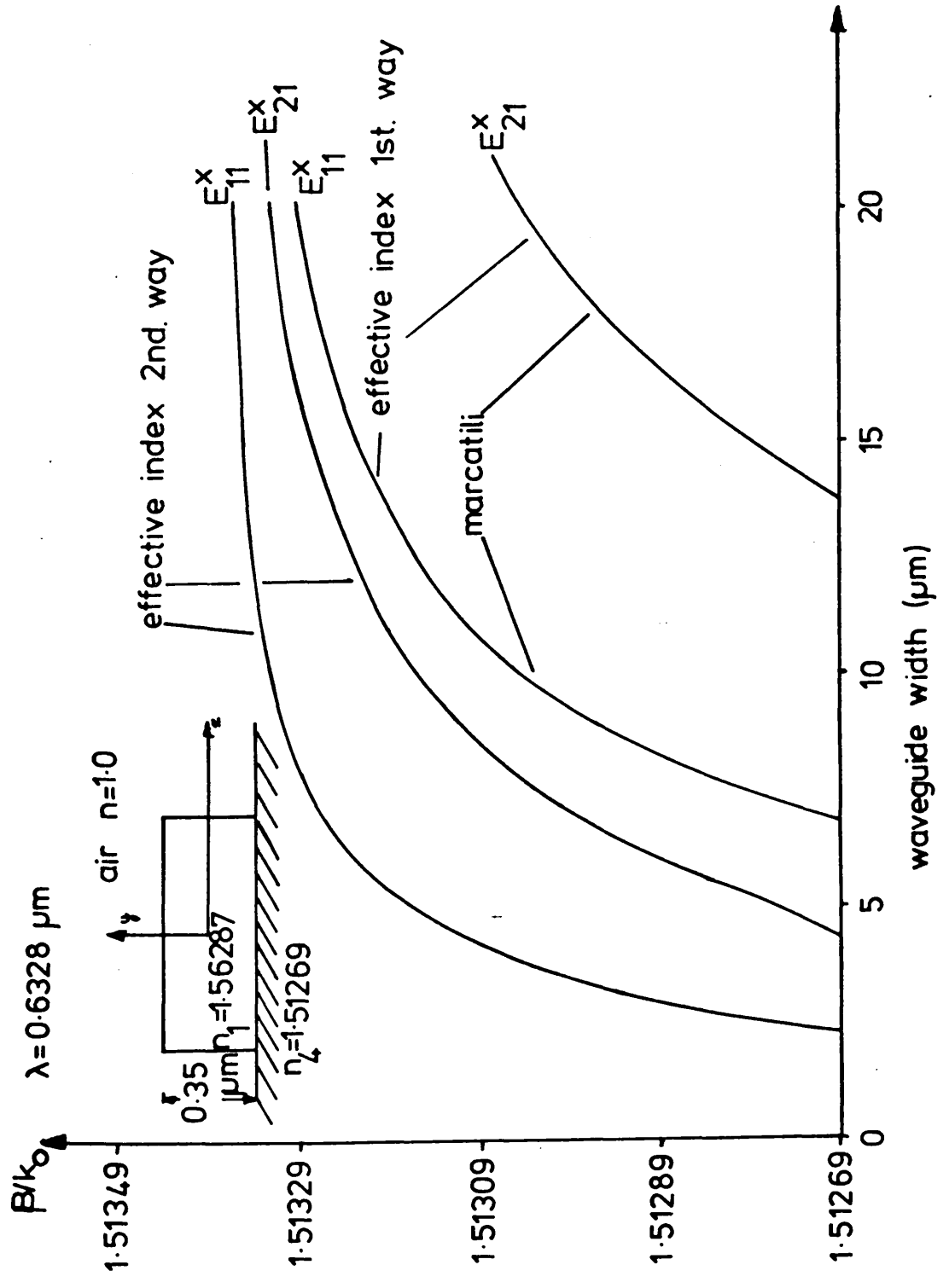

Fig.4.4 Comparison of MARCATILI and the effective index method

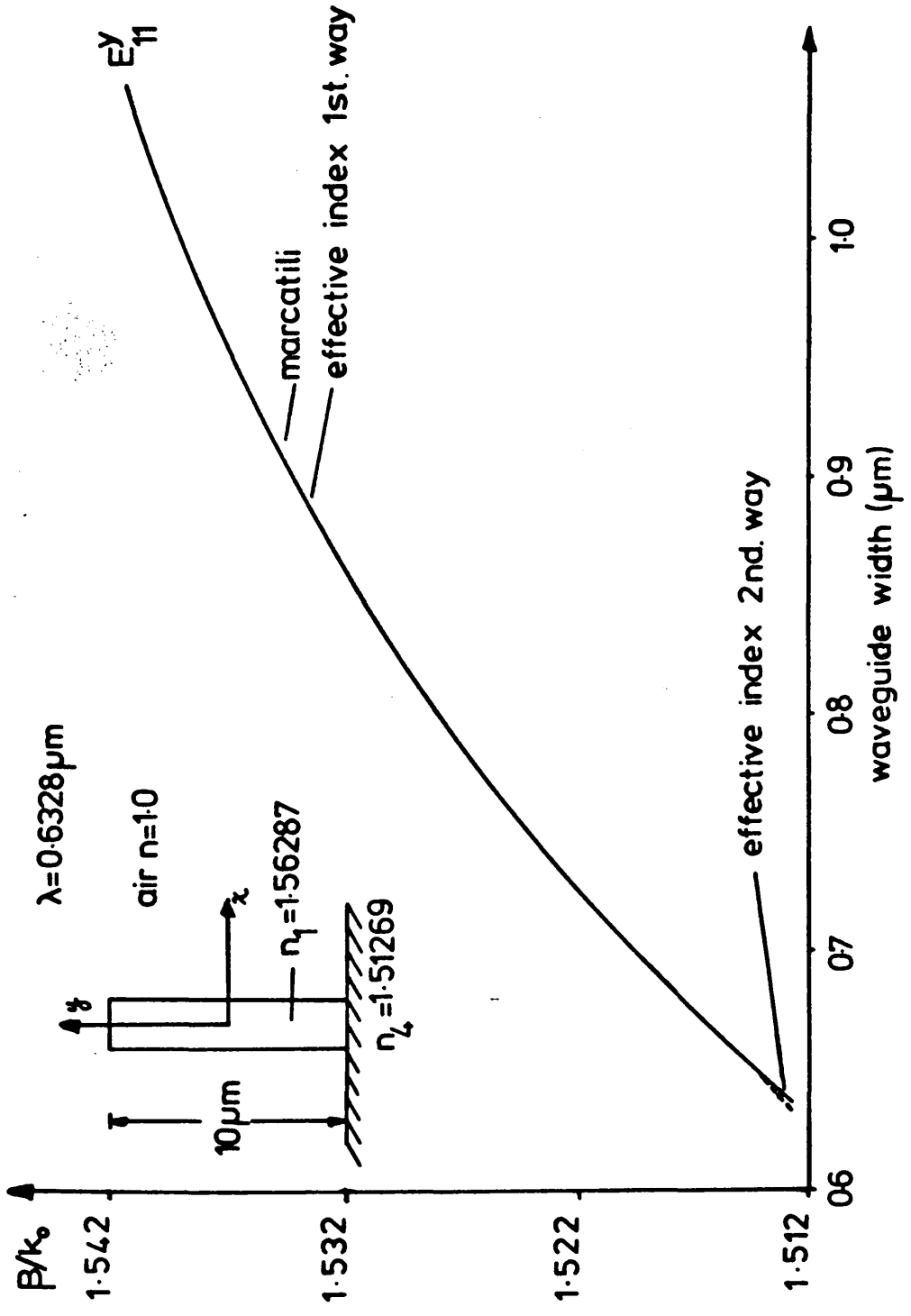

Fig. 4·5 Comparison of MARCATILI and the effective index method

Computer flow diagrams for the theories of Marcatili and the effective index methods are given in Appendices A2-A4.

4.2. Fabrication of Quasi-Rectangular (Trapezoidal) Stripe Waveguides from R.F. Sputtered 7059 Glass.

Ion beam etching (micro machining or ion milling) (63-65) is the only really satisfactory method of fabricating stripe waveguides in R.F. sputtered 7059 glass (43) mainly due to the resilient chemical and physical nature of the sputtered film. Chemical etching methods are ruled out due to the inertness of the sputtered film, while its hardness and brittleness precludes the use of any "lift off" procedure (88).

In an R.F. sputtering system it is desirable to allow only the minimum of materials into the sputtering chamber (15) to avoid target and system contamination through back sputtering. This criterion rules out the fabrication of stripe 7059 glass waveguides by sputtering the thin film glass onto "pre-masked" substrates, for fear of contaminating the sputtering system with the stripe waveguide mask material. For these reasons only clean "fisher" (46) soda-lime glass microscope slide substrates were allowed into the sputtering chamber. Thus ion-beam etching was regarded as the only feasible means of removing the unwanted thin film 7059 glass to produce stripe (quasi-rectangular) optical waveguides and associated devices.

4.2.1. Photolithographic Procedure.

Filtered "Shipley" AZ1350J (66) positive working photoresist was spun on-to newly sputtered 7059 glass thin films using a "Headaway Research" (89) photoresist spinner working at 4000 r.p.m. for 20 seconds. To avoid any problems associated

with atmospheric humidity the thin sputtered films were coated immediately after being removed from the sputtering chamber. After coating the samples were prebaked at 70°C for 30 minutes to drive off any remaining photoresist solvent. The desired waveguide pattern was then obtained by exposing the photoresist coated sample through a light-field photomask using an ultra violet lamp. By varying exposure time around the 4 minute optimum, it was possible to effect small changes in the replicated photoresist waveguide dimensions. This technique was employed regularly and proved invaluable in the fabrication of single mode stripe waveguide devices. After exposure the photoresist was removed by developing the sample in MF312 developer (66) mixed 1:1 with distilled water, for approximately 60 seconds. The actual development endpoint was judged by eye, when it became apparent that all the exposed photosensitive polymer had been removed. This was easily seen as large areas of the photoresist coated substrate were exposed, this being due to the light field photomask leaving only the narrow photoresist replicated stripe waveguide patterns standing proud on the thin film 7059 glass waveguide surface. Use of the above development technique was necessary due to small changes in ambient conditions controlling the absolute development time. Again it was possible, by over development, to reduce slightly the size of the photoresist replicated waveguides. After development the samples were washed in filtered deionised water for approximately 2 - 3 minutes, before being gently blown dry with a filtered nitrogen gas line. The samples were baked at 70°C for 30 minutes to allow the photoresist polymer to flow slightly and give waveguide patterns with smooth edges (66).

In order to ensure that the stripe waveguide photoresist masks could endure the relatively long ion-beam etching process, it proved necessary to further bake the samples for 1 hour at 150°C. This process drives off much of the remaining solvents in the photoresist and leaves a hard polymer film on top of the sputtered thin film (67). The samples were then ready to undergo the ion etching process as outlinedin Section 4.2.2 below.

4.2.2. Ion Beam Etching.

Ion beam etching (micro machining or ion milling) is now a well established thin film technology for replicating patterns by removal of the mask and substrate materials using high energy ions. It has been used in many applications over the past years (e.g. in integrated circuit manufacture and magnetic bubble memories), and has been described in a number of review articles (63-65). Its high resolution capability makes it a useful technique for integrated optics, since it will consistently reproduce any suitably masked pattern.

The ion beam etching of thin film 7059 glass introduces difficulties which do not occur with most other thin film materials. These difficulties are almost exclusively due to the relatively slow etch rate of the sputtered film compared to that of the photoresist (≈0.5μm/hour compared to ≈0.7 μm/hour), and results in devices of limited thickness and non-rectangular cross-sectional geometry. However, for the vast majority of stripe 7059 waveguide devices this is not a major problem.

As stated in Section 4.2.1 the photoresist must be baked for 1 hour at 150°C so as to form a hard polymer film that can withstand the ion-etching process. Baking, however, seriously alters the profile of the photoresist films, as can be seen from

the scanning electron micrographs of Figures 4.6a and 4.6b which show a rectangular waveguide photoresist pattern before and after baking. Baking first causes the photoresist to flow across the surface of the 7059 film and to take up a meniscus shape. The volatile constituents of the photoresist are then driven off by evaporation and the meniscus contracts while still retaining the same general shape. The photoresist in this form is able to withstand the high energy ion beam. However, as can be seen from Figure 4.6b, the photoresist mask is no longer rectangular and when etching takes place sloping rather than vertical walls are produced in the glass waveguide below. The etch rate is a complex function of angle of incidence of the ions (102,103) and Figure 4.6c shows schematically how this also produces sloping waveguide walls. A combination of both the above mentioned effects give a trapezoidal rather than rectangular waveguide profile. Figure 4.6d shows a scanning electron micrograph of a trapezoidal ridge waveguide fabricated in sputtered 7059 glass.

The trapezoidal geometry has the disadvantage that the sloping edges are rough (of the order of $\lambda/6$) and lead to large waveguide attenuation due to scattering. This roughness mainly arises from the differential etch rates of the waveguide and mask materials, (i.e. the R.F. sputtered 7059 glass and baked photoresist respectively). When the waveguide mask material (baked photoresist) is completely removed the roughness reproduces itself in the waveguide material. This is especially marked in the case when the waveguiding material etches at a faster etch rate than the mask material.

As well as using baked photoresist as the masking material,

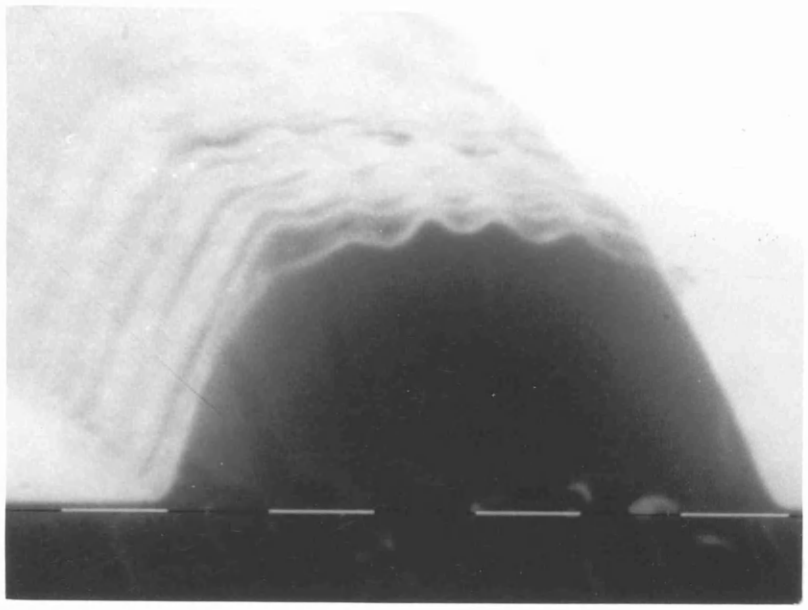

(a) before baking (1μm markers)

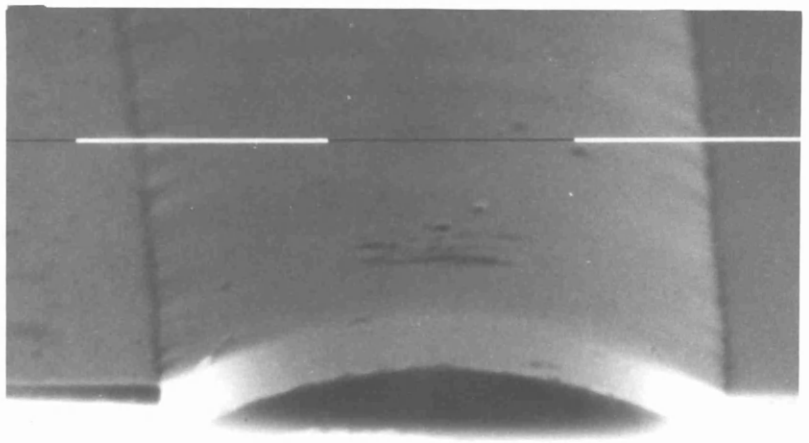

(b) after baking (10μm markers)

Fig. 4.6 Photoresist waveguide patterns before and after baking

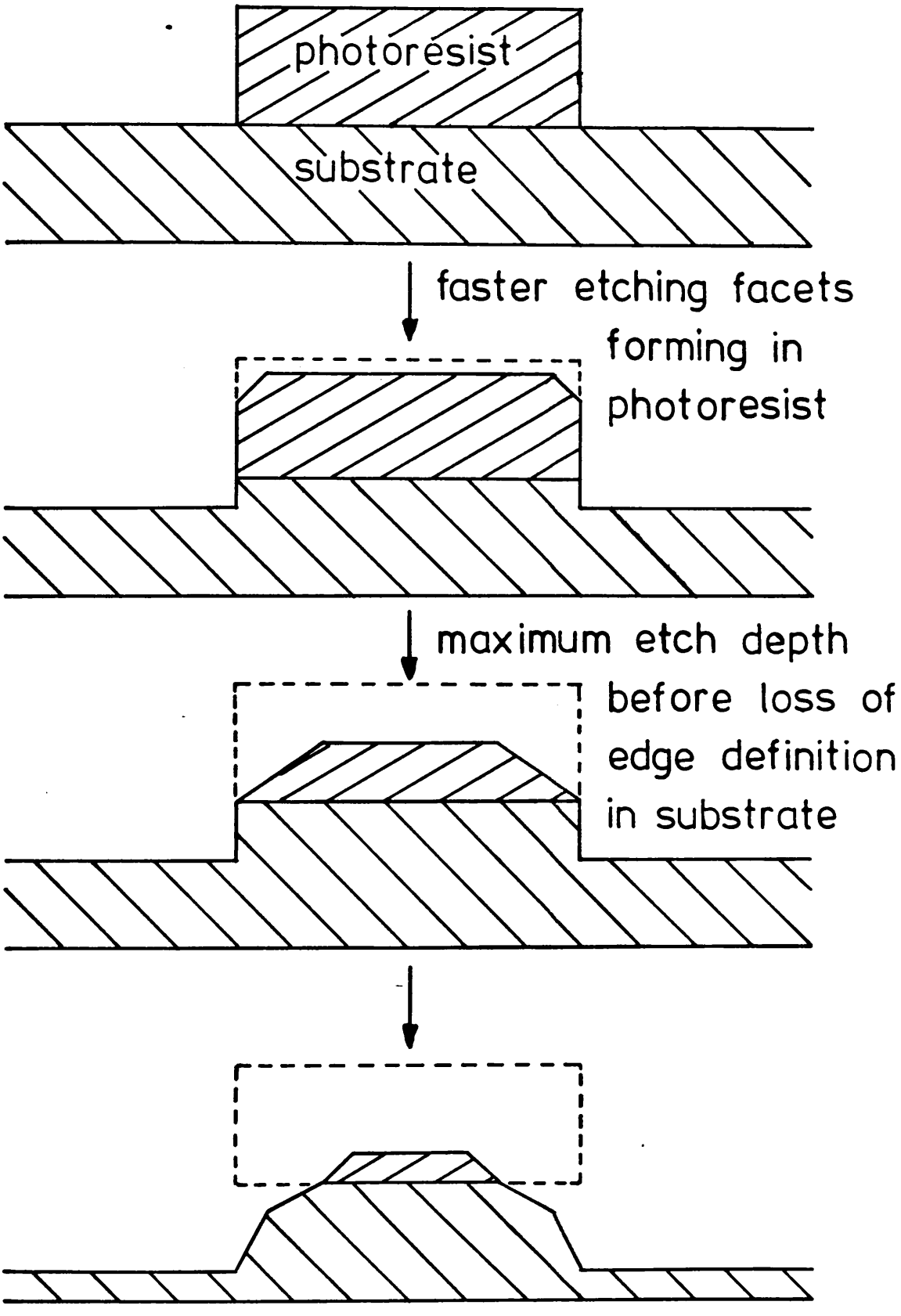

Fig. 4.6c Schematic diagram of the stages of ion-beam etching

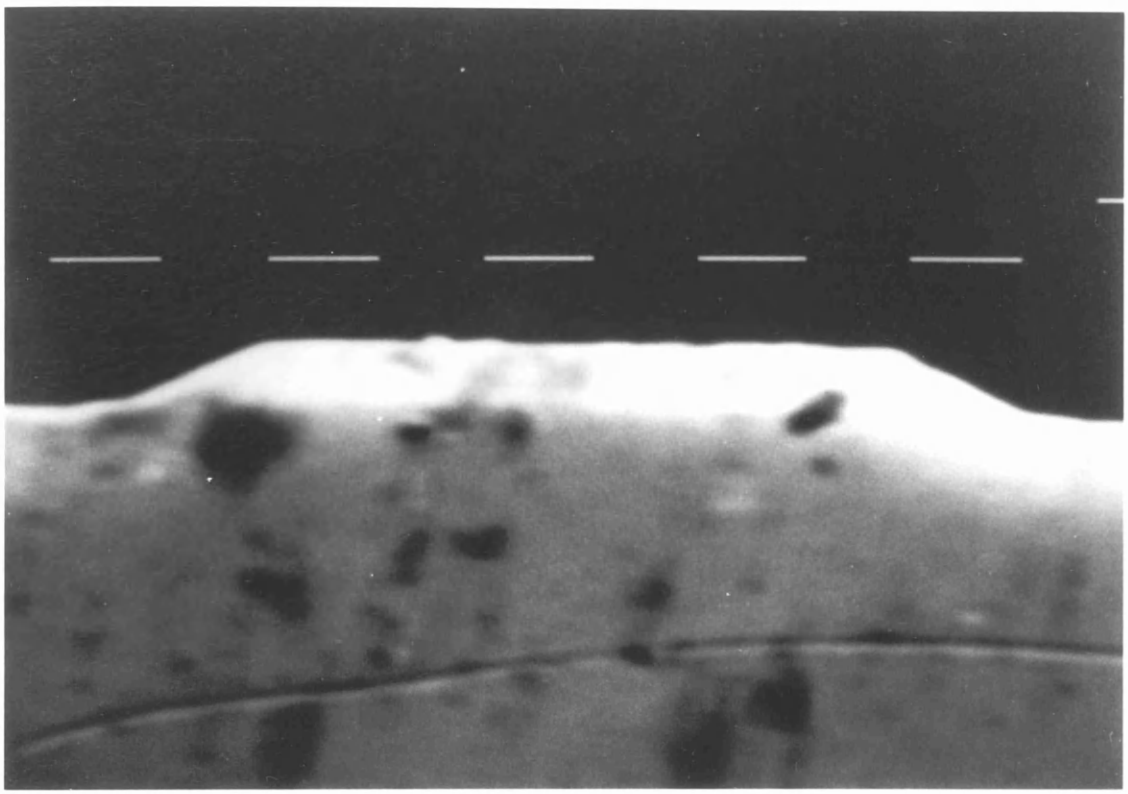

(d) S.E.M. micrograph of an ion-etched 7059 glass waveguide (1μm markers)

Fig. 4.6 Trapezoidal ridge waveguide

thin film aluminium and chrome were also tried. However, these investigations were dropped when it was discovered that they etched at a much faster rate than the photoresist. All stripe waveguides and devices were fabricated using the above procedure with baked photoresistas the masking material. It is interesting to note that apart from glass and carbon "Shipley" AZ1350J has one of the lowest etch rates of any material when subjected to a normally incident Argon ion beam (see Table 1, page T22 of reference 102).

The ion beam etching was carried out in a custom built pumping unit utilising fast "Edwards", diffusion and rotary pumps mounted with a G.V. Planar triode ion gun assembly (90). A photograph of this unit is shown in Figure 4.7. The substrates containing the thin films were mounted (two at a time), on a water cooled rotating substrate table using indium gallium eutectic to ensure good thermal contact with the substrate table. Etching was carried out in a pure argon atmosphere of 2×10^{-3} torr pressure with the ion gun operating at 5KV, 20 mA emission current. The etch rate of thin film sputtered 7059 glass was found to be 88.6Å/min, while that of baked AZ1350J photoresist was 120Å/min. Thus with a maximum photoresist thickness of ≈1.2 μm, the deepest guide that could be etched with safety was ≈0.8 μm. The relatively slow etch rate of the 7059 glass compared to that of the photoresist resulted in the stripe waveguides having a pronounced trapezoidal cross-sectional geometry (see earlier in this section).

After etching the samples were carefully washed in dilute hydrochloric acid to remove all traces of the indium gallium eutectic. They were then placed in a Tegal Plasmod (91)

Fig. 4.7 Ion-beam etching unit

plasma asher which removed all the remaining photoresist by ashing it in an R.F. excited oxygen plasma of 0.1 torr pressure. The time to remove all the remaining photoresist varied from sample to sample, but it was usually of the order of 2 hours. No evidence was observed of the oxygen plasma etching the thin film 7059 glass. After all the remaining photoresist deposits had been removed the samples were carefully cleaned using detergent and filtered deionised water, after which they were blown dry using a filtered nitrogen line. The waveguide samples were then stored in clean dry conditions prior to being tested.

4.3. Effective Width Modification for Waveguides with a Trapezoidal Cross-Sectional Geometry.

As stated in Section 4.2.2 it is not possible to fabricate rectangular stripe waveguides in sputtered 7059 glass using the present manufacturing techniques. This presents a major problem as there exists, to the author's knowledge, no analytical solution for propagation in waveguides with a trapezoidal cross-section.

Pelosi et al (60) have analysed ion etched trapezoidal waveguides using a finite element technique, while Gallagher (61) has analysed the same experimental data using the effective index method. In both cases agreement between theory and experiment was considered good; however, Gallagher assumed somewhat arbitrarily that the trapezoid base width was equivalent to a rectangular waveguide of the same width, while Pelosi's analysis required that each waveguide structure be analysed separately, thus making waveguide characterisation difficult. These methods gave reasonable results for waveguides that were nearly rectangular but returned values that became progressively worse as the

waveguides had a more pronounced trapezoidal geometry, e.g. in the case of over-etched waveguides (see Section 4.4).

During the course of experimental work it was noticed that somewhat better agreement between the theory of Marcatili (56) and experiment could be obtained by substituting a waveguide effective width in place of the base width. Initially the average waveguide width was used, but it soon became apparent that better agreement could be obtained by using an effective rectangular waveguide cut-off width as described below.

Referring to Figure 4.8 and recalling the rectangular waveguide analysis of Appendix B1, we may argue that there is little power flowing in the triangular sections of the waveguide whose heights are less than the equivalent rectangular waveguide cut-off thickness (see Figure 4.8). This follows directly from considerations of the trapezoidal stripe waveguide geometry, as to support a guided mode the equivalent rectangular waveguide must have some minimum value of waveguide thickness. This would appear to be a valid assumption since ion-etched 7059 glass stripe waveguides guide light for considerable distances (many 10,000's of λ), we may therefore conclude that there are no leaky modes caused by the sloping waveguide walls. From this we may deduce that the electric and magnetic fields of the guided mode inside the shaded triangular sections of the trapezoidal waveguide (see Figure 4.8) are very small. Thus we may argue that a trapezoidal waveguide may be represented by an equivalent rectangular waveguide whose width lies somewhere between the trapezoid base width and top width, i.e. $W_{top} < W_{effective} < W_{base}$.

The analysis of Appendix B1 has shown that the equations which describe the fields of a rectangular waveguide are similar

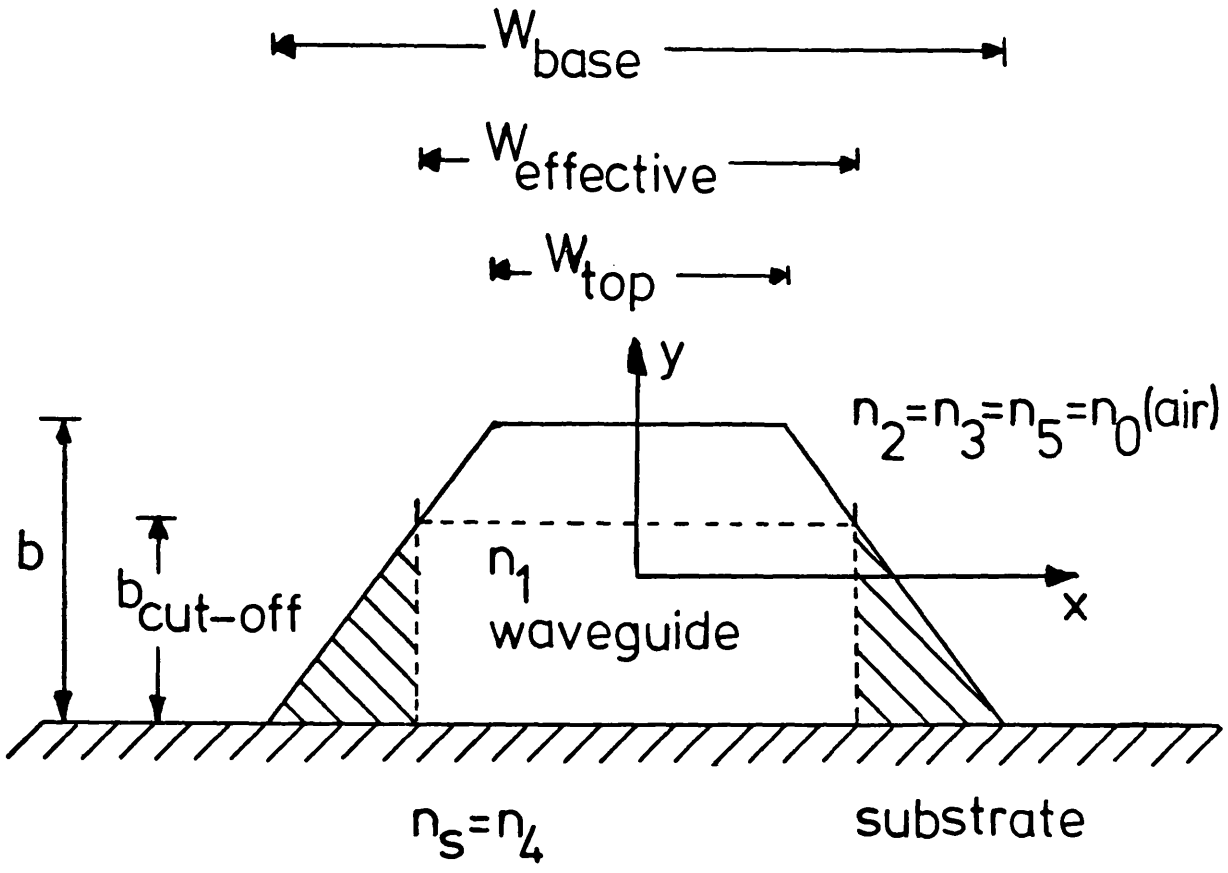

Fig. 4.8 Effective width modification for trapezoidal waveguides

to those of a planar waveguide. However, stripe waveguides, unlike planar waveguides (see Section 2.1) have both a minimum waveguide width and a minimum waveguide thickness. This leads to the waveguide being "cut-off" (i.e. unable to support a guided mode) whenever the waveguide width or thickness becomes so small that there is no solution to the rectangular waveguide transcendental mode equations (see Section 4.1.1.1, equations 4.2 through 4.5); or, the normalised propagation coefficient β_z/k_o falls to a value equal to that of the highest surrounding refractive index, i.e. $\beta_z = (n_1^2k_o^2-k_x^2-k_y^2)^{\frac{1}{2}} = nk_o$, n being the largest of the surrounding media refractive indices (n_2,n_3,n_4,n_5).

From the above result we see that the rectangular waveguide "cut-off" condition is a function of both the waveguide width and thickness (i.e. a function of both k_x and k_y). Thus using Marcatili's eigenvalue mode equations (see Section 4.1.1.1) we may define the following effective rectangular waveguide cut-off depths,

$$b_{\text{cut-off } E^x} = \left[q\pi - \tan^{-1}k_{yc.o.}\zeta_2 - \tan^{-1}k_{yc.o.}\zeta_4\right]/k_{yc.o.} \quad (4.10)$$

For E^x_{pq} modes, and

$$b_{\text{cut-off } E^y} = \left[q\pi - \tan^{-1}\frac{n_2^2}{n_1^2}k_{yc.o.}\zeta_2 - \tan^{-1}\frac{n_4^2}{n_1^2}k_{yc.o.}\zeta_4\right]/k_{yc.o.} \quad (4.11)$$

For E^y_{pq} modes. With,

$$k_{yc.o.} = k_{y\text{cut-off}} = (n_1^2k_o^2 - k_x^2 - n^2k_o^2)^{\frac{1}{2}} \quad (4.12)$$

and n being the largest of the surrounding media refractive indices (n_2,n_3,n_4,n_5), (usually the substrate n_4) and with $k_o = 2\pi/\lambda$. k_x is calculated from the trapezoid base width $W_{base} = a$ using equations (4.2) or (4.4), depending on the mode type (i.e. E^x_{pq} or E^y_{pq}).

W_{base} is chosen in preference to W_{top} as it contains the small triangular sections of waveguide which are less than the equivalent rectangular waveguide cut-off thickness. Therefore W_{base} corresponds to the largest value of equivalent rectangular waveguide width possible for a trapezoidal waveguide and we may expect, to a first approximation, that the following effective waveguide width corresponds to that of an equivalent rectangular waveguide.

Using the above cut-off depths we may define a corresponding waveguide effective width $W_{effective}$ which is dependent on the difference between the base and top widths of the trapezoid. Assuming that the etched waveguides have a perfectly symmetrical trapezoidal cross-section, we may calculate $W_{effective}$ using the following formula,

$$W_{effective} = W_{top} + (W_{base} - W_{top})(1 - b_{cut\text{-}off}/b) \qquad (4.13)$$

which follows from simple geometrical considerations of Figure 4.8. This enables a trapezoidal waveguide to be represented by an equivalent rectangular waveguide of width $W_{effective}$, thus allowing it to be analysed in a relatively straightforward manner using the theory of Marcatili (56).

Theoretical and experimental results using the above effective width theory and that of Marcatili are compared in Section 4.4. The validity of this analysis is checked using an independent computer solution. As will be seen in later chapters, the effective width theory coupled with that of Marcatili forms part of the fundamental design criteria for trapezoidal 7059 glass waveguide devices.

During the course of the project it became apparent that the above effective width theory of Section 4.3 may only

be an approximation to a more accurate equivalent width theory based on a numerical approximation technique.

The method proceeds by initially calculating a value of k_x using the trapezoidal waveguide refractive indices and base width (W_{base}), (see Figure 4.8). This value of k_x is then used to calculate the rectangular waveguide cut-off depth $b_{cut\text{-}off}$ using equations (4.10) through (4.12). $b_{cut\text{-}off}$ is then used to compute an equivalent rectangular waveguide effective width $W_{effective}$ using equation (4.13). This new value of equivalent rectangular waveguide effective width is then used to calculate a new value of $b_{cut\text{-}off}$, in an identical manner to the method described above. This in turn leads to another new value of equivalent rectangular waveguide effective width. This process is repeated until the difference between the old and new values of waveguide effective width becomes very small, at which point the iteration is terminated. The limiting value of waveguide effective width is then referred to as the two-dimensional waveguide effective width. A computer program to calculate the above two-dimensional waveguide effective width was written, a flow diagram of which may be found in Appendix A12.

The accuracy of the above effective width theory is believed to be better than that of the first approximation. However, the exact significance of this limiting value of waveguide effective width is still under review and at present its physical significance (if any) is unknown. Due to this fact no results using the above two-dimensional waveguide effective width are presented. However, some preliminary calculations reveal that the difference between the two-dimensional

waveguide effective width and the first order approximation is less than the estimated error of 0.25 μm in the S.E.M. waveguide width measurements (see Section 4.4.2) and is, therefore insignificant.

4.4. Two Dimensional (Stripe) Trapezoidal 7059 Glass Waveguides.

4.4.1. Measurement of Modal Propagation Constants.

Thin-film prism couplers (4) were used to couple light from a 0.6328 μm wavelength He-Ne laser into ion-etched stripe 7059 glass waveguides. Modal propagation constants were obtained by measurements of output synchronous coupling angles. Precise angle measurements were made by relating the direction of the normal from the output face of the prism to the output-coupled "m-line" angles by using a second laser to define a reference angle. Figure 4.9 shows a schematic of the experimental set-up used to measure these angles. The output "m-line" structure of the waveguides was projected onto a ground glass screen, and by careful alignment of the reference laser the output synchronous coupling angles could be measured. Details of calculating normalised propagation coefficients (β/k_o) from prism coupler measurements are given in Figure 4.10.

Figures 4.11,12,13 show "m-line" patterns for three stripe 7059 glass waveguides all supporting only a single "depth mode", (i.e. only one mode perpendicular to the plane of the thin 7059 glass film). The first is a wide multi-mode guide (in the transverse direction, i.e. the plane of the thin film), the second is a narrow guide supporting only two modes (i.e. E^x_{11} and E^x_{21}), whereas the third is a single mode guide propagating only the lowest order E^x mode (i.e. E^x_{11}). There is

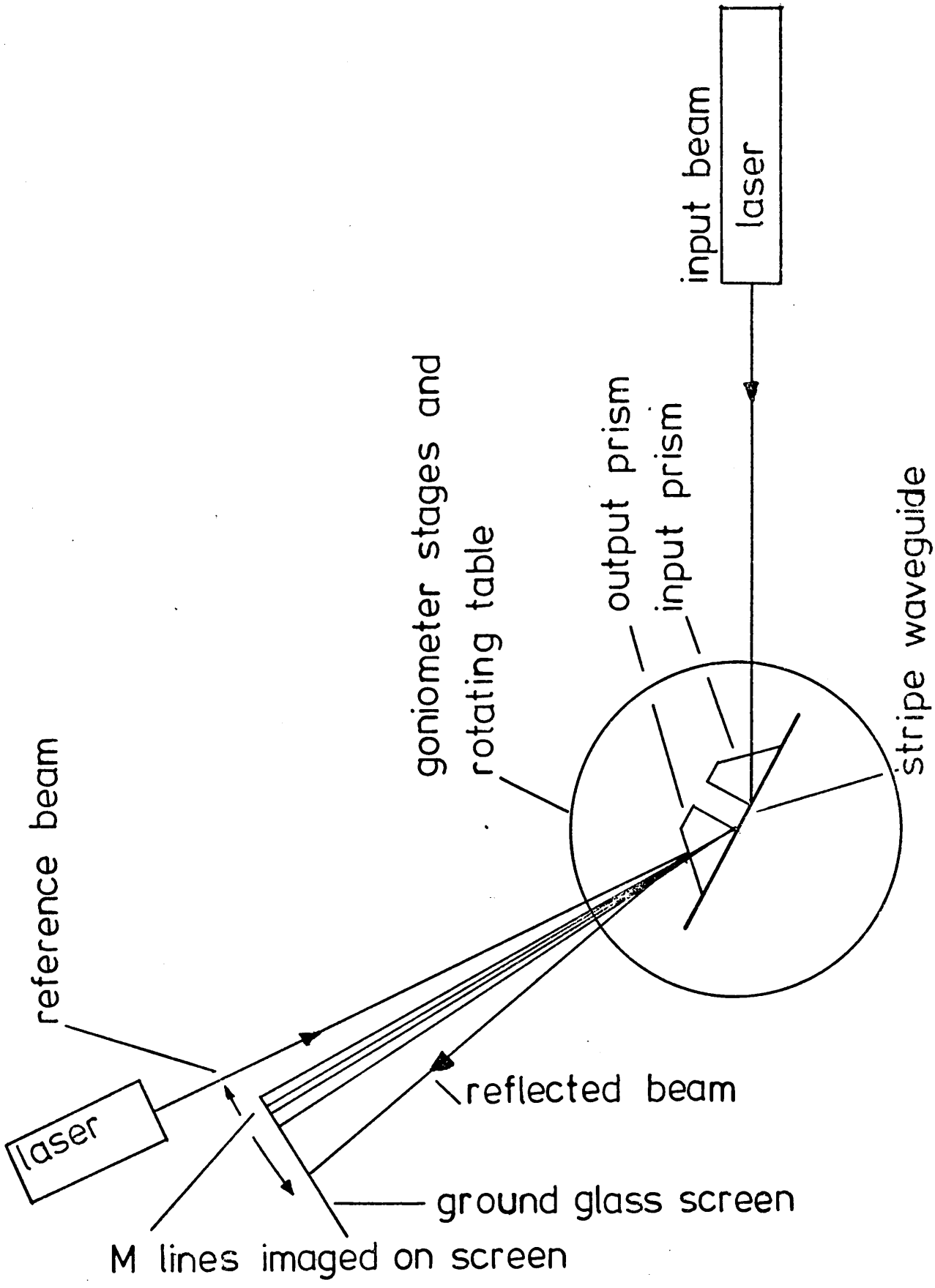

Fig. 4.9 Measurement of normalised modal propagation constants

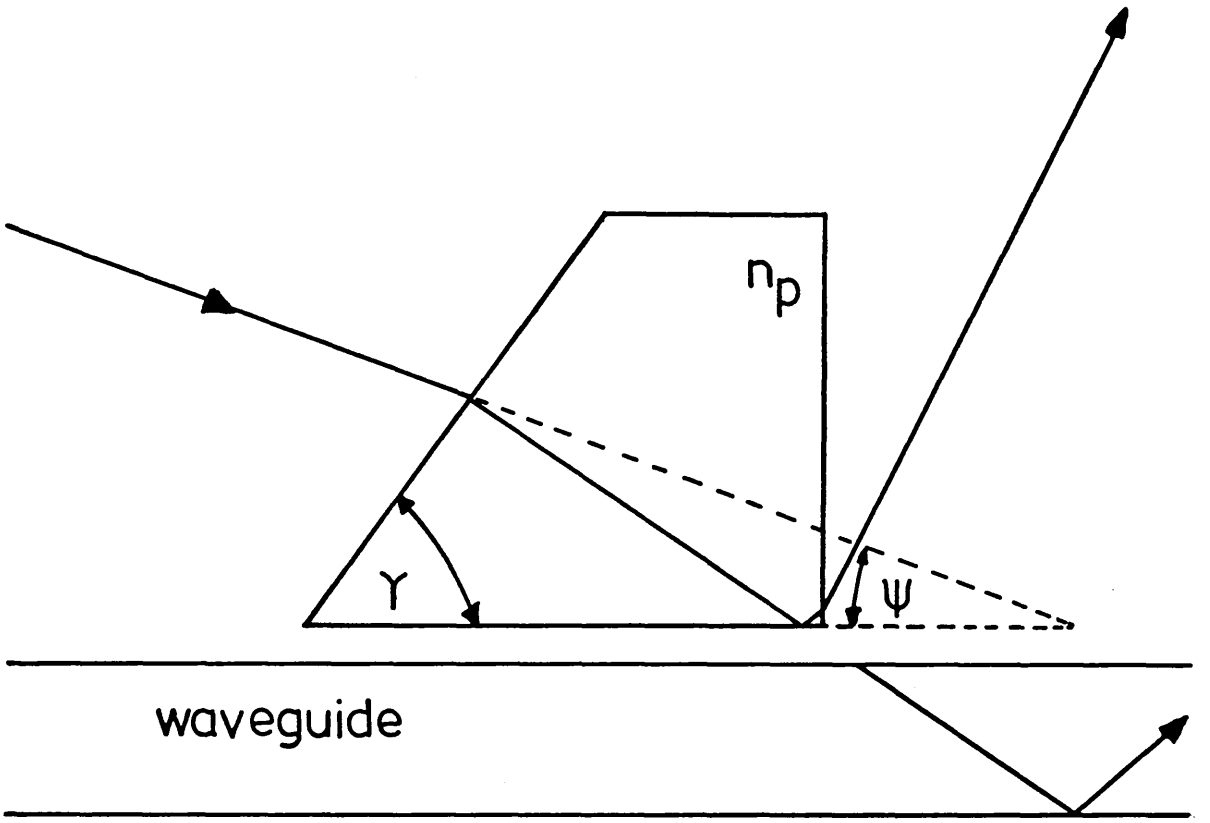

$$\beta/k_0 = n_p \sin\left(\sin^{-1}\left[\frac{1}{n_p}\cos[\gamma+\psi]\right] + \gamma\right)$$

Fig. 4.10 Measurement of waveguide mode propagation constants using a prism–film coupler

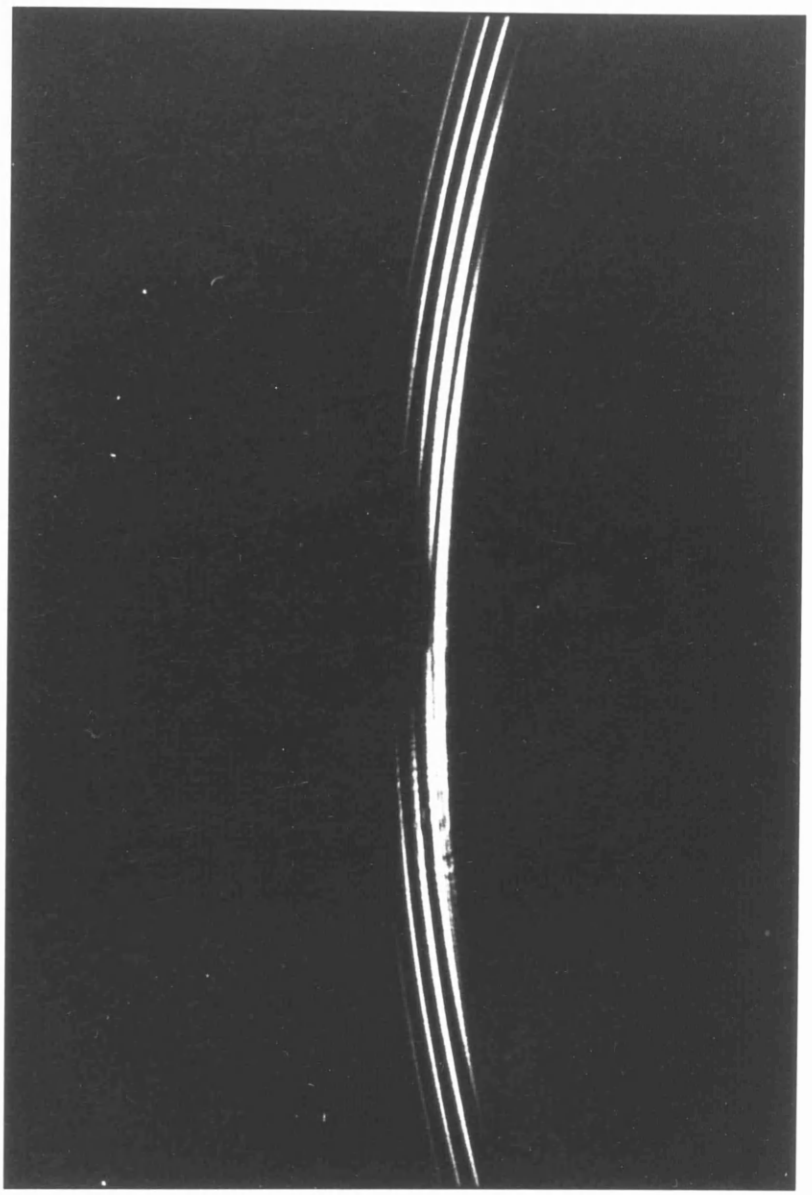

Fig. 4.11 Multi-mode waveguide M-line pattern

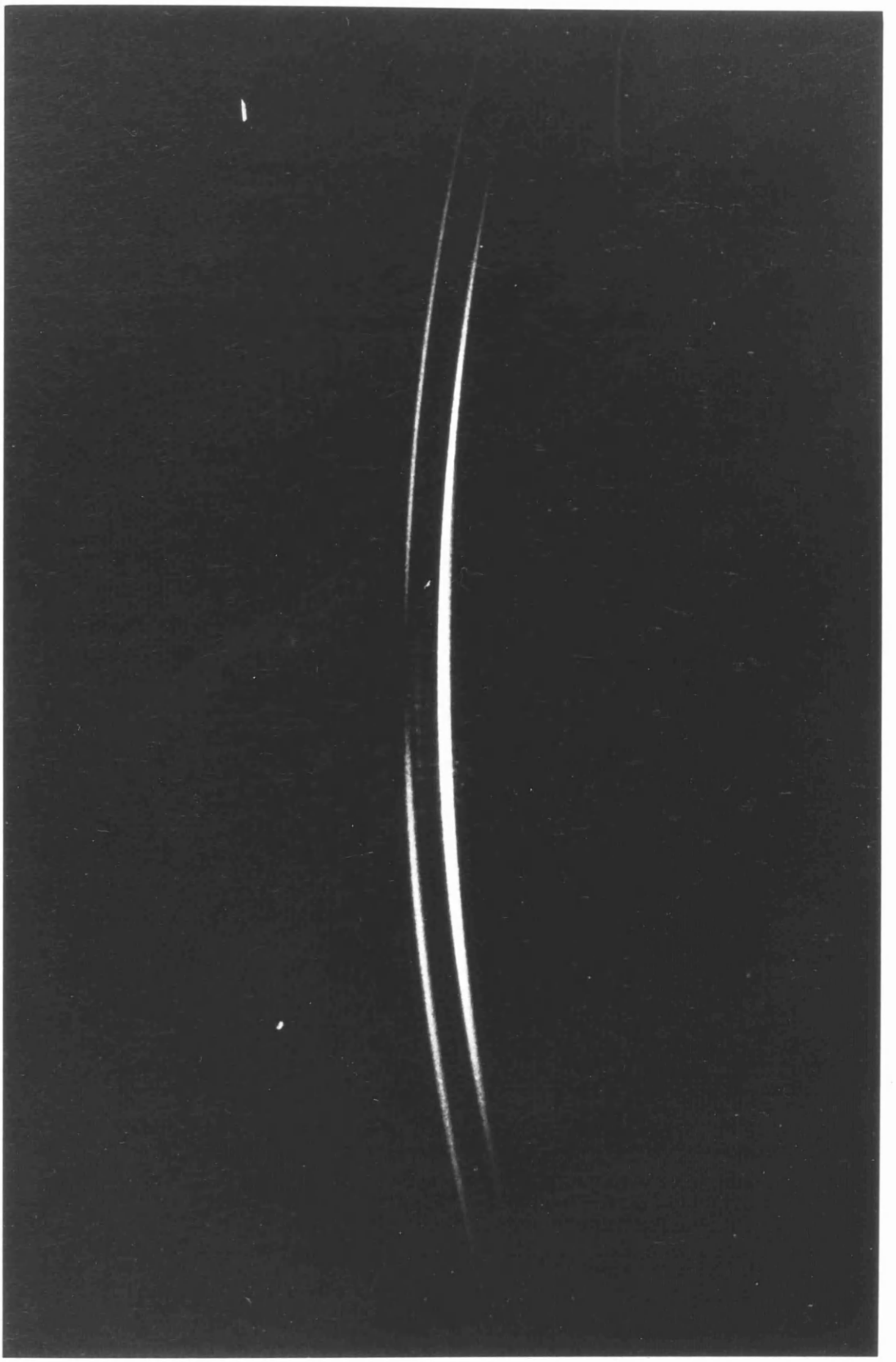

Fig. 4.12 Two transverse mode waveguide M-line pattern

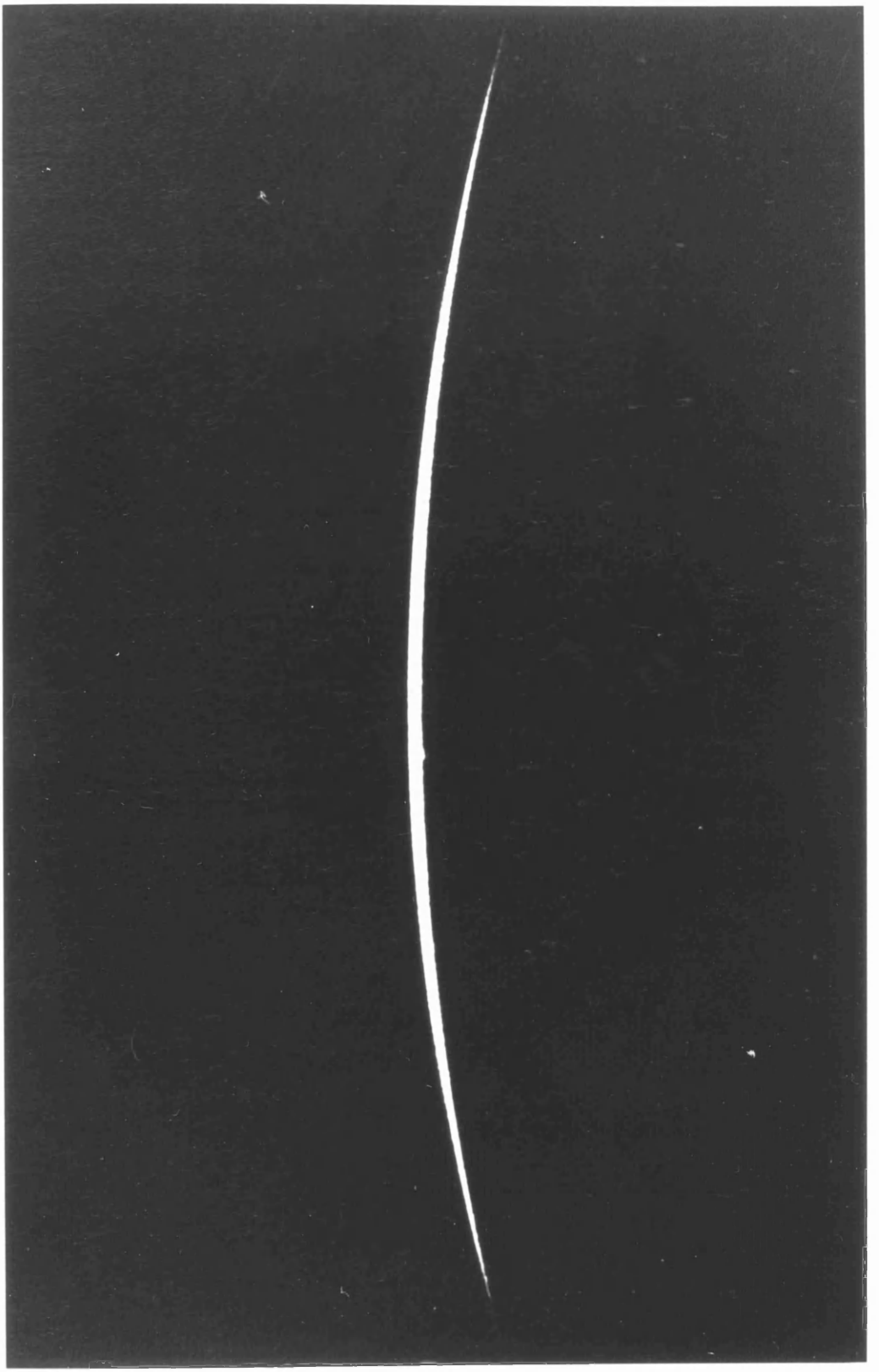

Fig. 4.13 Single mode waveguide M-line pattern

in general corresponding to each depth mode of a planar waveguide a group of transverse (i.e. in the plane of the film) "m-lines". The mode order of a specific transverse "m-line" is readily identified by noting the number of intensity maxima present in the output "m-line" pattern. Using the convention of Marcatili these intensity maxima correspond to the variable p while q specifies the number of intensity maxima in the depth direction.

The angular spacing of the transverse "m-lines" is critically dependent on the waveguide dimensions. Relatively large angular variations may be found in guides varying in width by only a micron or so, thus for repeatable results it is important to have an accurate knowledge of the waveguide dimensions. For this reason it was decided that all measurements of waveguide widths should be carried out using a scanning electron microscope (S.E.M.), utilising the electronically generated "Micron Markers" to measure accurately the waveguide width. The S.E.M. also proved invaluable in determining the base and top widths of the trapezoidal waveguides, and without its use it is doubtful whether any meaningful results could have been obtained. Accurate knowledge of the pre-etch 7059 glass thin film thickness was obtained by the calibration of the R.F. sputtering system, as described in Section 3.2. Accurate knowledge of these parameters is essential to the repeatable fabrication of single mode stripe waveguides.

The next section will present an experimental and theoretical study of 7059 glass stripe waveguides and will discuss the dimensional tolerances necessary to ensure the fabrication of single mode (E^{x}_{11}) waveguides.

4.4.2. Comparison Between Experimental and Theoretically Derived Modal Propagation Coefficients.

Normalised modal propagation coefficients for ion- etched, 7059 glass waveguides of various widths were measured using the procedure outlined in Section 4.4.1 above. The waveguide widths (see Figure 4.6d) were accurately determined to ±0.25 μm using the S.E.M., while the initial film thickness and etch depths were known from accurate calibrations of the sputtering system and ion-etcher respectively, (see Sections 3.2 and 4.2).

Figures 4.14 - 17 show experimental plots of normalised propagation coefficient (β/k_o) for E^x and E^y modes obtained from two experimental waveguides. As the two waveguide samples display similar characteristics, our discussion is limited to Figures (4.16,17). The graphs display waveguide top width/ base width, v.s. normalised propagation coefficient. The intersection of the horizontal and vertical error bars corresponds to the effective width point, as calculated from equation (4.13). The vertical error bars display the maximum uncertainty in the measurement of β/k_o corresponding to ±0.0006, while the theoretical curves are those of Marcatili's (56) eigenvalue mode equations.

By using the effective width theory of Section 4.3, the measured modal propagation coefficients of the trapezoidal ion-etched waveguides may be related to an equivalent rectangular waveguide and analysed using the theory of Marcatili (56). As Figures 4.14-17 show, agreement between theory and experiment is very good with the measured modal propagation coefficients being accurately predicted to within the experimental error. In particular the theory accurately predicts the waveguide

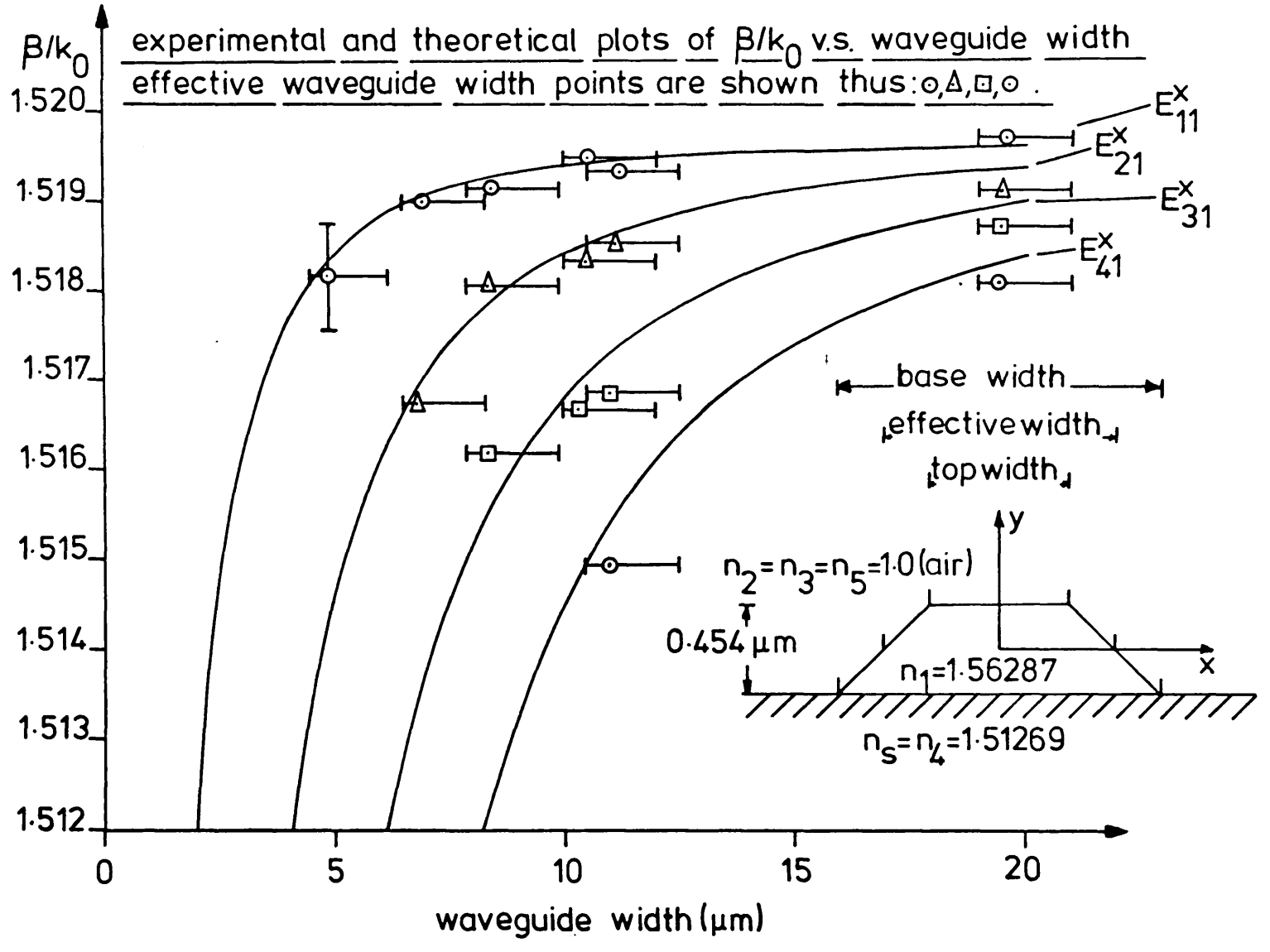
experimental and theoretical plots of β/k0 v.s. waveguide width
effective waveguide width points are shown thus: ⊙,Δ,⊡,⊙ .
β/k0
1·520
1·519
1·518
1·517
1·516
1·515
1·514
1·513
1·512
0
5
10
15
20
waveguide width (μm)
E11x
E21x
E31x
E41x
base width
effective width
top width
y
x
n2=n3=n5=1·0 (air)
0·454 μm
n1=1·56287
ns=n4=1·51269

Fig. 4.14

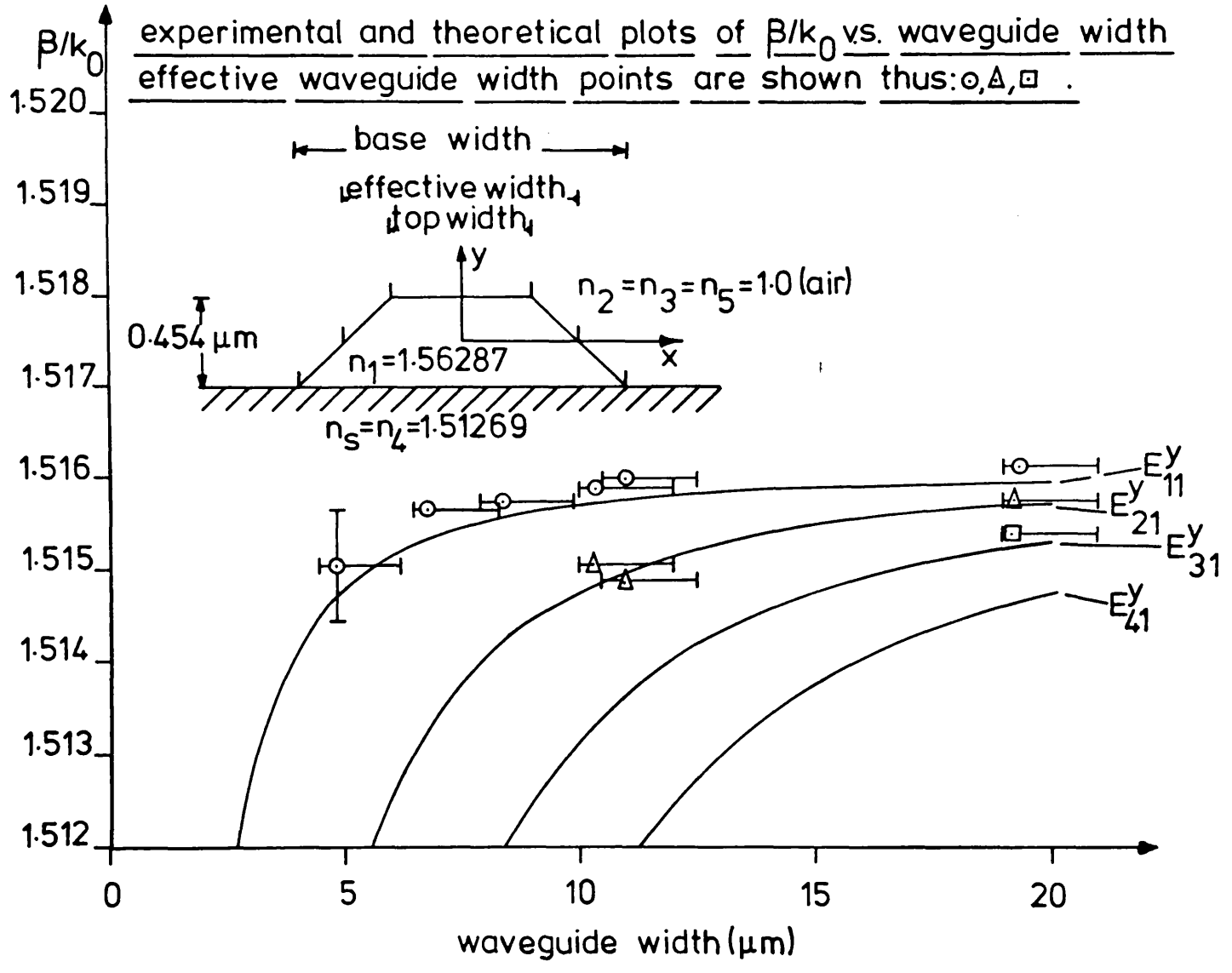
β/k0
experimental and theoretical plots of β/k0 v.s. waveguide width
effective waveguide width points are shown thus: ⊙, △, ⊡ .
1·520
1·519
1·518
1·517
1·516
1·515
1·514
1·513
1·512
base width
effective width
top width
y
x
n2 = n3 = n5 = 1·0 (air)
0·454 μm
n1 = 1·56287
ns = n4 = 1·51269
E11y
E21y
E31y
E41y
0
5
10
15
20
waveguide width (μm)

Fig. 4.15

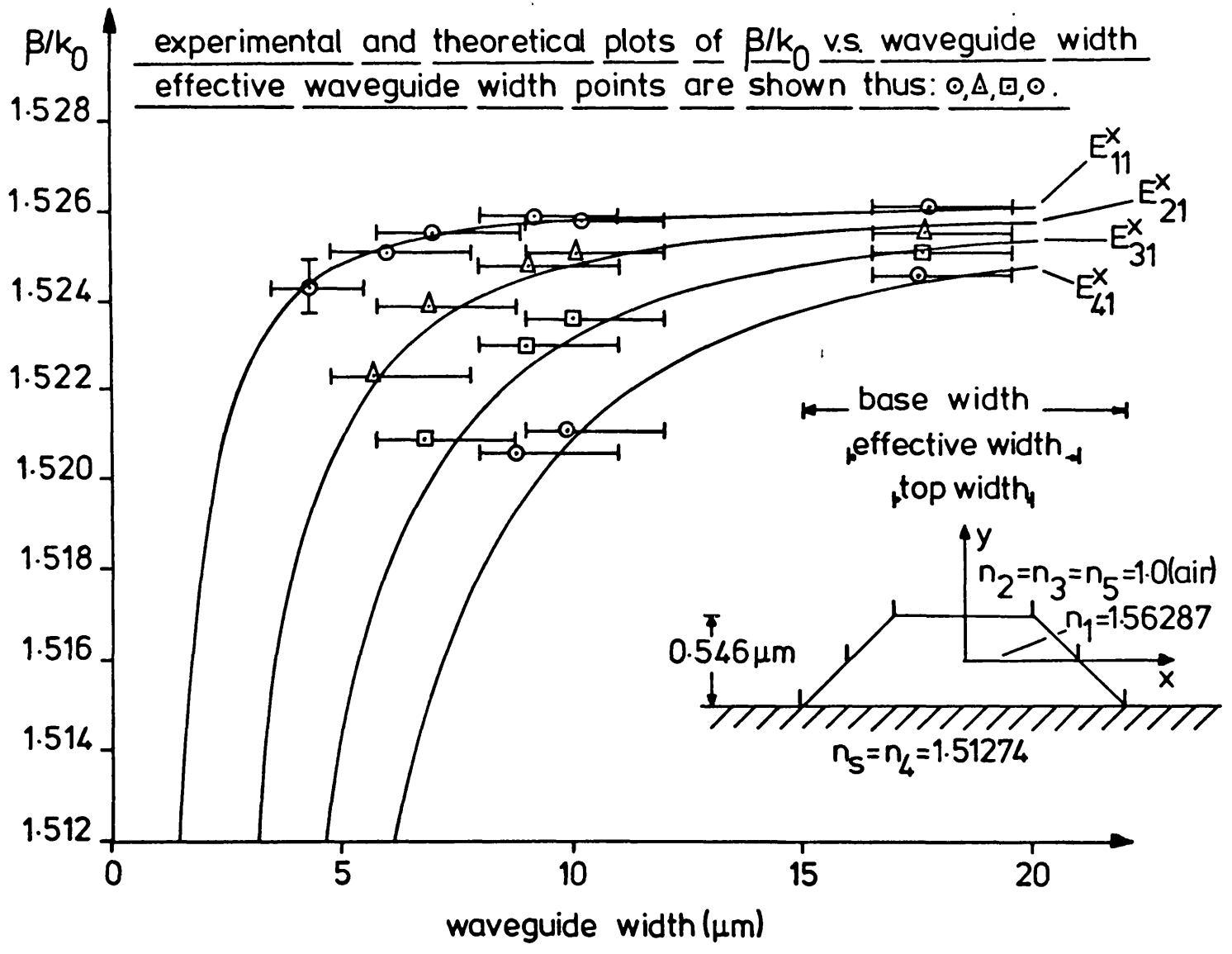
β/k0
experimental and theoretical plots of β/k0 v.s. waveguide width
effective waveguide width points are shown thus: ⊙,△,⊡,⊙.
1·528
1·526
1·524
1·522
1·520
1·518
1·516
1·514
1·512
0
5
10
15
20
waveguide width (μm)
E11x
E21x
E31x
E41x
base width
effective width
top width
y
n2=n3=n5=1·0(air)
n1=1·56287
0·546μm
x
ns=n4=1·51274

Fig. 4.16

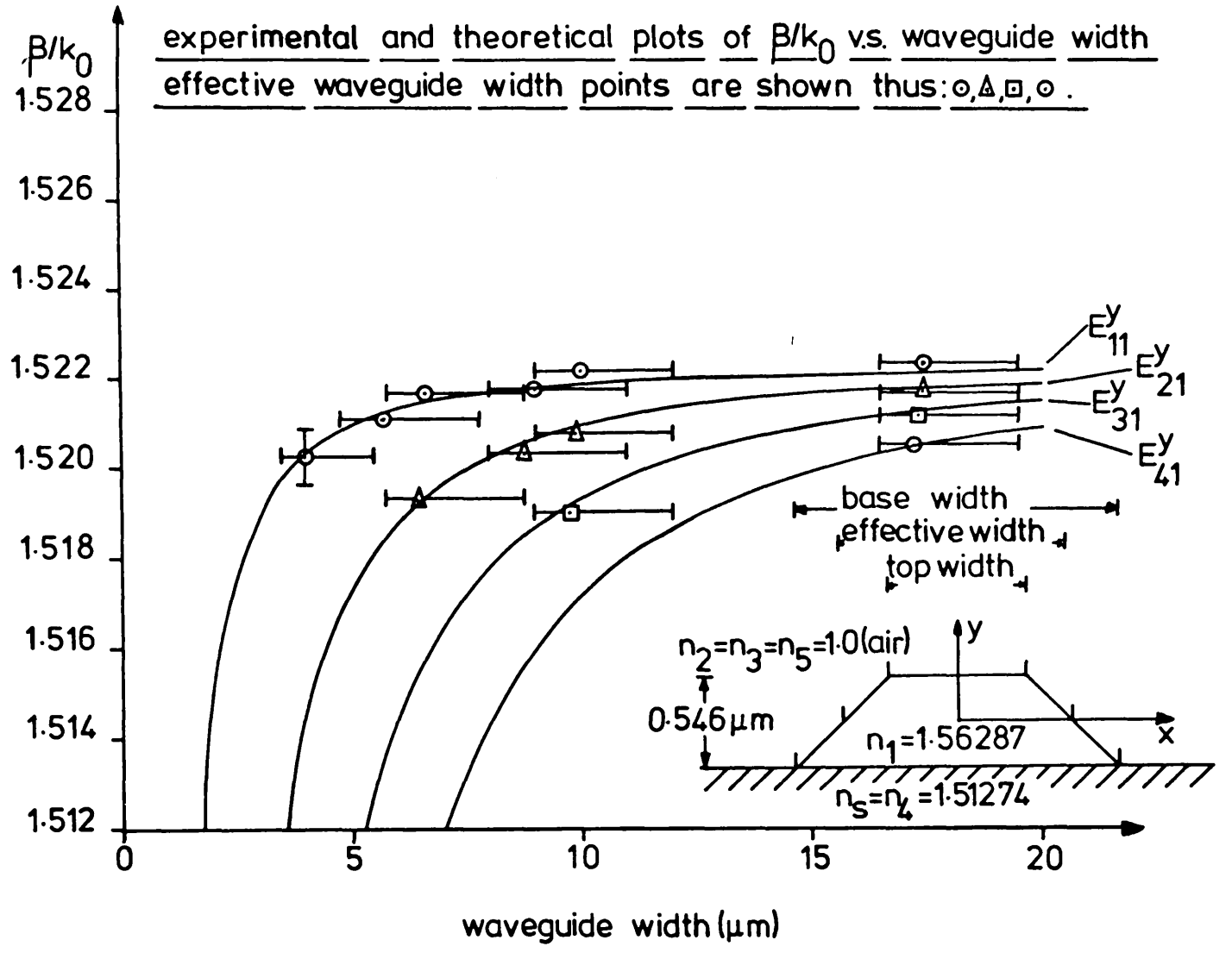
experimental and theoretical plots of β/k0 v.s. waveguide width
effective waveguide width points are shown thus: ⊙,△,⊡,⊙ .
β/k0
1·528
1·526
1·524
1·522
1·520
1·518
1·516
1·514
1·512
0
5
10
15
20
waveguide width (μm)
E11y
E21y
E31y
E41y
base width
effective width
top width
n2=n3=n5=1·0(air)
0·546μm
n1=1·56287
ns=n4=1·51274
y
x

Fig. 4.17

dimensions necessary to ensure single mode operation. This is a result that will prove essential in future chapters, where the design and fabrication of passive single mode stripe waveguide devices is undertaken. As can be seen from Figure 4.16 it is essential to have good control over the waveguide widths when fabricating single mode (E^x_{11}) waveguides. This is especially difficult, as in this case, when fabricating devices whose widths lie close to the limit of the optical lithographic process resolution, ($\simeq$1 μm waveguide width). This width restriction can be relaxed if the waveguide thickness is reduced. However, this imposes greater demands on the accuracy of the 7059 glass thin film thickness. As the film thickness approaches the cut-off limit of the planar waveguide mode, it is possible for minute changes in the film thickness to alter drastically the number of transverse modes that the waveguide can support. From practical experience it was found easier to couple light into a wide waveguide than a narrow one. This is due to the finite spot size of the focused laser beam being larger than the waveguide into which it is being coupled. This results in a considerable quantity of power being wasted and lower power levels in the narrower waveguides. However, relatively wide single mode waveguides place large demands on the film thickness tolerances required. Eventually a compromise waveguide width, in the range 3 - 6 μm, (depending on the device) was decided on, with the film thickness adjusted accordingly to ensure single mode (E^x_{11}) propagation.

Figure 4.18 shows a graph of rate of change of β/k_o with waveguide width using Marcatili's waveguide solutions (56). As can be seen there is a rapid change in the function value around the 3 - 5 μm region, thus making accurate control of the

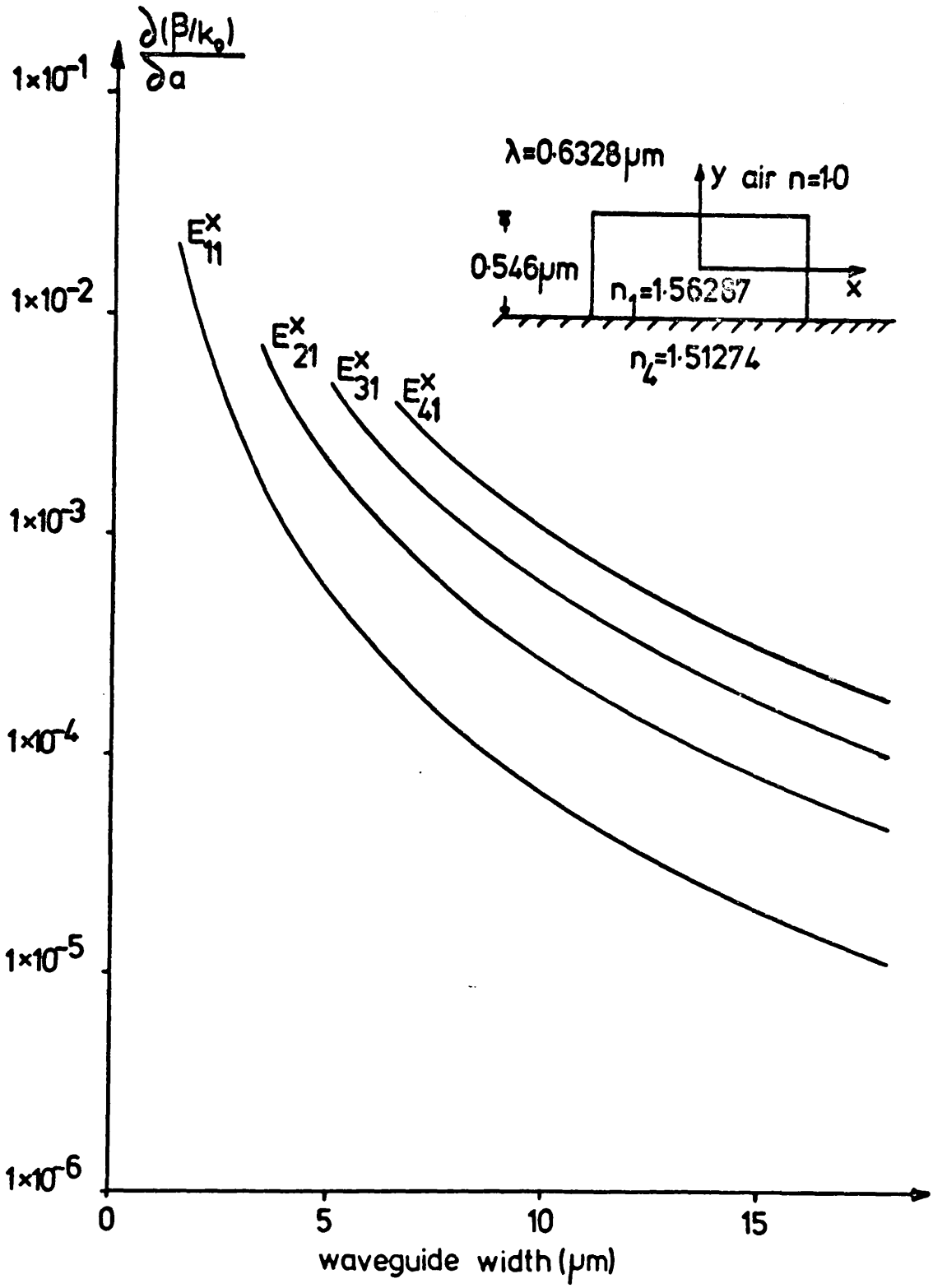

Fig. 4.18 Rate of change of normalised propagation constant with waveguide width

waveguide width essential. By reducing the waveguide widths by over-exposure and development of the photoresist, (see Section 4.2), it is possible to fabricate single mode waveguides with widths slightly narrower than those of the initial mask. This technique proved invaluable in the fabrication of single mode waveguide devices with widths of up to 7 μm. Another method of reducing the waveguide width to ensure single mode operation is to manufacture "over etched" stripe waveguides. Basically this involves ion-etching the waveguide well into the substrate leaving the stripe 7059 glass waveguide standing proud on a small unetched section of the substrate. As the etching process results in the formation of trapezoidal waveguides whose width at the top becomes narrower with increasing etch depth, it is possible to fabricate stripe waveguides whose widths are very much less than those of the initial baked photoresist mask. This reduction in waveguide width makes the fabrication of single mode waveguides relatively straightforward, even when starting from a large initial waveguide width of ≃8 μm. This method of fabrication, however, does have the drawback that it induces very large scattering losses (attributable to the etching process), into the waveguide, which limits its practical value.

Figures 4.19, 20 show theoretical and experimental plots of β/k_o v.s. effective waveguide width for an over-etched stripe waveguide; the corresponding waveguide dimensions are given in Figure 4.21. These over-etched stripe waveguides were fabricated in the same manner as normal ion etched waveguides (see Section 4.2), but with the ion-etching time extended so as to give etching well into the substrate. This ensured that the resulting waveguides had a very much smaller effective

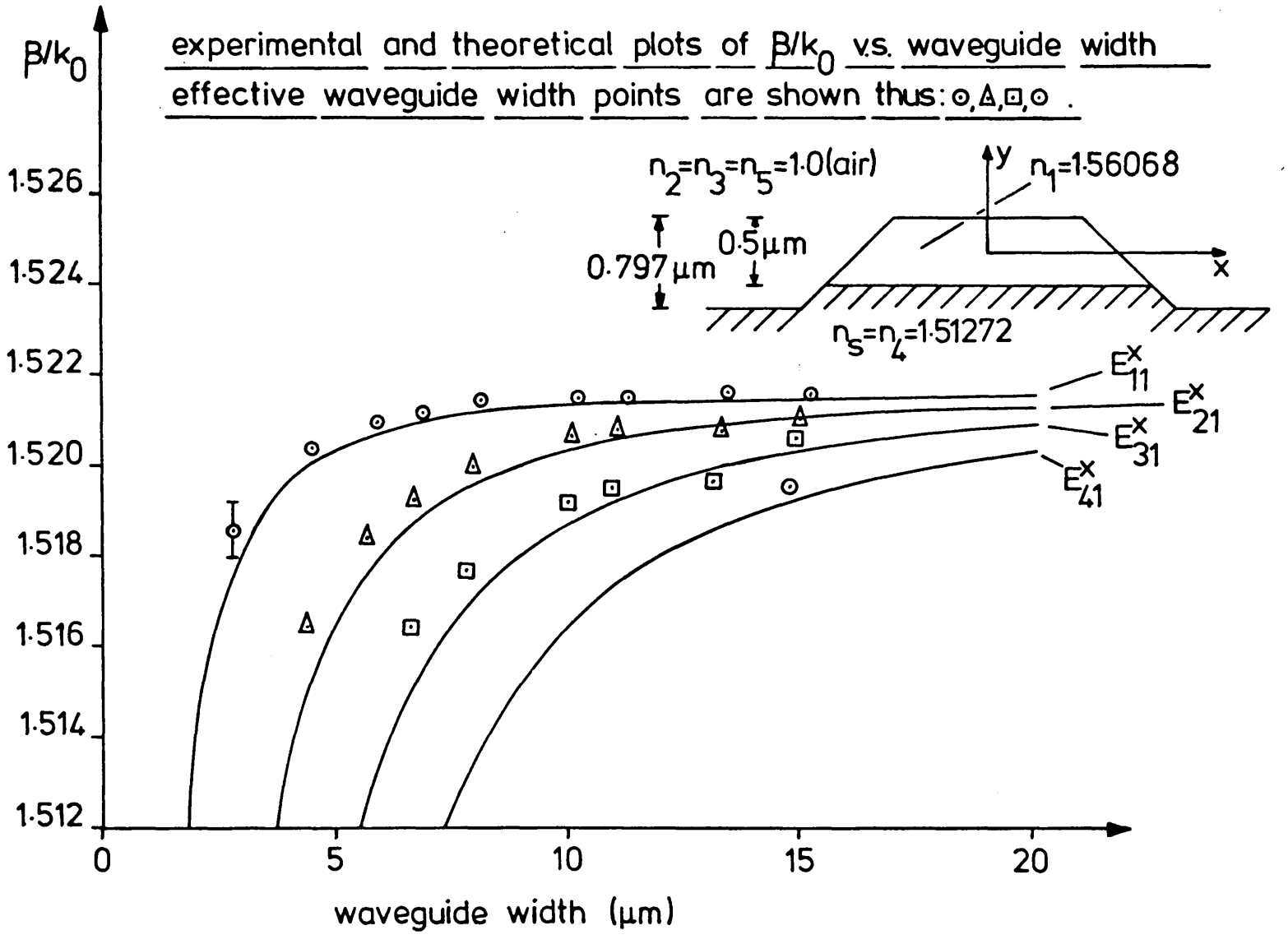
β/k0
experimental and theoretical plots of β/k0 v.s. waveguide width
effective waveguide width points are shown thus: ⊙,△,⊡,⊙ .
n2=n3=n5=1·0(air)
y
n1=1·56068
0·797 μm
0·5μm
x
n5=n4=1·51272
E11x
E21x
E31x
E41x
1·526
1·524
1·522
1·520
1·518
1·516
1·514
1·512
0
5
10
15
20
waveguide width (μm)

Fig. 4.19

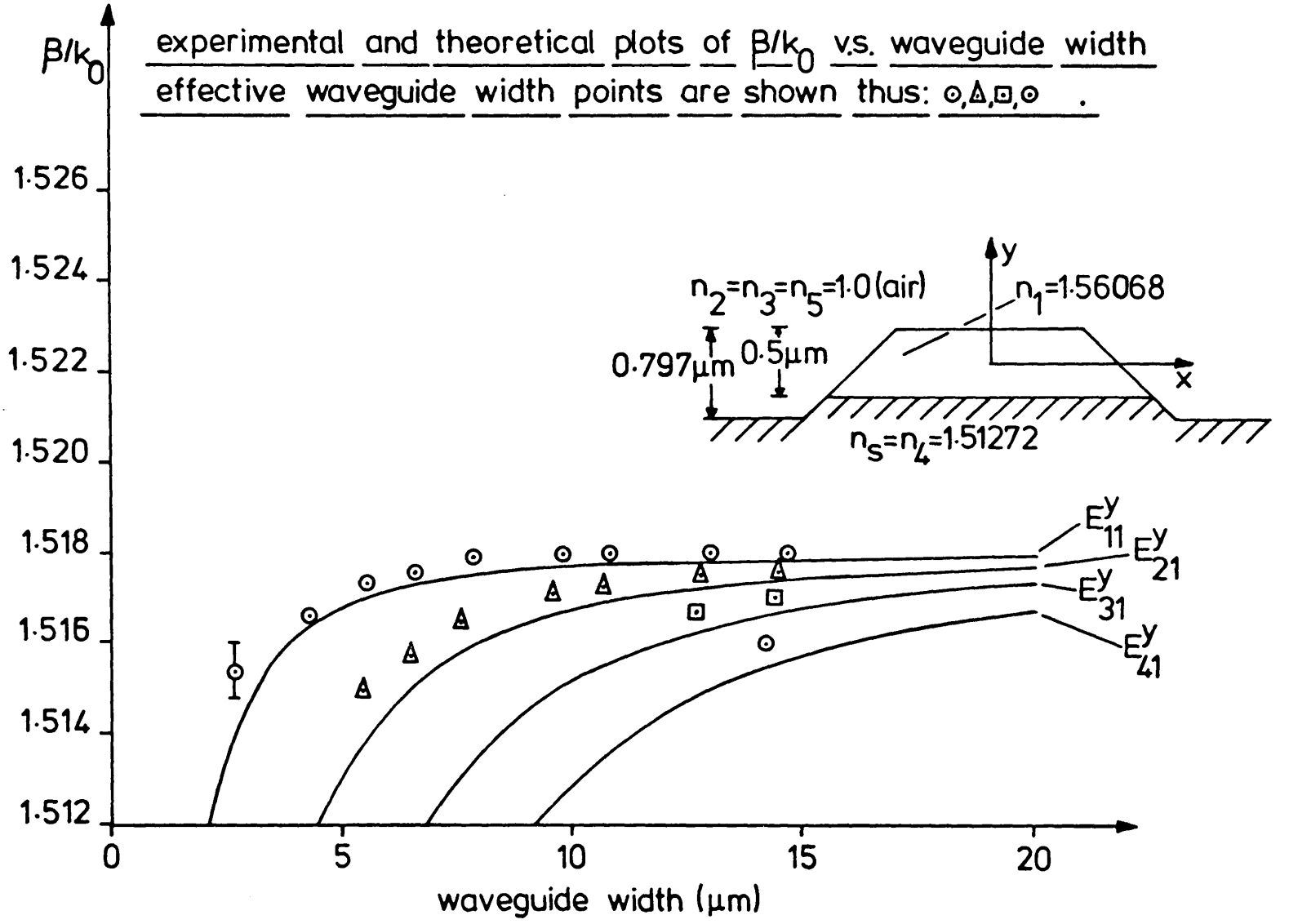
β/k0
experimental and theoretical plots of β/k0 v.s. waveguide width
effective waveguide width points are shown thus: ⊙,△,⊡,⊙ .
1·526
1·524
1·522
1·520
1·518
1·516
1·514
1·512
0
5
10
15
20
waveguide width (μm)
y
x
n2=n3=n5=1·0(air)
n1=1·56068
0·797μm
0·5μm
ns=n4=1·51272
E11y
E21y
E31y
E41y

Fig. 4.20

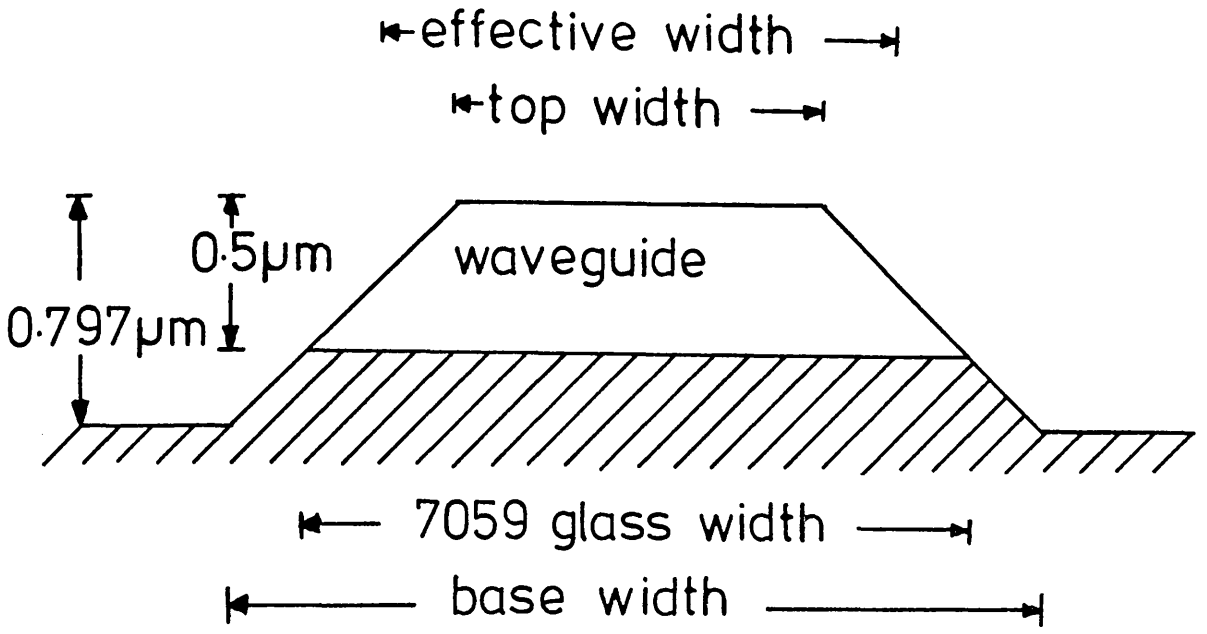

all dimensions in microns

BASE WIDTH (MEASURED)	TOP WIDTH (MEASURED)	7059 GLASS WIDTH (CALCULATED)	EFFECTIVE WAVEGUIDE WIDTH FOR THE E^x_{11} MODE (CALCULATED)
5.0	2.5	4.068	2.849
7.0	4.0	5.882	4.499
10.0	5.0	8.137	5.909
11.0	6.0	9.137	6.930
13.0	7.0	10.764	8.146
15.0	9.0	12.764	10.173
16.0	10.0	13.764	11.183
19.0	12.0	16.391	13.404
21.5	13.5	18.519	15.121

NOTE: IN THE INTERESTS OF CLARITY ONLY THE E^x_{11} MODE EFFECTIVE WAVEGUIDE WIDTHS ARE PRESENTED HERE.

Figure 4.21. Dimensions of Trapezoidal Waveguides Presented in Figures 4.19 and 4.20.

width than the initial baked photoresist waveguide mask patterns. The waveguide etch depths were known from calibrations of the ion-etcher and were checked using a G.V. Planar "sliding stylus", type surfometer (92). As can be seen from Figures 4.19,20 there is again good agreement between the over-etched trapezoidal waveguides and the effective width theory which uses Marcatili's (56) transcendental mode equations. The effective width points were calculated from S.E.M. measurements of "top width" and "base width" of the complete etched trapezoid (i.e. of the total trapezoidal height of the etched 7059 glass and substrate), and from a knowledge of the 7059 glass thin film thickness. These calculated effective width points relied on the fact (as in the normally etched waveguides), that the trapezoidal waveguides were perfectly symmetrical and had triangular waveguide walls; a fact justified from the photograph of Figure 4.6d. The estimated error in the measurement of β/k_o remains the same as before at ±0.0006.

We may conclude from the above results that over-etched stripe waveguides are a convenient means of producing single mode (E^x_{11}) waveguides, but will find little practical value due to the large waveguide losses induced by the fabrication procedure. Although it is slightly more difficult to fabricate conventional stripe waveguides (i.e. etched only to the top of the substrate), the reduced waveguide losses make them a much more attractive proposition for the fabrication of single mode stripe waveguide devices. Further details of stripe waveguide losses are found in Section 4.4.3 and a fuller and more detailed discussion of the above results will be found in Section 4.5.

4.4.2.1. Comparison of Experimental Theoretical and Numerical Computer Solutions.

Facilities exist in the department to check the above theories and experimental results using an independent numerical computer solution. This solution was primarily intended for the characterisation of two dimensional (stripe) silver ion exchange waveguides, as such it was extensively modified to enable the above stripe 7059 glass waveguides to be analysed.

Plots of theoretical (effective width), experimental and numerical (computer solution) points are shown in Figure 4.22. For the fundamental E^{x}_{11} mode both Marcatili and the computer solution give values well within the experimental error, while agreement for the other modes is good. A numerical study of an over-etched waveguide sample was also undertaken (see Figure 4.23). As can be seen the theoretical numerical and measured values are all in excellent agreement with each other, with little difference between measured and numerical solutions.

Due to the etch depth limitations of the baked photoresist waveguide masks, no stripe waveguides could be fabricated with a second thickness mode (i.e. q = 2). Thus it was impossible to test whether the effective width theory of Section 4.3 was valid for waveguides supporting more than one depth mode. However, good agreement between theoretical and numerical solutions was obtained for a hypothetical stripe waveguide of quasi-rectangular cross-section supporting two depth modes. Details of this waveguide and a comparison of results is given in Figure 4.24. Due to the length of computational time required to calculate each waveguide structure (up to 2 hours!), only a single representative hypothetical trapezoidal waveguide was considered. However, the results of this single calculation indicate

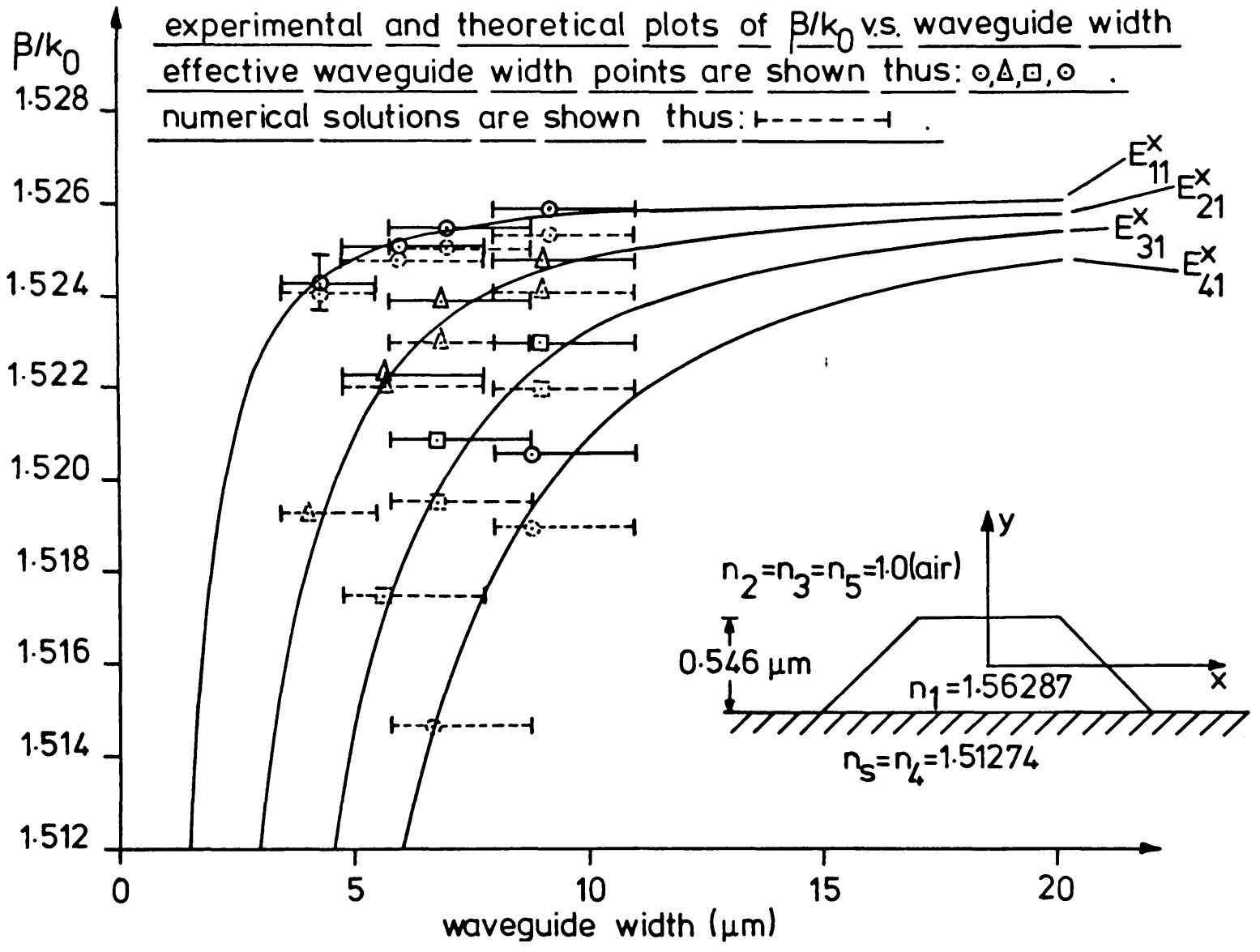
experimental and theoretical plots of β/k0 v.s. waveguide width
effective waveguide width points are shown thus: ⊙,Δ,⊡,⊙ .
numerical solutions are shown thus: ⊢------⊣ .
β/k0
1·528
1·526
1·524
1·522
1·520
1·518
1·516
1·514
1·512
0
5
10
15
20
waveguide width (μm)
E11x
E21x
E31x
E41x
n2=n3=n5=1·0(air)
0·546 μm
n1=1·56287
ns=n4=1·51274
y
x

Fig. 4.22

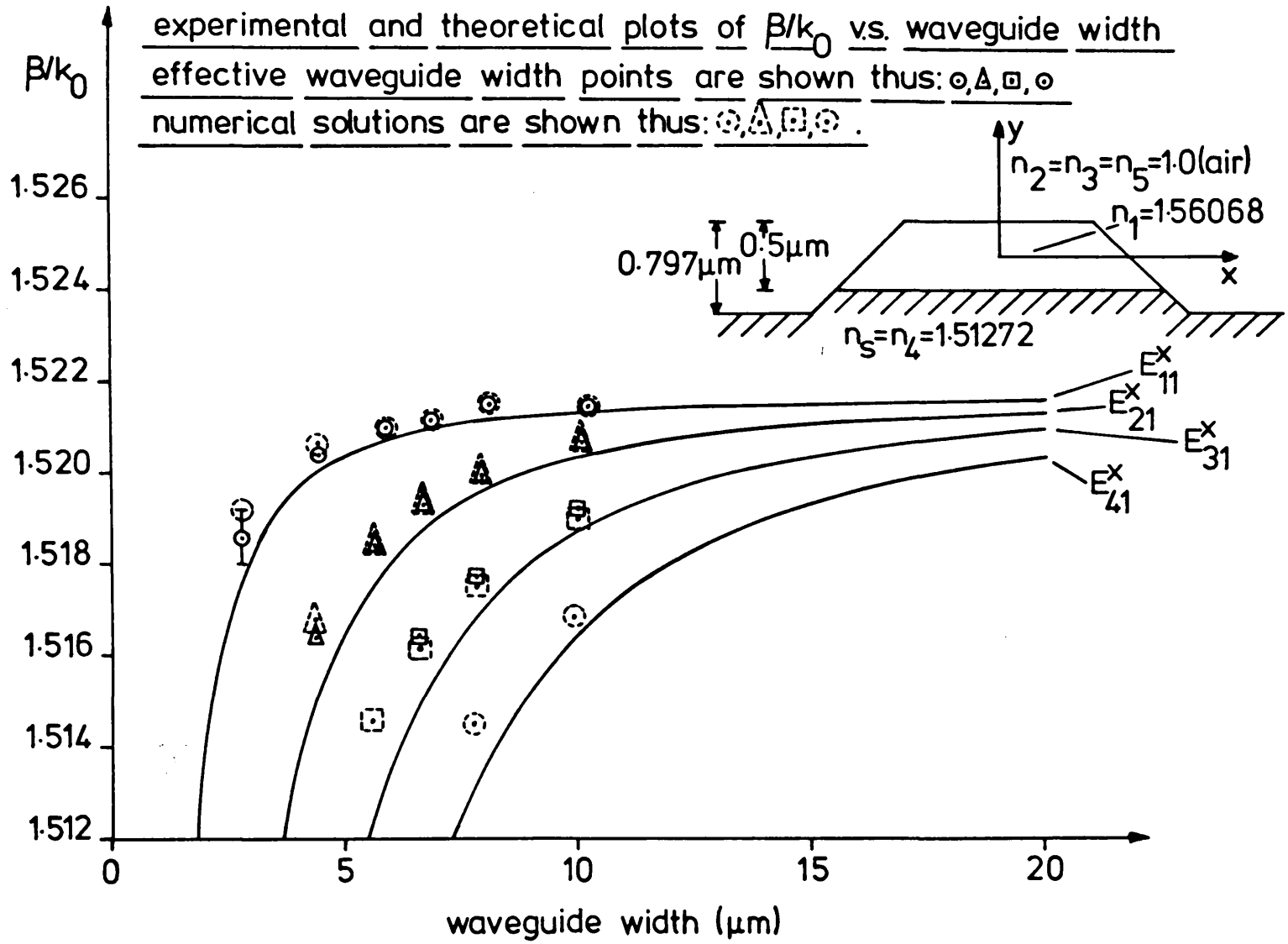
experimental and theoretical plots of β/k0 v.s. waveguide width
effective waveguide width points are shown thus: ⊙,△,⊡,⊙
numerical solutions are shown thus: ⊙,△,⊡,⊙ .
β/k0
1·526
1·524
1·522
1·520
1·518
1·516
1·514
1·512
0
5
10
15
20
waveguide width (μm)
y
x
n2=n3=n5=1·0(air)
n1=1·56068
0·797μm
0·5μm
ns=n4=1·51272
E11x
E21x
E31x
E41x

Fig. 4.23

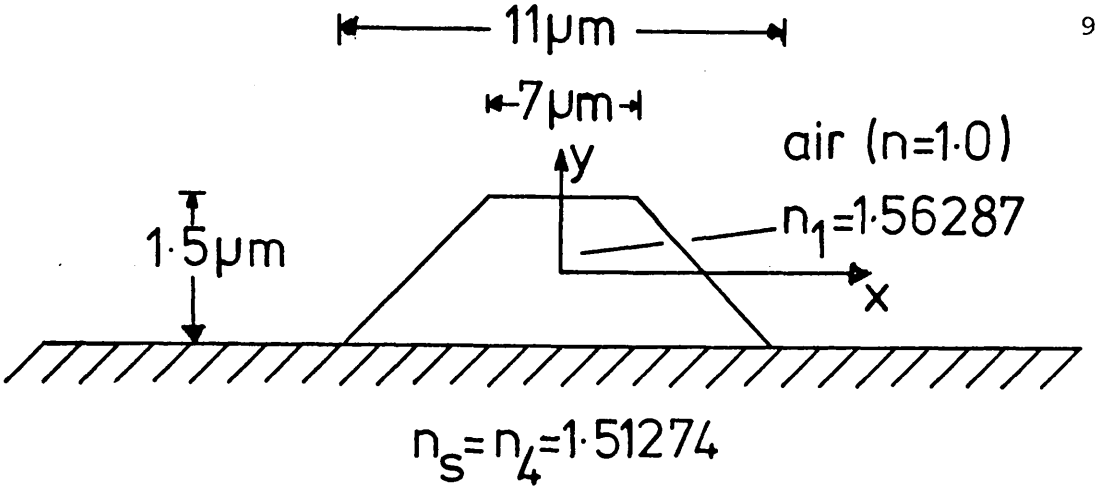

MODE TYPE	EFFECTIVE WAVEGUIDE WIDTH THEORY β/k_o	NUMERICAL COMPUTATION β/k_o	DIFFERENCE IN β/k_o VALUE
E^x_{11}	1.553168	1.552899	0.000269
E^x_{21}	1.552218	1.551558	0.000660
E^x_{31}	1.550600	1.549260	0.001340
E^x_{41}	1.548276	1.546245	0.002031
E^x_{51}	1.545187	1.542050	0.003137
E^x_{61}	1.541250	1.537587	0.003663
E^x_{12}	1.526150	1.525663	0.000487
E^x_{22}	1.524572	1.524476	0.000096
E^x_{32}	1.521836	1.521316	0.000520
E^x_{42}	1.517801	1.517292	0.000509
E^x_{52}	CUT-OFF	CUT-OFF	-
E^x_{62}	CUT-OFF	CUT-OFF	-

Figure 4.24. Comparison of Effective Waveguide Width Theory and Numerical Computer Solutions for a Trapezoidal Waveguide Supporting Two Depth Modes.

that the effective width theory should be applicable to quasi-rectangular stripe waveguides that support more than one depth mode. A fuller discussion of these results is given in Section 4.5.

We may conclude from the above results that the theory of Marcatili in conjunction with the effective width theory (see Section 4.3), accurately predicts the propagation coefficients of stripe 7059 glass waveguides. As such it proves a useful tool in the design of passive waveguide devices, being much easier to implement than an extensive numerical computation. Details of the numerical computer analysis are given in Appendix C.

4.4.3. Measurement of Stripe 7059 Glass Waveguide Losses.

One of the major problems of ion-etched stripe waveguides is that of waveguide attenuation, mainly attributable to the roughness induced in the waveguide walls during the fabrication stage (see Section 4.2).

Waveguide losses were measured using a thin film prism coupler (4) in a manner similar to that of Tien et al (13), and in an identical manner to the measurement of waveguide losses, as discussed in Chapter 3. The output prism "m-lines" from the stripe waveguide were focused down onto the detector head of the United Detector Technology (50) laser power meter using a large convex lens. The use of a narrow slit on the condensing lens removed unwanted scattered radiation whilst still allowing the "m-lines" to be detected. To avoid modifying subsequent measurements by damage to the waveguides, initial power readings were carried out as far from the input prism as possible. Power readings were then taken at points closer to the input

prism, with the inter-prism distance being measured with a micrometer. Since scattering losses and waveguide damage arise from clamping the prism-coupler onto the waveguide each measurement had to be made at the first attempt. Figure 4.25 shows light guiding in a stripe 7059 glass waveguide of approximately 6 μm width. It is only due to the large waveguide scattering loss that the waveguide may be clearly seen from the radiated light.

Using the above method losses were measured on a series of stripe 7059 glass waveguides. Most of the experimentally determined values of loss fell in the region of 4 - 20 dB/cm, and were dependent on the waveguide dimensions. These values are very much higher than those measured on planar waveguides of the same film thickness which exhibit losses of approximately 0.5 dB/cm. The higher loss is attributable to scattering from the waveguide walls due to the lateral confinement of the light, and is caused by roughness due to the fabrication method (see Section 4.2). A graph of waveguide loss in dB/cm v.s. reciprocal waveguide width (see Figure 4.26) is linear when drawn through the effective width points. This indicates that scattering loss varies directly with inverse waveguide width. This is to be expected as for constant amplitude of waveguide wall, constant scattering loss relates to a transmitted power proportional to the waveguide width; narrower waveguides, therefore, have a larger scattering loss due to the tighter field confinement of the guided mode(s). Marcuse (68) has presented a detailed theoretical discussion of radiation loss in planar dielectric waveguides due to periodic and random pertubations occurring in the waveguide walls. It was felt,

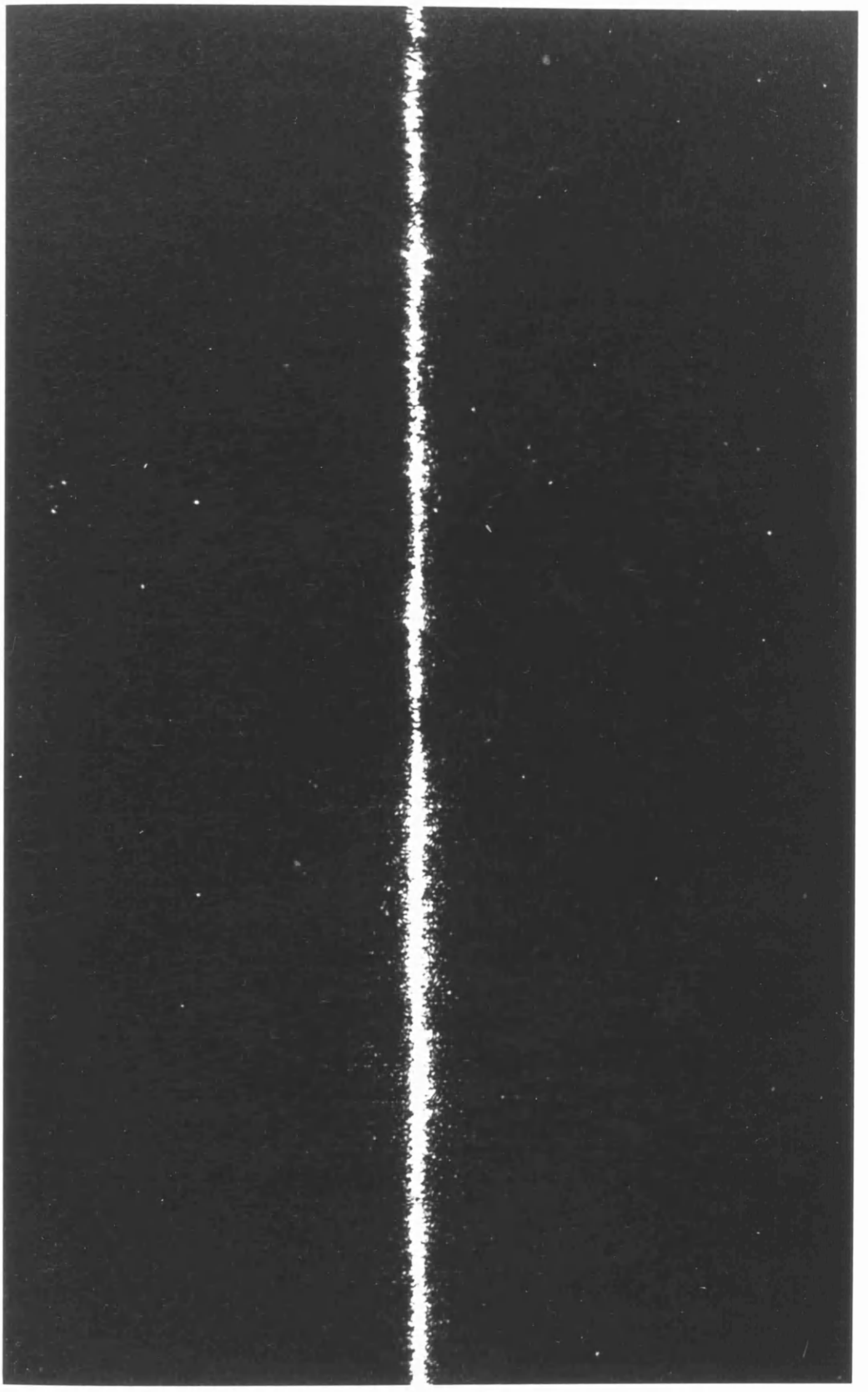

Fig. 4.25 He–Ne Laser light guiding in a stripe 7059 glass waveguide

Fig. 4.26

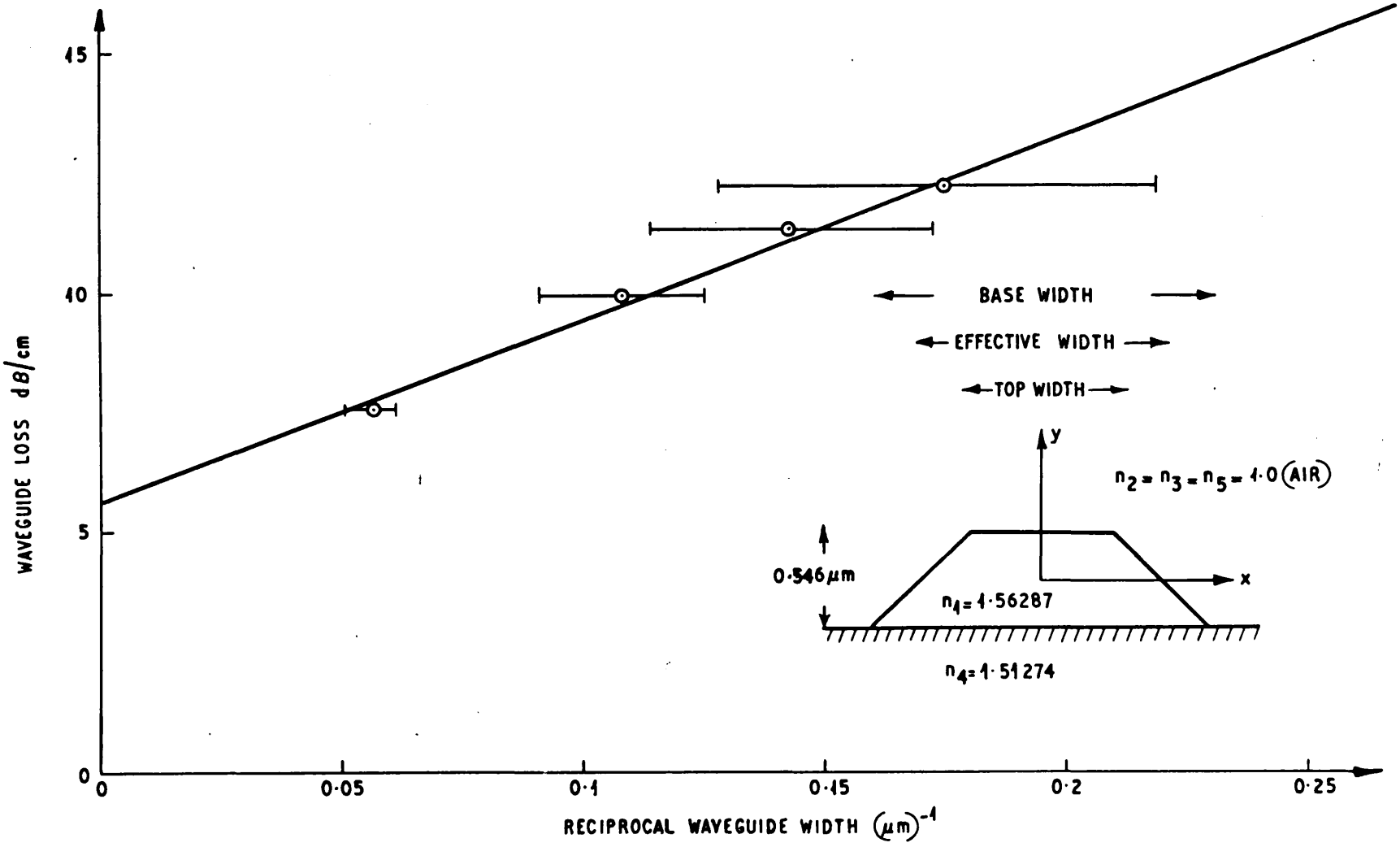

PLOT OF WAVEGUIDE LOSS V.S. RECIPROCAL WAVEGUIDE WIDTH
ERROR BARS SIGNIFY MAXIMUM AND MINIMUM WIDTH
EFFECTIVE WIDTH POINTS ARE SHOWN THUS: ⊙

however, that a detailed study of radiation loss was not within the scope of this project and more detailed investigations into radiation loss were not followed up.

Latterly acceptable low-loss (6 dB/cm) single mode waveguides were being fabricated, and it was decided to concentrate all efforts on the design of passive single mode (E_{11}^{x}) waveguide devices.

4.5. Discussion of Results.

Measurements carried out on trapezoidal stripe 7059 glass waveguides have been successfully related to the rectangular dielectric waveguide analysis of Marcatili (56), with an effective waveguide width substituted into the analysis to account for the trapezoidal shape of the waveguide cross-sectional geometry. A numerical computer solution allowing an independent analysis of propagation in the above waveguides was carried out. A comparison between experimental, theoretical and numerical solutions showed that agreement between the two methods of calculation was excellent for the fundamental mode and good for higher order modes. It was concluded that the relatively simple modification for effective width coupled with Marcatili's (56) transcendental mode equations could accurately predict the propagation coefficients of ion-etched 7059-glass stripe waveguides of trapezoidal cross-section, thus enabling the design of single mode stripe waveguide devices to be undertaken. Over-etched stripe waveguide modal propagation constants were also found to be accurately predicted using the effective width theory. Experiments revealed that it was easier to fabricate single mode waveguides, even when starting

from relatively large waveguide mask dimensions. The practical value of these waveguides is, however, limited due to the very large waveguide losses induced by the fabrication process.

The introduction of high definition waveguide masks resulted in the fabrication of single mode stripe waveguides with relatively low losses of 6 dB/cm, making feasible the design and fabrication of single mode waveguide devices. We may conclude from the results presented in this chapter that the effective width theory coupled with Marcatili's transcendental mode equations allows trapezoidal stripe waveguides with known modal propagation characteristics to be manufactured.

The above results should also be equally applicable to other forms of homogeneous, isotropic stripe waveguides, but care should be exercised if the difference between the waveguide and surrounding refractive indices is small. This could lead to more power being propagated in the ignored corner regions of the waveguide (see Marcatili, 56), thus making the predicted values inaccurate. This problem does not arise with 7059 glass waveguides where there is a relatively large refractive index difference between the waveguide and the surrounding media.

This concludes the discussion on trapezoidal stripe waveguides, the remaining chapters in this thesis consider the design of single mode passive waveguide devices using the above results as a design reference.

4.6. Conclusions.

Experimental stripe trapezoidal 7059 glass waveguides have been analysed using an effective waveguide width theory which uses Marcatili's transcendental mode equations. Agreement between theory and experiment is good with the modal propagation coefficients being accurately predicted. This result forms the basis of a design criterion for the fabrication of stripe waveguide passive devices, considered in following chapters.

CHAPTER 5.

CHAPTER 5. DESIGN, FABRICATION AND EVALUATION OF STRIPE SINGLE MODE 7059 GLASS WAVEGUIDE TILTS.

Single mode waveguide tilts (i.e. abrupt bends, see Figure 5.1) could form important elements in future integrated optical communications systems where dielectric waveguide are required to make small changes in direction. These tilts offer a good practical alternative to waveguide bends, are much easier to fabricate by photolithography for which straight lines are much easier to draw than curves and, if the angles of the tilt are kept small enough, transmission losses of only a few percent may be achieved. Waveguide tilts have already been incorporated into a practical device; Sasaki (6) has used them in the fabrication of an electro-optic, Mach-Zender (93) type modulator in titanium diffused lithium niobate for which the tilts are used to make parallel the output waveguides from the branching arms of a Y-junction.

Taylor (69) has carried out a theoretical analysis of tilts, but as far as is known this has not been verified experimentally. However, Taylor's analysis is primarily concerned with multimode waveguides and mode conversion, whereas the problem considered here deals with the transmission performance of single mode waveguide tilts. Taylor's analysis is, therefore, unsuited for the characterisation of single mode waveguide tilts. Clearly, if such devices are to be designed, the transmission performance must be related to the waveguide dimensions, refractive index and tilt angle. Accordingly, a single mode waveguide tilt analysis is derived.

This chapter presents an analytical solution for planar waveguide tilts (see Figure 5.1). The planar waveguide analysis

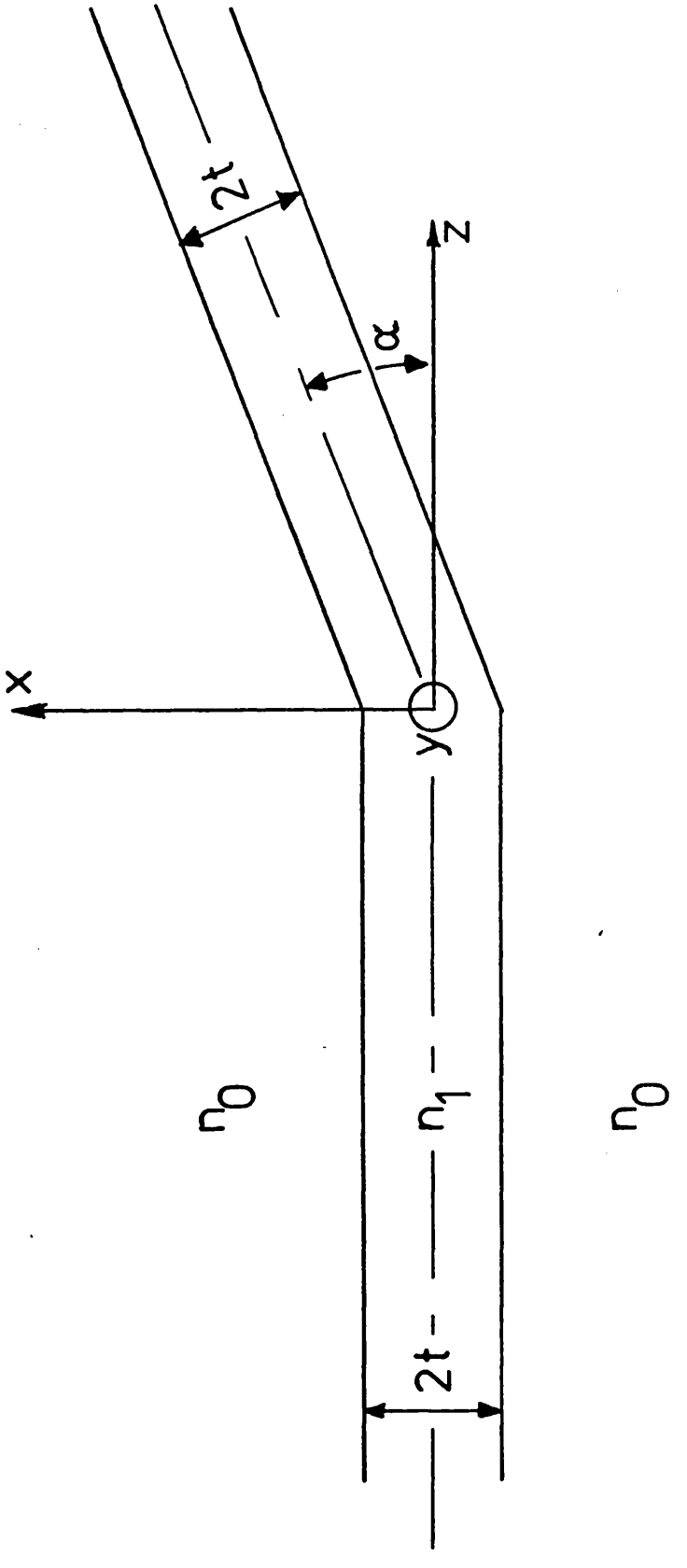

Fig.5.1 Planar waveguide tilt

is then extended to the case of two dimensional (stripe) waveguides (see Figure 5.6). Experimental investigation of tilts in trapezoidal ion-etched 7059 glass waveguides are described in Section 5.3.

5.1. Planar Waveguide Tilt Analysis.

This analysis is based on a method due to Anderson. A more detailed description of this method is found in reference (70). In this analytical solution backward radiation from the tilt region is ignored; the need for this assumption is explained below and the justification is presented in Appendix D1. The analysis is greatly simplified by considering only the fundamental TE_o mode.

Referring to Figure 5.1, for $z<0$ the incident electric fields of the TE_o mode of the symmetrical planar waveguide are:-

$$E_y^i(x,z) = A \cos(h_a x) \exp(-j\beta_a z) \qquad |x| \leq t \tag{5.1}$$

$$E_y^i(x,z) = A \cos(h_a t) \exp(-p_a(|x|-t)-j\beta_a z)) \qquad |x| \geq t \tag{5.2}$$

with,

$$p_a = h_a \tan(h_a t) \tag{5.3}$$

$$\beta_a^2 = k_o^2 + p_a^2 = (n_1 k_o)^2 - h_a^2 \tag{5.4}$$

defining the eigenvalue equation for β_a.

From Maxwell's equations we have,

$$H_x^i = \frac{-\beta_a}{\omega\mu_o} E_y^i(x,z) \tag{5.5}$$

where μ_o is the permeability of free space.

The coefficient A is now normalised to correspond to a mode power of unity (per unit length in the y direction), i.e.

$$\frac{1}{2}\,\mathrm{Re}\int_{-\infty}^{\infty} E_y^i(x,z).H_x^{i*}(x,z).dx \;=\; 1 \qquad (5.6)$$

where Re denotes "real part off", and the asterisk indicates the complex conjugate. Integration and algebraic manipulation lead to,

$$A = \sqrt{\frac{2\omega\mu_o}{\beta_a}}\left[t + \frac{\sin(2h_a t)}{2h_a} + \frac{\cos^2(h_a t)}{p_a}\right]^{-\frac{1}{2}} \qquad (5.7)$$

which, only for the symmetric planar waveguide case, as considered here, further reduces to

$$A = \left[\frac{2\omega\mu_o}{\beta_a(t+1/p_a)}\right]^{\frac{1}{2}} \qquad (5.8)$$

by use of (5.3).

The transmitted mode in the region $z > 0$ has the same waveguide propagation coefficient, β_a. However, the field expressions for the transmitted mode contain a term $\exp(-j\alpha\beta_a x)$, to account for the small linear phase tilt of α radians in the positive x direction about the y axis of Figure 5.1. For $z > 0$ the transmitted field components are, to this approximation,

$$E_y^t(x,z) = B\cos(h_a x)\exp(-j\alpha\beta_a x - j\beta_a z) \qquad |x| \leq t \qquad (5.9)$$

$$E_y^t(x,z) = B\cos(h_a t)\exp(-p_a(|x|-t) - j\alpha\beta_a x - j\beta_a z) \qquad |x| \geq t \qquad (5.10)$$

where p_a, β_a and h_a are again given by (5.3) and (5.4).
The value of B is normalised as before to correspond to a mode power of unity (per unit length in the y direction) i.e.,

$$\frac{1}{2}\,\mathrm{Re}\int_{-\infty}^{\infty} E_y^t(x,z).H_x^{t*}(x,z).dx \;=\; 1 \qquad (5.11)$$

which of course gives a value identical to that of A in (5.7) and (5.8), i.e.

$$B = \left[\frac{2\omega\mu_o}{\beta_a(t+1/p_a)}\right]^{\frac{1}{2}} \qquad (5.12)$$

With reference to Figure 5.1 the mode E_y^i is incident on the tilt at z = 0 and excites a transmitted mode TE_y^t in the angled section of waveguide for z > 0. As both the incident and transmitted modes have the same propagation coefficient β_a (varying only in phase constant $\exp(-j\alpha\beta_a x)$) we have, to a first order approximation, provided that $\alpha<<1$, from consideration of similar problems (69,71,107), that, there is no reflected power in the incident waveguide mode from the z = 0 plane.* Matching the tangential electric and magnetic fields on the z = 0 plane gives:-

$$E_y^i(x,o) + E_y^-(x,o) = TE_y^t(x,o) + E_y^+(x,o) \tag{5.13}$$

$$H_x^i(x,o) + H_x^-(x,o) = TH_x^t(x,o) + H_x^+(x,o) \tag{5.14}$$

where T is the transmission coefficient to be determined. E_y^- and E_y^+ are the radiation electric fields in the backward and forward directions respectively, with similar notations applying to the magnetic fields.

By using the result obtained in Appendix D1, we may argue that there is very little radiation in the backward direction, and this suggests that E_y^- and H_x^- may be neglected (70, 71,72). This allows an approximate solution to be found for T. Accordingly multiplication of (5.13) by $E_y^{t*}(x,o)$ or (5.14) by $H_x^{t*}(x,o)$ followed by integration with respect to x over the z = 0 plane gives,

$$T = \frac{\beta_a}{2\omega\mu_o} \int_{-\infty}^{\infty} E_y^i(x,o).E_y^{t*}(x,o).dx \tag{5.15}$$

*Strictly speaking, there should be some reflected power in the section of incoming waveguide, due to the tilted output waveguide in the region z > 0 introducing a small waveguide impedance variation at the junction. In general an accurate solution of problems such as this is complex; a method of general solution based on variational techniques may be found in Chapter 8 of Collin, (106).

Modal othogonality ensures that the integral of the forward radiation fields is zero; i.e.,

$$\int_{-\infty}^{\infty} E_y^{+}(x,o).E_y^{t*}(x,o).dx \;=\; 0 \;=\; \int_{-\infty}^{\infty} H_x^{+}(x,o).H_x^{t*}(x,o).dx \tag{5.16}$$

By conservation of power, the fraction S scattered into the surrounding media is

$$S = 1 - |T|^2 \tag{5.17}$$

The final step in the evaluation of T is the determination of the integral in (5.15). This may be split into three parts, viz,

$$\int_{-\infty}^{\infty} E_y^{i}(x,o).E_y^{t*}(x,o).dx \;= I_1 + I_2 + I_3 \tag{5.18}$$

$$I_1 = \int_{-\infty}^{-t} E_y^{i}(x,o).E_y^{t*}(x,o).dx \tag{5.19}$$

$$I_2 = \int_{-t}^{t} E_y^{i}(x,o).E_y^{t*}(x,o).dx \tag{5.20}$$

$$I_3 = \int_{t}^{\infty} E_y^{i}(x,o).E_y^{t*}(x,o).dx \tag{5.21}$$

Each reduces to a trival integration of trignometric functions, full details are omitted. The result for T is:-

$$T = \frac{1}{t+1/p_a}\left[\frac{\sin(t(\alpha\beta_a+2h_a))}{2(\alpha\beta_a+2h_a)} + \frac{\sin(t(\alpha\beta_a-2h_a))}{2(\alpha\beta_a-2h_a)} + \frac{\sin(\alpha\beta_a t)}{\alpha\beta_a} + 2\cos^2(h_a t)\left[\frac{2p_a\cos(\alpha\beta_a t)-\alpha\beta_a\sin(\alpha\beta_a t)}{4p_a^2+(\alpha\beta_a)^2}\right]\right] \tag{5.22}$$

To verify the above result we may check that the transmission is unity when $\alpha = 0$. Substituting into (5.22) gives

$$T = \frac{1}{t + 1/p_a}\left[\frac{\sin(2h_a t)}{2h_a} + t + \frac{\cos^2(h_a t)}{p_a}\right] \qquad (5.23)$$

which by use of (5.3) reduces to T = 1, as required.

A computer program to obtain the eigenvalue solutions and evaluate the above expression (5.22) was written, a flow diagram of which may be found in Appendix A5. Figure 5.2 shows a theoretical plot of transmission v.s. tilt angle for a series of planar 7059 glass waveguides surrounded by air. It can be noted that for reasonably small angles, the transmission is close to unity. However, above a certain point the transmission rapidly falls with increasing tilt angle. This is caused by the relative phase mismatch between the incident and transmitted modes. As the tilt angle becomes greater the relative phase mismatch $\exp(-j\alpha\beta_a x)$ also increases, reducing the transmitted power $|T|^2$ across the z= 0 plane. This effect is more pronounced in wider waveguides for which the guided mode is less tightly confined and also in waveguides for which there is only a small difference in refractive index between the waveguide and the surrounding media, e.g. for Ti diffused $LiNbO_3$. Figure 5.3 shows a plot of power transmission v.s. tilt angle for a series of hypothetical Ti diffused $LiNbO_3$ planar waveguide tilts. As can be seen the fall in transmission with angle is much more pronounced than in the 7059 glass case. This is primarily due to the small refractive index difference between the waveguide and the surrounding media resulting in a weakly guided mode which is very sensitive to abrupt changes in direction. This effect can be explained more easily using a "ray optics" approach rather than the wave approach used in the analysis.

In weakly guiding modes the "rays" of the guided mode

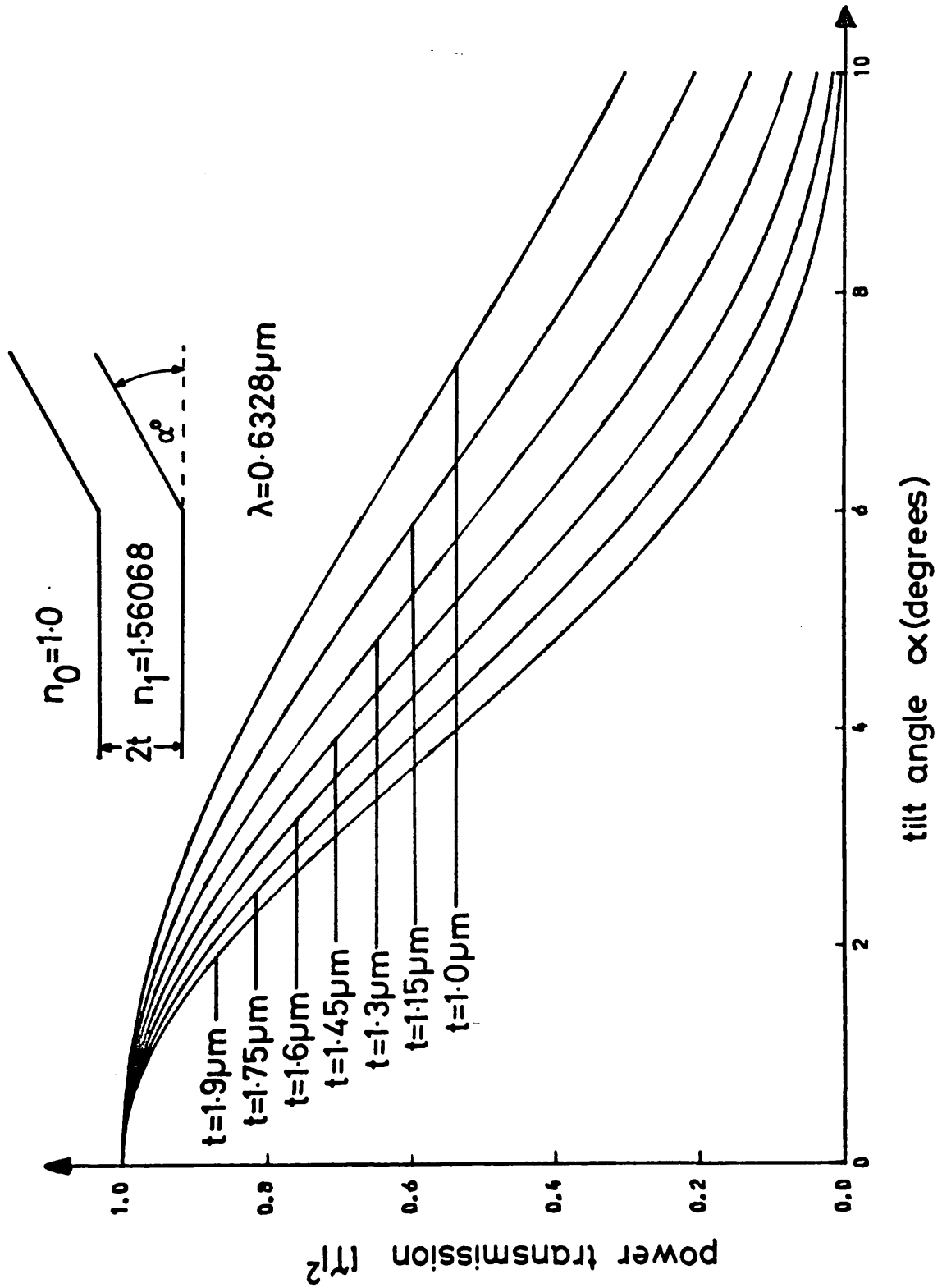

Fig. 5.2 Plot of power transmission versus tilt angle for a 7059 glass planar waveguide tilt

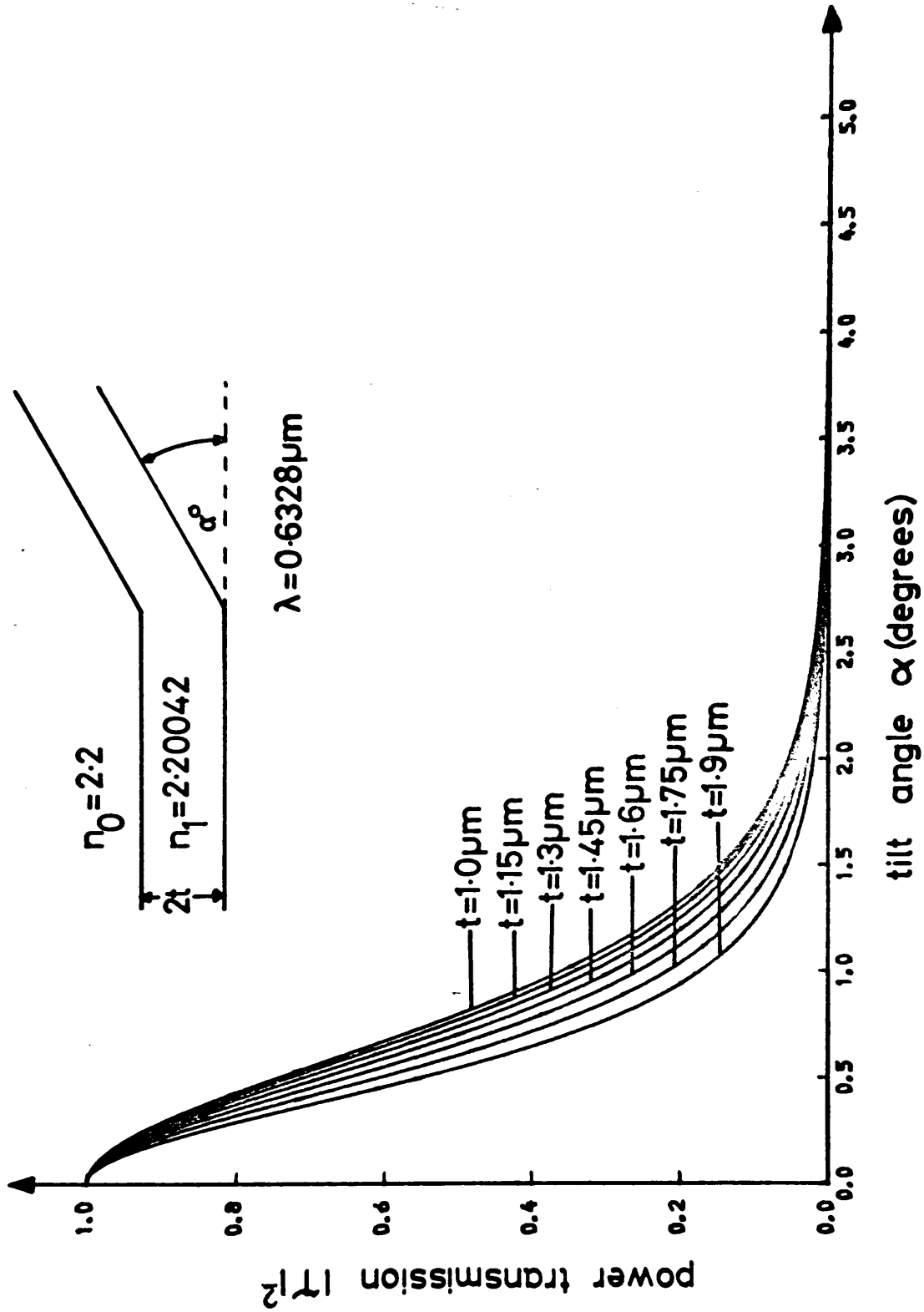

Fig. 5.3 Plot of power transmission versus tilt angle for a $LiNbO_3$ planar waveguide tilt

impinge at shallow glancing angles on the waveguide/surrounding media interface. If an abrupt tilt is introduced into the waveguide, then some of the "rays" of the weakly guiding mode will impinge on the interface with the surrounding medium at an angle greater than the critical angle and will not undergo total internal reflection. This leads to the formation of "leaky rays" which lose power at every interface reflection and are rapidly attenuated. The transmitted power in the output section of the waveguide thus decreases. As the tilt angle increases the effect becomes more pronounced until at large angles all the incident power is lost to radiation leading to zero transmitted power. This effect is shown pictorially in Figure 5.4. It is also interesting to note that the "ray optics" approach also indicates that radiation in the backward direction may be ignored. Any guided mode "ray" impinges on the waveguide/ surrounding media interface at small grazing angles. Thus, when such a guided mode is incident on a tilted section of waveguide and results in a "leaky mode", decaying ray, the radiated power is lost almost exclusively in a direction to the right of the $z = 0$ plane, except for very large tilt angles ($>10^{o}$). However, even in this case radiation is predominantly in the forward direction with only a very small fraction of the incident power finding its way across the $x = 0$ plane. This effect is also shown pictorially in Figure 5.5. Large tilt angles ($>10^{o}$) do not concern us as no practical device is envisaged with such a sharp change of direction.

Figures 5.2, 5.3 show that, provided the waveguide is formed in suitable materials with appropriate choices of waveguide width, then waveguide tilts with angles of up to around 1^{o} may be fabricated with little transmission loss.

Section 5.2 shows how the above planar waveguide analysis

increasing proportion of incident power lost to radiation. as α increases

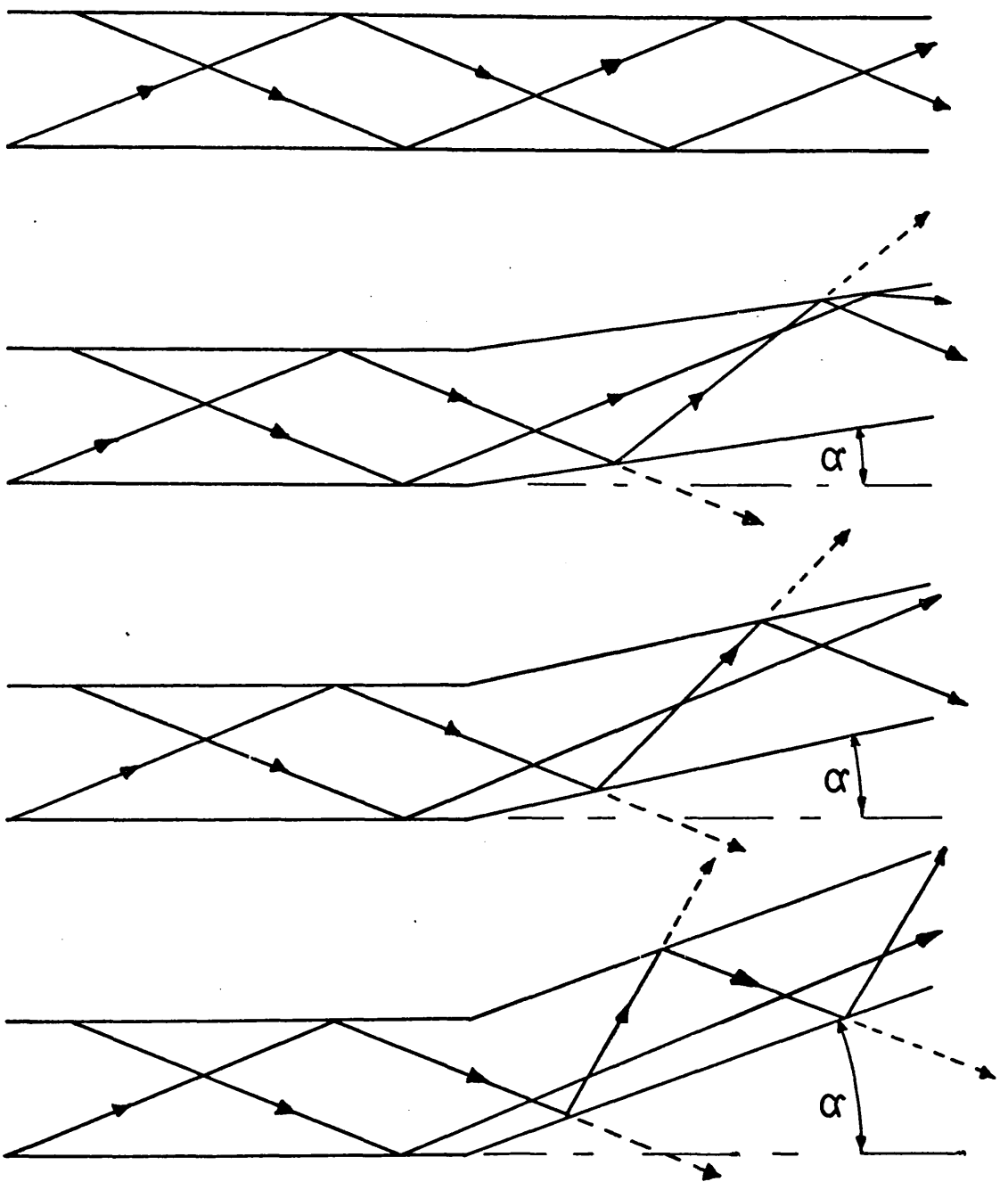

Fig. 5.4 Pictorial representation of power loss with increasing tilt angle α

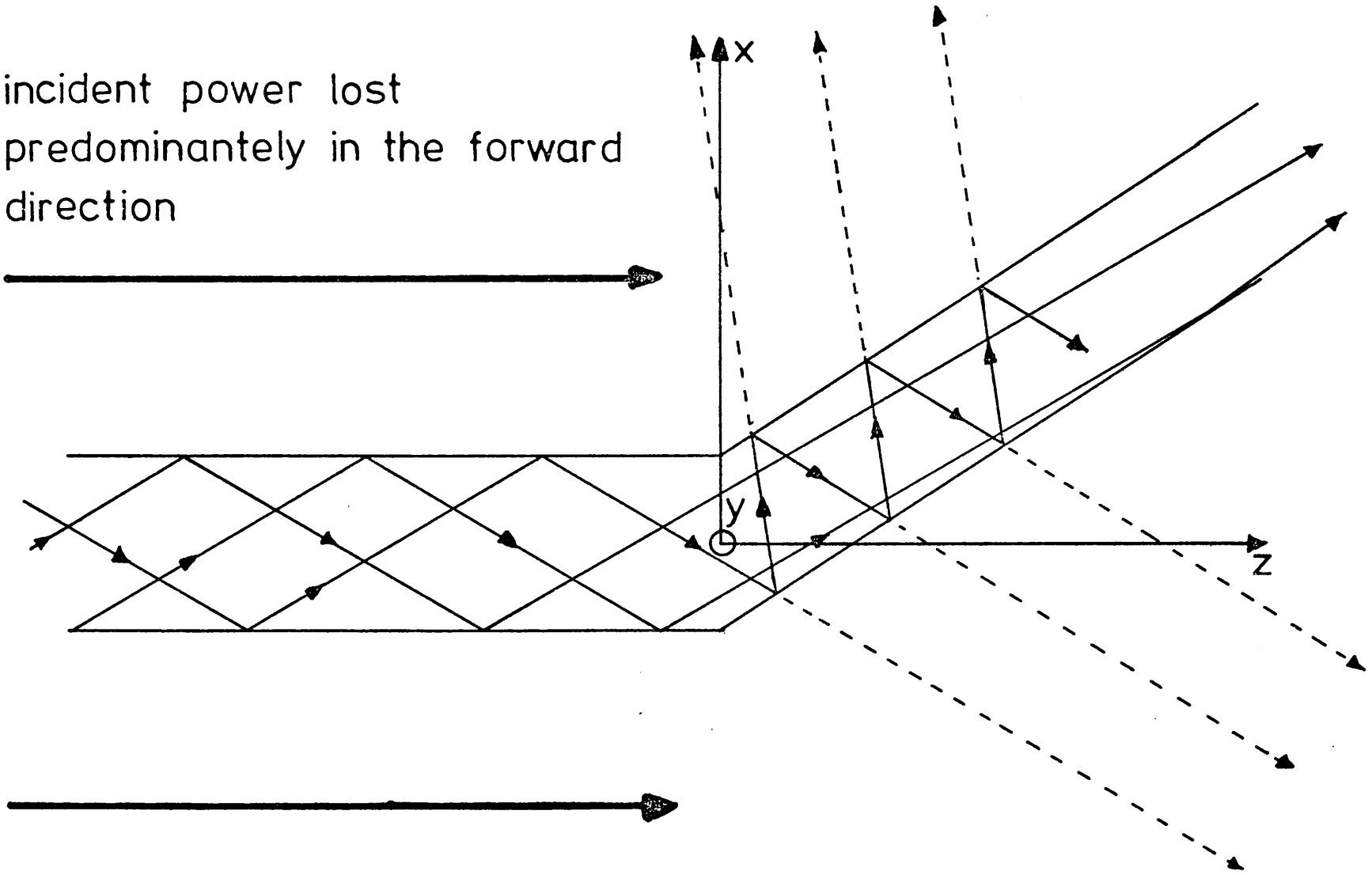
incident power lost
predominantely in the forward
direction
x
y
z

Fig. 5.5

may be used to predict the transmission performance of trapezoidal stripe waveguides formed in ion-etched 7059 glass.

5.2. Stripe Waveguide Tilt Transmission Using a Planar Waveguide Analysis.

Referring to Appendix B2, we may think of the functions which describe the electric and magnetic fields in a two dimensional (stripe) waveguide as being uncoupled, i.e. separable. This follows immediately from the theory of Marcatili (56) and from the analysis of Appendix B1, and implies that the transverse fields of a waveguide in the x direction are independent of the transverse fields in the y direction and vice versa. Consequently the transmission performance of a single mode stripe waveguide tilt, for which the waveguide is tilted in the x direction only (see Figure 5.6), may be calculated directly using the planar waveguide analysis of Section 5.1, but with the stripe waveguide propagation coefficient β_z substituted in place of the planar waveguide propagation coefficient β_a (see Appendix B2). Using the result of Appendix B2 and recalling the parameters used in Section 5.1, the following changes are made to allow the planar waveguide analysis of Section 5.1 to be used in the design of single mode stripe waveguide tilts. Using the notation of Marcatili (56),

$$\beta_a \text{ becomes } \beta_z = k_z \tag{5.24}$$

$$h_a \text{ becomes } k_x \tag{5.25}$$

$$p_a \text{ becomes } 1/\xi_3 = 1/\xi_5 \tag{5.26}$$

Thus we may use the theory of Marcatili (56) to calculate the various two dimensional waveguide parameters, which are in turn

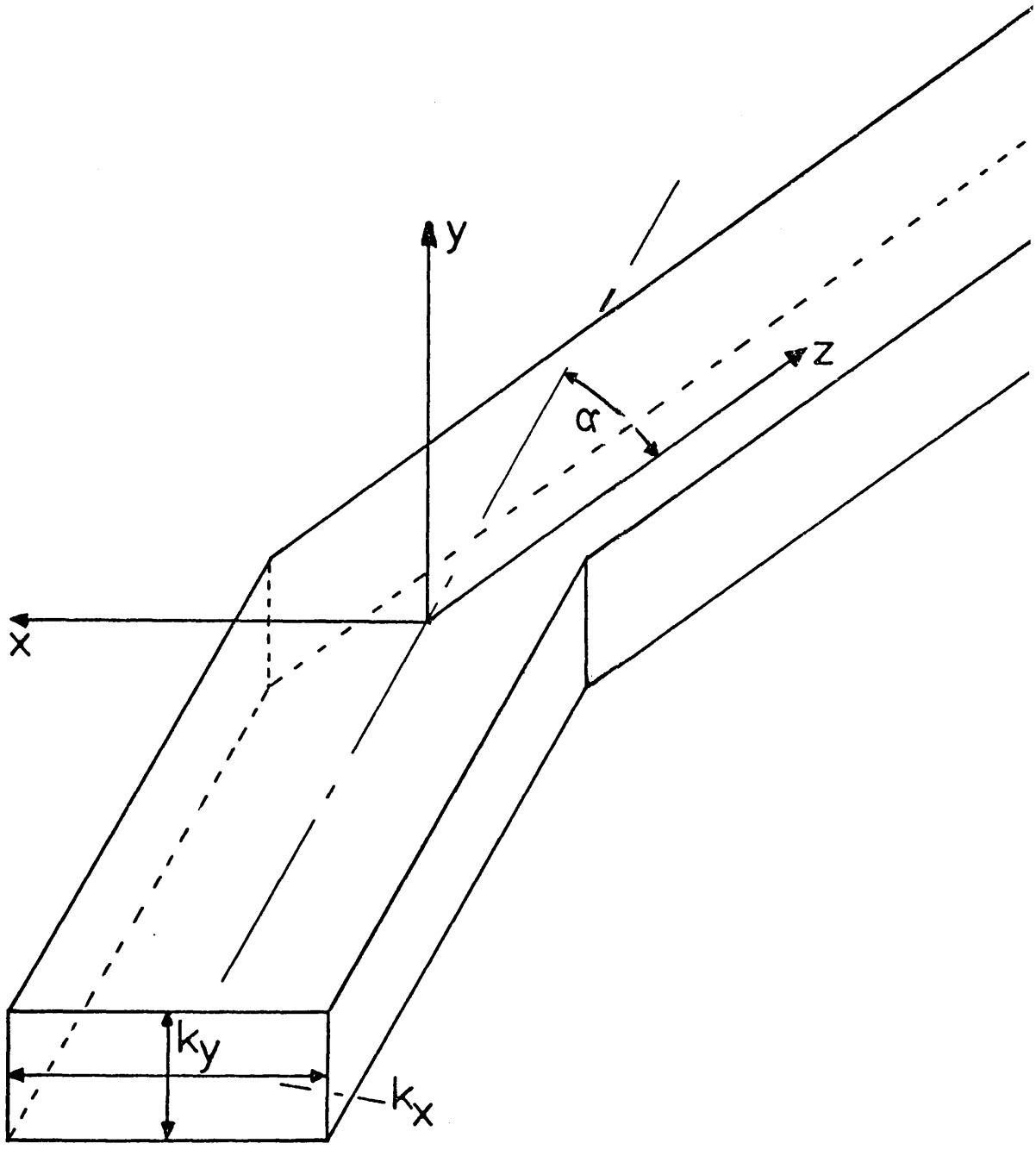

Fig. 5.6 Pictorial representation of uncoupled wave vectors in a stripe waveguide tilt

used to predict the transmission performance of stripe waveguide tilts. The planar waveguide tilt power transmission equation (5.22) is modified to become,

$$|T|^2 = \left[\frac{1}{\left[t + \frac{\sin(2k_x t)}{2k_x} + \frac{\cos^2(k_x t)}{1/\xi_3} \right]} \left[\frac{\sin(t(\alpha\beta_z + 2k_x))}{2(\alpha\beta_z + 2k_x)} + \right. \right.$$

$$\frac{\sin(t(\alpha\beta_z - 2k_x))}{2(\alpha\beta_z - 2k_x)} + \frac{\sin(\alpha\beta_z t)}{\alpha\beta_z} + 2\cos^2(k_x t)\left[\right.$$

$$\left. \left. \left. \frac{2(1/\xi_3)\cos(\alpha\beta_z t) - \alpha\beta_z \sin(\alpha\beta_z t)}{4(1/\xi_3)^2 + (\alpha\beta_z)^2} \right] \right] \right]^2 \qquad (5.27)$$

Figure 5.7 shows a plot of theoretical transmission performance v.s. tilt angle for three hypothetical waveguides all of the same width. One is a planar waveguide supporting only the fundamental TE_o mode while the other two are stripe waveguides guiding the E^x_{11} and E^y_{11} modes respectively. As can be seen, there is virtually no difference in transmission performance between the TE_o mode planar waveguide and the E^y_{11} mode stripe waveguide. This is to be expected, as the analysis of Appendix B2 shows that a planar waveguide device analysis may be used to predict the transmission performance of the corresponding stripe waveguide device. Thus we would expect very little difference between the transmission curves for a planar waveguide supporting the TE_o mode and a stripe waveguide supporting the E^y_{11} mode, as the stripe waveguide E^y_{11} mode corresponds effectively to a planar waveguide TE_o mode in the plane of the tilt. It is interesting to note that there is very little difference (<3%) between the stripe waveguide E^y_{11} mode, (effectively a planar

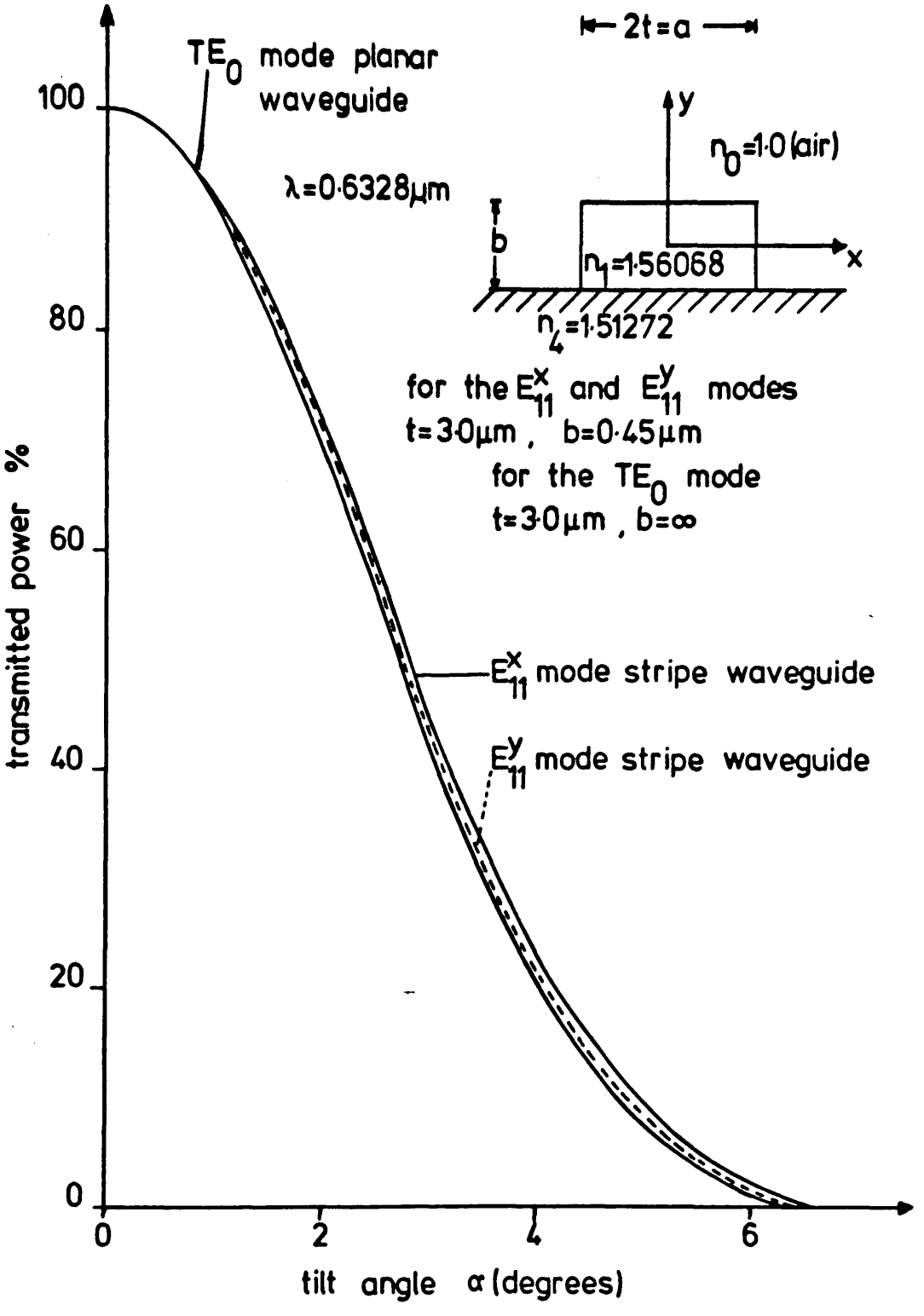

Fig. 5.7 Comparison of power transmission versus tilt angle for TE_0, E_{11}^x and E_{11}^y modes

waveguide TE_o mode in the plane of the tilt) and the E_{11}^x mode, (effectively a planar waveguide TM_o mode in the plane of the tilt). This suggests that the waveguide tilt analysis may be used to predict the transmission performance of E_{11}^x single mode stripe waveguide tilts as well as E_{11}^y single mode tilts. This makes the design of stripe waveguide tilts which support only the fundamental E_{11}^x mode much easier, because the analysis of a planar waveguide tilt propagating the fundamental TM_o mode is more complicated than that of the fundamental TE_o mode. It should be noted that the above 7059 glass examples display probably the largest difference in modal propagation parameters between the modes (i.e. between the TE_o, E_{11}^y and E_{11}^x), of any practical device. Many future practical integrated optical devices will be based on active substrates, e.g. Lithium Niobate or Gallium Arsenide. As both have little refractive index difference between the waveguide and the surrounding media, the difference between the TE_o, E_{11}^y and E_{11}^x modal propagation parameters will be much less than in the above 7059 glass example. Thus we may conclude that the above tilt analysis applies with increasing accuracy to practical waveguides which display only small refractive index differences between the waveguide and the surrounding media. For these cases the above tilt analysis may be used with confidence to predict the transmission performance of stripe waveguide tilts propagating either the E_{11}^x or E_{11}^y modes.

The above tilt analysis is compared in Section 5.3 with experimental, ion-etched, waveguide tilts, which guide only the E_{11}^x mode.

5.3. Experimental Investigation of the Transmission Performance of Trapezoidal, Ion-Etched, 7059 Glass, Waveguide Tilts.

5.3.1. Waveguide Design Considerations.

Two dimensional (stripe) 7059 glass waveguide tilts are fabricated using the process outlined in Section 4.2. By suitable choice of the waveguide thickness only the lowest order E^x_{11} mode is supported in a waveguide of approximately 6 μm nominal effective width, (see Section 4.4). In the waveguides with a>>b (i.e. a = 6 μm, b = 0.4 μm) the lowest order (and only) propagating mode is the E^x_{11} mode (see Section 4.4). It is not possible using this waveguide geometry to fabricate a waveguide with E^y_{11} as the lowest order mode. To do so we would have to reverse the roles of a and b, i.e. to make b = 6 μm and a = 0.4 μm. This is not possible using the current fabrication procedure, as it would involve etching waveguides 6 μm deep with a width of 0.4 μm -, hardly compatable with the current tehcnological limit of ∿0.8 μm depth using ion-etching and ∿1.0 μm width using photolithographic techniques (see Section 4.2).

It is possible to make stripe waveguides which support only the lowest order E^x and E^y modes, i.e. E^x_{11} and E^y_{11}, and to excite selectively each in turn using a suitably polarised laser light source. However, in practice, mode scattering occurs and it is not possible to excite one mode without waveguide discontinuities scattering power into the other, causing it in turn to be excited (see Section 4.4). After only a small distance both modes are propagated together although one of them is at a much reduced power level. This is especially true when selectively exciting the E^y_{11} mode; after only a small distance the E^x_{11} mode can be observed strongly in evidence in the output

"m-line" mode-structure pattern. It was thought undesirable to have more than one mode type present when testing experimental waveguide tilts, mainly due to the possibility that mode conversion modifies the power transmission measurements. The effect of this, however, should be small if the waveguide is capable of supporting only the fundamental E^x and E^y modes, (see Section 5.2). Waveguides capable of supporting both E^x_{11} and E^y_{11} modes need only small fluctuations in width and thickness to enable them to guide the E^x_{21} mode which would have large effects on the measured power transmission. As the theory of Section 5.2 deals only with single mode guides it could not be used to predict the transmission performance of multimode guides, and as a result correlation between it and the experimentally measured values would be expected to be poor. It is interesting to note that some initial stripe waveguide tilt measurements carried out on multimode waveguides displayed large discrepencies between theory and experiment for tilt angles greater than 2.5^o. Therefore to eliminate this problem stripe waveguide tilts were designed to propagate only the E^x_{11} mode, even although the theory is more directly applicable to E^y_{11} modes (quasi TE_o mode), (see Section 5.2).

5.3.2. Transmission Loss Measurement.

Transmission loss measurements were carried out on ion-etched 7059 glass stripe waveguide tilts in a similar manner to the measurements of the stripe waveguide losses, as outlined in Section 4.4. Power measurements along the guide were taken initially at points after the tilt, and then before the tilt using a prism coupler. Use of this technique avoided the possibility that the power reading at the output is modified by damage from clamping the prism to the input. As the initial power measurements were obtained on sections of waveguide

furthest away from the input prism and then progressively moved towards it, a measure of waveguide attenuation could be obtained. This measurement of waveguide loss was then compared with a "control" section of straight waveguide fabricated at the same time as the tilts and of the same width and film thickness. From these results an estimated error of $\pm 5\%$ was calculated in the power measurement. An average waveguide attenuation of between 6 - 8 dB/cm for single mode stripe waveguides of ~ 6 μm effective width and 0.4μm film thickness was recorded. Use of a better waveguide mask with smoother edges would undoubtably lower this figure to a more acceptable level. The waveguide tilt transmission losses were then obtained by subtracting the average waveguide attenuation from the overall transmission loss of the tilt section of waveguide.

The next section compares the above measured results with the theory developed in Section 5.2.

5.3.3. Comparison of Experimental and Theoretical Stripe Waveguide Tilts.

5.3.3.1. Waveguide Width Measurements.

After making the transmission loss measurements the stripe waveguide tilt samples were examined in a scanning electron microscope (S.E.M.). This was necessary to obtain accurate values of the trapezoidal waveguide top width and base width, so as to calculate the waveguide effective width (see Sections 4.2, 4.3, 4.4). Although the waveguide widths were known approximately from the initial waveguide mask dimensions and the single mode nature of the waveguides, accurate

knowledge of the waveguide widths is essential due to the rapid fall in power transmission with increasing waveguide width (see Figures 5.2, 5.3). The S.E.M. measurements are essential for the accurate determination of the waveguide widths and calculation of the power transmission curves. Waveguide width measurements obtained from the S.E.M. have an estimated maximum error of ±0.25 μm, (see Section 4.4). Theoretical curves of power transmission v.s. tilt angle using the single mode E^x_{11} stripe waveguide tilt theory of Section 5.2 were drawn for the widths found using the S.E.M. measurements and the film thickness deduced from the sputtering unit calibration, (see Sections 3.1, 3.2). A flow diagram of the computer program used to calculate this is given in Appendix A6.

5.3.3.2. Theory and Experiment.

Experimental and theoretical plots of power transmission v.s. tilt angle for ion-etched 7059 glass waveguide tilts are shown in Figures 5.8, 5.9. Figure 5.8 clearly demonstrates the effect that waveguide width has on power transmission for constant tilt angle. As can be seen, the choice of waveguide width greatly influences the theoretical power transmission curve. It is, therefore, gratifying to find such good agreement between theory and experiment when using the effective waveguide width theory of Section 4.3. Experimental evidence of this kind adds further weight to the trapezoidal waveguide effective width theory, and shows that it may be used in the design of single mode stripe waveguide components.

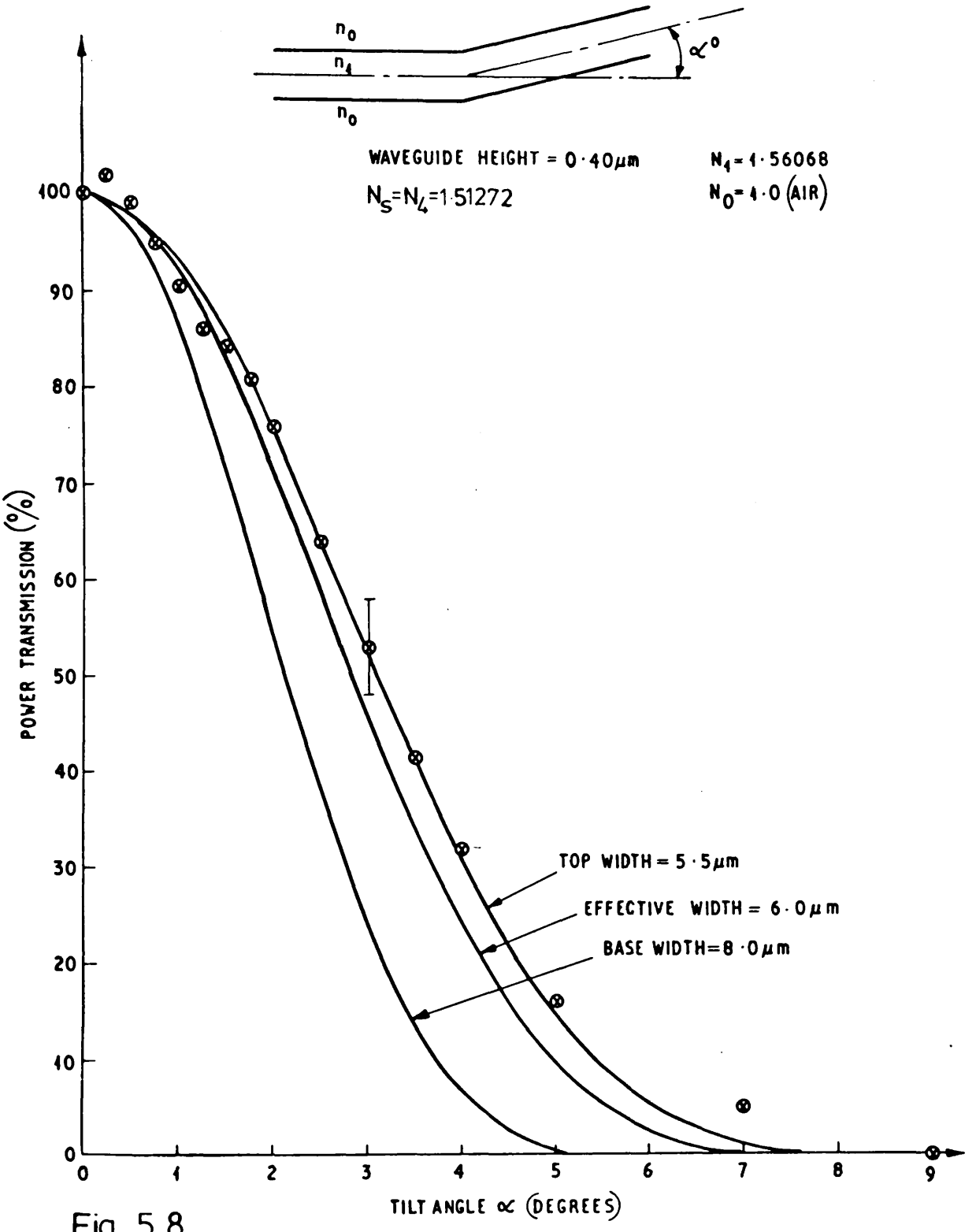

Fig 5.8

EXPERIMENTAL AND THEORETICAL PLOTS OF TRANSMISSION V.S. TILT ANGLE

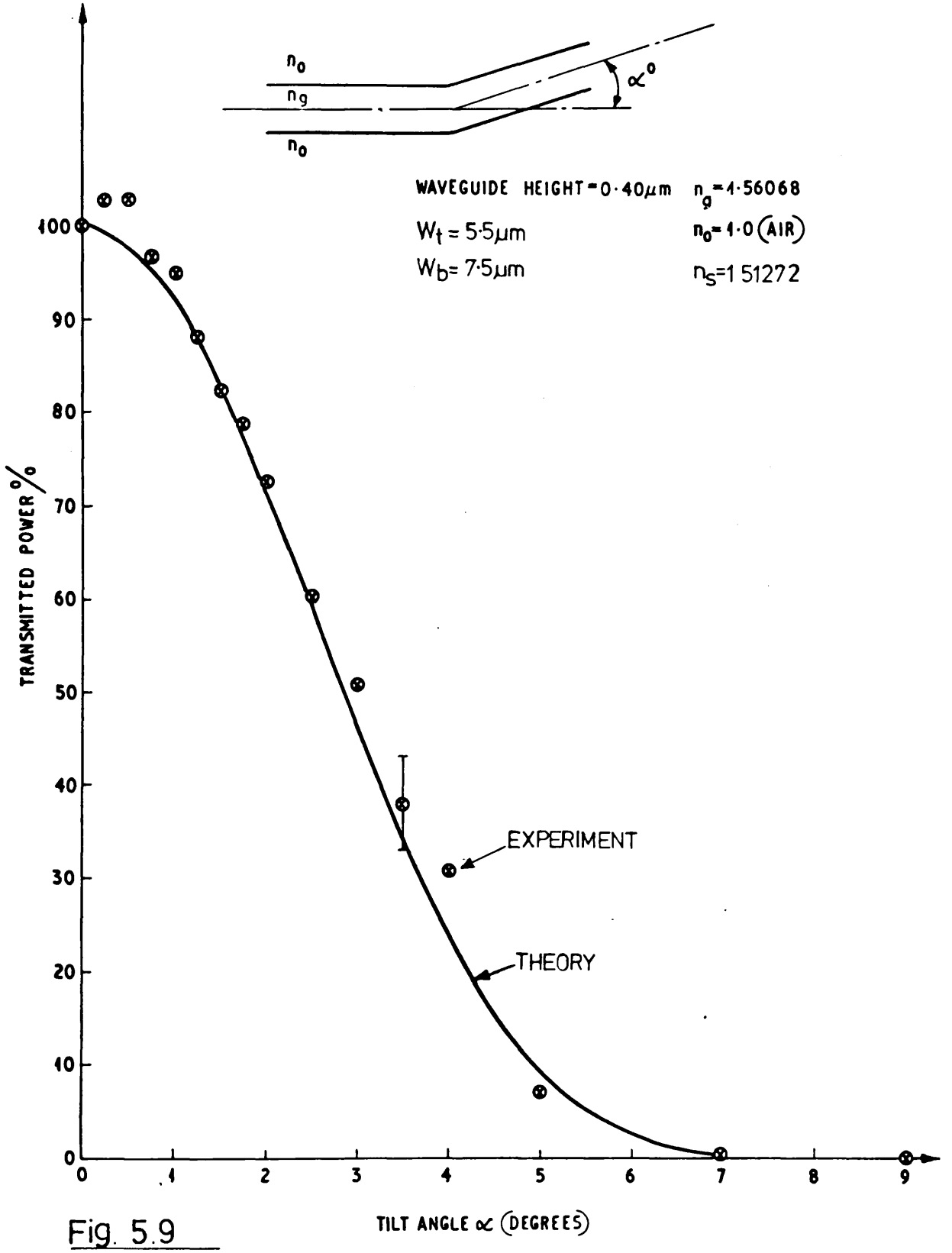

Fig. 5.9

EXPERIMENTAL AND THEORETICAL PLOTS OF TRANSMISSION V.S. TILT ANGLE

5.4. Discussion of Results.

Figures 5.8, 5.9 show clearly a close correlation between the theoretical transmission and the experimentally measured values when using the effective width theory (see Section 4.3). Figure 5.8 shows how the choice of waveguide width dramatically alters the transmission performance of the device. This result supports the effective width theory, further increasing its usefulness in the design of 7059 glass ion-etched stripe waveguides and at the same time verifies that the waveguide tilt analysis accurately predicts the transmission performance of single mode stripe waveguide tilts which support only the fundamental E_{11}^{x} mode (see Section 5.2). Use of this fact greatly simplifies the design of single mode stripe waveguide tilts, and allows a simple analytical solution to be applied to a problem which otherwise would require a complex, computer orientated, numerical solution.

The assumption of ignoring radiation in the backward direction in the analysis of Section 5.1 would appear to be a valid one, as the experimentally measured results compare well with the theoretically calculated values, using the theory of Section 5.2. All of the experimental waveguides measured and observed displayed no sign of any radiation in the backward direction from the tilt region. Thus we may conclude that the assumption in the analysis of neglecting radiation in the backward direction is quite justified.

The rapid fall in transmission with tilt angle is clearly shown in the above diagrams of Figures 5.8, 5.9. It can also be shown to greater effect photographically. Figure 5.10 shows the effect of increasing tilt angle on overall device

power transmission. These photographs show clearly how the light level intensity in the output section of the waveguide tilt decreases rapidly with increasing tilt angle. To obtain these photographs some of the films had to be overexposed on the input section of waveguide so as to show the very much reduced power levels in the output sections of waveguide. As some of the output power levels were extrmely low, exposure times of several hours using fairly fast film, (400 A.S.A.) were common.

Input power levels into these waveguides were never much greater than 2×10^{-6} watts using a 7×10^{-3} watt 0.6328 μm wavelength He-Ne laser source (94), thus showing the inefficiency in the power coupling to the waveguide. As explained in Section 4.4, the maximum power input into stripe waveguides is very dependent on the waveguide width, such that it becomes increasingly difficult to obtain reasonable power levels in waveguides as they are reduced in width. To fabricate single mode stripe waveguides one must keep the waveguide width as small as possible (see Section 4.4.). Thus the above waveguides represent a compromise in terms of power level, (i.e. stripe waveguide width) and single mode (E^x_{11}) propagation. The above waveguide dimensions were chosen for relatively easy fabrication of single mode (E^x_{11}) waveguides while at the same time maintaining a reasonably large waveguide width, so as to enable experimental measurements to be carried out accurately and easily using readily measurable power levels.

When designing the waveguide mask, no thought was given to the effect of the waveguide dimensions on transmission, as the experiments were primarily intended to test the validity of the theory. Thus the waveguide dimensions chosen are not

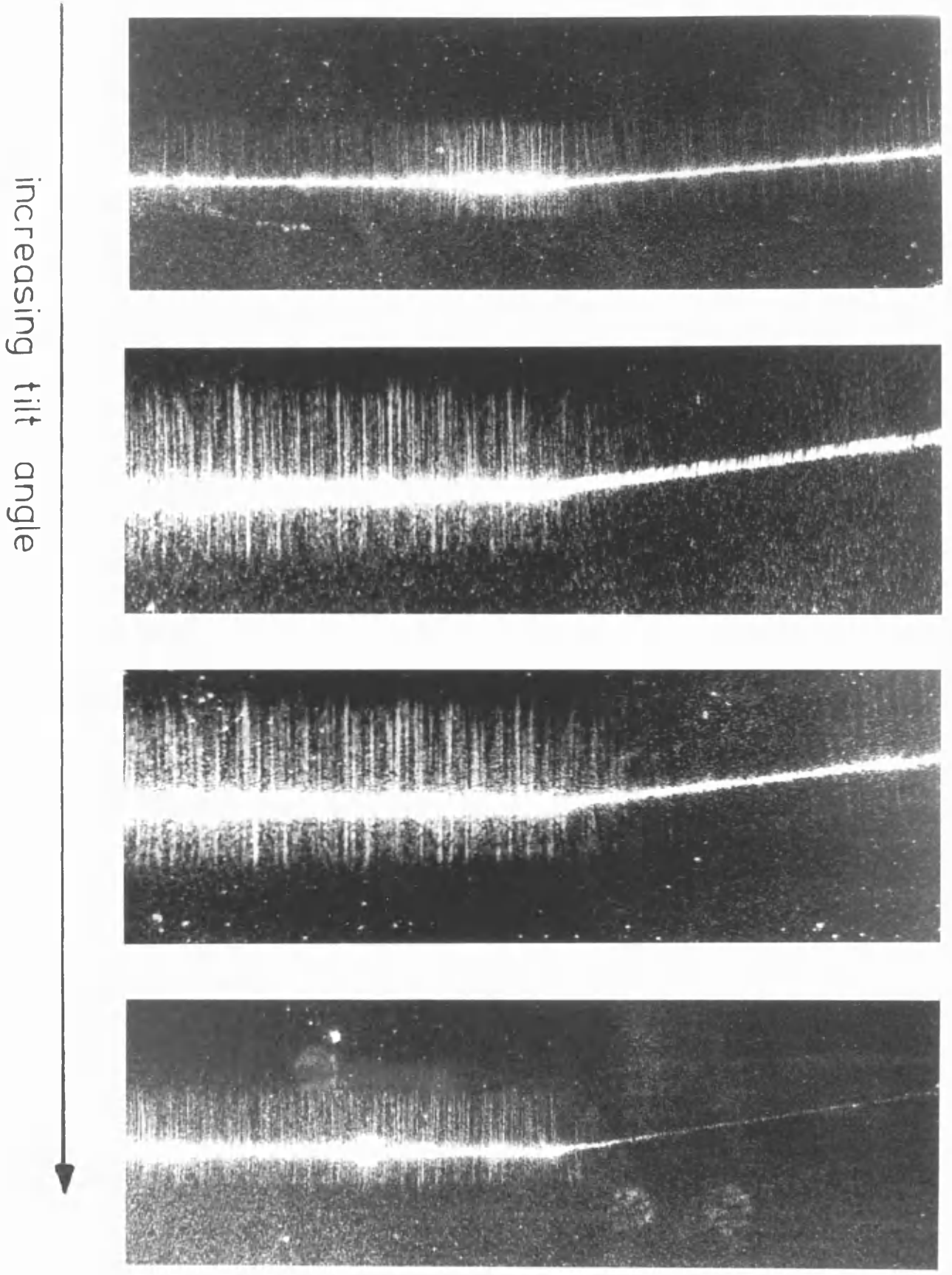

Fig. 5.10 Micrographs of working tilts showing the effect of increasing tilt angle on power transmission

representative of a practical device in which a much smaller waveguide width would be used. Any practical system based on 7059 glass will probably have a waveguide width around the 1 μm region. This will have the effect of increasing the useful tilt working angle up to around 3^{o}- 4^{o}. It should be noted that the above results apply only to a 7059 glass ion-etched ridge waveguide supported on a lower index soda lime glass substrate. If the waveguide is to be embedded in a lower index surrounding medium, then the power transmission with increasing tilt angle will fall rapidly, due to the less well confined guided mode leaking into the surrounding medium more easily.

We may conclude that the planar waveguide tilt analysis of Section 5.1 can accurately predict the transmission performance of single mode (E^{x}_{11}) ion-etched 7059 glass stripe waveguide tilts, when the planar waveguide value is replaced by that of the corresponding two-dimensional waveguide. Recalling the discussion of Section 5.2, we may expect the above analysis to become even more accurate for waveguides with only small refractive index differences between the waveguide and the surrounding media, and also for waveguides whose fundamental mode is the E^{y}_{11} instead of the E^{x}_{11} . Experimentally this could be verified using an as yet undiscovered stripe waveguide fabrication technology which would ensure that the fundamental stripe waveguide mode was the E^{y}_{11}, or alternatively by use of a planar waveguide structure similar to that of Yajima (76). There is still ample scope for further work in this field, particularly in the optimisation of tilt angle for various waveguide widths and materials, e.g. $LiNbO_3$, where the above theory may be used to optimise an electro-optic Mach-Zender phase modulator.

Chapter 6 extends the methods of analysis developed here, and uses them in a planar waveguide Y-junction analysis.

5.5. Conclusions.

A relatively simple analytical solution for transmission through a planar waveguide tilt has been used successfully to predict the transmission performance of single mode (E_{11}^{x}) ion-etched 7059 glass stripe waveguide tilts. Results indicate that the theory may be even more accurate when used on waveguides that have only a small refractive index difference between the waveguide and the surrounding media, or on waveguides that can only support the E_{11}^{y} mode.

CHAPTER 6.

CHAPTER 6. DESIGN FABRICATION AND EVALUATION OF STRIPE SINGLE MODE 7059 GLASS WAVEGUIDE Y-JUNCTIONS.

A Y-junction formed in stripe dielectric waveguide is capable of performing two different functions. It may act as a mode filter or as a power divider (74,76). Single mode stripe waveguide Y-junctions have already been used in optical waveguide devices. Sasaki (6) has demonstrated an active waveguide optical switch, while Gallagher has studied passive silver ion exchanged Y-junctions (73). It was the failure of the above two devices to behave in the manner predicted by Anderson (53, 70) that the following study was undertaken.

Single mode Y-junctions could form important components in any future integrated optical communications system. These include switching devices performing logic functions, or passive power splitting devices (73). Clearly there is a need to relate experimental transmission performance to a theoretical model. Both Yajima (74) and Burns and Milton (75) have analysed an asymmetrical Y-junction. Yajima (76) has shown that an asymmetric planar waveguide Y-junction with one of the output guides co-planar with the input guide will act either as a power divider or as a mode filter, depending on the degree of asymmetry in the structure. Both the above authors neglect the effect of phase tilt and consider only coupling between the output waveguides. Their analyses are, therefore, restricted to very small junction angles only.

It is the purpose of this chapter to compare predicted and experimental values of transmission for Y-junctions formed in stripe ion-etched 7059 glass waveguides. Anderson's theory (70), which does make due allowance for phase tilt, is modified to account for defects in the junction area, formed in the fabrication stage.

This theory provides a close lower bound for the power transmission of a symmetrical Y-junction formed in planar waveguide. This theoretical value is then used in a manner similar to that of the waveguide tilt of Chapter 5 in which the planar waveguide analysis is extended to the case of two dimensional (stripe) waveguides. The transmission performance of experimental ion-etched 7059 glass Y-junctions is then compared with the above theory.

6.1. Planar Waveguide Analysis of a Y-Junction with a Blunt Wedge.

This planar waveguide Y-junction analysis follows closely the method developed by Anderson (70). The method of analysis is identical, only the waveguide geometry being altered. Referring to Figure 6.1 the perfect wedge in the Y-junction discussed by Anderson is replaced by a straight waveguide section of width 2d. This modification to the geometry approximates closely with that of experimental Y-junctions (see Figure 6.2a, 6.2b), and may explain the large discrepancies between the measured and theoretical values of power transmission. This defect arises due to limitations in the photolithography and also from the nature of the ion-etching process (see Section 4.2).

In this analysis radiation in the backward direction from the junction area is ignored. The need for this is explained below and its justification is given in Appendix D1, (see also Chapter 5). The method of analysis is similar to that of the waveguide tilt (Chapter 5), and many areas are common to both. As most of the analysis is identical to that of Anderson (70) it is presented only briefly except where there is a difference in expressions and the evaluation of integrals. All the basic assumptions made by Anderson are equally valid in this analysis. Only the fundamental TE_o mode as considered by Anderson will be dealt with here.

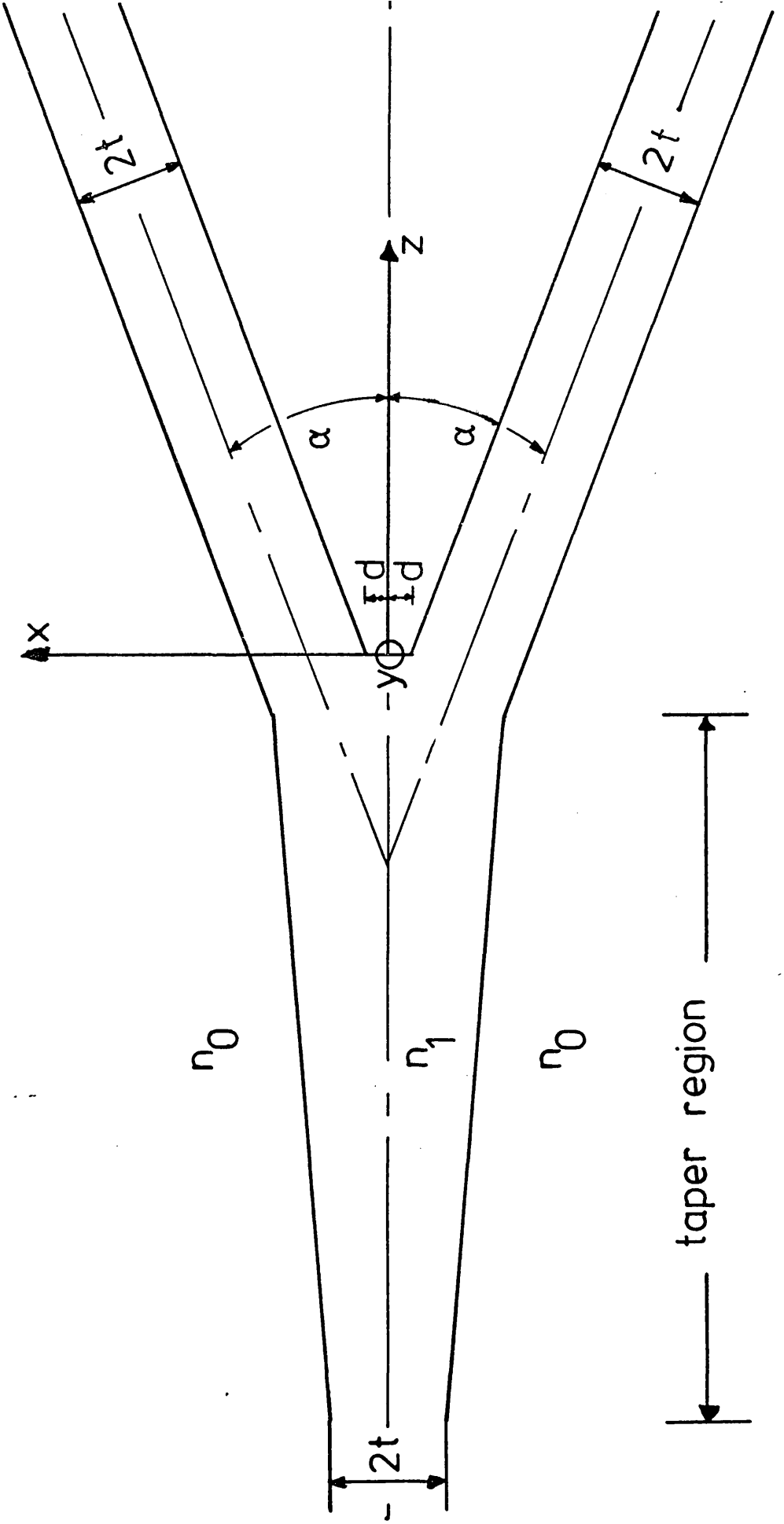

Fig. 6.1 Planar waveguide Y-junction with a blunt wedge

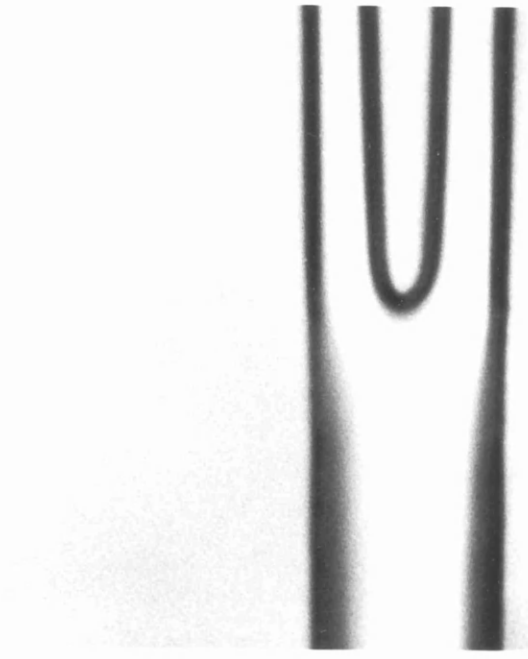

(a) baked photoresist Y-junction

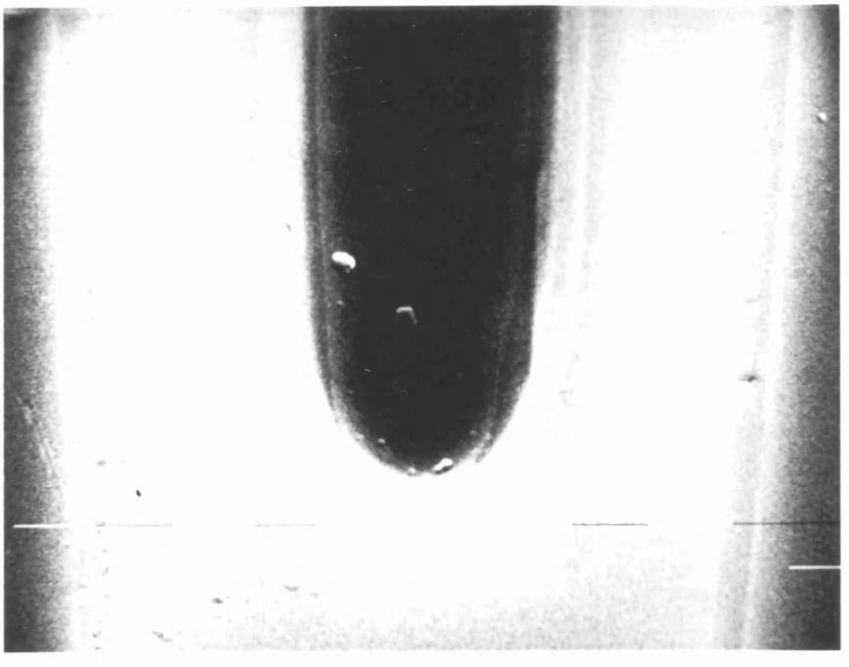

(b) ion-etched Y-junction (1μm markers)

Fig. 6.2 Y-Junction waveguide patterns

Referring to Figure 6.1, it is assumed that the transmission coefficient of the tapered section of waveguide directly before the junction is close to unity, so that any interaction between the taper and the output waveguides is negligible. For $z \leqslant 0$ the incident electric fields of the fundamental TE_o mode are:-

$$E_y^i(x,z) = A \cos(h_a x)\exp(-j\beta_a z) \qquad |x| \leqslant 2t+d \tag{6.1}$$

$$E_y^i(x,z) = A \cos(h_a(2t+d))\exp(-p_a(|x|-2t-d)-j\beta_a z) \qquad |x| \geqslant 2t+d \tag{6.2}$$

with

$$p_a = h_a \tan(h_a(2t+d)) \tag{6.3}$$

$$\beta_a^2 = k_o^2 + p_a^2 = (n_1 k_o)^2 - h_a^2 \tag{6.4}$$

and $k_o = 2\pi/\lambda$. The suffix "a" corresponds to parameters associated with the incident mode. From Maxwell's equations the corresponding magnetic field component in the x direction is:-

$$H_x^i(x,z) = \frac{-\beta_a}{\omega\mu_o} E_y^i(x,z) = Y_a E_y^i(x,z) \tag{6.5}$$

with μ_o the permeability of free space and $Y_a = -\beta_a/\omega\mu_o$, the wave admittance of the incident mode. The coefficient A in (6.1) and (6.2) is now selected such that the incident mode power is unity (per unit length in the y direction) i.e.

$$\frac{1}{2}\mathrm{Re}\int_{-\infty}^{\infty} E_y^i(x,z).H_x^{i*}(x,z).dx = 1 \tag{6.6}$$

where Re denotes "real part off" and * the complex conjugate. After integration,

$$A = \left[\frac{2\omega\mu_o}{\beta_a}\right]^{\frac{1}{4}}\left[2t+d + \frac{\sin(2h_a(2t+d))}{2h_a} + \frac{\cos^2(h_a(2t+d))}{p_a}\right]^{-\frac{1}{2}} \tag{6.7}$$

which only for the symmetrical planar case, as considered here,

reduces to,

$$A = \left[\frac{2\omega\mu_o}{\beta_a(2t+d+1/p_a)}\right]^{\frac{1}{2}} \tag{6.8}$$

by use of (6.3).

We now consider the transmitted fields for the region $z > 0$. From considerations of symmetry the coupled mode in $z > 0$ may be approximated by the superposition of the guided mode in each (isolated) output waveguide that lies in $x > 0$, $z > 0$ at an angle α to the z axis of Figure 6.1 (70), (see also reference (98). i.e.

$$E_y^t(x,z) = B(z)\left[e_y^t(x,z) + e_y^t(-x,z)\right] \tag{6.9}$$

with $e_y^t(x,z)$ the guided mode of the output waveguide that lies in $x>0$, $z> 0$ in isolation. The coefficient $B(z)$ is selected such that the transmitted mode power is unity across any plane parallel to $z = 0$. For small values of α, $B(z)$ is a slowly varying function of z. Thus the x component of magnetic field associated with (6.9) is,

$$H_x^t(x,z) = \frac{-\beta_b}{\omega\mu_o} E_y^t(x,z)\cos(\alpha) = Y_b E_y^t(x,z)\cos(\alpha) \tag{6.10}$$

The suffix "b" refers to parameters associated with the transmitted mode. Calculating $B(z)$ we have:-

$$B(z) = \sqrt{\frac{2}{Y_b}}\left[\int_{-\infty}^{\infty} \left|e_y^t(x,z) + e_y^t(-x,z)\right|^2 dx\right]^{-\frac{1}{2}} \tag{6.11}$$

$B_o = B(z = 0)$ gives,

$$B_o = \sqrt{\frac{1}{Y_b}}\left[\int_{-\infty}^{\infty} \left|e_y^t(x,0)\right|^2 dx + 2\mathrm{Re}\int_{o}^{\infty} e_y^t(x,0).e_y^{t*}(-x,0)\,dx\right]^{-\frac{1}{2}} \tag{6.12}$$

For a small phase tilt of α radians about the y axis of Figure 6.1, the transmitted fields are:-

$$e_y^t(x,0) = \cos(h_b(x-t-d))\ \exp(-j\alpha\beta_b x) \qquad |x-t-d| \leq t \qquad (6.13)$$

$$e_y^t(x,0) = \cos(h_b t)\exp(-p_b(|x-t-d| - t) - j\alpha\beta_b x) \qquad |x-t-d| \geq t \qquad (6.14)$$

$$e_y^t(-x,0) = \cos(h_b(x+t+d))\exp(+j\alpha\beta_b x) \qquad |x+t+d| \leq t \qquad (6.15)$$

$$e_y^t(-x,0) = \cos(h_b t)\exp(-p_b(|x+t+d| - t) + j\alpha\beta_b x) \qquad |x+t+d| \geq t \qquad (6.16)$$

with $$p_b = h_b \tan(h_b t) \qquad (6.17)$$

$$\beta_b^2 = k_o^2 + p_b^2 = (n_1 k_o)^2 - h_b^2 \qquad (6.18)$$

B_o is now evaluated as in (6.12)

$$B_o = \sqrt{\frac{1}{Y_b}}\left[t + \frac{\sin(2h_b t)}{2h_b} + \frac{\cos^2(h_b t)}{p_b} + \text{Re}\cos^2(h_b t)\left[\frac{\exp(-2p_b d)\left[1-\exp(-2j\alpha\beta_b d)\right]}{j\alpha\beta_b} + \frac{\exp\left[-2p_b(t+d)-2j\alpha\beta_b(2t+d)\right]}{p_b + j\alpha\beta_b}\right] + 2\text{Re}\cos(h_b t)\ \exp\left[-p_b(t+2d)-2j\alpha\beta_b(t+d)\right]\left[C(h_b)+C(-h_b)\right]\right]^{-\frac{1}{2}} \qquad (6.19)$$

$$\text{with } C(h_b) = \frac{\sin(t(h_b - 2\alpha\beta_b + jp_b))}{h_b - 2\alpha\beta_b + jp_b} \qquad (6.20)$$

If d is set equal to zero then (6.19) reduces to the same expression as calculated by Anderson (70).

If $e_y^+(x,z)$ is the radiation field in $z > 0$ associated with the guided mode $e_y^t(x,z)$ then, by superposition, the total radiation field in the presence of both output waveguides is,

$$E_y^+(x,z) = e_y^+(x,z) + e_y^+(-x,z) \quad \text{for } z > 0 \qquad (6.21)$$

Using modal othogonality we obtain,

$$\int_{-\infty}^{\infty} e_y^+(x,0).e_y^{t*}(x,0).dx = \int_{-\infty}^{\infty} e_y^+(-x,0).e_y^{t*}(-x,0).dx = 0 \qquad (6.22)$$

which may be written as

$$\int_{-\infty}^{\infty} E_y^+(x,0).E_y^{t*}(x,0).dx = 0 \qquad (6.23)$$

with similar expressions applying to the magnetic field components.

Referring to Figure 6.1 the incident mode at the junction E_y^i excites a transmitted mode TE_y^t. Due to the change in waveguide impedance there is a reflected mode ρE_y^i and radiation fields E_y^- in $z < 0$ and E_y^+ in $z > 0$. Matching the tangential electric and magnetic fields on $z = 0$ plane gives,

$$(1 + \rho)E_y^i(x,0) + E_y^-(x,0) = TE_y^t(x,0) + E_y^+(x,0) \qquad (6.24)$$

$$(1 - \rho)H_x^i(x,0) + H_x^-(x,0) = TH_x^t(x,0) + H_x^+(x,0) \qquad (6.25)$$

It is known (108), that radiation at surface waveguide discontinuities, of type similar to that considered here, is predominantly in the forward direction and this suggests that $E_y^-(x,0)$, $H_x^-(x,0)$ be neglected (70,71,72,75) in equations (6.24) and (6.25) so as to obtain an approximate solution for T and ρ. Accordingly multiplication of (6.24) by $E_y^{t*}(x,0)$ and (6.25) by $H_x^{t*}(x,0)$, followed by integration with respect to x over the $x = 0$ plane, gives, with (6.23),

$$T = \frac{\beta_a\beta_b}{\beta_a+\beta_b} \cdot \frac{1}{\omega\mu_o} \int_{-\infty}^{\infty} E_y^i(x,0).E_y^{t*}(x,0).dx \qquad (6.26)$$

$$\rho = \frac{\beta_a-\beta_b}{\beta_a+\beta_b} \qquad (6.27)$$

The fractions of incident power transmitted to the output waveguides and reflected in the input waveguides are

$$T = |T|^2 \quad \text{and} \quad R = |\rho|^2 \qquad (6.28)$$

respectively. By conservation of power the fraction S

scattered into the surrounding medium is

$$S = 1 - R - T \tag{6.29}$$

Finally we evaluate the integral in (6.26),

$$\int_{-\infty}^{\infty} E_y^i(x,0).E_y^{t*}(x,0).dx = 2B_o \int_o^{\infty} E_y^i(x,0)\left[e_y^{t*}(x,0)+e_y^{t*}(-x,0)\right].dx \tag{6.30}$$

which may be reduced to three parts,

$$I_1 = 2B_o \int_o^d E_y^i(x,0).\left[e_y^{t*}(x,0) + e_y^{t*}(-x,0)\right] .dx \tag{6.31}$$

$$I_2 = 2B_o \int_d^{d+2t} E_y^i(x,0).\left[e_y^{t*}(x,0) + e_y^{t*}(-x,0)\right] .dx \tag{6.32}$$

$$I_3 = 2B_o \int_{d+2t}^{\infty} E_y^i(x,0).\left[e_y^{t*}(x,0) + e_y^{t*}(-x,0)\right].dx \tag{6.33}$$

Omitting details we obtain:-

$$I_1 = AB_o \cos(h_b t)\left[Q(h_a) + Q(-h_a) + R(h_a)+R(-h_a)\right] \tag{6.34}$$

with

$$Q(h_a) = \frac{\exp\left[jd(h_a + \alpha\beta_b)\right] - \exp(-p_b d)}{+ p_b + j(h_a + \alpha\beta_b)} \tag{6.35}$$

$$R(h_a) = \frac{\exp\left[jd(h_a - \alpha\beta_b) - 2p_b d\right] - \exp(-p_b d)}{-p_b + j(h_a - \alpha\beta_b)} \tag{6.36}$$

$$\begin{aligned} I_2 = AB_o \Big[& \exp\left[j(d+t)(h_a+\alpha\beta_b)\right]\left[S(h_b) + S(-h_b)\right] + \\ & \exp\left[j(d+t)(-h_a+\alpha\beta_b)\right]\left[U(h_b) + U(-h_b)\right] + \\ & \cos(h_b t)\left[V(h_a) + V(-h_a)\right]\Big] \end{aligned} \tag{6.37}$$

With,

$$S(h_b) = \frac{\sin(t(h_a + h_b + \alpha\beta_b))}{h_a + h_b + \alpha\beta_b} \tag{6.38}$$

$$U(h_b) = \frac{\sin(t(-h_a + h_b + \alpha\beta_b))}{-h_a + h_b + \alpha\beta_b} \tag{6.39}$$

$$V(h_a) = \frac{\exp\left[-2p_b d + jd(h_a - \alpha\beta_b)\right]\left[\exp\left[-2p_b t + j2t(h_a - \alpha\beta_b)\right] - 1\right]}{-p_a + j(h_a - \alpha\beta_b)} \tag{6.40}$$

$$I_3 = 2AB_o \cos(h_a(2t+d))\cos(h_b t)\left[\frac{\exp(j\alpha\beta_b(2t+d))}{p_a + p_b - j\alpha\beta_b} + \frac{\exp(-2p_b(t+d) - j\alpha\beta_b(2t+d))}{p_a + p_b + j\alpha\beta_b}\right] \tag{6.41}$$

Again, if d is set equal to zero then the above expressions reduce to those calculated by Anderson (70). A computer program to evaluate power transmission for varying junction angle and defect size was written, a flow diagram of which may be found in Appendix A7.

Figures 6.3 and 6.4 show theoretical plots of power transmission v.s. junction half angle for planar waveguide Y-junctions with varying junction defect size propagating the TE_o mode. The device in Figure 6.3 is formed in titanium diffused lithium niobate, while the device shown in Figure 6.4 is fabricated in 7059 glass. In both cases the junction defect is presumed to arise from simple fabrication imperfections, as considered in the above analysis. The effect of junction defects is clearly apparent in the 7059 glass waveguide case, with the power transmission being dramatically reduced, even by relatively small junction defects. However, simple junction defects of this kind do not affect Ti diffused $LiNbO_3$ Y-junctions (Figure 6.3) to the same degree as their 7059 glass counterparts. This is due to the small refractive index difference between the waveguide and the surrounding media, resulting in large evanescent fields which carry a fair proportion of the propagating power. Thus when a guided mode in a Ti diffused $LiNbO_3$ Y-junction

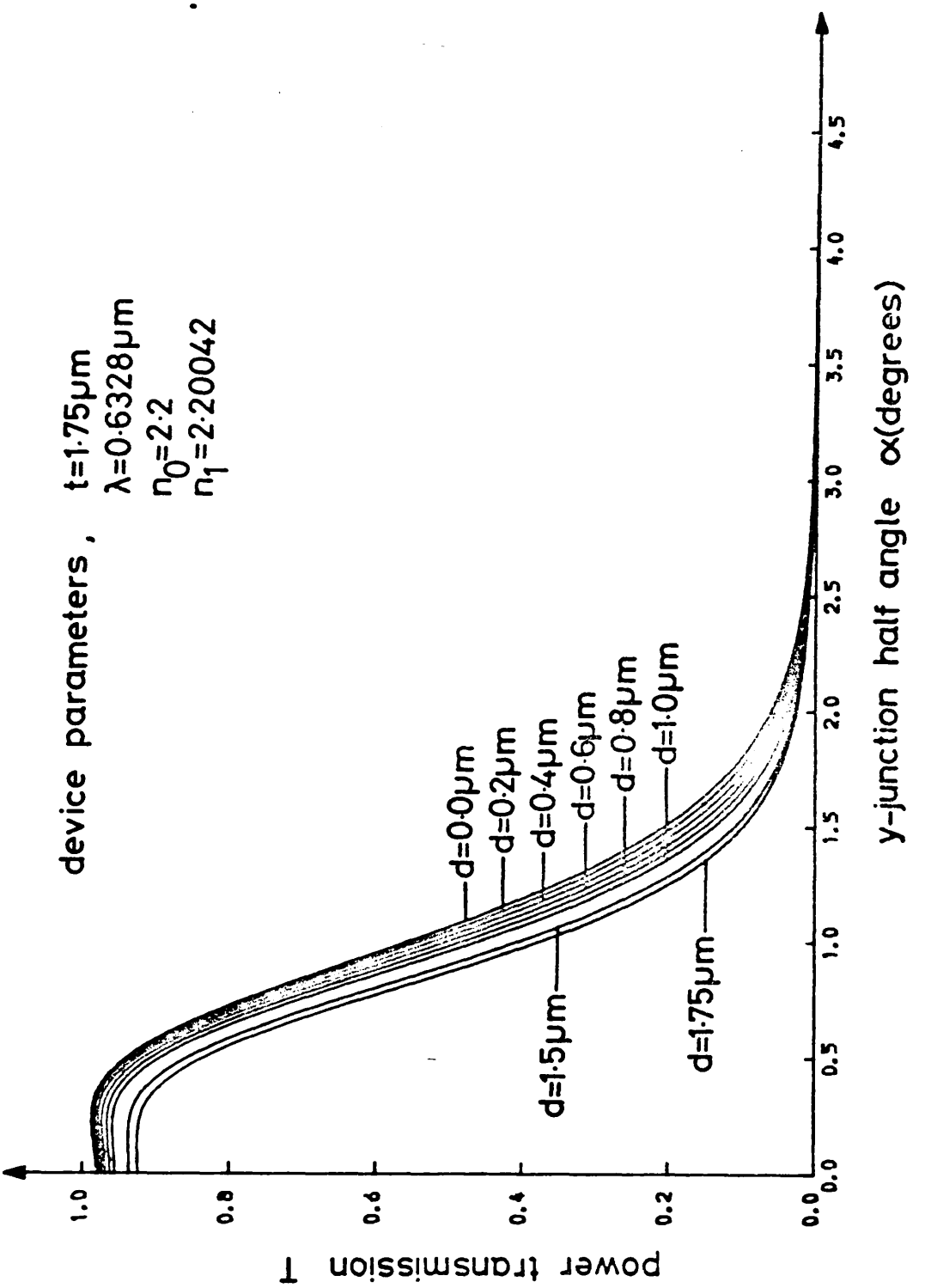

Fig. 6.3 Plot of power transmission for increasing defect size in a $LiNbO_3$ planar waveguide Y-junction

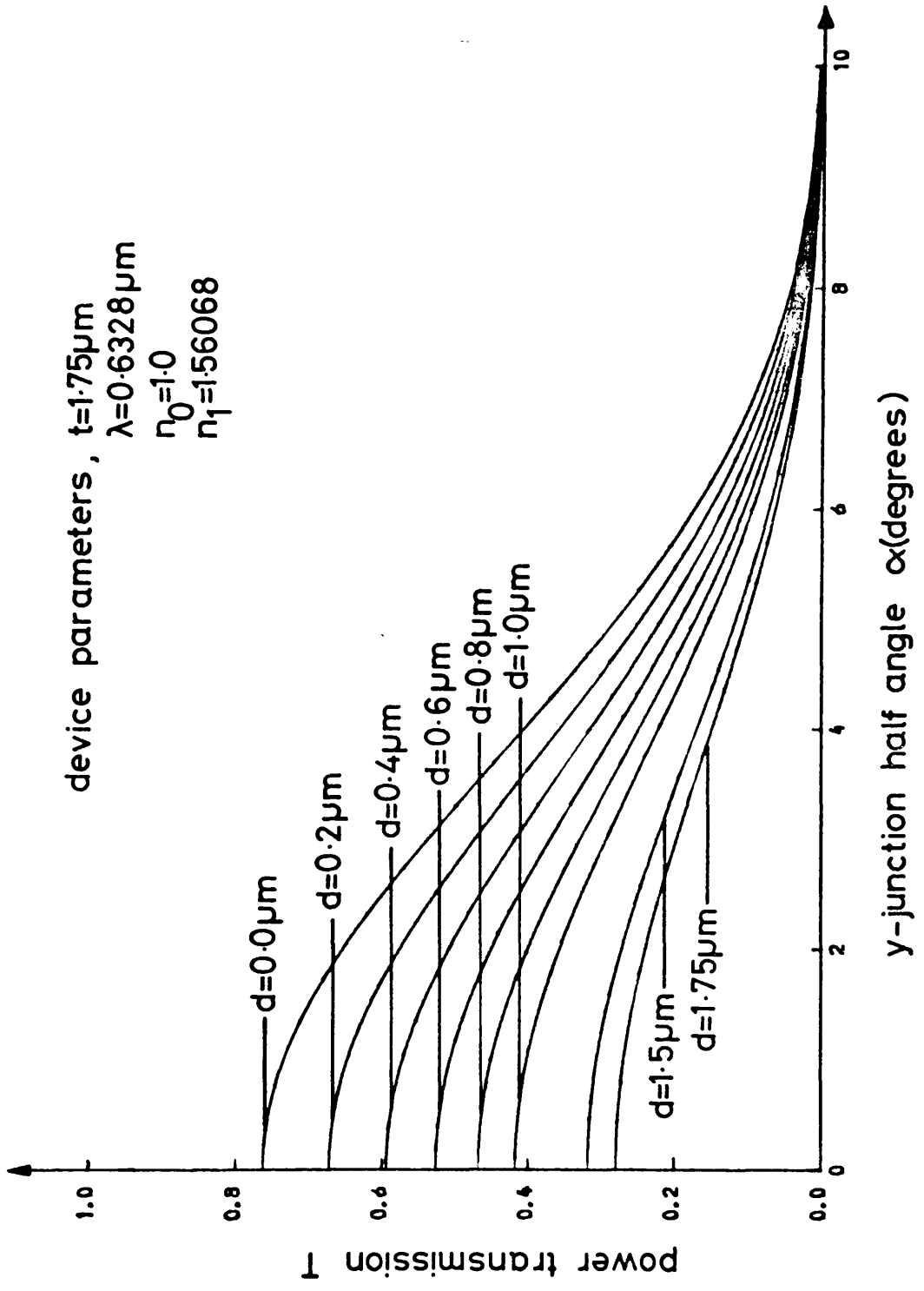

Fig. 6.4 Plot of power transmission for increasing defect size in a 7059 glass planar waveguide Y-junction

encounters a blunt junction wedge, little power is lost to radiation in the junction region as the defect appears only as a small perturbation in the waveguide structure. Junction defects of this kind do not seriously degrade the transmission performance of Ti diffused $LiNbO_3$ Y-junctions. On the other hand, 7059 glass Y-junctions do suffer large junction losses due to the tight field confinement brought about by the comparatively large difference in refractive index between the waveguide and the surrounding media. Even small defects appear as large perturbations in the waveguide structure, causing appreciable amounts of incoming power to be released as radiation at the junction. This effect may also be explained in terms of the "ray optics" approach.

In weakly guiding modes the "rays" of a guided mode impinge at shallow glancing angles on the waveguide/surrounding media interface. As the junction defect becomes larger, a greater proportion of the incident guided mode "rays" impinge on the junction defect at an angle greater than the critical angle and do not undergo total internal reflection. This causes the incident guided mode "rays" to be released as radiation into the surrounding media. This is shown pictorially in Figure 6.5. This effect is in addition to the manner in which the tilted output waveguides affect the device power transmission. As the tilt angle of the output waveguides is increased, then some of the "rays" in the tilted output waveguide arms will impinge on the waveguide/surrounding media interface at an angle greater than the critical angle and will not undergo total internal reflection. This leads to the formation of leaky rays which lose power at

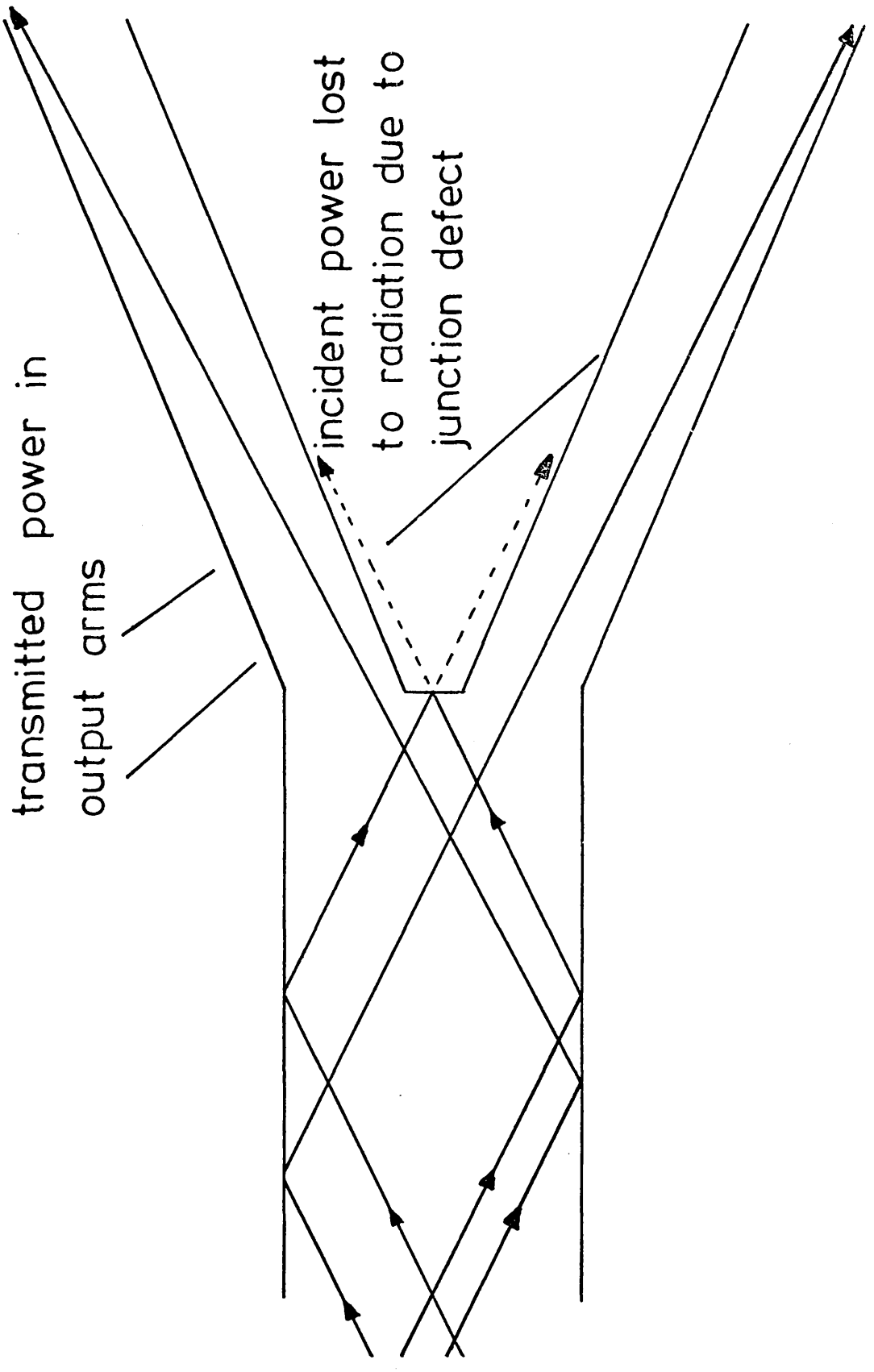

Fig. 6.5 Schematic diagram of junction defect loss mechanism using a RAY OPTICS model

every interface reflection and are rapidly attenuated. This effect decreases the power in the output waveguides. The effect becomes more and more pronounced with increasing tilt angle until at sufficiently large angles all the incident power is lost to radiation, resulting in zero transmitted power. This is the same loss mechanism theory as proposed for the waveguide tilt and the same arguments of Section 5.1 apply to the planar Y-junction, considered here. A pictorial representation of this loss mechanism is shown in Figure 6.6. The "ray optics" approach also indicates that radiation in the backward direction may be ignored. Further details of this will be found in the discussion of Section 5.1.

In both Figures 6.3,4 it should be noted that the transmission of the Y-junction is not unity when α and $d = 0$, as would be expected from physical considerations. This is due to the nature of the analysis which assumes that the waveguide admittance changes discontinuously at $z = 0$, rather than gradually (70, 71). Since superposition implies a greater discontinuity in waveguide admittance than actually exists at the junction, the calculated power transmission T is a lower bound to the actual value (70). For increasing α, the actual variation of waveguide admittance at the junction will tend to the assumed discontinuous variation and the lower bound T will become increasingly accurate as α increases. Thus for the $LiNbO_3$ example for which there is only a small change in waveguide admittance at the junction, i.e. $\beta_a \simeq \beta_b$ and the abrupt change of impedance assumed in the analysis is a close approximation. However, for the 7059 glass example, $\beta_a \neq \beta_b$ there is a large change in waveguide admittance and the assumed abrupt change is no longer such a close approximation.

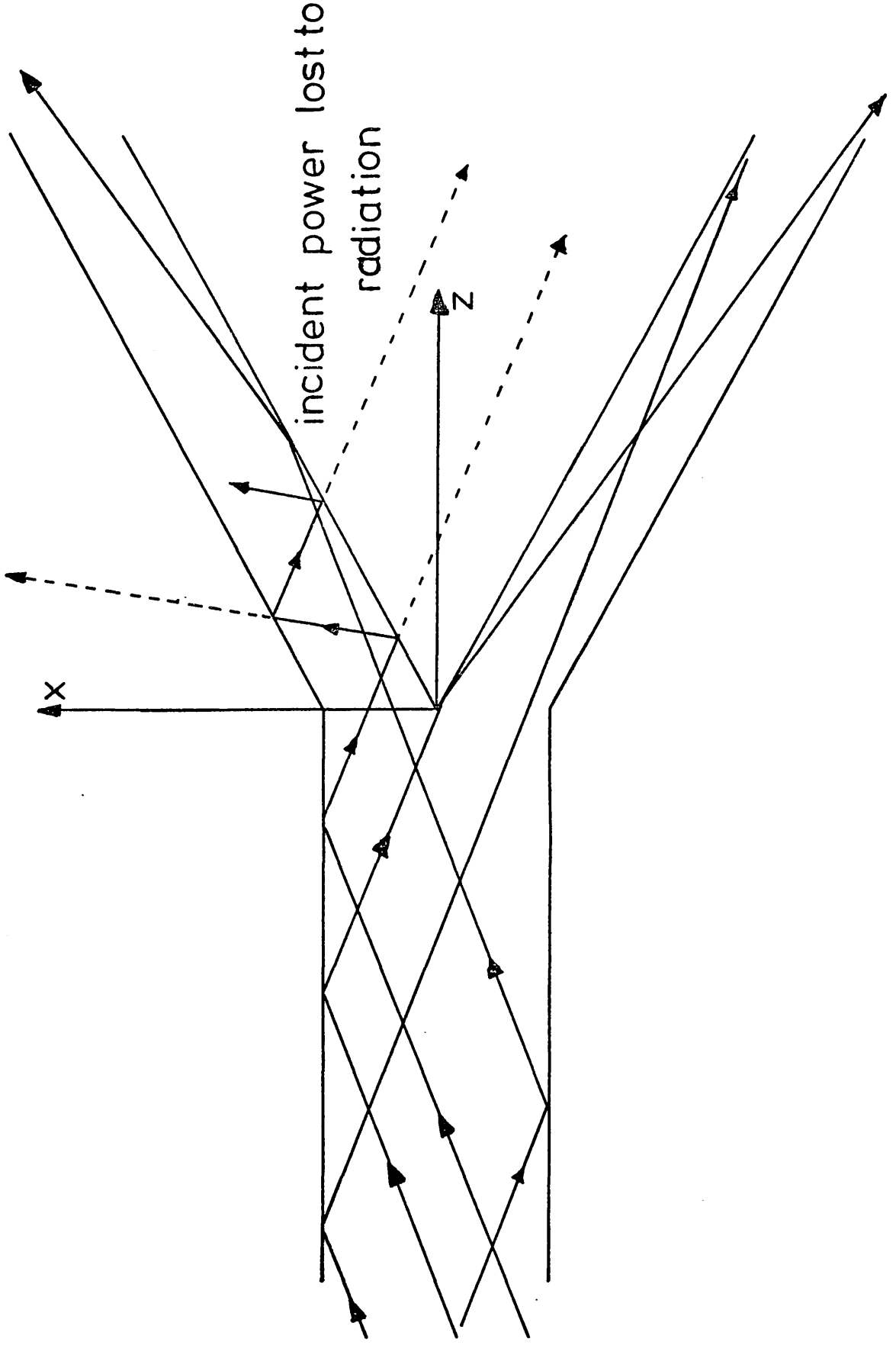

Fig. 6.6 Schematic diagram of power loss due to tilted output waveguides using a RAY OPTICS model

It may be noted from Figures 6.3,4 that as long as the junction defects are kept small, large power transmissions are available over a useful range of angles. This is particularly marked in the case of a large refractive index difference between the waveguide and the surrounding media, i.e. for the 7059 glass example. This fact proves important in later sections, in which the design of single mode stripe waveguide Y-junctions is undertaken.

It is interesting to note that the "ray optics" approach also predicts the small rise in waveguide power transmission with angle, around the 0.25^{o} region in the planar waveguide $LiNbO_3$ Y-junction example of Figure 6.3. This phenomenon arises from a phase matching condition when the difference angle between the incident ($\theta_a = \pm\tan^{-1}(h_a/\beta_a)$) and transmitted ($\theta_b = \pm\tan^{-1}(h_b/\beta_b)$) guided modes corresponds to the Y-junction half angle α_o, i.e. $\alpha = \alpha_o = |\theta_b| - |\theta_a|$. A more detailed and thorough description of this effect will be found in the original paper of Anderson (70).

Section 6.2 shows how the above planar waveguide analysis may be used to predict the transmission performance of trapezoidal stripe waveguide Y-junctions formed in ion etched 7059 glass.

6.2. Stripe Waveguide Y-Junction Power Transmission Using a Modified Planar Waveguide Analysis.

The following method of relating planar waveguide Y-junction power transmission to that of a practical stripe waveguide device is identical to the method described in Section 5.2 and it is only summarised here, although the differences are discussed.

Referring to Appendix B2, we may think of the functions which describe the transverse variation of the electric and

magnetic fields in a two dimensional (stripe) waveguide as being separable. This follows directly from the theory of Marcatili (56) and from the analysis of Appendix B1, and implies that the transverse fields of a waveguide mode in the x direction are independent of the transverse fields in the y direction and vice-versa. Consequently the transmission performance of a stripe single mode Y-junction, which varies only in the x direction (see Figure 6.7), may be calculated directly using the planar waveguide analysis of Section 6.1, but with the planar waveguide device propagation coefficients, β_a and β_b replaced by those of the stripe waveguide device, i.e. β_{za} and β_{zb} (see Appendix B2). Using the result of Appendix B2 and recalling the parameters used in Section 6.1, the following changes are made to allow the theory of Section 6.1 to be used in the design of single mode stripe waveguide Y-junctions. Using Marcatili's (56) notation,

$$\beta_a \text{ becomes } \beta_{za} = k_{za} \tag{6.42}$$

$$h_a \text{ becomes } k_{xa} \tag{6.43}$$

$$p_a \text{ becomes } 1/\xi_{3a} = 1/\xi_{5a} \tag{6.44}$$

$$\beta_b \text{ becomes } \beta_{zb} = k_{zb} \tag{6.45}$$

$$h_b \text{ becomes } k_{xb} \tag{6.46}$$

$$p_b \text{ becomes } 1/\xi_{3b} = 1/\xi_{5b} \tag{6.47}$$

Thus by replacing all the parameters associated with the above variables in the planar waveguide Y-junction analysis of Section 6.1 we may predict the transmission performance of a stripe waveguide (two-dimensional) Y-junction.

Figure 6.8 shows a plot of Y-junction power transmission performance v.s. junction angle for three theoretical waveguides all of the same width. One is a planar Y-junction supporting

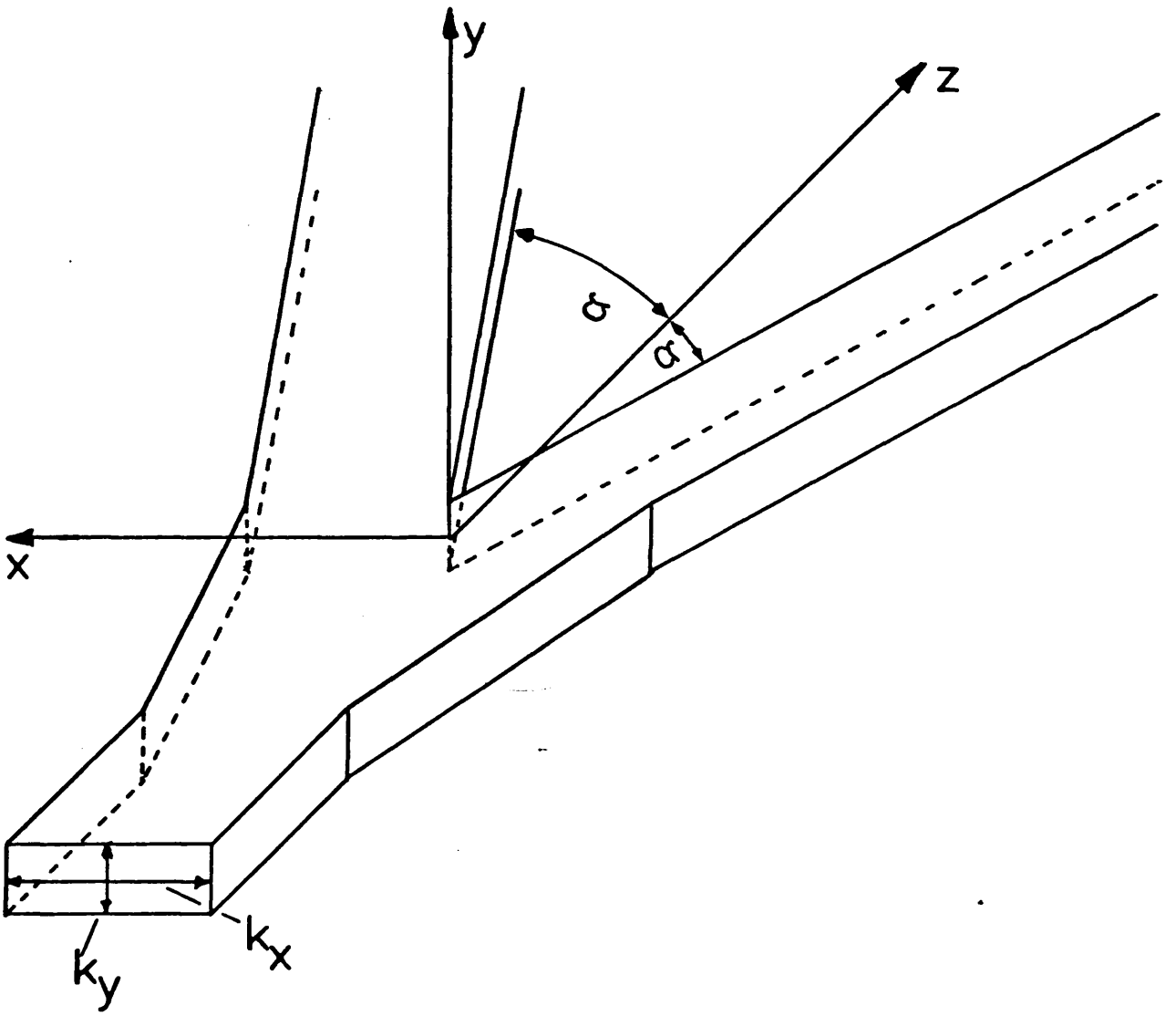

Fig. 6.7 Pictorial representation of uncoupled wave vectors in a stripe waveguide Y-junction

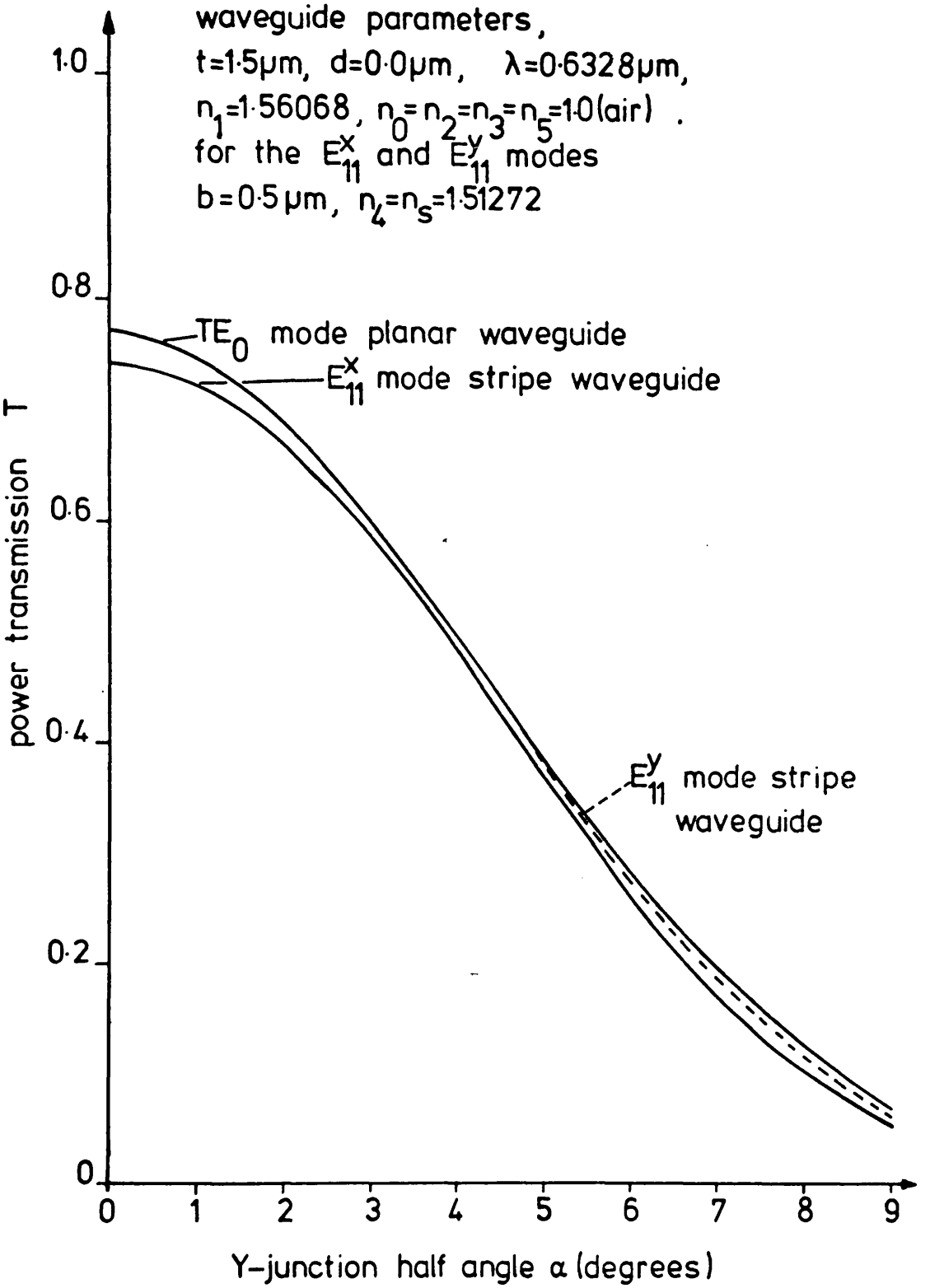

Fig. 6.8 Comparison of power transmission versus junction half angle for TE_0, E^x_{11} and E^y_{11} modes

only the fundamental TE_o mode while the other two are stripe Y-junctions guiding the E_{11}^x and E_{11}^y modes respectively. As can be seen, there is virtually no difference in transmission performance between the TE_o mode planar waveguide and the E_{11}^y mode stripe waveguide. This is to be expected, as the analysis of Appendix B2 shows that a planar waveguide device analysis may be used to predict the transmission performance of the corresponding stripe waveguide device. Thus we would expect very little difference between the transmission curves for a planar waveguide supporting the TE_o mode and a stripe waveguide supporting the E_{11}^y mode, as the stripe waveguide E_{11}^y mode corresponds effectively to a planar waveguide TE_o mode in the plane of the tilt. It is interesting to note that there is very little difference (<3%) between the stripe waveguide E_{11}^y mode, (effectively a planar waveguide TE_o mode in the plane of the tilt) and the E_{11}^x mode, (effectively a planar waveguide TM_o mode in the plane of the tilt). This suggests that the Y-junction analysis may be used to predict the transmission performance of E_{11}^x single mode Y-junctions as well as E_{11}^y single mode Y-junctions. This makes the design of stripe waveguide Y-junctions which support only the fundamental E_{11}^x mode much easier, because the analysis of a planar waveguide Y-junction propagating the fundamental TM_o mode is more complicated than that of the fundamental TE_o mode. It should be noted that the above 7059 glass example of Figure 6.8 displays probably the largest difference in modal propagation parameters between the modes (i.e. between the TE_o, E_{11}^y and E_{11}^x), of any practical device. Many future practical integrated optical devices will be based on active substrates,

e.g. Lithium Niobate or Gallium Arsenide. As both have little refractive index difference between the waveguide and the surrounding media, the difference between the TE_o, E_{11}^y and E_{11}^x modal propagation parameters will be much less than in the above example of Figure 6.8. We may conclude that the above Y-junction analysis will become even more accurate in practical waveguides which display only small refractive index differences between the waveguide and the surrounding media. The lower bound solution of Section 6.1 will also become increasingly more accurate as the difference in refractive index between the waveguide and the surrounding media becomes less. This is due to the fact that waveguides which have only a small refractive index difference between the waveguide and the surrounding media show only a small change in waveguide admittance at the junction, i.e. $Y_a \approx Y_b$ and the assumed abrupt change of admittance used in the analysis is a close approximation (70, 71). This however does not hold so well for the 7059 glass examples, which do display large changes in waveguide admittance at the junction, i.e. $Y_a \not\approx Y_b$, and the assumed abrupt change in admittance is no longer such a close approximation. The lower bound solution of Section 6.1 becomes increasingly inaccurate as the difference in refractive index between the waveguide and the surrounding media becomes larger. However, for most stripe waveguide Y-junctions, the difference in refractive index is such that the lower bound solution should provide a reasonably good idea of expected practical stripe waveguide Y-junction transmission.

The above stripe waveguide Y-junction analysis is compared in Section 6.3 with the transmission performance of experimental ion etched 7059 glass stripe waveguide Y-junctions propagating only the E_{11}^x mode.

6.3. Experimental Investigation of the Transmission Performance of Ion-Etched 7059 Glass Stripe Waveguide Y-Junctions.

6.3.1. Waveguide Design Considerations.

Stripe waveguide 7059 glass Y-junctions were fabricated using the process outlined in Section 4.2. Suitable choice of the waveguide thickness enabled only the lowest order E_{11}^{x} mode to be supported in both the output waveguides, (width 2t) and the tapered input waveguide section, (width at the junction 4t+2d), see Figure 6.1. To fulfil the condition of overall E_{11}^{x} mode propagation calls for careful design of the waveguide mask dimensions. A suitable choice of device dimensions is a waveguide of width 2t = 3 μm tapering to a 6 μm waveguide at the junction before splitting into two 3 μm output arms. Single mode (E_{11}^{x}) operation of the junction section of 6 μm width waveguide required that the 3 μm width output waveguides operated very close to the waveguide cut-off width, thus necessitating accurate control of the waveguide thickness, (see Section 3.2). As explained in Section 5.3 it is not possible using the techniques of Section 4.2 to fabricate stripe waveguides which have the E_{11}^{y} mode as their fundamental, as this would involve making b>>a and $a \simeq \lambda/2$. Thus for the same reasons given in Section 5.3 the waveguide dimensions were chosen such that only the E_{11}^{x} mode could be propagated, even although the theory of Section 6.1 is more directly applicable to E_{11}^{y} modes (quasi TE_{o} mode in the plane of the device), see Sections 6.1 and 6.2.

Due to the nature of the fabrication process (see Section 4.2), Y-junctions with non-perfect wedge tips were formed. As well as reducing the overall device power transmission these defects also effectively increased the size of the junction taper region

waveguide width to 4t+2d, (see Figure 6.1). Depending on the size of d this increase in waveguide width may allow the tapered section of the junction to support more than the fundamental E_{11}^{x} mode. The implications of this effect on device transmission are discussed in the experimental results section.

To correlate the experimental results all waveguide parameters (widths, refractive index etc), are given in a separate table along with each set of power transmission measurements.

6.3.2. Transmission Loss Measurements.

Experimental stripe waveguide Y-junction power transmission measurements were carried out in an identical manner to those of the waveguide tilts (see Section 6.3.2). Due to the limited length of the experimental devices it was possible to measure the propagating power at only two positions; after and before the junction. Thus average waveguide attenuation measurements were restricted to a section of straight waveguide of the same width as the Y-junction output arms (width 2t), which was present on the same substrate. This method was adopted to measure all the experimental stripe waveguide Y-junctions. Due to the limited length of the devices, approximately 15 mm maximum, the accuracy in the measurement of the average waveguide attenuation was limited to ±10%. An average waveguide attenuation of between 4 and 8 dB/cm for single mode stripe waveguides of approximately 3 μm effective width and 0.44 μm thickness was recorded. Use of a better waveguide mask with smoother edges would undoubtedly reduce this figure to a more acceptable level. The reason for this large range in the average waveguide attenuation is thought

to arise from small differences in processing techniques, resulting in waveguides which have rougher edges (see Section 4.2). The next section will compare the above measured results with the theory developed in Section 6.2.

6.3.3. Comparison of Experimental and Theoretical 7059 Glass Stripe Waveguide Y-Junctions.

6.3.3.1. Waveguide Width Measurements.

After the transmission loss measurements were made the Y-junction samples were examined in a scanning electron microscope (S.E.M.) to obtain the waveguide dimensions. Accurate knowledge of these is essential due to the rapid fall in power transmission with increasing junction defect size (2d), and also to enable calculation of the waveguide effective widths. Waveguide width measurements obtained from the S.E.M. have an estimated maximum error of $\pm 0.25\,\mu m$, (see Sections 4.4 and 5.3.3.1). Figure 6.2 clearly shows the blunting effect of the fabrication process on the Y-junction wedge, resulting in the waveguide defect of width 2d.

Using the S.E.M. measurements and knowing the film thickness from the sputtering unit calibration (see Sections 3.1 and 3.2), theoretical curves of power transmission v.s. Y-junction half angle α^{o} using the stripe waveguide Y-junction theory of Section 6.2 were drawn. A flow diagram of the computer program used to calculate this is given in Appendix A8.

6.3.3.2. Theory and Experiment.

Experimental and theoretical plots of power transmission v.s. junction half angle α^{o} for ion-etched 7059 glass Y-junctions are shown in Figures 6.9a, 10a with the corresponding waveguide dimensions being shown in Figures 6.9b, 10b.

Due to the nature of the fabrication process it proved impossible to fabricate Y-junctions with the same defect size for varying angles, therefore the experimental devices could not all be plotted on the same theoretical curve. Thus no theoretical curves were drawn and each experimental point was compared with a theoretical point calculated from the waveguide widths measured on the S.E.M. Figures 6.9a, 10a show measured experimental points and corresponding computed theoretical points with the S.E.M. determined dimensions given in Figures 6.9b, 10b. As can be seen there is reasonably good agreement between theory and experiment, indicating that the theoretical model of Section 6.2 can accurately predict the transmission performance of a stripe 7059 glass ion-etched waveguide Y-junction which has a simple fabrication defect at the junction tip.

6.3.3.3. Discussion of Results.

Figures 6.9a, 10a show a close correlation between experimental and theoretically predicted values of Y-junction transmission performance. Although these diagrams indicate that a junction defect may drastically reduce the transmission performance of a device, they do not illustrate the fall in transmitted power with angle. Figure 6.11 shows a theoretical curve of power transmission v.s. junction half angle for a 7059 glass stripe waveguide Y-junction of $\simeq 3$ μm nominal effective width. Unfortunately only one point on the curve could be verified experimentally as the other devices on the waveguide mask were unable to transmit any power due to the large junction angles involved. Again theory and experiment for this particular point agree well within the estimated experimental error.

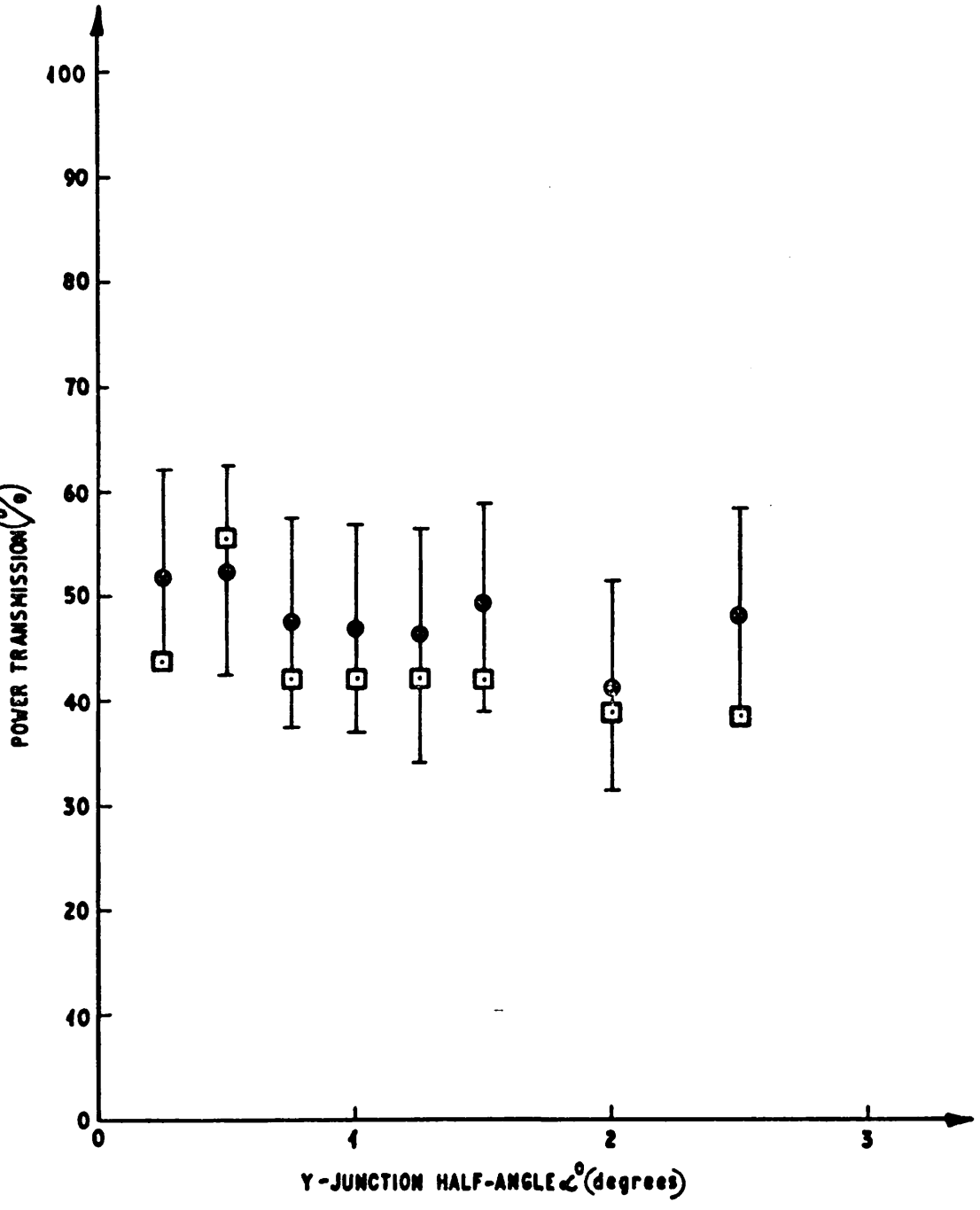

EXPERIMENTAL ● AND THEORETICAL ⊡ POWER TRANSMISSION V.S. Y-JUNCTION HALF ANGLE

Fig 6.9a

TABLE OF EXPERIMENTAL Y-JUNCTION PARAMETERS

Y-JUNCTION HALF ANGLE α (DEGREES)	WAVEGUIDE EFFECTIVE HALF WIDTH t(μm)	WAVEGUIDE DEFECT EFFECTIVE HALF WIDTH d(μm)
0.25	1.96	0.47
0.50	1.80	0.86
0.75	1.78	0.90
1.00	1.78	0.87
1.25	1.78	0.83
1.50	1.78	0.80
2.00	1.86	0.83
2.50	1.81	0.69

WAVEGUIDE THICKNESS b = 0.44 μm

$n_1 = 1.56068$

$n_2 = n_3 = n_5 = n_o = 1.0$ (AIR)

$n_4 = n_s = 1.51272$

Figure 6.9b. Details of Waveguide Dimensions of Figure 6.9a.

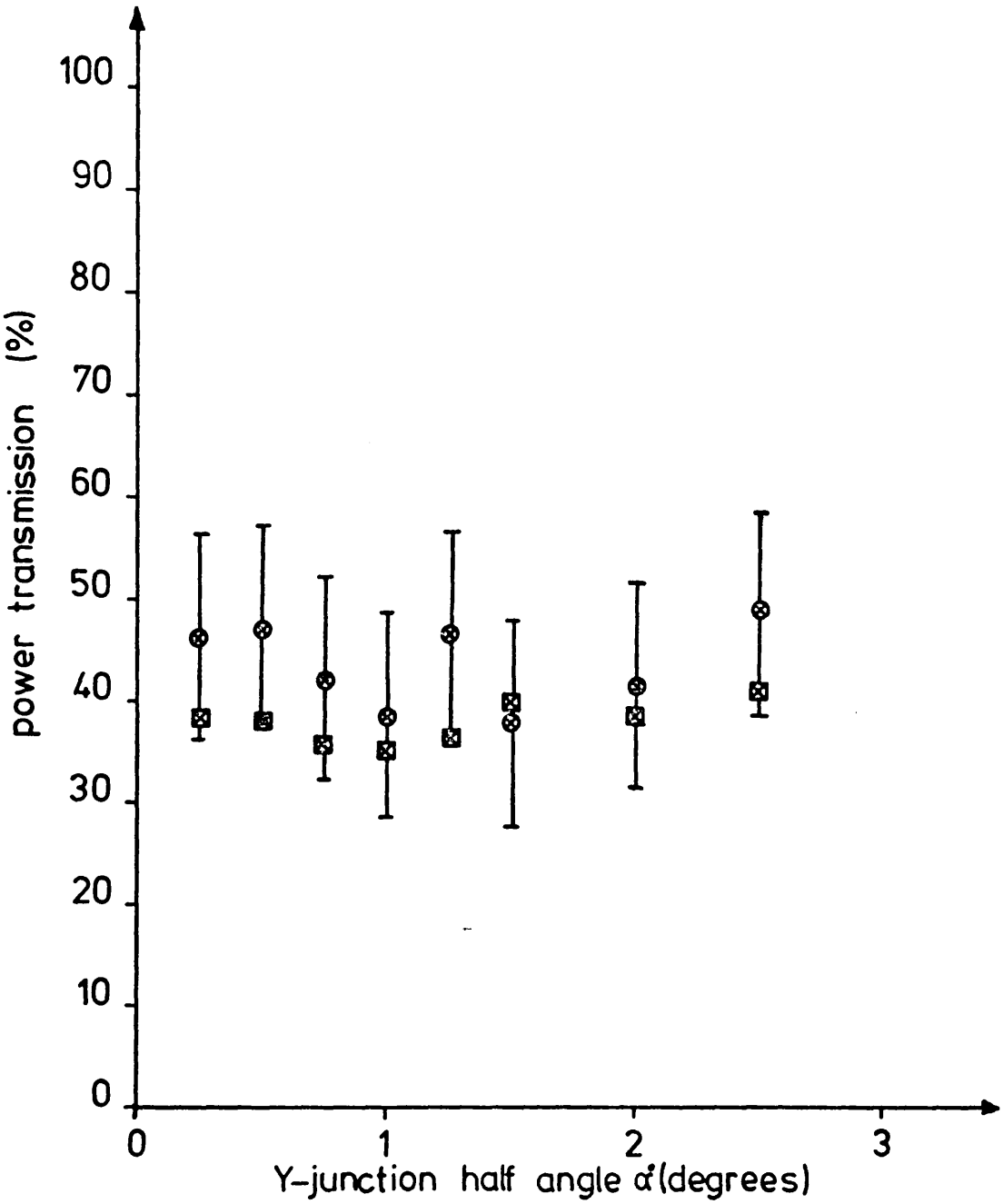

Experimental ⊗ and theoretical ⊠ power transmission v.s. Y-junction half angle

Fig 6.10 a

TABLE OF EXPERIMENTAL Y-JUNCTION PARAMETERS

Y-JUNCTION HALF ANGLE α (DEGREES)	WAVEGUIDE EFFECTIVE HALF WIDTH t(μm)	WAVEGUIDE DEFECT EFFECTIVE HALF WIDTH d(μm)
0.25	1.79	1.11
0.50	1.79	1.11
0.75	1.79	1.21
1.00	1.79	1.21
1.25	1.79	1.09
1.50	1.79	0.90
2.00	1.79	0.84
2.50	1.79	0.59

WAVEGUIDE THICKNESS b = 0.44 μm

$n_1 = 1.56068$

$n_2 = n_3 = n_5 = n_o = 1.0$ (AIR)

$n_4 = n_s = 1.51272$

Figure 6.10b. Details of Waveguide Dimensions of Figure 6.10a.

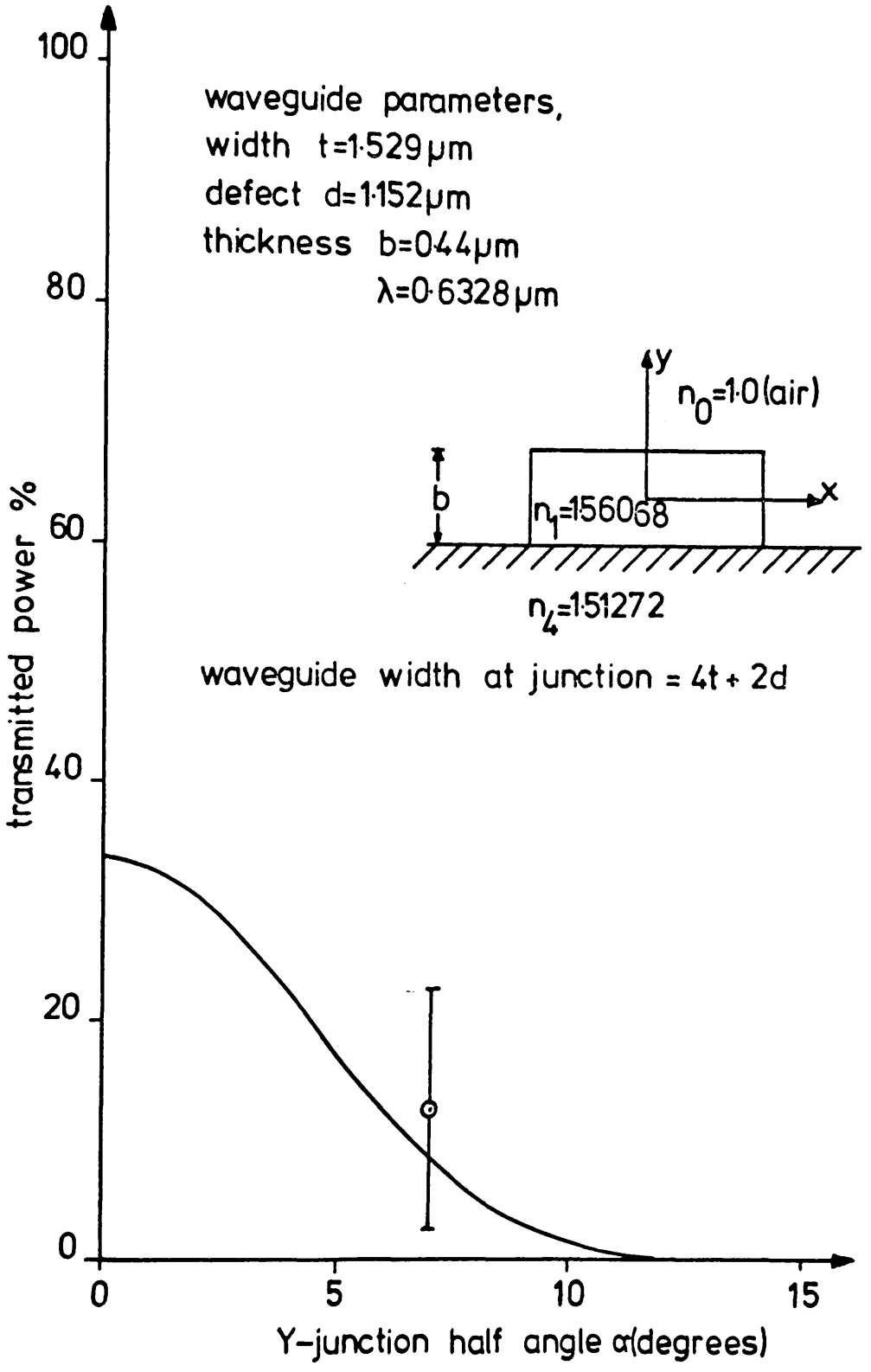

Fig. 6.11 Comparison of theoretical and experimental power transmission for a 7° Y-junction

We may conclude that the theory derived in Sections 6.1 and 6.2 can accurately predict the transmission performance of stripe waveguide Y-junctions. This is especially true when there is little change in admittance between the input and output waveguides. In this case the lower bound solution of Section 6.1 may be regarded as an almost exact solution.

Figures 6.12,13 show the operation of typical ion-etched 7059 glass waveguide Y-junctions. The large power transmission loss induced by the wedge tip fabrication defect is clearly visible as an abrupt change in light intensity at the junction. This indicates that a large proportion of the incident guided mode power is being released to radiation at the junction. This abrupt power loss is much more noticeable than the average waveguide loss of 4 - 8 dB/cm and results in almost 50% of the guided incoming mode power being lost to radiation at the junction. This presents a formidable problem in the design of an efficient stripe 7059 glass waveguide power splitter, and until a more suitable fabrication process is found it would appear that 7059 glass devices of this kind will continue to display large fabrication defects.

As mentioned earlier the ion-etching process tends to increase the size of the waveguide width at the junction, from 4t of the perfect device to 4t+2d of the device with a defect. This allows the possibility of more than one mode type to be present in the junction region due to power being scattered into a higher order mode(s) in the tapered section of waveguide directly before the junction. It is thought likely (although no experimental evidence was found), that in many of the devices tested a small proportion of the incident power was being

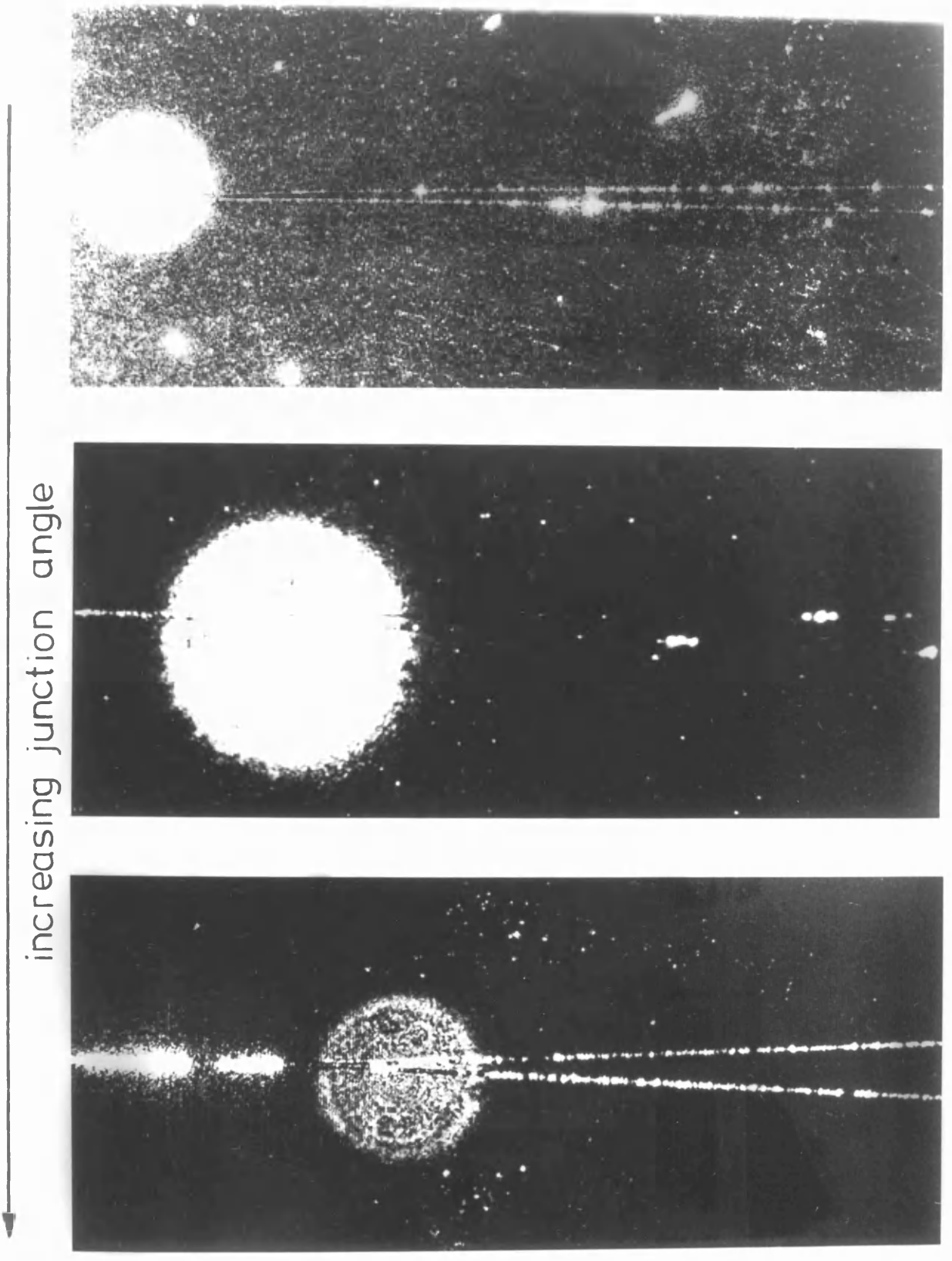

Fig. 6.12 Micrographs of typical working ion-etched 7059 glass Y-junctions

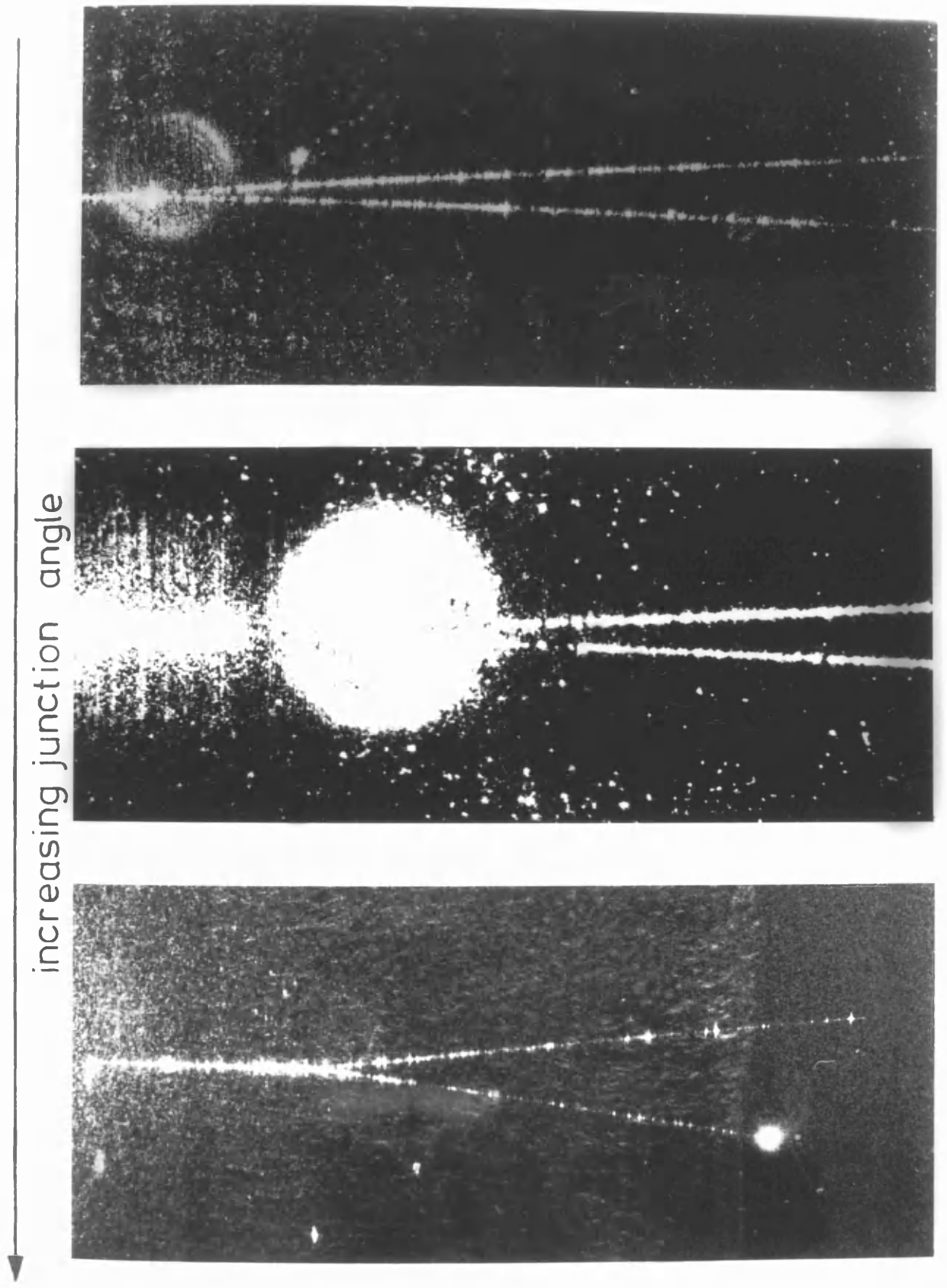

Fig. 6.13 Micrographs of typical working ion-etched 7059 glass Y-junctions

propagated in the E_{21}^{x} mode in addition to the major power contribution from the fundamental E_{11}^{x} mode. As the E_{21}^{x} mode is antisymmetric about the axis of propagation (z axis) there is a field intensity minimum at $x = 0$. Thus when the E_{21}^{x} mode encounters a blunt junction of the kind present in ion-etched 7059 glass waveguides, the power lost to radiation should be much reduced over the E_{11}^{x} mode which has a point of maximum field intensity at $x = 0$. This will have the effect of reducing the loss effect of the blunt wedge, thus increasing the overall device power transmission. From these considerations an ion-etched 7059 glass Y-junction may be more useful as a mode convertor than as a power divider, being able to split an incident E_{21}^{x} mode into two E_{11}^{x} modes which are in antiphase with respect to each other in the output waveguides. This effect may find uses in an active waveguide medium where an active Y-junction could perform some signal processing function.

An interesting by-product of the ion-etching process is the formation of a steep waveguide taper in the junction wedge. This is formed in an identical manner to the trapezoidal edges of the waveguide and results in a form of taper coupler (36) which allows some of the incident guided mode power to leak into the substrate and thus to radiation. Tien et al (37) have already reported on such a device in planar form, and it is interesting to note the near-field radiation pattern observed by us is identical to that observed by Tien. Figure 6.14 shows such a near-field pattern observed in a stripe single mode 7059 glass Y-junction. The nature of this taper coupler type loss mechanism is more akin to that proposed for titanium diffused lithium niobate Y-junctions (see Section 6.4) than to that of the simple junction defect kind, as considered in the

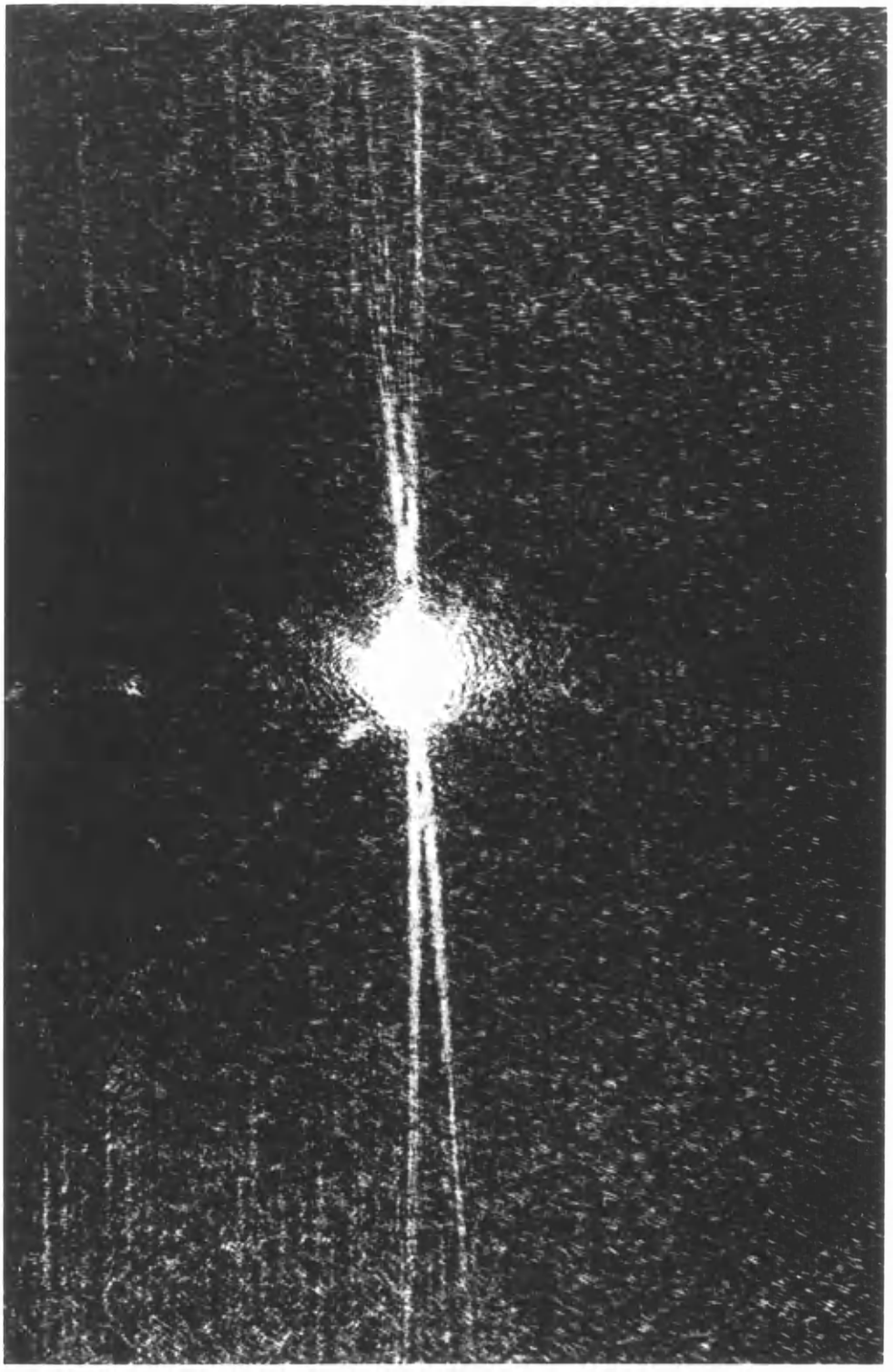

Fig. 6.14 Near field radiation pattern from the junction taper of an ion-etched 7059 glass Y-junction

analysis of Section 6.1. However, the above near-field radiation pattern was not observed in every experimental ion-etched 7059 glass Y-junction and was not observed at all in any of the experimental ion-etched 7059 glass waveguide power splitters (see Section 7.3.4.3). Therefore, it would seem most likely that the main power loss mechanism of 7059 glass branching waveguide devices (Y-junction, power splitter, etc.) is that of the simple junction defect kind, as included in the analyses of Section 6.1 and 7.1.

An attempt was made to measure the reverse power transmission performance of a stripe waveguide Y-junction by launching light into the two branching waveguide output arms and measuring the transmitted power in the input waveguide. However, this proved impracticable due to the small length of the output branching waveguides, approximately 4 mm in a total device length of 15 mm, which made it impossible to measure the power in the branching waveguides before the junction, due to the close proximity of the input prism. A purely visual observation of the device indicated that it may work better in reverse due to the junction defect having little effect when the device is used with inputs and outputs interchanged. Figure 6.15 shows a photograph of a Y-junction operating in this manner. As can be seen there is little radiation from the junction region, indicating a more efficient transfer of power. At first sight this would tend to violate reciprocity (99), as being a passive device in isotropic media the Y-junction should also be a reciprocal device. This can be easily shown to be the case by considering the analysis of the waveguide structure of Section 6.1 the other way round. That is, by launching

the incident mode into the two branching waveguides and combining the power at the junction into a transmitted mode in the tapered section of waveguide after the junction. Carrying out the analysis in this way results in exactly the same expressions for transmitted, reflected and radiated power as those found in Section 6.1 (equations 6.28 and 6.29). However, this analysis relies on the fact that the incident mode(s)in each of the branching waveguides is launched with the same phase and power level. If this is not the case the power transmission need not be the same for both propagation directions. This may be the cause of the apparent increase in power transmission of the device shown in Figure 6.15, as it is impossible to guarantee when using a prism coupler that each of the guided modes in the branching waveguides was launched with the same phase and power. Therefore, it is most likely that the device was not operating under the usual Y-junction excitation conditions when power was launched into the two branching waveguides. Due to the lack of any quantitative measurements, caution should be exercised as it is possible that the apparent increase in device transmission was not actually taking place. Because of this, no conclusions can be drawn from the above observation other than the fact that a further more quantitative investigation is required.

Since ion-etched 7059 glass waveguides have a large refractive index difference between the waveguide and the surrounding media, the phase mismatch between the incident and transmitted modes at the junction is small (70), (see earlier). Thus they are relatively insensitive to junction angle, and

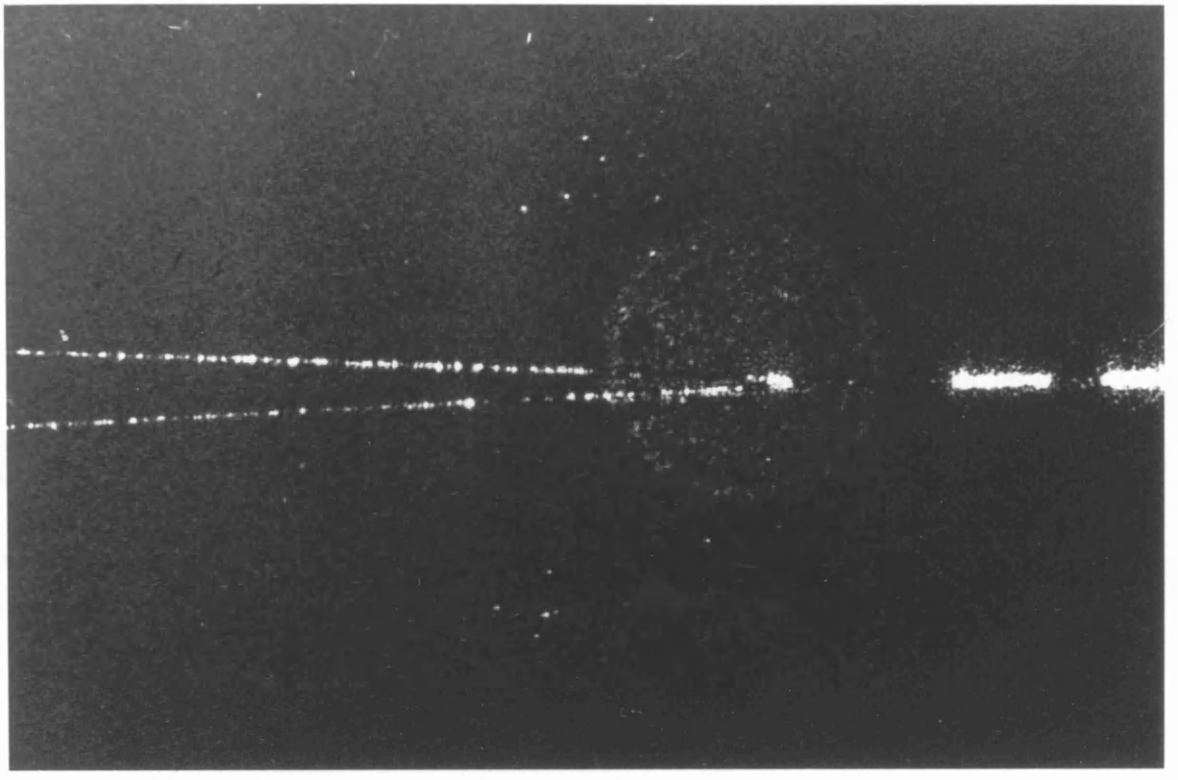

Fig. 6.15 Micrograph of a Y-junction operating in reverse. The light is being launched from the two branching arms

useful devices may be manufactured with total enclosed angles of 10^{o} or more. If the large junction loss can be eliminated by the use of an alternative fabrication technique, then stripe waveguide 7059 glass Y-junctions could find many applications in passive integrated optical circuits.

6.4. Experimental and Theoretical Comparison of the Transmission Performance of Titanium Diffused Lithium Niobate Stripe Waveguide Y-Junctions.

The incentive for most of the research presented in this chapter was brought about by the failure of the theoretical model of Anderson (70) to predict accurately the transmission performance of active stripe waveguide Y-junctions formed in Ti diffused $LiNbO_3$ (53). Measurements show that the experimentally determined power transmission of a symmetric passive Y-junction formed in Ti diffused $LiNbO_3$ is much less than would be expected from the theoretical calculations of Anderson (70), (see Figure 6.16).

6.4.1. Theoretical Loss Model.

To account for the discrepancy between theory and experiment in the curves of Figure 6.16 the loss model in the analysis of Section 6.1 was modified.

The junction defects arising in the fabrication of Ti diffused $LiNbO_3$ Y-junctions are not of the straight forward wedge defect kind as considered in Section 6.1, but arise from the lateral diffusion of Ti occurring in the junction region during the fabrication process. Sideways diffusion of the Ti in the $LiNbO_3$ will tend to increase the blunting effect of a non-perfect wedge formed during the lithographic

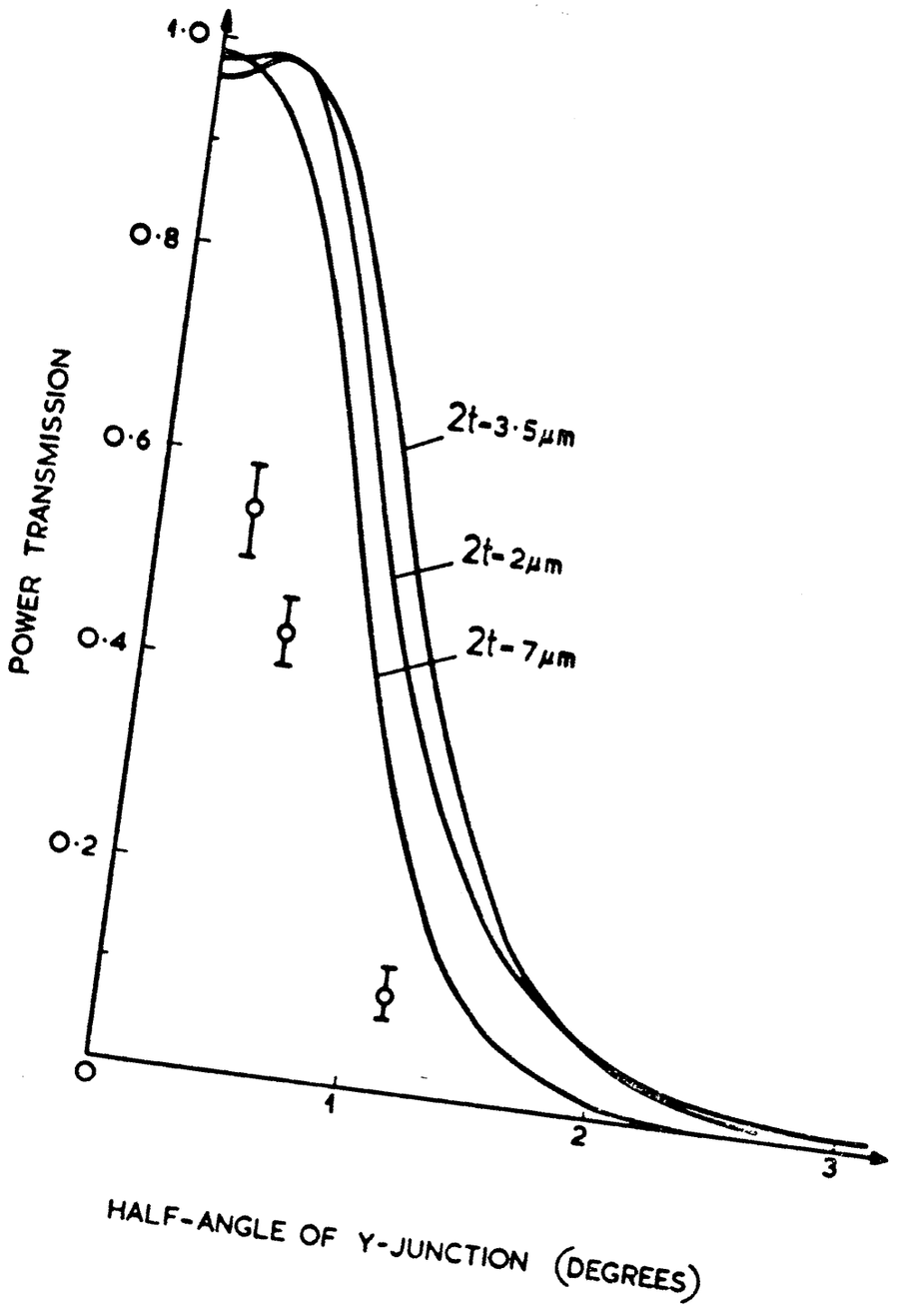

Fig. 6.16 Plot of power transmission v.s. junction half angle for $LiNbO_3$ stripe waveguide Y-junctions (after reference [53], fig. 3)

stage and, in addition will result in a local increase in refractive index in the vicinity of the junction tip. Any power incident on this area is immediately converted to guided mode of this higher index region. As the power propagates away from the junction the effect of the lateral Ti diffusion becomes less and less as the branching output waveguides move further apart. Thus the power incident at the junction encounters a refractive index taper which gradually falls to the substrate value some distance from the junction. The effect of this is to form a type of taper coupler (37) similar in operation to that discussed in Section 6.3.3.3, which removes all the power incident on the defect and releases it to radiation in the substrate. This results in a Y-junction with a highly absorbing tip.

To model this theoretically we consider all the power incident on the defect region 2d to be perfectly absorbed and make no contribution to the transmitted mode power. This requires that certain expressions in the analysis of Section 6.1 are set equal to zero. Thus when evaluating the integral in (6.12) we ignore the term

$$2\ \mathrm{Re}\int_{o}^{d} e_y^{t}(x,0).e_y^{t*}(-x,0).dx$$

and set it equal to zero, as this area deals with the superposition of fields across the defect region. Since the defect region is of a higher refractive index than that of the waveguides, all the power in the evanescent fields of this area is absorbed. Similarly we set I_1 of (6.31) equal to zero for the same reasons, as there can be no transmitted mode in this region of higher refractive index. When d = 0, the modified analysis again correctly reduces to that of the simpler case considered by Anderson (70).

As the fundamental mode of Ti diffused $LiNbO_3$ stripe

waveguides is weakly guided, the β values of the waveguides are close to their planar waveguide equivalents and we may use the planar waveguide analysis of Section 6.1 to predict the transmission performance, (see reference 53 for full details). As such all the theoretical curves of power transmission v.s. junction half angle presented in this section are obtained from the planar analysis of Section 6.1 with the modified loss model changes, as detailed above, included.

6.4.2. Results.

Figure 6.17 shows a graph containing experimental points and theoretical curves for stripe waveguide Y-junctions formed in Ti diffused $LiNbO_3$. Three of the points were measured by Sasaki (53) and are identical to those of Figure 6.16. The fourth point was obtained by R. Esdaile (95) on a device fabricated and measured in an identical manner to those of Sasaki's. The theoretical curves are drawn for various sizes of junction defect, with the curve for d = 1.2 μm chosen as it gives the best curve fit to the measured experimental points. As can be seen the experimental and theoretical curves agree to within the estimated error of measurement.

As d increases we see that the overall power transmission is less for small angles but tends to increase again around 1.8°, to give a value of transmission larger than would be expected from a perfect Y-junction (i.e. d = 0). This effect can be related to the incident and transmitted mode phase mismatch combining with the junction defect to form a complex transmission function. For small defects very little power is lost at the junction and the phase mismatch, i.e. the wavefront tilt between the incident and transmitted modes is the dominant factor,

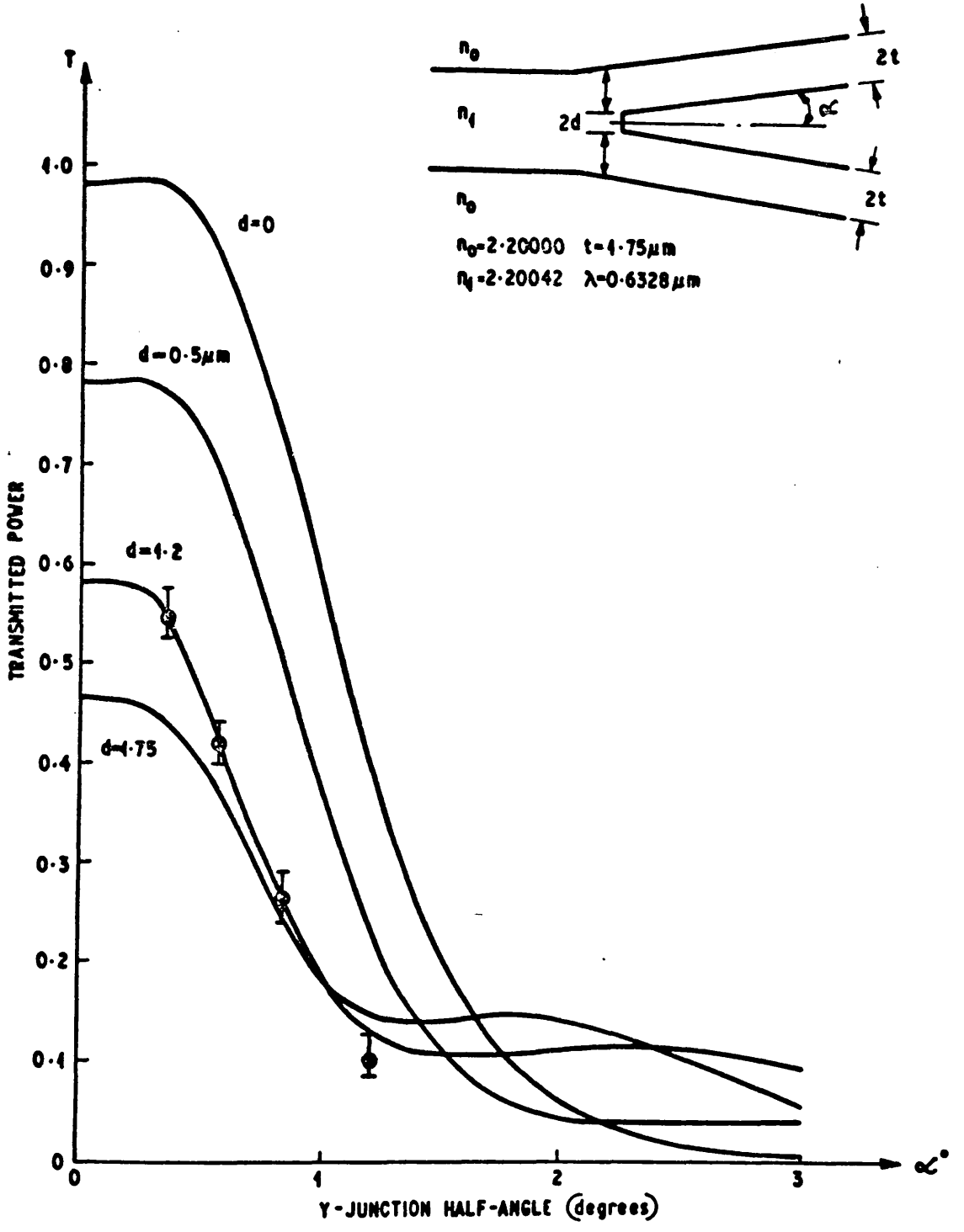

Fig. 6.17 EFFECT OF WEDGE-TIP IMPERFECTION UPON Y-JUNCTION TRANSMISSION

reducing the power transmission rapidly with increasing angle α. However, as the junction defect becomes larger more transmitted power is lost to the increased defect size, but at the same time the effect of the phase mismatch is reduced due to the separation of the output waveguides becoming larger with increasing defect size. This leads, (theoretically at least) to larger power transmissions becoming available at certain angles of α that could not be obtained from a perfect device (see Figure 6.17). This effect is only noticeable in waveguides which have a very small refractive index difference between the waveguide and the surrounding media, and would not, for example, be found in ion-etched 7059 glass waveguides which have a large refractive index difference. As the above mentioned effect is of second order, it has no real practical usefulness and as such will be discussed no further.

6.4.3. Conclusion.

By introducing a perfectly absorbing wedge tip defect into the theoretical model of Section 6.1 the transmission performance of experimental Ti diffused $LiNbO_3$ Y-junctions may be predicted more accurately. Due to the non-availability of the defect parameters (size, refractive index, etc.), a curve fit to the measured experimental points had to be employed. For the analysis to become more directly applicable to practical devices, knowledge of the afore-mentioned parameters is essential.

6.5. Conclusions.

By introducing a modification into the waveguide geometry of the perfect planar waveguide Y-junction considered by

Anderson (70), the transmission performance of stripe single mode Y-junctions fabricated in both ion-etched 7059 glass and Ti diffused $LiNbO_3$ may be predicted. Results obtained indicate that the analysis is equally valid for both E_{11}^x and E_{11}^y modes, and in the Ti diffused $LiNbO_3$ waveguide case the planar waveguide model may be used. In order to construct efficient Y-junctions with low transmission loss a means must be found to fabricate more precise Y-junction wedges. This criterion may be offset by the use of waveguides which have a small refractive index difference between the waveguide and the surrounding media.

CHAPTER 7.

CHAPTER 7. DESIGN FABRICATION AND EVALUATION OF 7059 GLASS SINGLE MODE STRIPE WAVEGUIDE POWER SPLITTERS.

This device follows logically from the stripe waveguide Y-junctions of Chapter 6. In essence it consists of a Y-junction with only one of the output arms at an angle to the input arm which passes straight through, (see Figure 7.1). By varying the angle of the side output arm, the ratio of the powers in the two output arms may be varied. Yajima (76) has already reported a planar version of this device and has shown that it may be used as a mode filter or mode convertor.

The object of this study was to design and fabricate a single mode stripe waveguide power splitter which could be used to provide a reference power level of a known ratio to the power in the main waveguide. A device of this type could find important applications in future integrated optical signal processing devices. By extending the idea to an active medium such as Ti diffused $LiNbO_3$, an electro-optic variable power switch could be conceived, similar to that of Sasaki's (6) but with the advantage of having a preset power ratio in the output arms, depending on the angle of the tilted arm.

Both Yajima (74) and Burns and Milton (75) have analysed an asymmetrical Y-junction (power splitter); however, both analyses neglect the effect of phase tilt (70) and consider only coupling between the output waveguides. The analyses are restricted to very small angles only.

It is the purpose of this chapter to compare predicted and experimental values of power transmission and power ratio between the output waveguides for power splitters formed in stripe ion-etched 7059 glass waveguides. Anderson's (70)

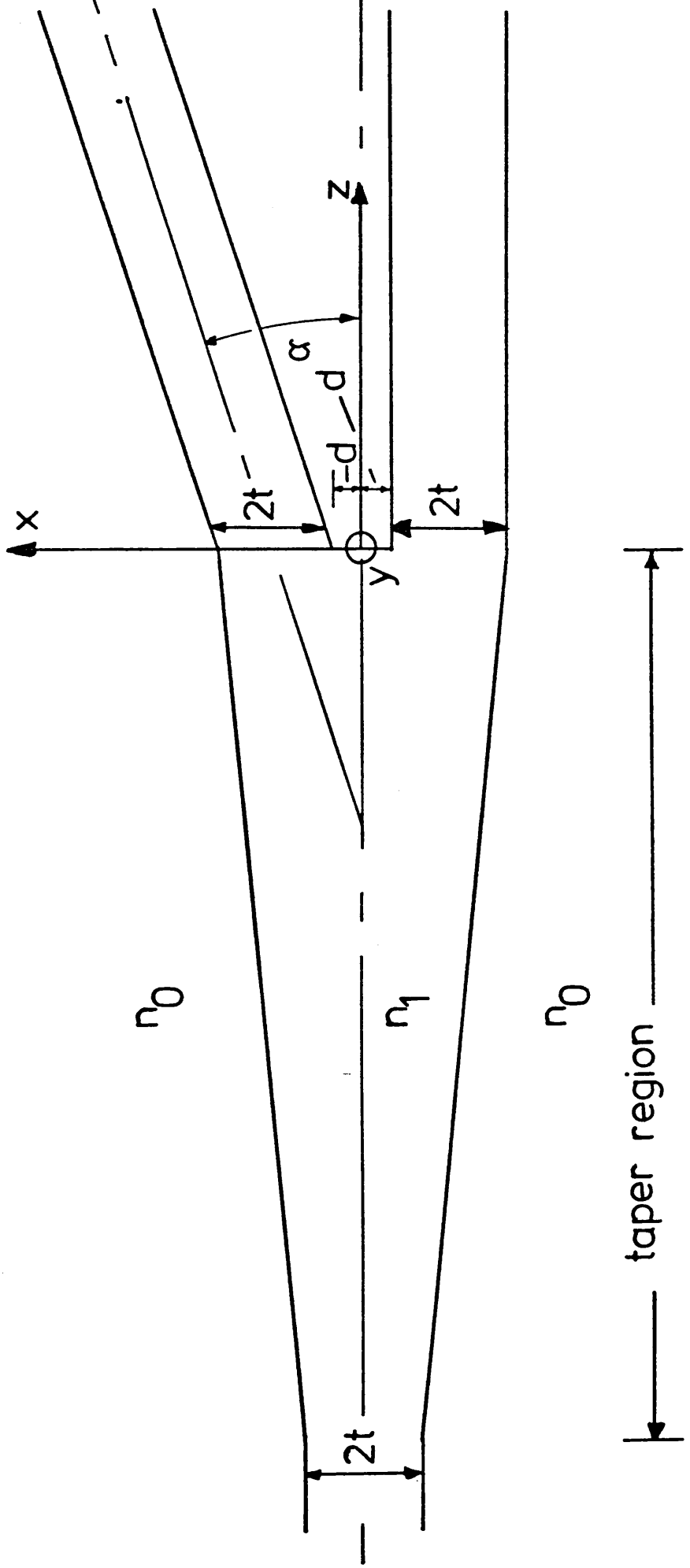

Fig. 7.1 Planar waveguide power splitter with a blunt wedge

theory, which makes due allowance for phase tilt, is modified to account for the asymmetric nature of the power splitter and also for the wedge defect formed in the junction as a result of the fabrication process. This theory provides a close lower bound for the power transmission of a power splitter formed in symmetrical planar waveguide. This theoretical lower bound is then used in an identical manner to that of Chapter 6 and is extended to the case of two dimensional (stripe) waveguides. The transmission performance of experimental stripe 7059 glass power splitters is then compared with the theoretically computed values.

7.1. Theoretical Analysis of the Transmission Performance of a Planar Waveguide Power Splitter.

This analysis follows closely the methods developed by Anderson in (70) and (53). Referring to Figure 7.1 the structure to be analysed consists of an asymmetric Y-junction (power splitter) with a blunt wedge at the junction tip. Inclusion of this defect is necessary, as blunting of the wedge tip occurs during the fabrication process as in the Y-junction case (see Section 6.1).

As usual the solution obtained in this analysis requires that radiation in the backward direction from the junction be ignored. The reasons for this are explained below and the justification for the assumption is presented in Appendix D1. The method of analysis is almost identical to that of the Y-junction and many expressions are the same. As most of the assumptions made in the analysis are identical to those of Anderson (70), (and of Chapter 6), many small stages of the analysis

are omitted in the interests of brevity. Only the fundamental TE_o mode is considered.

Referring to Figure 7.1 it is assumed that the transmission coefficient of the tapered section of waveguide at the junction is close to unity, so that interaction between the taper and the output waveguides is negligible (70, 71). For $z \leqslant 0$, the incident electric fields of the fundamental TE_o mode are,

$$E_y^i(x,z) = A \cos(h_a x)\exp(-j\beta_a z) \qquad |x| \leqslant 2t+d \tag{7.1}$$

$$E_y^i(x,z) = A \cos(h_a(2t+d))\exp(-p_a(|x|-2t-d)-j\beta_a z) \qquad |x| \geqslant 2t+d \tag{7.2}$$

with $$p_a = h_a \tan(h_a(2t+d)) \tag{7.3}$$

$$\beta_a^2 = k_o^2 + p_a^2 = (n_1 k_o)^2 - h_a^2 \tag{7.4}$$

with $k_o = 2\pi/\lambda$. The suffix "a" corresponds to parameters associated with the incident mode. From Maxwell's equations we have,

$$H_x^i(x,z) = \frac{-\beta_a}{\omega\mu_o} E_y^i(x,z) = Y_a E_y^i(x,z) \tag{7.5}$$

The coefficient A in (7.1) and (7.2) is as usual chosen such that the incident mode power is unity (per unit y length) i.e.,

$$\frac{1}{2}\,\mathrm{Re}\int_{-\infty}^{\infty} E_y^i(x,z).H_x^{i*}(x,z).dx = 1 \tag{7.6}$$

After integration,

$$A = \sqrt{\frac{2\omega\mu_o}{\beta_a}}\left[2t+d + \frac{\sin(2h_a(2t+d))}{2h_a} + \frac{\cos^2(h_a(2t+d))}{p_a}\right]^{-\frac{1}{2}} \tag{7.7}$$

which only for the symmetrical planar case, as considered here, reduces to

$$A = \sqrt{\frac{2\omega\mu_o}{\beta_a}}\left[2t+d+1/p_a\right]^{-\frac{1}{2}} \tag{7.8}$$

by use of (7.3).

We now consider the transmitted fields for the region $z>0$.

The coupled mode in $z>0$ may be approximated by,

$$E_y^t(x,z) = B(z)\left[\gamma e_1^t(x,z) + e_2^t(x,z)\right] \tag{7.9}$$

with $e_{1,2}^t(x,z)$ the guided mode of the output waveguide in isolation. γ is a constant to account for the difference in power levels in the two output waveguides. The coefficient $B(z)$ is now selected such that the transmitted mode power is unity across any plane parallel to $z = 0$. For small values of α, $B(z)$ is a slowly varying function of z, thus the magnetic field component associated with (7.9) is,

$$H_x^t(x,z) = \frac{-\beta_b}{\omega\mu_o} E_y^t(x,z)\cos(\alpha) = Y_b E_y^t(x,z)\cos(\alpha) \tag{7.10}$$

For small α $\cos(\alpha) \approx 1$, $\sin(\alpha) \approx \alpha$, calculating $B(z)$ we have,

$$B(z) = \sqrt{\frac{2}{Y_b}}\left[\mathrm{Re}\int_{-\infty}^{\infty}\left[\gamma e_1^t(x,z)+e_2^t(x,z)\right]\left[\gamma e_1^t(x,z)+e_2^t(x,z)\right]^*.dx\right]^{-\frac{1}{2}} \tag{7.11}$$

and for $B_o = B(z=o)$,

$$B_o = \sqrt{\frac{2}{Y_b}}\left[\mathrm{Re}\int_{-\infty}^{\infty}\left[\gamma e_1^t(x,o)+e_2^t(x,o)\right]\left[\gamma e_1^t(x,o)+e_2^t(x,o)\right]^*.dx\right]^{-\frac{1}{2}} \tag{7.12}$$

For a small phase tilt of α radians about the y axis, the transmitted field components are,

$$e_1^t(x,o) = \cos(h_b(x-t-d))\exp(-j\alpha\beta_b x) \qquad |x-t-d| \leq t \tag{7.13}$$

$$e_1^t(x,o) = \cos(h_b t)\exp(-p_b(|x-t-d| - t) - j\alpha\beta_b x) \qquad |x-t-d| \geq t \tag{7.14}$$

$$e_2^t(x,o) = \cos(h_b(x+t+d)) \qquad |x+t+d| \leq t \tag{7.15}$$

$$e_2^t(x,o) = \cos(h_b t)\exp(-p_b(|x+t+d| - t)) \qquad |x+t+d| \geq t \tag{7.16}$$

with $p_b = h_b \tan(h_b t)$ (7.17)

$$\beta_b^2 = k_o^2 + p_b^2 = (n_1 k_o)^2 - h_b^2 \tag{7.18}$$

B_o may be evaluated as in (7.7), suppressing all superscripts, we have:-

$$B_o = \sqrt{\frac{2}{Y_b}} \left[\mathrm{Re} \int_{-\infty}^{\infty} \left[\gamma.\gamma^*.e_1.e_1^* + e_2.e_2^* + \gamma e_1 e_2^* + \gamma^* e_1^* e_2 \right] dx \right]^{-\frac{1}{2}} \qquad (7.19)$$

noting that $e_1 e_1^* = |e_1|^2 = |e_2|^2$ (7.19) reduces to,

$$B_o = \sqrt{\frac{2}{Y_b}} \left[(1+|\gamma|^2) I_2 + \mathrm{Re}\left[\gamma I_5 + \gamma^* I_3 \right] \right]^{-\frac{1}{2}} \qquad (7.20))$$

with,

$$I_2 = \int_{-\infty}^{\infty} e_1.e_1^*.dx = \int_{-\infty}^{\infty} |e_1|^2 dx = t + \frac{\sin(2h_b t)}{2h_b} + \frac{\cos^2(h_b t)}{P_b} \qquad (7.21)$$

$$I_3 = \int_{-\infty}^{\infty} e_1^*.e_2.dx = \cos^2(h_b t) \left[\frac{\exp(-2p_b(t+d) - j\alpha\beta_b(2t+d))}{2p_b + j\alpha\beta_b} + \right.$$

$$\left. \frac{\exp(-2p_b(t+d) + j\alpha\beta_b(2t+d))}{2p_b - j\alpha\beta_b} + 2\exp(-2p_b d) . \frac{\sin(\alpha\beta_b d)}{\alpha\beta_b} \right] +$$

$$\frac{\cos(h_b t)}{2} \exp(-p_b d) \left[S(h_b) + S(-h_b) + T(h_b) + T(-h_b) \right] \qquad (7.22)$$

with,

$$s(h_b) = \exp(jh_b(t+d)) \left[\frac{\exp(-jd(h_b + \alpha\beta_b - jp_b)) - \exp(-j(2t+d)(h_b + \alpha\beta_b - jp_b))}{j(h_b + \alpha\beta_b - jp_b)} \right] \qquad (7.23)$$

$$T(h_b) = \exp(-jh_b(t+d)) \left[\frac{\exp(j(2t+d)(h_b + \alpha\beta_b + jp_b)) - \exp(jd(h_b + \alpha\beta_b + jp_b))}{j(h_b + \alpha\beta_b + jp_b)} \right] \qquad (7.24)$$

$$I_5 = \int_{-\infty}^{\infty} e_1.e_2^* dx = \int_{-\infty}^{\infty} e_1.e_2 dx = I_3^* \qquad (7.25)$$

If $E_y^+(x,z)$ is the radiation field in $z \geq 0$ associated with the guided mode $E_y^t(x,z)$ then from modal othogonality we obtain,

$$\int_{-\infty}^{\infty} E_y^+(x,0).E_y^{t*}(x,0).dx = 0 \qquad (7.26)$$

with similar results holding for the magnetic field components.

Referring to Figure 7.1 the incident mode at the junction E_y^i excites a transmitted mode TE_y^t. Due to the change in waveguide impedance there is a reflected mode ρE_y^i and radiation fields E_y^- in $z<0$ and E_y^+ in $z>0$. Matching the tangential electric and magnetic fields over the $z = 0$ plane gives,

$$(1+\rho)E_y^i + E_y^- = {}^TB_o(\gamma e_1^t + e_2^t) + E_y^+ \qquad (7.27)$$

$$(1-\rho)H_x^i + H_x^- = {}^TB_o(\gamma h_1^t + h_2^t) + H_x^+ \qquad (7.28)$$

By neglecting radiation in the backward direction (see Appendix D1), E_y^- and H_x^- may be ignored (70, 71, 72, 75). Accordingly multiplication of (7.27) by e_1^{t*} and (7.28) by h_1^{t*} followed by integration with respect to x over the $z = 0$ plane gives,

$$(1+\rho)I_1 = {}^TB_o(\gamma I_2 + I_3) \qquad (7.29)$$

$$(1-\rho)I_1Y_a = {}^TB_oY_b(\gamma I_2+I_3) \qquad (7.30)$$

Similarly multiplication of 7.27) by e_2^{t*} and (7.28) by h_2^{t*} gives,

$$(1+\rho)I_4 = {}^TB_o(\gamma I_5 + I_6) \qquad (7.31)$$

$$(1-\rho)I_4Y_a = {}^TB_oY_b(\gamma I_5+I_6) \qquad (7.32)$$

with,

$$I_1 = \int_{-\infty}^{\infty} E_y^i e_1^{t*}dx = A\cos(h_a(2t+d))\cos(h_bt)\left[\frac{\exp(-2p_b(t+d)-j\alpha\beta_b(2t+d))}{p_a+p_b+j\alpha\beta_b} + \frac{\exp(j\alpha\beta_b(2t+d))}{p_a+p_b-j\alpha\beta_b}\right] +$$

$$\frac{A\cos(h_bt)}{2}\exp(-p_bd)\left[U(h_b) + U(-h_b)\right] +$$

$$\frac{A}{4}\left[\exp(j(d+t)(h_a+\alpha\beta_b))\left[R(h_b)+R(-h_b)\right] + \exp(j(d+t)(-h_a+\alpha\beta_b))\left[V(h_b) + V(-h_b)\right]\right] \qquad (7.33)$$

With,

$$U(h_b) = \frac{\exp(d(p_b+j(h_a+\alpha\beta_b)))-\exp((-2t-d)(p_b+j(h_a+\alpha\beta_b)))}{p_b + j(h_a+\alpha\beta_b)} \tag{7.34}$$

$$R(h_b) = \frac{2\sin(t(h_a + h_b + \alpha\beta_b))}{h_a + h_b + \alpha\beta_b} \tag{7.35}$$

$$V(h_b) = \frac{2\sin(t(-h_a + h_b + \alpha\beta_b))}{-h_a + h_b + \alpha\beta_b} \tag{7.36}$$

$$I_4 = \int_{-\infty}^{\infty} E_y^i e_2^{t*} dx = A\cos(h_a(2t+d))\cos(h_b t)\left[\frac{1+\exp(-2p_b(t+d))}{p_a + p_b}\right] +$$

$$\frac{A}{2}\left[W(h_b)+W(-h_b)+X(h_b)+X(-h_b)\right] + \frac{A\cos(h_b t)\exp(-p_b d)}{2}\left[Y(h_a)+Y(-h_a)\right] \tag{7.37}$$

With,

$$W(h_b) = \frac{\sin(h_b t - h_a d)}{h_a + h_b} \tag{7.38}$$

$$X(h_b) = \frac{\sin(h_b t + h_a(2t+d))}{h_a + h_b} \tag{7.39}$$

$$Y(h_a) = \frac{\exp((2t+d)(-p_b+jh_a)) - \exp(-d(-p_b+jh_a))}{-p_b + jh_a} \tag{7.40}$$

$$I_6 = \int_{-\infty}^{\infty} e_2^t e_2^{t*} dx = \int_{-\infty}^{\infty} |e_2|^2 dx = I_2 \tag{7.41}$$

(7.29) and (7.31) together give,

$$\gamma = \frac{I_3 I_4 - I_1 I_6}{I_1 I_5 - I_2 I_4} \tag{7.42}$$

while (7.29) and (7.30) give,

$$T = \frac{1}{B_o} \cdot \frac{Y_a}{Y_a+Y_b} \cdot \frac{2I_1}{\gamma I_2 + I_3} \tag{7.43}$$

and $$\rho = \frac{Y_a - Y_b}{Y_a + Y_b} \tag{7.44}$$

The fractions of incident power transmitted to the output waveguides and reflected in the input waveguide are

$$T = |T|^2 \quad \text{and} \quad R = |\rho|^2 \tag{7.45}$$

respectively. By conservation of power, the fraction

S scattered into the surrounding medium is

$$S = 1 - R - T \tag{7.46}$$

Recalling that the mode powers are normalised to unity, we find that the fractions of power transmitted to the tilted upper and straight lower output waveguides are,

$$P_1 = \frac{|\gamma T|^2}{1+|\gamma|^2} \tag{7.47}$$

$$P_2 = \frac{|T|^2}{1+|\gamma|^2} \tag{7.48}$$

respectively.

If α is set equal to zero, then it may be shown that (7.43) reduces to equation (6.26) in Chapter 6, with α also equal to zero. This is to be expected as both waveguide structures are identical in this situation.

A computer program to calculate power transmission for varying output waveguide tilt angles was written, a flow diagram of which may be found in Appendix A9.

Figure (7.2) shows a theoretical plot of the transmitted power in each waveguide for varying angle (α), and junction defect (2d) for a planar 7059 glass waveguide guiding the TE_o mode. As in the Y-junction case (see Figure 6.4), even modest junction defects drastically reduce the device power transmission. This effect can be reduced by using waveguides which have a small refractive index difference between the waveguide and the surrounding media, e.g. Ti diffused $LiNbO_3$ waveguides resulting in weakly guided modes with large evanescent fields which are relatively insensitive to waveguide defects of this kind. However, waveguides of this type are sensitive to abrupt changes in direction and as a result the power in the angled output waveguide falls rapidly with increasing angle (α). This is

the same loss mechanism as associated with the Y-junction analysis of Chapter 6 and the waveguide tilt analysis of Chapter 5. A more complete and detailed description of the loss mechanism is given in Section 5.1 and 6.1.

As in the Y-junction case it should be noted that the power transmission of the device is not unity when α and d equal zero, as would be expected. This is due to the nature of the analysis which assumes that the waveguide admittance changes discontinuously at $z = 0$, rather than gradually (70, 71). Since superposition implies a greater discontinuity in waveguide admittance than actually exists at the junction, the calculated power transmission T is a lower bound to the actual value (70). For increasing α the actual variation of waveguide admittance at the junction will tend to the assumed discontinuous variation and the lower bound T will become increasingly accurate as α increases. Thus for the $LiNbO_3$ example (Figure 7.3) where there is only a small change in waveguide admittance at the junction (i.e. $\beta_a \simeq \beta_b$), and the abrupt change of impedance assumed in the analysis is a close approximation. However, for the 7059 glass example (Figure 7.2), ($\beta_a \neq \beta_b$), and there is a large change in waveguide admittance and the assumed abrupt change is no longer such a close approximation.

Another interesting aspect of the $LiNbO_3$ power splitter of Figure 7.3 is that as the angle (α) of the tilted output waveguide increases the transmitted power present in the waveguide decreases rapidly. However, this does not drastically affect the overall device power transmission, as the non-angled output waveguide supports an ever increasing proportion of the transmitted power, (see Figure 7.3). Thus

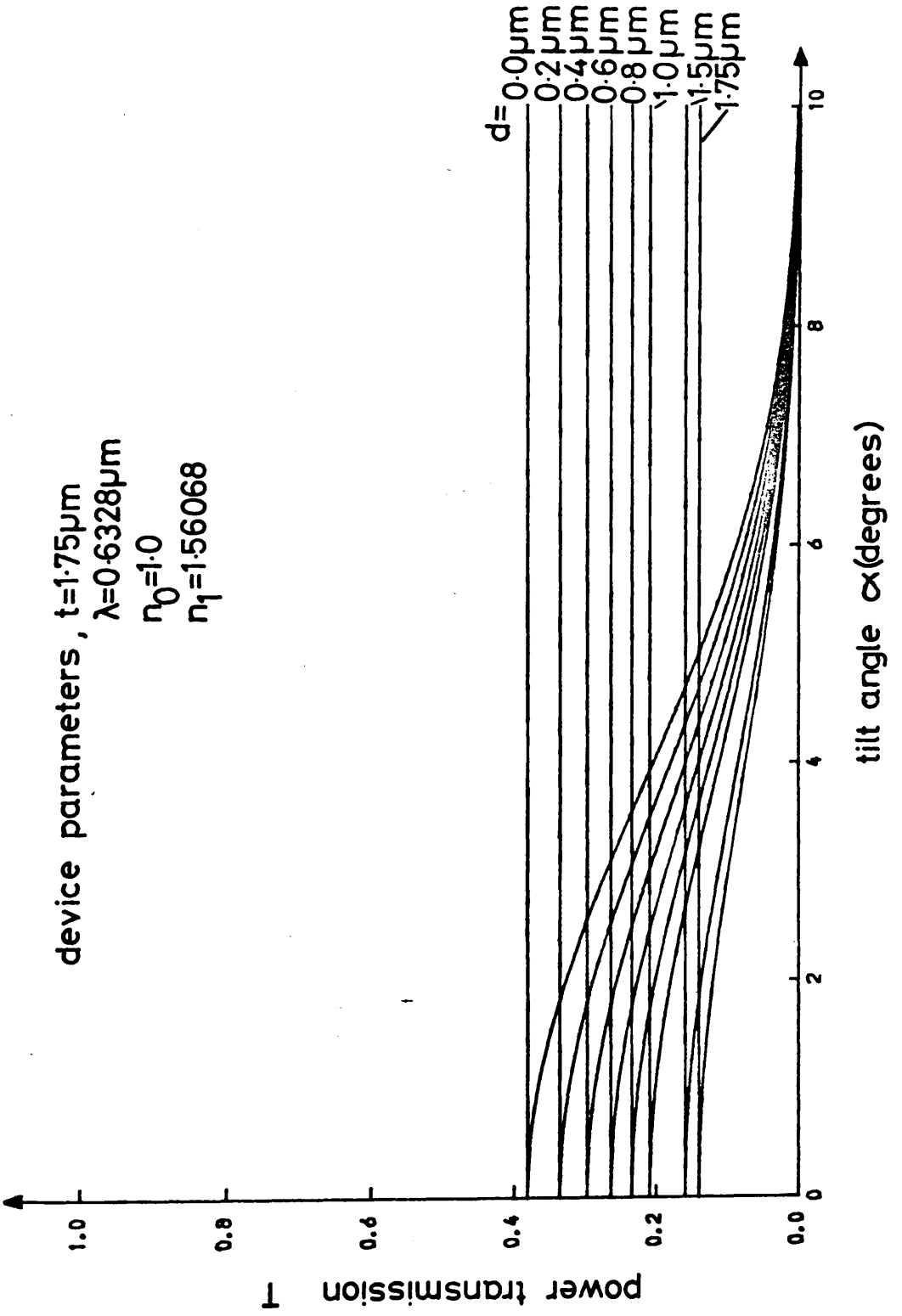

Fig. 7.2 Plot of power transmission for increasing defect size in a 7059 glass planar waveguide power splitter

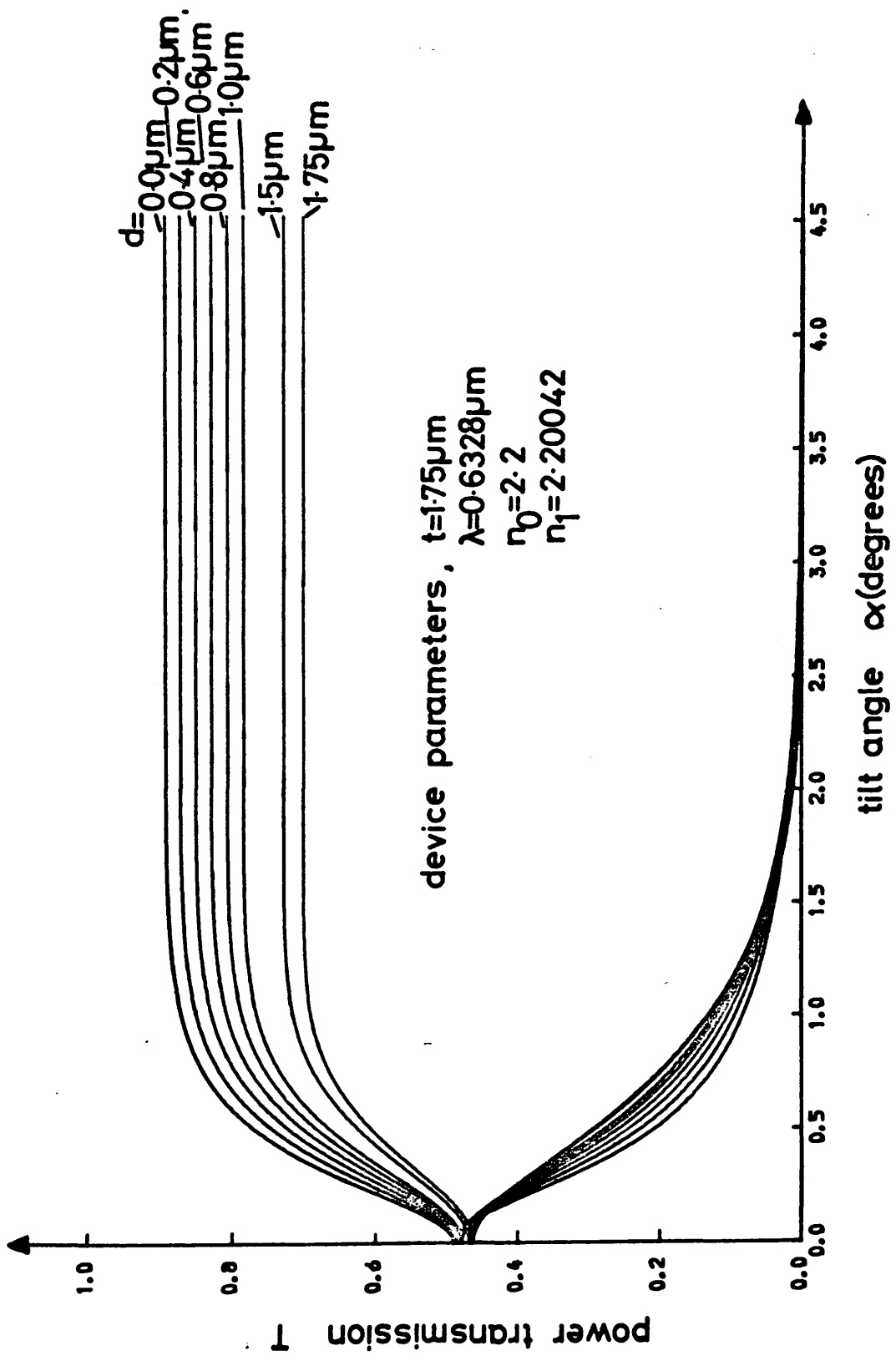

Fig. 7.3 Plot of power transmission for increasing defect size in a $LiNbO_3$ planar waveguide power splitter

the overall device power transmission is only slightly reduced, even when there is no power present in the angled output waveguide. This indicates that modes propagating in a waveguide formed from Ti diffused $LiNbO_3$ can suffer large changes in waveguide dimensions, i.e. from 4t + 2d to 2t (see Figure 7.1), with very little power loss. This is to be expected, as waveguides formed in materials which have small differences in refractive index between the waveguide and the surrounding medium are insensitive to waveguide defects, due to a large proportion of the guided mode power being carried in the evanescent fields, which propagate outside the waveguide. However, referring to Figure 7.2 we see that as the angle of the tilted output waveguide formed in 7059 glass is increased, the transmitted power falls slowly with increasing α to reach a steady state value of exactly half of the $\alpha = 0$ value. This is due to the large refractive index difference between the waveguide and the surrounding media, resulting in a waveguide which has a tightly confined field structure and is insensitive to abrupt changes of direction (see Section 6.1).

As can be seen from Figures 7.2,3 large power ratios of at least 10:1 may be obtained in the output waveguides of a power splitter if α is made large enough. This makes the above waveguide power splitter a potentially useful signal processing device, and if waveguide defect losses can be reduced to a minimal level, then power splitters of this kind could be used as a practical alternative to waveguide couplers which rely on evanescent field coupling between two adjacent waveguides. It is envisaged that until stripe dielectric waveguides can be fabricated with submicron dimensions and separations then power

splitters of this kind may be one of the few methods available of obtaining directive couplers with accurate power ratios.

Section 7.2 shows how the above planar waveguide analysis may be used to predict the transmission performance of trapezoidal stripe 7059 glass waveguide power splitters.

7.2. Stripe Waveguide Power Splitter Transmission Performance Using a Planar Waveguide Analysis.

The following method of relating planar waveguide power splitter transmission to that of a practical stripe waveguide device is identical to the method described in Section 6.2 when discussing the Y-junction. The discussion here is kept brief; a fuller description of the method, which is equally applicable to the power splitter, can be found in Section 6.2.

Using the result of Appendix B2 and recalling the parameters used in Section 7.1, the following changes are made to allow the planar waveguide device analysis of Section 7.1 to be used in the design of single mode stripe waveguide power splitters (see Figure 7.4). Using Marcatili's (56) notation,

$$\beta_a \text{ becomes } \beta_{za} = k_{za} \tag{7.49}$$

$$h_a \text{ becomes } k_{xa} \tag{7.50}$$

$$p_a \text{ becomes } 1/\xi_{3a} = 1/\xi_{5a} \tag{7.51}$$

$$\beta_b \text{ becomes } \beta_{zb} = k_{zb} \tag{7.52}$$

$$h_b \text{ becomes } k_{xb} \tag{7.53}$$

$$p_b \text{ becomes } 1/\xi_{3b} = 1/\xi_{5b} \tag{7.54}$$

As stated in the Y-junction analysis of Section 6.2 the planar waveguide model of Section 6.1 is more suited to predicting the

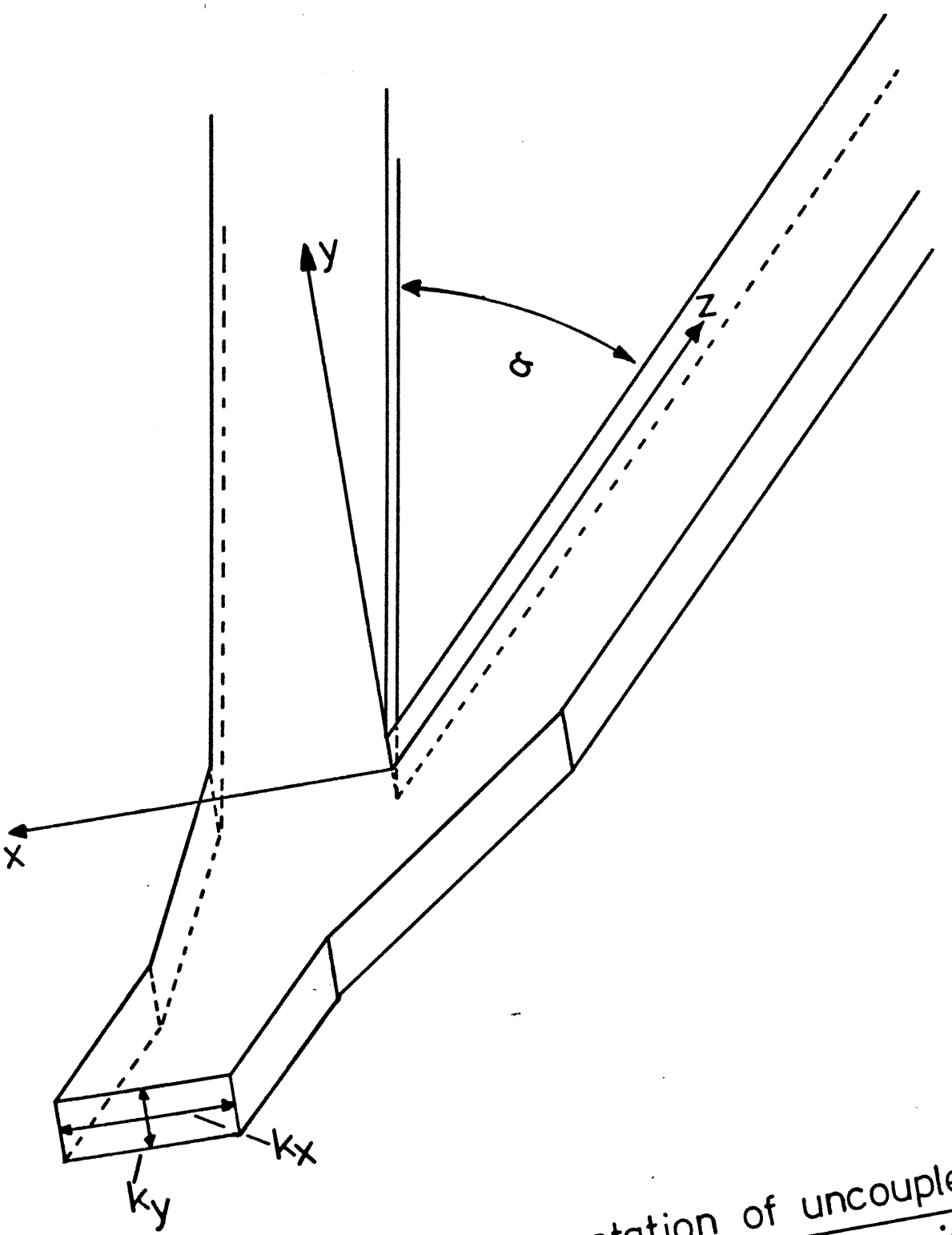

Fig. 7.4 Pictorial representation of uncoupled wave vectors in a stripe waveguide power splitter

power transmission of a stripe waveguide Y-junction propagating the E_{11}^{y} mode (quasi TE_o mode in the plane of the device), than the E_{11}^{x} mode (quasi TM_o mode in the plane of the device). However, as the TM_o mode planar waveguide analysis is much more complicated than that of the TE_o mode analysis, and as little difference in power transmission is expected between the two modes (see Section 6.2 and Figure 6.8), we may conclude that the planar waveguide device analysis can be used to predict the transmission performance of both the E_{11}^{x} and E_{11}^{y} modes, with minimal error, when the planar waveguide device propagation coefficients, β_a and β_b, are replaced by those of the stripe waveguide device, β_{za} and β_{zb} (see Appendix B2). The same reasoning applies to the power splitter analysis for which the planar waveguide TE_o mode model of Section 7.1 is used to predict the transmission performance of a stripe waveguide power splitter propagating the E_{11}^{x} mode. As stated in Chapter 6, the stripe waveguide power splitter theory is expected to become more accurate as the difference in refractive index between the waveguide and the surrounding media becomes less. As such the lower bound solution of Section 7.1 should become almost exact for devices fabricated in Ti diffused $LiNbO_3$. However, the accuracy for ion-etched 7059 glass waveguides with large refractive index differences is not expected to be as good, although it should still remain acceptable.

The above stripe waveguide power splitter analysis is used in Section 7.3 to predict the transmission performance of experimental ion-etched 7059 glass stripe waveguide power splitters propagating the E_{11}^{x} mode and to compare with the measured values.

7.3. Experimental Investigation of the Transmission Performance of Ion-Etched 7059 Glass Stripe Waveguide Power Splitters.

7.3.1. Waveguide Design Considerations.

Stripe waveguide 7059 glass power splitters were fabricated using the process outlined in Section 4.2. As the power splitter device is almost identical to that of the Y-junction (with only the angle between the output waveguides varying), the same waveguide design considerations apply (see Section 6.3.1). Because of this only a brief description is given here.

The same waveguide dimensions used in the Y-junction mask were also used for the power splitter, i.e. a waveguide of width $2t = 3$ μm tapering to 6 μm at the junction before splitting into two 3 μm output arms. Again, as in the Y-junction case, single mode (E_{11}^{x}) operation of the junction section of 6 μm waveguide width required that the 3 μm output waveguides operated close to cut-off, necessitating accurate control of the waveguide thickness (see Section 3.2). Again the fabrication process of Section 4.2 resulted in devices with junction defects. As well as reducing the overall device power transmission these defects also effectively increased the size of the input waveguide, (from $4t$ to $4t+2d$). Depending on the size of d this increase in waveguide width was sometimes sufficient to allow the input waveguide to support more than the fundamental E_{11}^{x} mode. The implications of this are discussed in the experimental results section.

To correlate the experimental results all waveguide parameters, (widths, refractive index, etc) are given in a separate table along with each set of power transmission measurements.

7.3.2. Transmission Loss Measurements.

The method of measuring device power transmission was identical to that of Section 6.3.2, thus all the experimentally measured parameters mentioned there are equally applicable to the power splitter measurements.

7.3.3. Output Waveguide Power Ratio Measurements.

Due to the small angular separation between the branching output waveguides ($< 10^{o}$) and due to the limited output waveguide length (useful length of output waveguides $\simeq$4mm), it proved impossible to couple out the guided mode power selectively from each of the branching output waveguides independently, when using a prism coupler. Thus power ratio measurements between the two output waveguides, unlike the power transmission measurements of Section 7.3.2, could not be obtained in this way. Therefore another means of measuring the power ratio in the two branching output waveguides had to be developed. This problem was solved by scanning the output "m-line" structure of the two branching waveguides using the laser power meter detector head (50), and measuring the peak power in each. Figure 7.5 shows a photograph of a typical output "m-line", obtained from a single mode stripe waveguide power splitter. By comparing the peak power in each waveguide we may obtain a measure of the relative power transmitted into each of the branching arms. However, this method was beset by problems, the major one of which was scattered background illumination from the laser modifying the relative power ratios of the output "m-lines", and giving a false measurement of the relative peak power intensity ratio. Another problem was that of the laser power meter detector head having a very large area, which resulted in power readings which

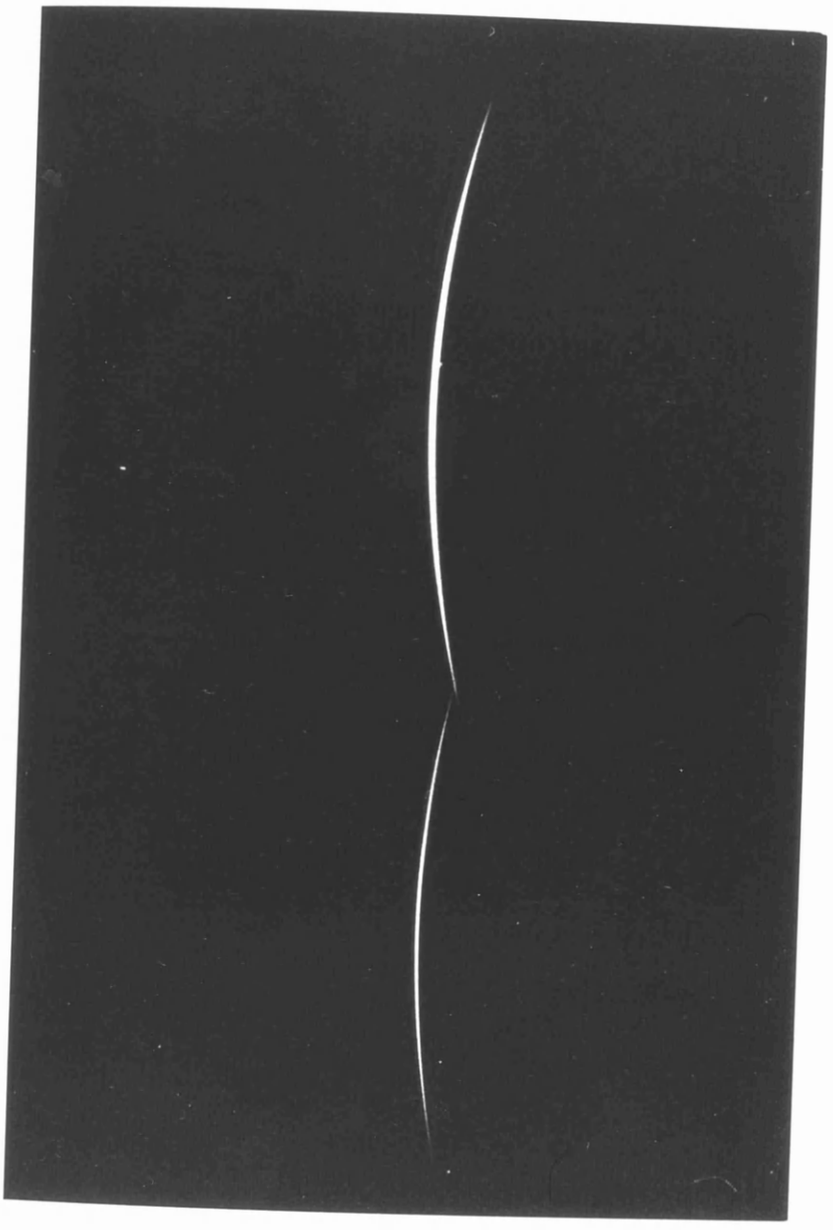

Fig. 7.5 Typical power splitter M-line pattern

were more of an average value than of a peak value. Again this resulted in misleading power ratio measurements due to the measured average power levels tending to smooth out the difference between the relative power levels of the output waveguides. This problem was overcome to some extent by using a narrow aperture slit on the front of the detector head assembly, thus increasing the selectivity of the arrangement and allowing a more precise determination of the peak power levels of the output "m-lines". However, this increase in selectivity was offset by the reduction of available power reaching the detector head, thus making peak power measurements more difficult. The accuracy of the above power ratio measurement technique is therefore limited and an error of at least ±10% is estimated in each measurement. This is especially true for power splitters which have small angular separations between the output waveguides resulting in "m-lines" with peak power levels close together. Figure 7.5 shows the "m-line" structure of such a device. As the angle between the two output waveguides is small, there is little difference in the intensity levels of the two output "m-lines".

Another method that was tried for the measurement of relative power intensity levels was the use of micrographs showing light guiding in working devices, coupled with a micro-densitometer to measure the photographic density of the exposed film. By measuring the relative photographic density of each of the output arms, a measure of the power being scattered from the walls of each output waveguide could be obtained. As each of the output arms is identical in every respect (i.e. waveguide losses, width, etc), a measure of the relative power propagating

in each may be obtained. However, caution must be exercised if accurate relative power levels are required, as this demands that the photographic film is operated in the "linear" region.

Unfortunately, although excellent microdensitometer facilities existed and were readily available, the above technique was deemed impractical due to the large amount of time required to characterise and calibrate the film being used. However, preliminary measurements obtained from some non-characterised micrographs indicated that the technique showed much promise, giving a reasonable indication of relative power levels.

If more time had been available then the above technique would undoubtedly have been a better experimental method than that of measuring the peak power levels, as described above. With a little more development work, especially in the characterisation of the film, the photographic technique could be extended to include measuring waveguide attenuation and stripe waveguide device power transmission losses (e.g. Y-junctions, waveguide tilts, etc). Had this technique been available earlier, it would have undoubtedly increased the ease and accuracy of experimental measurements, as well as making them less time-consuming.

The next section compares the results obtained in Sections 7.3.2 and 7.3.3 with the theory developed in Section 7.2.

7.3.4. Comparison of Experimental and Theoretical 7059 Glass Stripe Waveguide Power Splitters.

7.3.4.1. Waveguide Width Measurements.

Waveguide width measurements were obtained using the scanning electron microscope (S.E.M.), in an identical manner to those of Section 6.3.3.1. Using these measurements

and knowing the film thickness from the sputtering unit calibration (see Sections 3.1,2) theoretical curves of power transmission v.s. tilt angle α^{o} were drawn using the theory of Section 7.2. A flow diagram of the computer program is given in Appendix A10.

7.3.4.2. Theory and Experiment.

Experimental and theoretical plots of power transmission and relative power ratio v.s. tilt angle α^{o} for ion-etched 7059 glass power splitters are shown in Figures 7.6a and 7.6b with the corresponding device waveguide dimensions being shown in Figure 7.6c. As in the Y-junction case it proved impossible to fabricate power splitters with the same defect size for different tilt angles, thus each theoretical point had to be calculated individually using the device dimensions measured on the S.E.M. Thus Figures 7.6a, 6b show measured experimental points and corresponding computed theoretical points with the S.E.M. measured dimensions given in Figure 7.6c. The experimental device tilt angles were known accurately from the angles scribed in the master mask at the "cutting" stage, thus any error associated with them is minimal.

Referring to Figures 7.6a, 6b, we see that there is reasonably good agreement between theory and experiment. As can be seen there is much better agreement for the transmission loss measurements Figure 7.6a, than there is for the power ratio measurements Figure 7.6b. This reflects on the discussion of Section 7.3.3 where the accuracy of the power ratio measurements was questioned. However, most of the measured and theoretical points would appear to agree reasonably well and we may conclude that the theoretical model of Section 7.2 can accurately predict

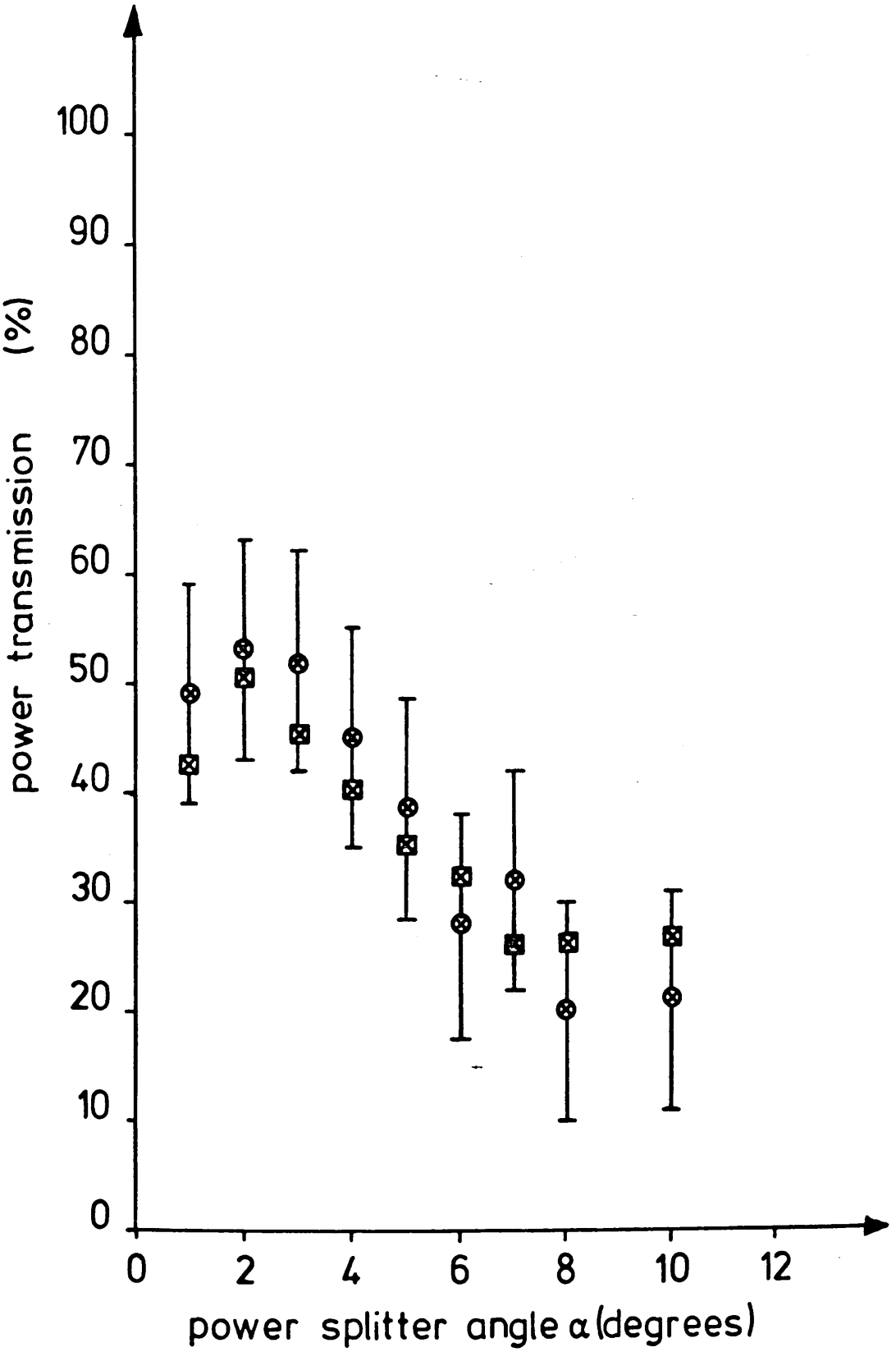

Fig. 7.6a Experimental ⊗ and theoretical ⊠ power transmission v.s. power splitter angle

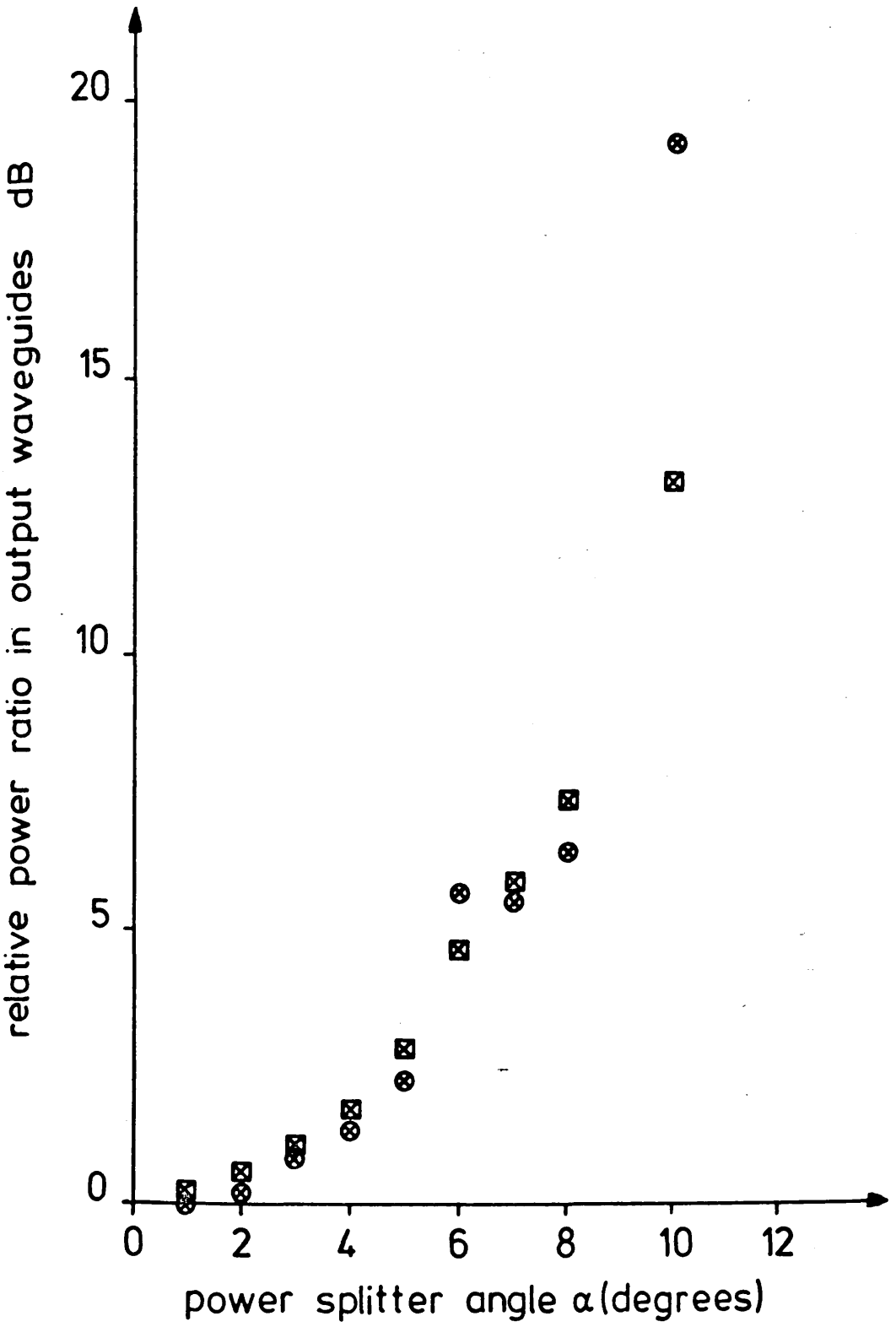

Fig. 7.6b Experimental ⊗ and theoretical ⊠ power ratio v.s. power splitter angle

TABLE OF EXPERIMENTAL POWER SPLITTER PARAMETERS

POWER SPLITTER ANGLE α (DEGREES)	WAVEGUIDE EFFECTIVE HALF WIDTH t(μm)	WAVEGUIDE DEFECT EFFECTIVE HALF WIDTH d(μm)
1	1.57	0.77
2	1.57	0.46
3	1.57	0.53
4	1.46	0.57
5	1.49	0.64
6	1.60	0.61
7	1.51	0.80
8	1.47	0.69
9	DEVICE NOT TESTED DUE TO MASK DEFECTS	
10	1.52	0.51

WAVEGUIDE THICKNESS b = 0.44 μm

$n_1 = 1.56068$

$n_2 = n_3 = n_5 = n_o = 1.0$ (AIR)

$n_4 = n_s = 1.51272$

Figure 7.6c. Details of Waveguide Dimensions of Figure 7.6a and Figure 7.6b.

the transmission performance of a stripe waveguide power splitter propagating the fundamental E_{11}^{x} mode.

7.3.4.3. Discussion of Results.

Figure 7.6a shows a reasonably close correlation between the experimentally measured and theoretically computed values of waveguide power splitter transmission performance. As can be seen, the fall in transmitted power with increasing tilt angle α is reasonably well predicted, as is the overall power loss, the major part of which can be attributed to the blunt wedge tip imperfection formed in the fabrication stage. This is to be expected from the results of Chapter 6, where results show that ion-etched 7059 glass Y-junctions also suffer large waveguide losses due to the same fabrication imperfection. Figure 7.6b shows a plot of measured and theoretical power ratios for the two output waveguides for varying tilt angles. As can be seen the agreement between theory and experiment is reasonable. The reasons for this are mainly thought to arise from the uncertainty involved in measuring the relative power ratio between the two output waveguides (see Section 7.3.3), and not from any serious defects in the theory, as the power transmission measurements of Figure 7.6a and the results of Chapter 6 indicate that overall the theory is reasonably accurate. If a more accurate means of measuring the power ratio had been available, then it is thought that much better agreement between theory and experiment could have been obtained.

The operation of the power splitter is shown to best effect photographically by the differences in exposure levels which indicate the relative difference in light intensity of the two output arms. Figures 7.7,8,9 are photographs of

(a) $\alpha=1^{\circ}$

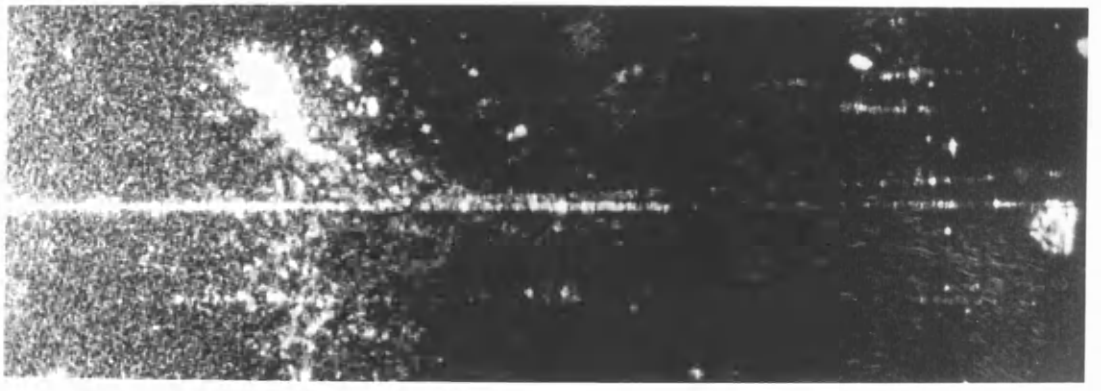

(b) $\alpha=2^{\circ}$

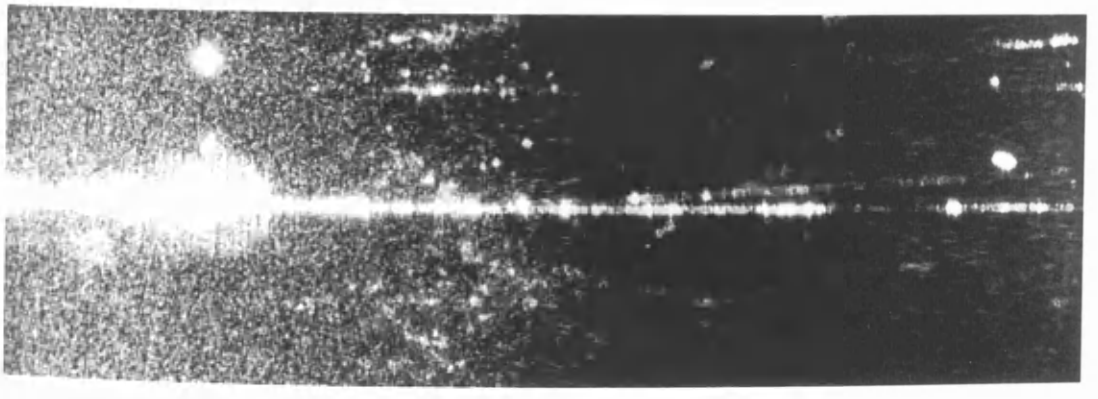

(c) $\alpha=3^{\circ}$

Fig. 7.7 Micrographs of working power splitters

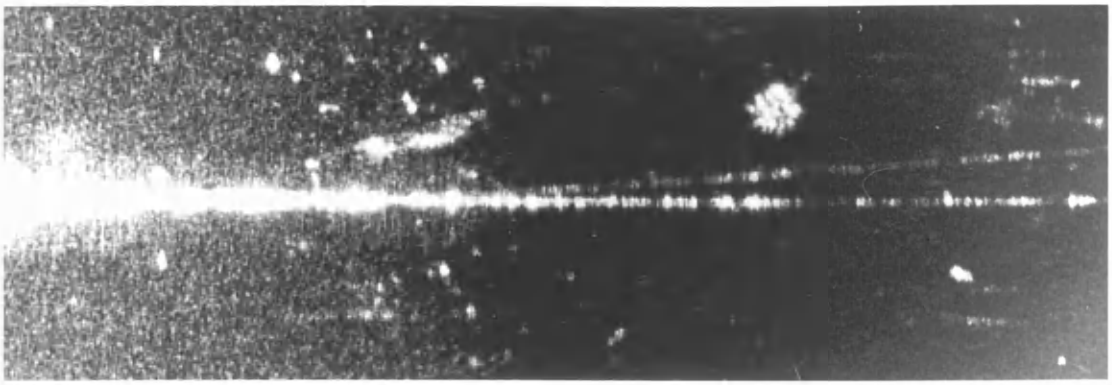

(a) $\alpha=4^{\circ}$

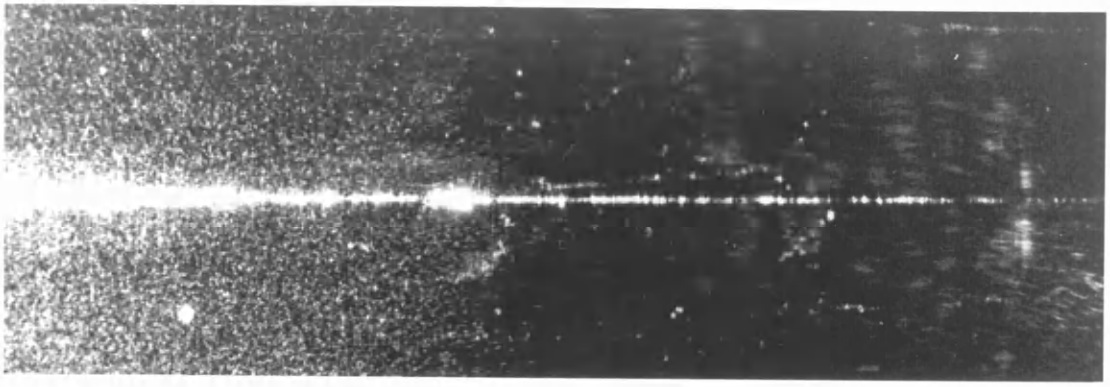

(b) $\alpha=5^{\circ}$

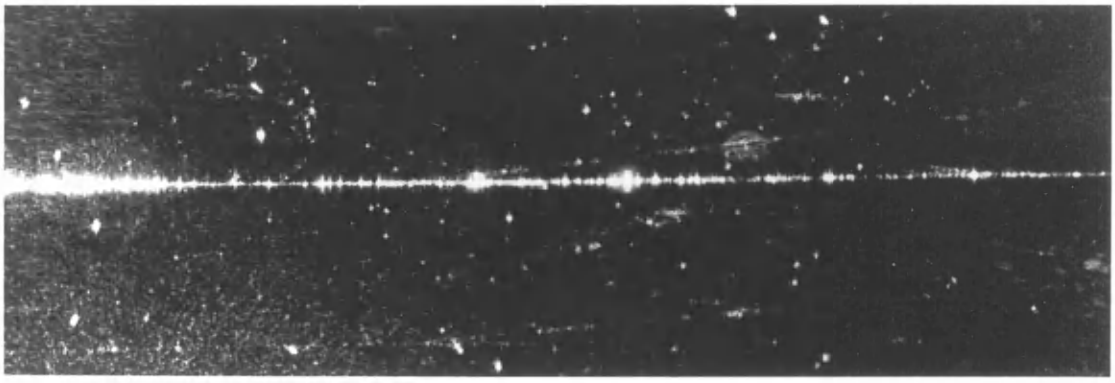

(c) $\alpha=6^{\circ}$

Fig. 7.8 Micrographs of working power splitters

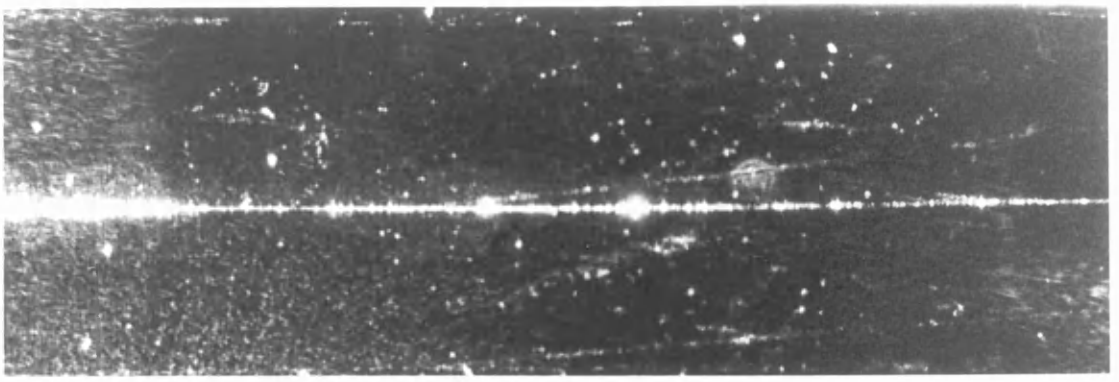

(a) $\alpha = 7^{\circ}$

(b) $\alpha = 8^{\circ}$

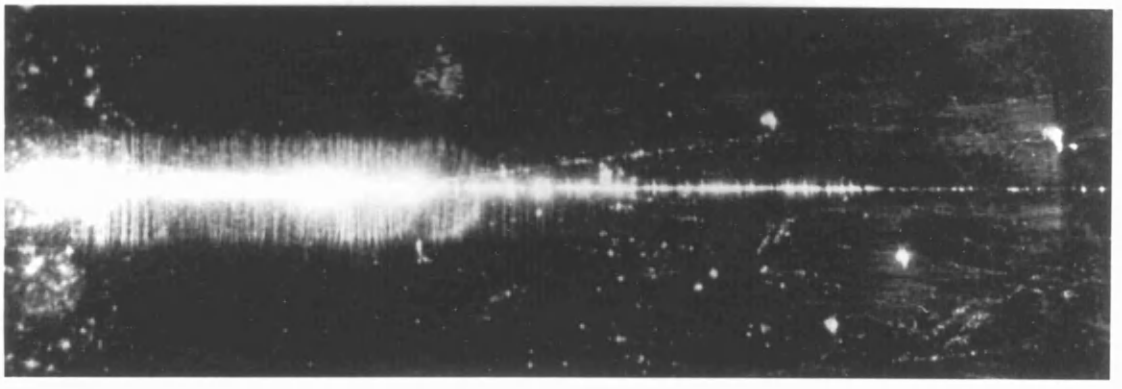

(c) $\alpha = 10^{\circ}$

Fig. 7.9 Micrographs of working power splitters

power splitters operating at various junction angles. The variation in power levels before and after the junction is clearly visible, as is the decrease in power in the upper waveguide with increasing tilt angle. The large difference in transmitted power at the junction gives an abrupt change in light intensity, while the decrease in power with increasing tilt angle of the upper tilted waveguide appears as a decrease in light intensity. The radiation loss mechanism associated with these devices is identical to that of the Y-junction and waveguide tilt, further details of this are found in Sections 5.1,5.4,6.2,6.3.3.3. As in the Y-junction case, the large power loss at the junction presents a formidable obstacle to the efficient design of a 7059 glass stripe waveguide power splitter, and until a more suitable fabrication process is found it would appear that 7059 glass devices of this kind will continue to display large fabrication defects.

As mentioned earlier, the ion-etching process tends to increase the waveguide width at the junction, from 4t of the perfect device to 4t+2d of a device with a defect. This allows the possibility that more than one mode type is present in the junction region due to power being scattered into a higher order mode(s) in the tapered section of the waveguide directly before the junction. It is thought likely (although no experimental evidence was found), that in many of the devices tested a small proportion of the incident power was being propagated in the E^x_{21} mode as well as the major power contribution of the fundamental E^x_{11} mode. As the E^x_{21} mode is antisymmetric about the axis of propagation (z axis) there is a field intensity minimum at $x = 0$. Thus when the E^x_{21} mode encounters a blunt

junction of the kind present in ion-etched 7059 glass waveguides, the power lost to radiation should be much reduced over the E_{11}^{x} mode which has a point of maximum field intensity at x = 0. This will have the effect of reducing the loss effect of the blunt wedge, thus increasing the overall device power transmission. From these considerations an ion-etched 7059 glass power splitter may be more useful as a mode convertor, providing a fixed power ratio between the output waveguides, than as a single mode power splitter.

In contrast to the case of the Y-junction, no taper coupler effects at the junction were observed (see Section 6.3.3.3). The reason for this is not clear, but it is thought that steeper waveguide wall tapers allowed the power to radiate directly into the air at the junction, rather than via a shallower taper into the substrate, as in the Y-junction case.

Since ion-etched 7059 glass waveguides have a large refractive index difference between the waveguide and the surrounding media, the phase mismatch between the incident and transmitted modes at the junction is small. Thus 7059 glass waveguide devices are relatively insensitive to tilt angle, and useful devices may be fabricated with angles of 10^{o} or more. If the large junction loss can be eliminated by the use of an alternative fabrication technique, then stripe waveguide 7059 glass power splitters could find many applications in passive integrated optical circuits.

We may conclude that the theory derived in Sections 7.1 and 7.2 can accurately predict the transmission performance of ion-etched 7059 glass power splitters. This is especially true for waveguides with little change in waveguide admittance

between the input and output waveguides. In this case the lower bound solution of Section 7.1 gives an almost exact solution.

4.4. Conclusions.

The transmission performance of experimental stripe waveguide power splitters fabricated in R.F. sputtered 7059 glass has been successfully related to a relatively simple analytical solution based on the theory of Anderson (70,53). This solution may be used to design waveguide devices which have known fixed power ratios between the two output arms. The solution should be adaptable to other materials better suited to active waveguide devices(e.g. Ti diffused $LiNbO_3$) and could lead to the design of 10 and 20 dB reference power splitters.

However, to fabricate efficient devices a means must be found to reduce the level of junction defect losses to an acceptable level.

P A R T I I I

CONCLUDING DISCUSSION

CHAPTER 8.

CHAPTER 8. CONCLUSIONS AND FUTURE WORK.

8.1. Conclusions.

8.1.1. Thin Film R.F. Sputtered 7059 Glass Waveguides.

It has been confirmed that thin films of Corning type 7059 glass (43) can be deposited onto microscope slide substrates using a radio frequency (R.F.) sputtering technique in an 80/20 Ar/O_2 gas mixture of 2×10^{-3} torr pressure (see Chapter 3). The thin films produced are of a high optical quality with a precisely defined refractive index and thickness. Thin-film prism-coupler mode-angle measurements confirmed that the films were homogeneous and isotropic, and that the thin film deposition rate was linear with time. Thin film waveguide losses were found to be as low as 0.1 dB/cm at 0.6328 μm wavelength, being mainly attributable to small substrate scattering centres caused by imperfect substrate preparation (see Section 3.2.2). These losses are amongst the lowest measured to date on R.F. sputtered thin films, and lie close to the limit of the measuring technique (13). Planar 7059 glass waveguides, therefore, provide a useful source of good low loss optical films of known refractive index and thickness and should prove useful in the fabrication of passive integrated optical waveguide devices.

8.1.2. Two-Dimensional (Stripe) Ion-Etched 7059 Glass Waveguides.

A practical monolithic integrated optical communications system must have a reasonably large packing density, while at the same time maintaining single mode operation to allow the system bandwidth to approach the theoretical limit and minimise crosstalk. To achieve this one must look to two-dimensional (rectangular) waveguides which impose lateral confinement of the

guided light allowing higher packing densities. It is foreseen that two-dimensional dielectric optical waveguides will form the basic building blocks in any future integrated optical communications system, interconnecting the various active and passive devices and providing input and output coupling parts for direct connection to optical fibre data highways. To ensure compatability with the high data transmission rates of the current single mode optical fibres, the rectangular waveguides (and devices) must also be capable of supporting only a single mode.

The fabrication of multimode two-dimensional 7059 glass waveguides is relatively straightforward although the manufacture of single mode waveguides and devices calls for stringent tolerences on the waveguide dimensions and refractive index. Indeed, the realisation of consistently low loss single mode stripe waveguides and devices was probably the most complex aspect of the research undertaken and, although many single mode stripe waveguides and devices have been fabricated and tested, the technological problems are still immense.

Single mode stripe waveguides formed by use of the ion-etching process showed typical waveguide losses in the region of 4-8 dB/cm, depending on the waveguide width. The above losses are somewhat higher than average for stripe waveguides formed using other fabrication techniques (e.g. diffusion or ion exchange), and limit the useful practical length of an ion-etched 7059 glass waveguide to around 2 - 3 cm. However, for any practical integrated optical waveguide system utilising waveguides of 4 μm width (or less), large waveguide attenuations should not present a problem due to the small interconnecting lengths of waveguide envisaged. The development of a better

ion-etching mask material (e.g. thick film carbon) or the introduction of a better etching method (e.g. plasma etching) would probably result in waveguides with reduced attenuation figures. By surrounding the ion-etched waveguides with a slightly lower refractive index medium, the tolerances on waveguide dimensions and refractive index, necessary to ensure only single mode guiding, could be reduced. By use of a suitable material this "passivation" would also reduce the waveguide losses due to scattering and would permit a reduction in waveguide losses with more of the guided mode power being carried in the evanescent fields. However, for all of the experimental waveguide devices tested, the above loss figures, although being on the high side, allowed a more than adequate length of waveguide to be available for the fabrication and evaluation of waveguide devices.

Many stripe waveguides of varying widths were fabricated and tested. It was found that the modal propagation characteristics could be successfully related to a simple theoretical model, the same as Marcatili's (56) but with an effective waveguide width substituted in place of the rectangular width to account for the trapezoidal cross-sectional geometry of the ion-etched waveguide, which is a product of the fabrication process (see Chapter 4). Single mode (E_{11}^{x}) guiding has been readily achieved in waveguides of 3 μm effective width and 0.44 μm depth operating close to the "cut-off" width of approximately 2 μm. Such waveguides have been routinely fabricated with good reproducability in the production of stripe waveguide devices (Y-junctions etc, see Chapters 5 - 7). It is possible to fabricate single mode (E_{11}^{x}) waveguides with guide widths of up to 8 μm. However, to ensure single mode operation it is necessary

that, as the waveguide width is increased, the waveguide thickness decreases rapidly to approach the "cut-off" thickness. This condition places heavy demands on the film thickness tolerances and at 8 μm guide width a change of only +10Å in film thickness may bring in the next order mode and allow it to propagate. This condition may be relaxed if a substrate with a refractive index close to that of the thin film is used, but this is not always a practical proposition. By extending the idea in the opposite direction and making the waveguide very narrow and increasing the film thickness, it is possible to control the modal propagation characteristics accurately. However, it is difficult to fabricate waveguides with widths of less than 2 - 3 μm over large areas. Therefore, it was decided to concentrate on the fabrication of single mode stripe waveguide devices with waveguide widths in the 3 - 6 μm range. This was mainly for the ease of predicting modal propagation characteristics for a known film thickness, but also to allow a reasonable amount of laser light to be launched into the waveguide (see Chapter 4).

8.1.2.1. Over-Etched Stripe Waveguides.

A novel extension of the ion-etching process allows relatively wide waveguides of 5 - 6 μm to be over-etched past the film/substrate interface into the substrate, thus leaving the resultant waveguide raised on a small unetched section of substrate standing proud over the rest of the general substrate level. As the waveguide effective width decreases with increasing etch depth it is possible to fabricate waveguides with a 2 μm effective width over a relatively large area starting from a 5 μm wide initial waveguide photomask (see Chapter 4). This allows the fabrication of narrow

waveguides with extremely large lengths. Unfortunately this fabrication technique results in waveguides with more pronounced trapezoidal geometries with larger area ion-etched waveguide walls, thus resulting in higher waveguide losses due to scattering from the relatively rough ion-etched walls. However, it is still thought that this novel technique will find many applications in the fabrication of single mode stripe optical waveguides, as a reduction in waveguide width greatly relaxes the tolerances for the design of single mode waveguides.

8.1.2.2. Comparison of Numerical Measured and Calculated Modal Propagation Constants.

Measured modal propagation coefficients of ion-etched 7059 glass stripe waveguides were compared with an independent, computer orientated numerical solution. In all cases agreement was good and in some cases excellent, with the measured and computed values all lying within the estimated experimental error (see Section 4.4.2). Modal propagation coefficients were also compared with theoretical values obtained using the effective index method. In all cases this method returns a value almost identical to that of Marcatili (56) when using the equivalent rectangular waveguide effective width theory of Section 4.3, but since it appears to have no simple physical interpretation, it was decided to concentrate on Marcatili's solution. For 7059 glass stripe waveguides it has been shown (see Section 4.4.2) that the trapezoidal waveguide effective width theory together with Marcatili's eigenvalue mode equations provides solutions valid over all ranges of practical interest, even for waveguides close to "cut-off" and gives useful information as to the field distributions both inside and outside the

waveguide which proves useful in the design of stripe waveguide devices. We have shown, therefore, that Marcatili's theory accurately predicts the modal propagation characteristics of ion-etched 7059 glass waveguides with an effective waveguide width substituted in place of the rectangular width to account for the trapezoidal geometry of the waveguide (see Section 4.3).

8.1.3. Stripe Ion-Etched 7059 Glass Waveguide Devices.

With these thoughts in mind, attention was turned to the design of stripe single mode passive waveguide devices including waveguide tilts, Y-junctions and power splitters. In analysing each case a planar waveguide model was employed which neglects radiation in the backward direction. Since the stripe waveguide devices considered display only dimensional and directional changes in the x direction, it is possible to use the planar waveguide model analysis coupled with the relevant x direction waveguide parameters to predict accurately the transmission performance of single mode (E_{11}^{x}) stripe waveguide devices (see Sections 5.2, 6.2, 7.2 and also Appendices B1 and B2).

8.1.3.1. Waveguide Tilts.

In the waveguide tilt case, experimentally measured values of power transmission plotted against tilt angle showed a close correlation with the values calculated from the theoretical model (see Chapter 5). Tilt angles of up to 3^{o} may be used but the rapid fall in power transmission above this precludes larger angles. It is foreseen that waveguide tilts will find many applications in integrated optical circuits for which dielectric waveguides require small changes in direction, for example, making parallel the branching arms of a Y-junction formed in $LiNbO_3$ so as to fabricate a modulator (6). However, in this case it

should be noted that due to the extremely small refractive index difference between the waveguide and the surrounding media the range of useful angles are limited to around 1^{o}.

8.1.3.2. Y-Junctions.

Another device which was considered is the Y-junction (see Chapter 6). The problem here was to investigate the loss mechanism of the device and to relate it to a theoretical model which can accurately predict the transmission performance of practical devices. The planar waveguide analysis of Anderson (70) was modified to take into account a defect formed in the junction wedge during the fabrication process. Using the method outlined for the waveguide tilt analysis, the planar Y-junction model was used to predict the transmission performance of stripe waveguide Y-junctions. Experimental results showed good agreement with the theoretically calculated values of transmission, with the wedge defect causing almost half of the total incident power to be lost by radiation at the junction. The effects of junction defects are pronounced in ion-etched 7059 glass waveguides due to the large refractive index difference between the waveguide and the surrounding media. This effect should not be so marked for other waveguide materials which display a smaller change in refractive index, e.g. Ti diffused $LiNbO_3$. By modifying the planar waveguide Y-junction analysis it is possible to model the loss mechanism present in Ti diffused $LiNbO_3$ Y-junctions and hence predict the power transmission of practical devices (see Section 6.4). The loss mechanism associated with $LiNbO_3$ stripe Y-junctions is somewhat different from that of the 7059 glass case in that there is a section of waveguide with a larger refractive index present at the junction,

due to the lateral diffusion of the titanium. Thus all the power incident on this higher index region is refracted into the surrounding media and then lost by radiation, rather than being reflected and scattered and lost to radiation directly, (see Section 6.4.1). This results in a larger transmission loss at the junction than at first would be expected when considering the simpler loss mechanism of the ion-etched 7059 glass Y-junctions. A modified $LiNbO_3$ Y-junction loss model was applied to several experimentally measured Ti diffused $LiNbO_3$ Y-junctions (see Section 6.4.2). A best curve fit to the measured experimental points was employed, results showed that all the experimental points were predicted to within experimental error. We may conclude, therefore, that the planar Y-junction analysis with the modified loss mechanism can predict accurately the transmission performance of practical stripe waveguide Y-junctions formed in $LiNbO_3$. This should optimise the design of both passive and active devices based on Ti diffused $LiNbO_3$ Y-junctions and should allow the accurate design and fabrication of highly efficient electro-optic modulators and switches with low insertion loss (6,53). The introduction of this modified loss model has done much for the understanding of Ti diffused $LiNbO_3$ Y-junctions.

8.1.3.3. Waveguide Power Splitters.

The other device considered was the waveguide power splitter. Basically it consists of an asymmetric Y-junction, i.e. one output arm is straight and the other tilted (see Chapter 7). Measurements showed that this device had the same overall power loss as the Y-junction (as would be expected), (see Section 7.3.4). However, due to the

asymmetric nature of the device, the straight waveguide supports more transmitted power than does the angled waveguide. This results in a useful waveguide power splitter. Measurements showed that it is possible to fabricate a device with a 10 dB power ratio between the output waveguides (see Section 7.3.4).

The power splitter is easier to make than the corresponding evanescent field type of directional coupler in 7059 glass stripe waveguides, which requires a smaller gap between the two adjacent waveguides than can be achieved by conventional photo-lithography. This device is sure to find application in future integrated optical communications systems which include signal processing.

8.1.4. Conclusions.

We conclude that a number of stripe waveguides and associated devices had been fabricated and evaluated. Marcatili's modified theory (56) was found to predict accurately the waveguide modal propagation characteristics and could be used to design single mode stripe waveguides. Single mode stripe waveguides were then used in the fabrication of waveguide tilts, Y-junctions and power splitters. By considering a planar waveguide analysis of the relevant stripe waveguide device it was possible, using the field configurations of Marcatili, to predict accurately the stripe waveguide device power transmission performance. This should make the efficient design of the relevant stripe waveguide components relatively straightforward thus allowing for an optimum system design. In this respect the research undertaken has achieved its goal, namely the design of passive waveguide components for integrated optics.

One of the limiting factors in this investigation has been the need to work with waveguides which are long enough for

convenient and accurate measurement (i.e. at least 3 cm). The need for long waveguides limits the narrowest guide width to around 5 μm and restricts the fabrication conditions necessary for single mode guiding. Due to a recent upgrade in the photolithographic facilities, it is now possible to design waveguide masks which have a good edge quality and guide widths of around 3 μm, with waveguide lengths sufficient to allow reasonably accurate measurements to be made. Unfortunately, this facility became available too late in the course of experimental work to be of assistance. All waveguides and devices were, therefore, made using the pre-upgrade photolithographic facilities.

Skill, patience, dedication and care were required in all of the measurements undertaken due to the small size of the devices. This greatly hindered the rate of progress that was attained. In retrospect it might have been better to model these devices at microwave frequencies for which, due to the much increased size of the waveguides, measurements could be made more accurately and more quickly. This may have to be contemplated in future device development as the waveguides become smaller and smaller and the power levels drop accordingly. It is possible in the future that microwave modelling may become a useful technique in the design of sub-micron, single mode, stripe waveguides and components, where the microscopic size of the waveguides makes measurement impossible.

8.2. Future Work.

There is ample scope for further work. Thin film, R.F. sputtered, 7059 glass is ideally suited to the fabrication of passive integrated optical waveguide devices in both planar

and stripe waveguide form. However, in the latter case it should be noted that the maximum useful length of waveguide is about 3 cm because of the high loss associated with the method of preparation.

Another potentially useful integrated optical device is a waveguide cross-over (X-junction), much work has still to be carried out on both large and small angle versions of these devices. From the work completed on the stripe waveguide Y-junctions and power splitters it may be expected that small angle X-junctions could be analysed in much the same way, with the transmission performance v.s. junction angle behaving in a similar manner.

From the results presented in this thesis, it should be possible to fabricate and design a small scale integrated optical system incorporating some active elements. A suitable material could be Ti diffused $LiNbO_3$. The integrated optical device could consist of several modulators/switches (active Y-junctions) feeding into several input/output waveguides and perform some high speed digital processing, e.g. multiplexer/de-multiplexer. The technology to fabricate such a device is available and the only remaining problem is that of coupling input and output optical fibres to the device. Work is in fact underway in this department into this problem, using arsenic trisulphide ribbon fibres to taper-velocity-couple both into and out of Ti diffused $LiNbO_3$ waveguides transmitting the near infrared (1.15 μm) (96,109).

Work could also be carried out on "Slab-Coupled Waveguides" (45,97). The waveguides could be fabricated in an identical manner to the ion-etched waveguides of Chapter 4, but instead

of etching the guide down to the substrate, only a small section of the guiding film is removed. This results in a raised ridge of higher guide effective index (β/k_o) which tends to channel the guided mode(s) into a region directly below the etched ridge. In this manner the etched ridge acts as a waveguide and allows the direction and nature of the guided mode(s) to be controlled and modified. Waveguides fabricated in this way have large evanescent fields and small waveguide losses due to the reduced size of the rough ion-etched waveguide walls. It is envisaged that all the single mode stripe waveguide devices considered in this thesis could be fabricated in this type of waveguide. Due to the small etch depth of the waveguide walls, waveguide losses and junction defects would be reduced, however, so also would be the available range of device angles. This type of waveguide would also make feasible the fabrication of an evanescent field waveguide coupler, due to the small effective index difference between the waveguide and the surrounding thin film, resulting in large evanescent fields. In many cases devices fabricated in this type of waveguide would show enhanced operational characteristics of reduced device transmission loss due to defects. However, it should be noted that analysis of a "slab coupled waveguide" is not trivial, and the consistent fabrication of single mode waveguides may prove difficult. All things considered, characterisation of this type of waveguide is a project in itself and should not be undertaken lightly.

Another device considered is a directional coupler. Basically it consists of two long stripe waveguides separated by a small gap (approximately 1.5 μm), onto which is sputtered a marginally lower refractive index 7059 glass film (approximately

0.005% change in index). This may be readily achieved by altering the R.F. power in the sputtering chamber plasma. Due to the extremely small refractive index difference, the evanescent fields of the propagating mode should couple across the gap in a reasonably small distance (≃ 1 mm), and with both guides being fabricated at the same time, their β values should be similar, thus allowing almost total transfer of power (98) between them. A coupler is also being considered in another form for which two large radius circular stripe 7059 glass waveguides touch tangentially. Calculations suggest that a 3dB coupler may be fabricated from two 3 μm wide single mode stripe waveguides with a 0.171 metre radius (77), (see Appendix E1). However, this theory and calculations have still to be verified experimentally.

With waveguides fabricated in materials exhibiting a small refractive index difference between the waveguide and the surrounding media small radius bends become a problem due to the large evanescent fields present in the substrate leaking into radiation modes as the guided mode traverses the bend. This is not such a great problem for 7059 glass waveguides due to the large refractive index difference between the waveguide and the surrounding media. To the author's knowledge, little is known about stripe waveguide bending loss. Single mode stripe 7059 glass waveguides provide an ideal medium for carrying out an experimental investigation into waveguide bending loss and its dependance on radius of curvature. Work of this kind would have been beneficial for inclusion in the thesis, as bends in stripe waveguides will form a necessary part of a practical future integrated optical communications system. Information on bending loss will be of value in the design of the waveguide

coupler based on two tangentially touching curved waveguides (77), (see also Appendix E1).

It is hoped that some of the devices investigated in this thesis will find their way into a future integrated optical communications system. A practical system will be unlikely to use a passive material such as sputtered glass and it is envisaged that some systems will be based on GaAs and its associated compounds and be able to perform all the functions required on a single substrate.

APPENDICES

APPENDIX A. COMPUTER FLOW DIAGRAMS

During the course of the project many varied computer programs were written to aid the design of waveguides and associated devices. Many of the problems solved required the use of extensive iterative procedures (e.g. solving transcendental equations), and the use of complex number routines (e.g. the Y-junction and power splitter analyses of Chapters 6 and 7). All the programs were written in extended "Fortran", language using "Double Precision", arithmetic and were implemented on large I.B.M. and I.C.L. machines. The use of "Double Precision" arithmetic was necessary to avoid the possibility of cumulative "round off" errors having a detrimental effect on the accuracy of the calculation. This was especially true in the effective index calculations of Chapter 4, for which a change in the sixth decimal place of one calculation could seriously affect the results of subsequent calculations, inducing large errors into the final result. Round-off errors were also significant in the calculation of the Y-junction and power splitter equations due to the large number of calculations. The use of "Double Precision" arithmetic ensured that round off errors were insignificant.

Only flow diagrams are given in the following sections as complete program listings were thought to be bulky and unnecessary. Many smaller programs are not listed here as the implementation is trivial. Many of the programs that are mentioned here use several common subroutines and differ only in the calculation of a specific parameter. However in the interests of clarity this will not be indicated, and each section will be treated separately.

APPENDIX A1. COMPUTER FLOW DIAGRAM OF PROGRAM FOR CALCULATING WAVEGUIDE REFRACTIVE INDEX AND THICKNESS FROM THE SYNCHRONOUS MODE COUPLING ANGLES.

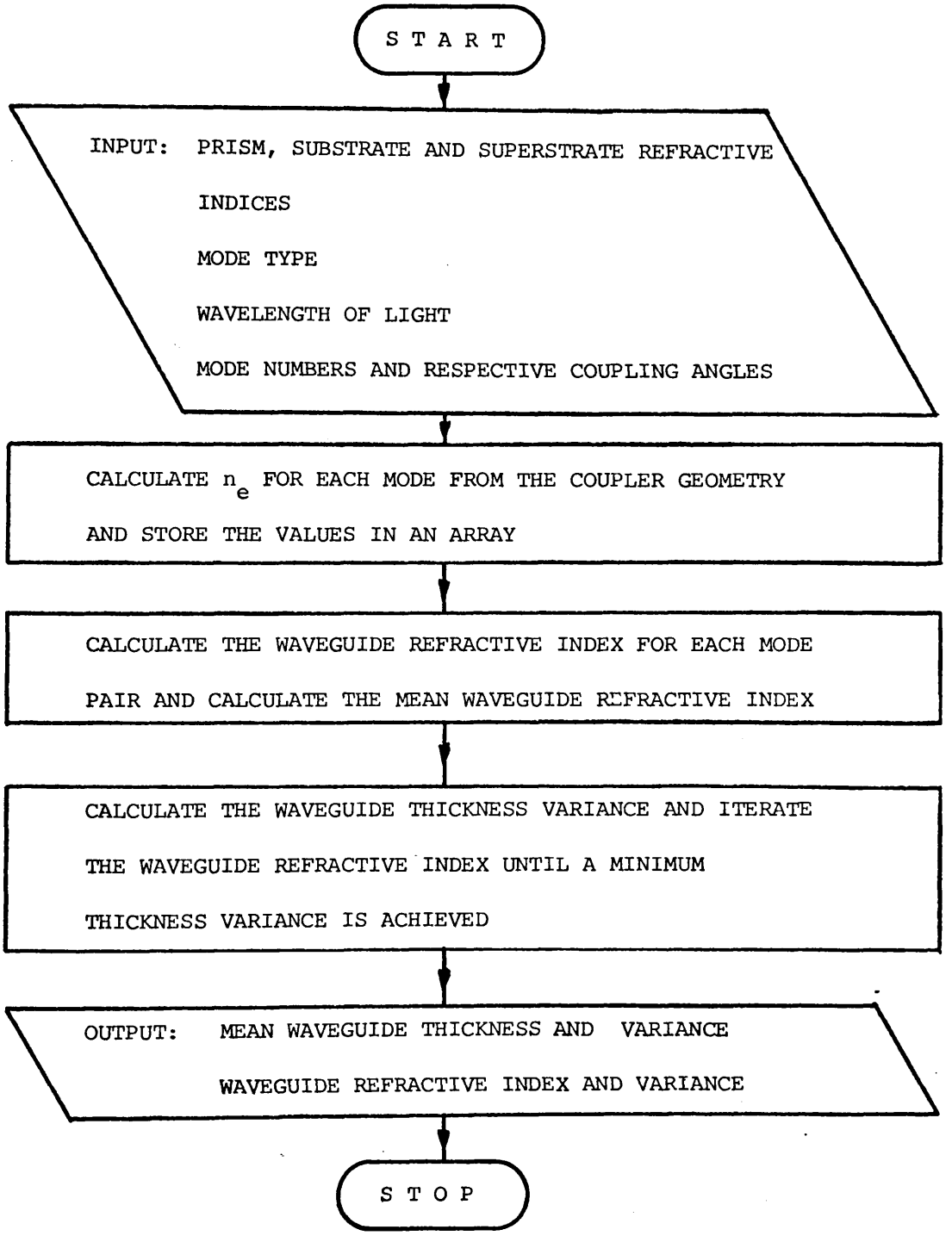

APPENDIX A2. COMPUTER FLOW DIAGRAM OF PROGRAM FOR CALCULATING WAVEGUIDE PROPAGATION COEFFICIENTS USING MARCATILI'S TRANSCENDENTAL WAVEGUIDE EQUATIONS.

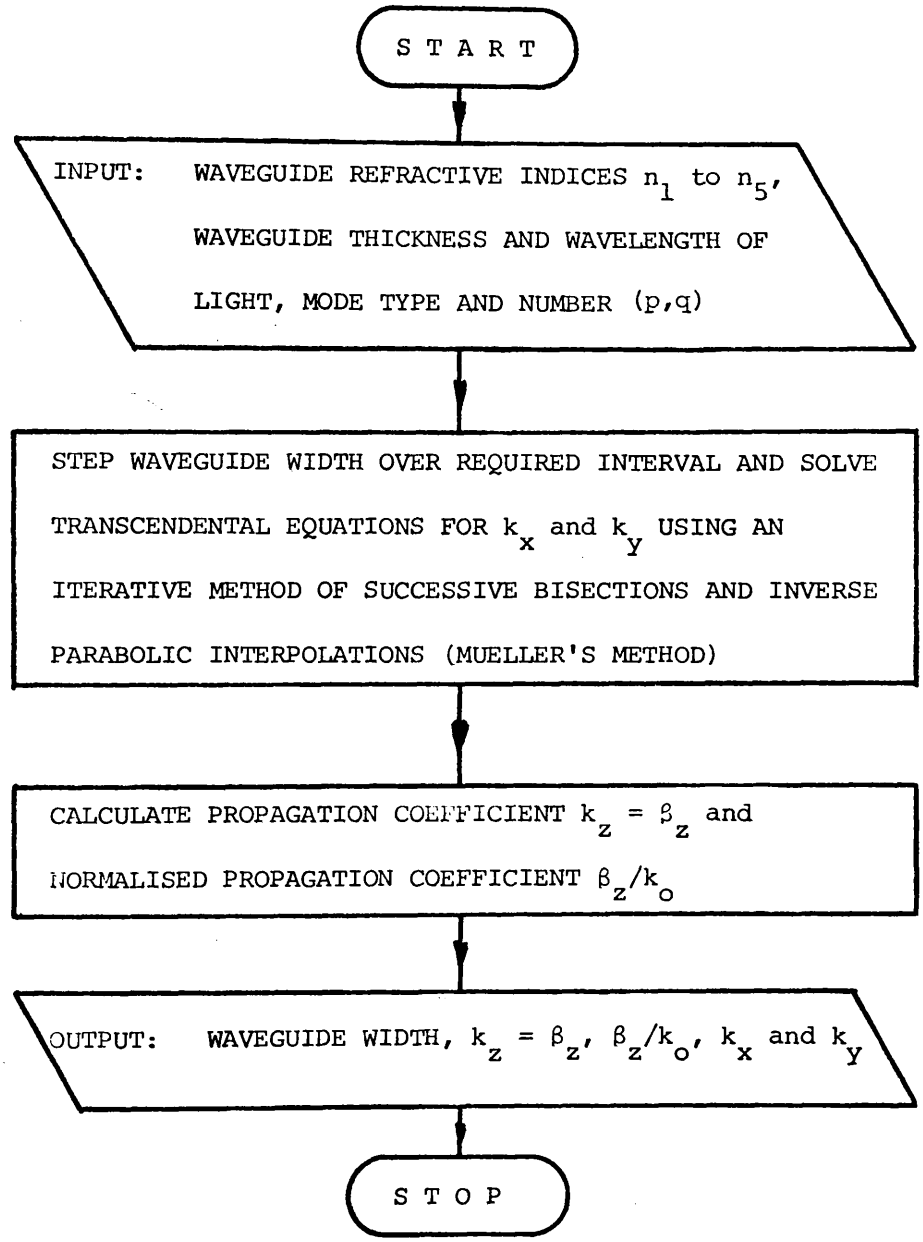

APPENDIX A3. COMPUTER FLOW DIAGRAM OF PROGRAM FOR CALCULATING WAVEGUIDE PROPAGATION COEFFICIENTS USING THE EFFECTIVE INDEX METHOD OF FIG. 4.2.

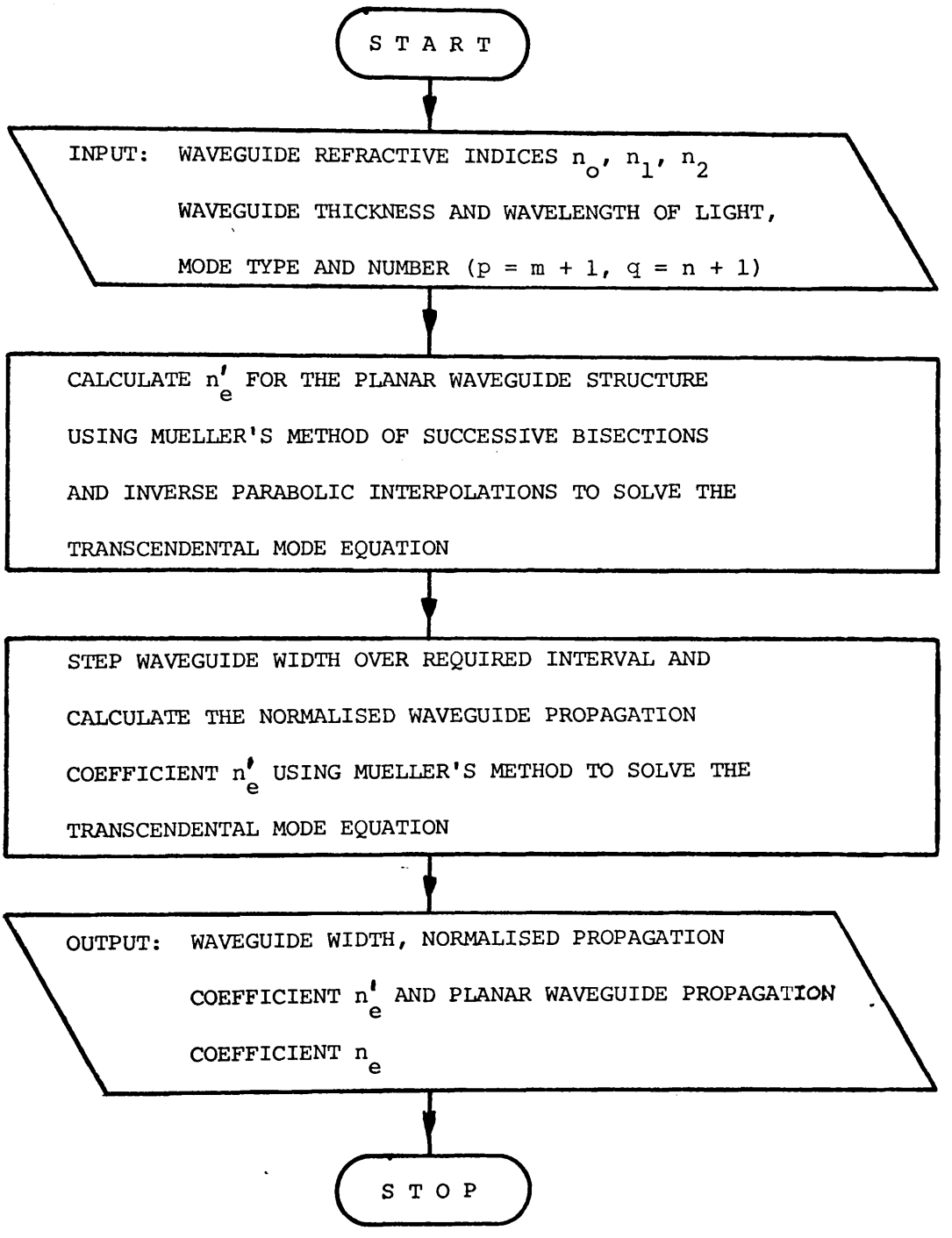

APPENDIX A4. COMPUTER FLOW DIAGRAM OF PROGRAM FOR CALCULATING WAVEGUIDE PROPAGATION COEFFICIENTS USING THE EFFECTIVE INDEX METHOD OF FIG. 4.3.

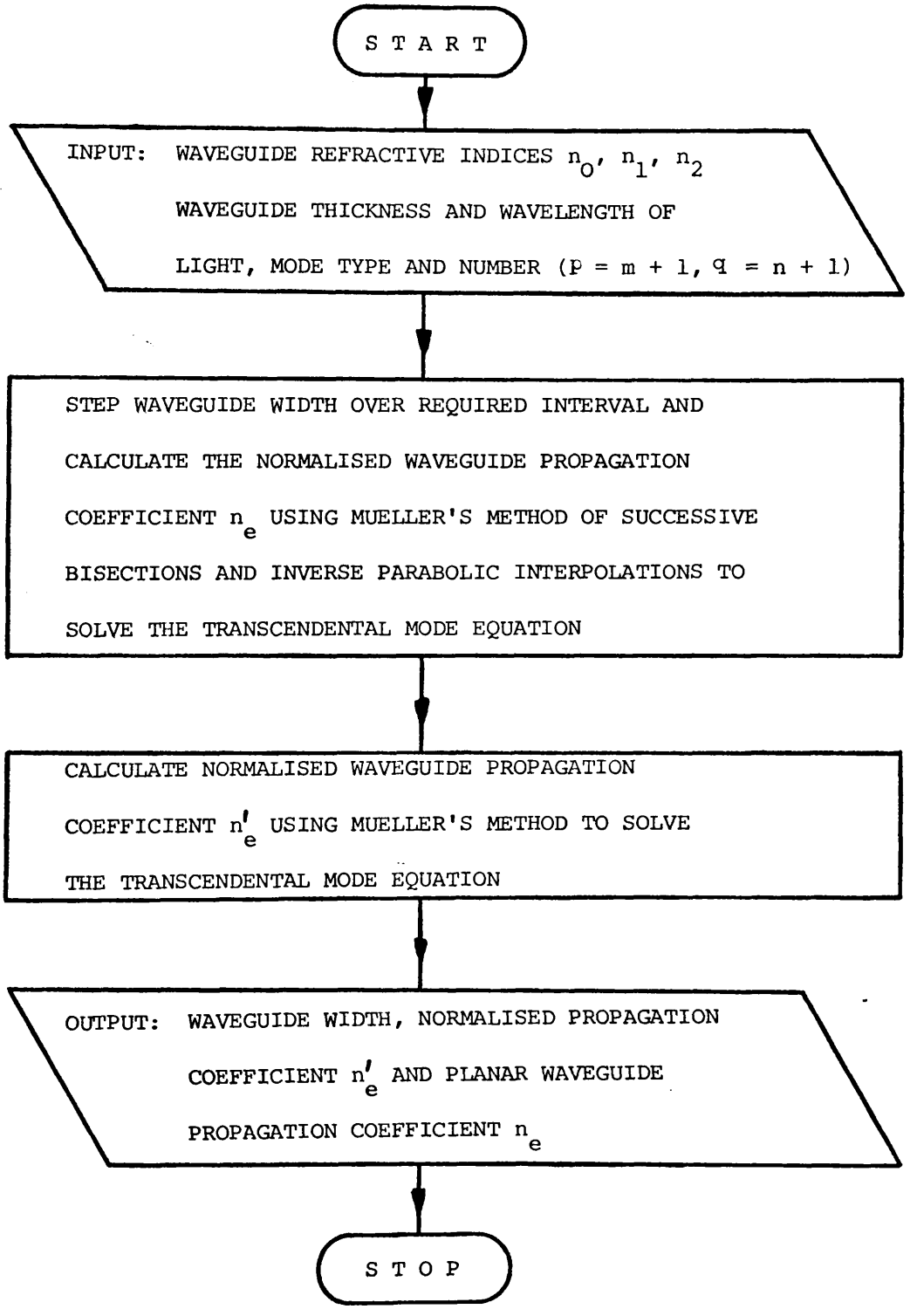

APPENDIX A5. COMPUTER FLOW DIAGRAM OF PROGRAM FOR CALCULATING THE POWER TRANSMISSION OF A PLANAR WAVEGUIDE TILT.

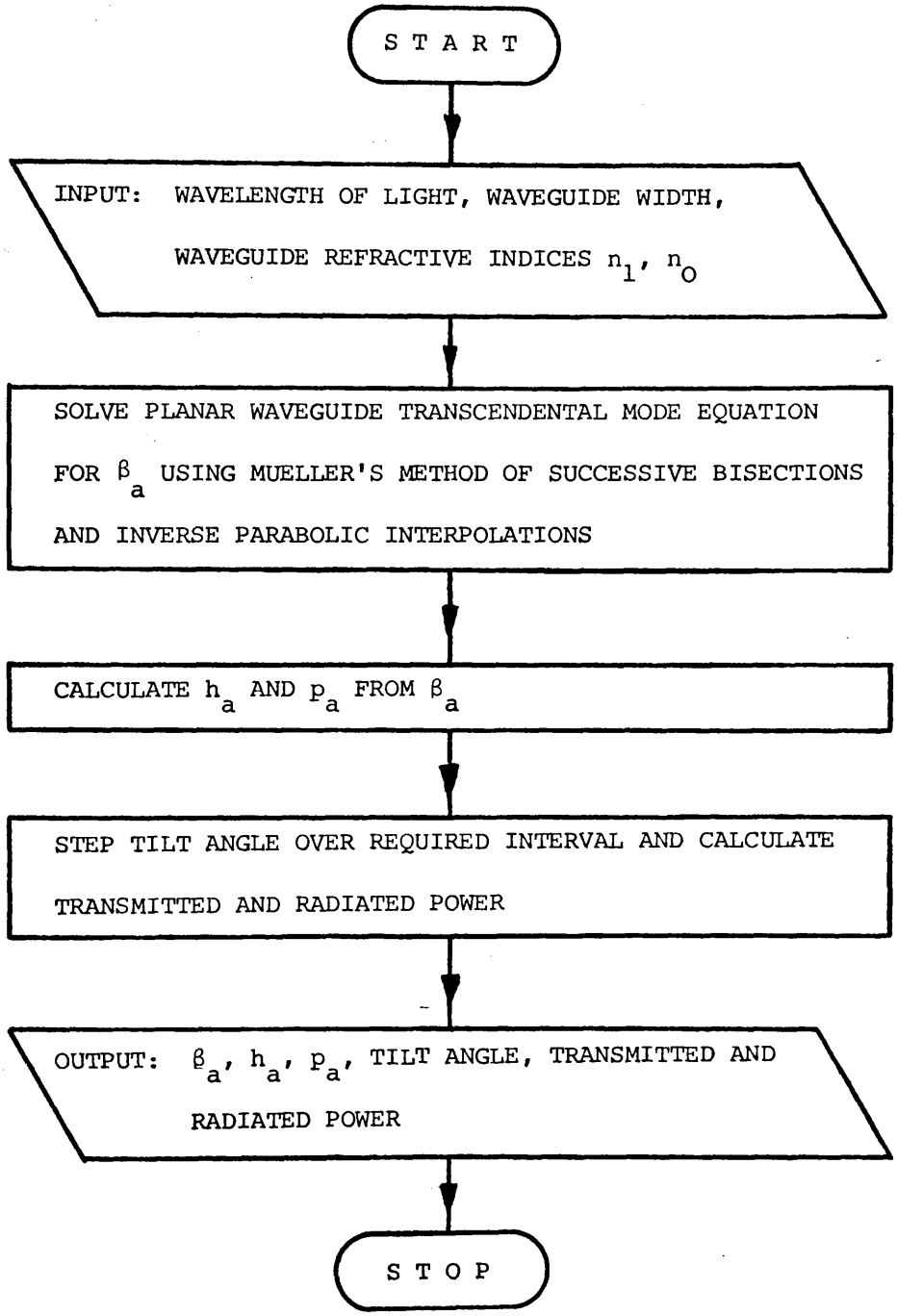

APPENDIX A6. COMPUTER FLOW DIAGRAM OF PROGRAM FOR CALCULATING THE POWER TRANSMISSION OF A STRIPE WAVEGUIDE TILT.

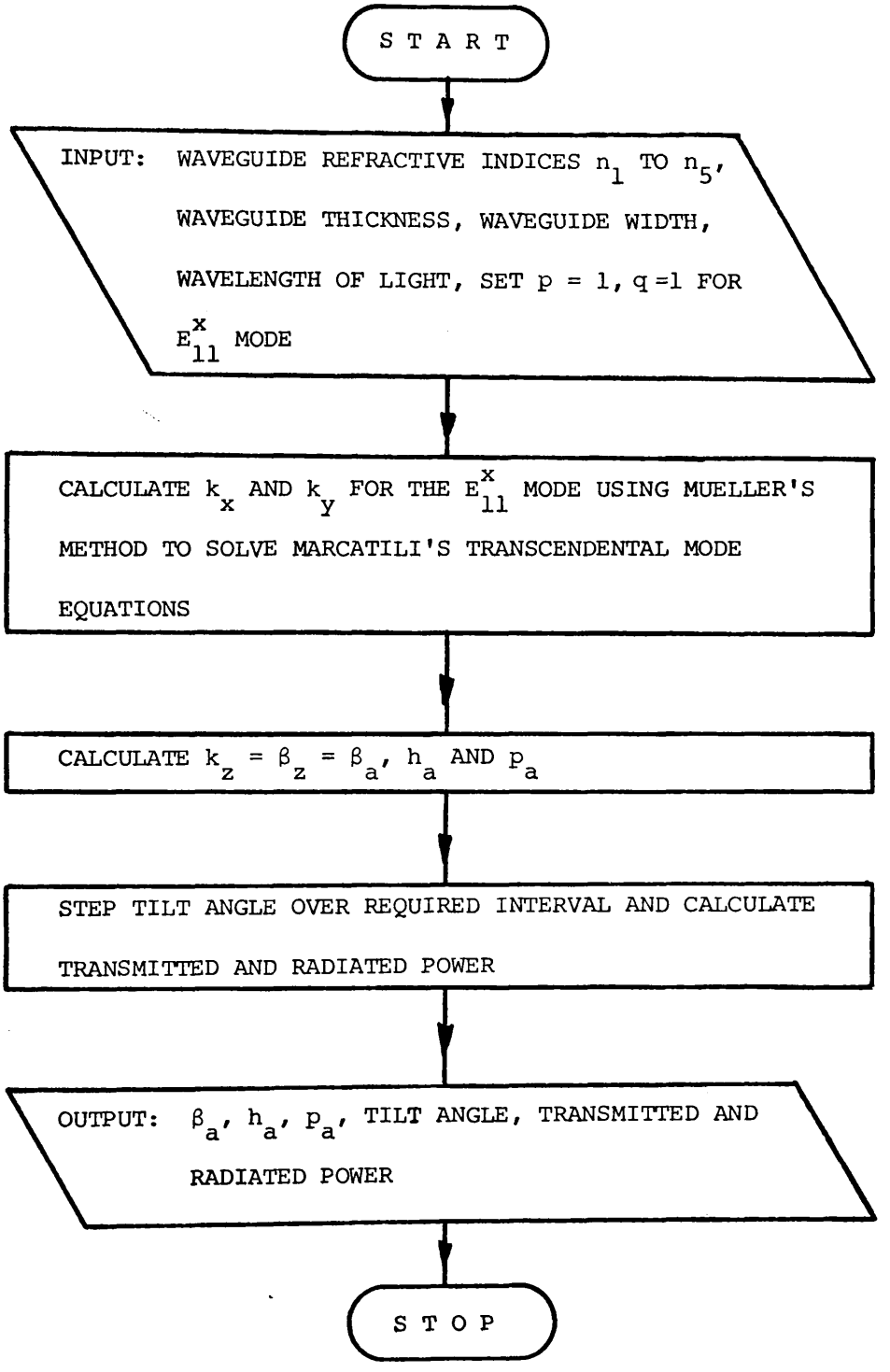

APPENDIX A7. COMPUTER FLOW DIAGRAM OF PROGRAM FOR CALCULATING THE POWER TRANSMISSION OF A PLANAR WAVEGUIDE Y-JUNCTION WITH A BLUNT WEDGE.

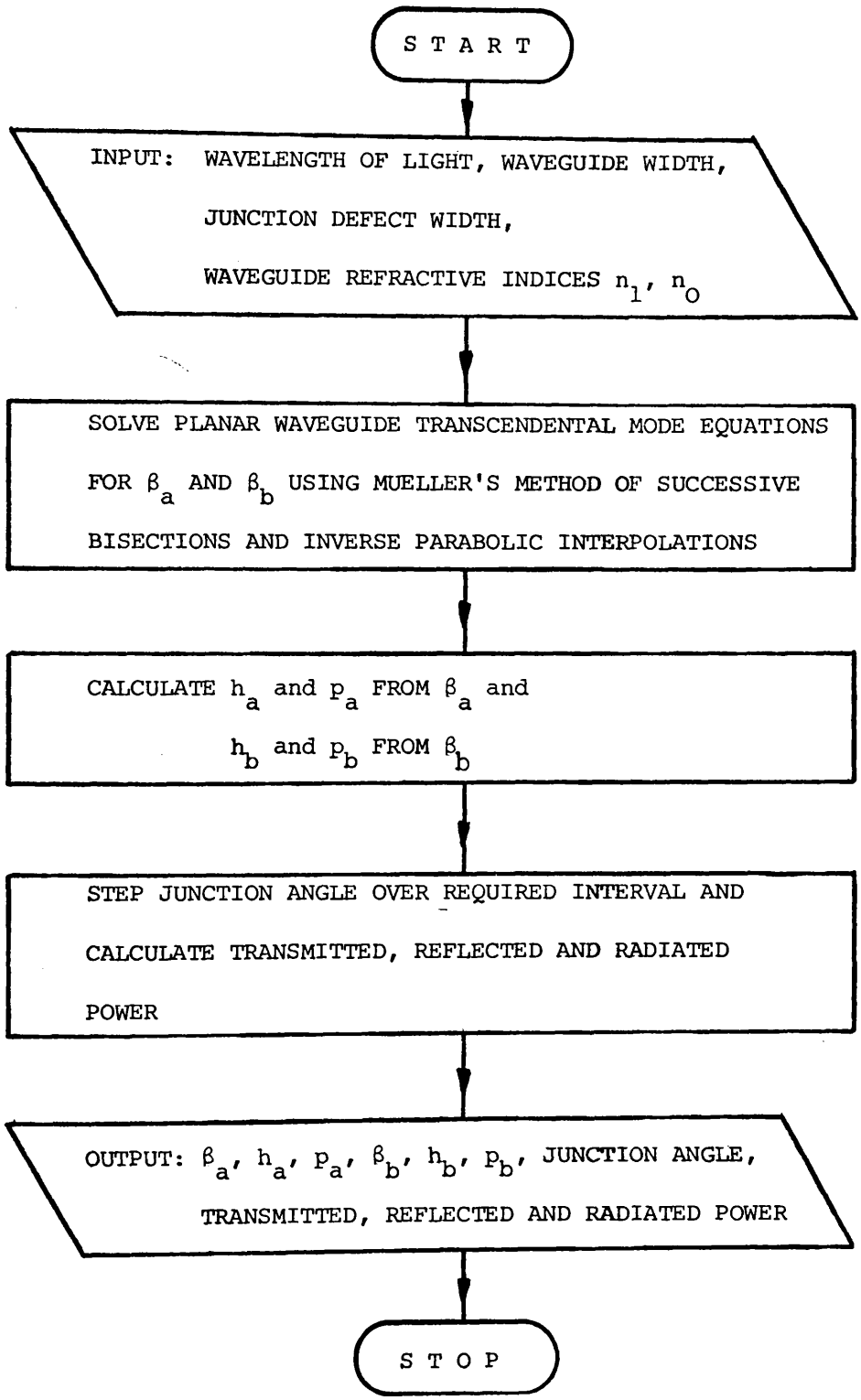

APPENDIX A8. COMPUTER FLOW DIAGRAM OF PROGRAM FOR CALCULATING THE POWER TRANSMISSION OF A STRIPE WAVEGUIDE Y-JUNCTION WITH A BLUNT WEDGE.

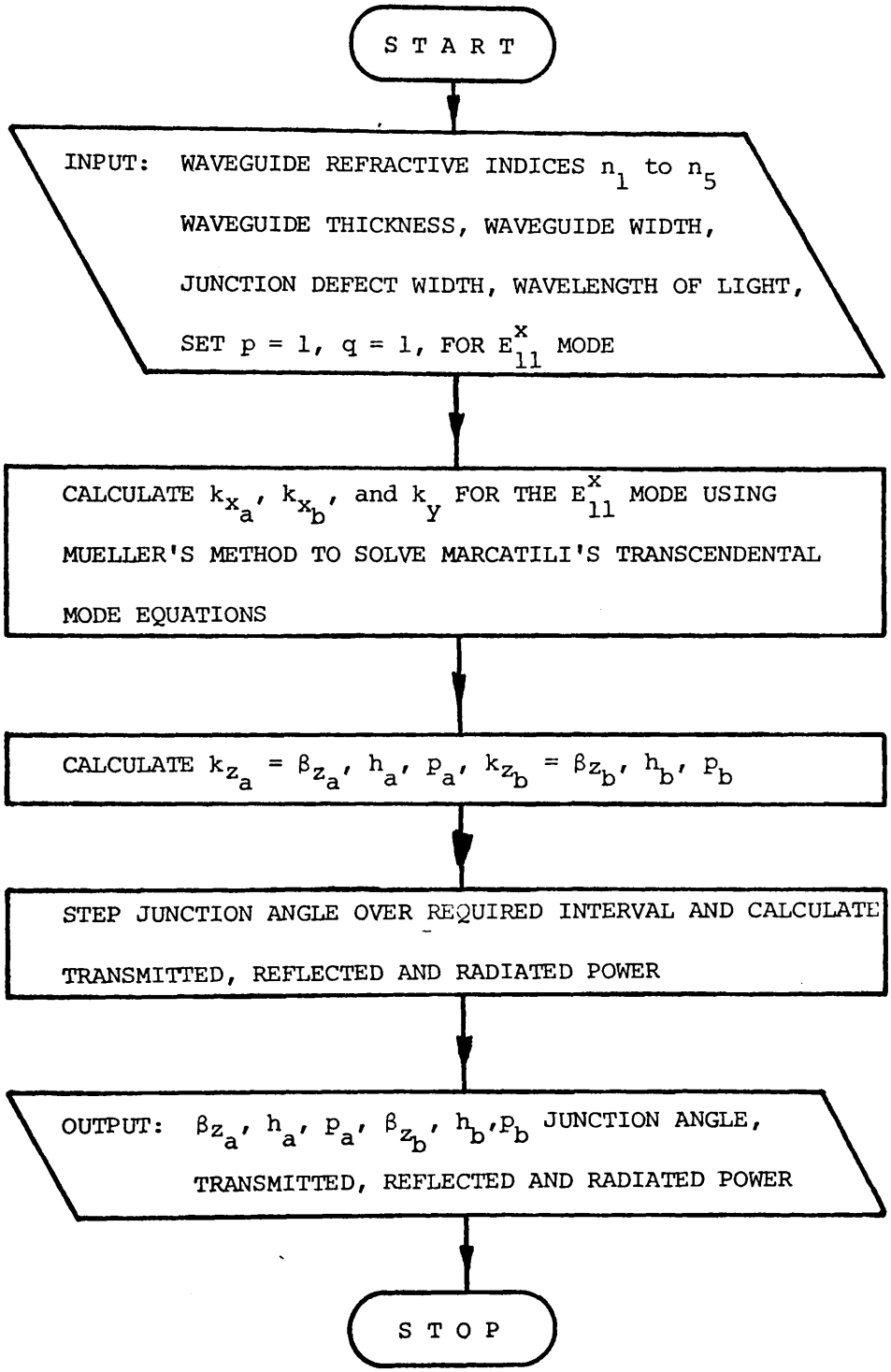

APPENDIX A9. COMPUTER FLOW DIAGRAM OF PROGRAM FOR CALCULATING THE POWER TRANSMISSION OF A PLANAR WAVEGUIDE POWER SPLITTER WITH A BLUNT WEDGE.

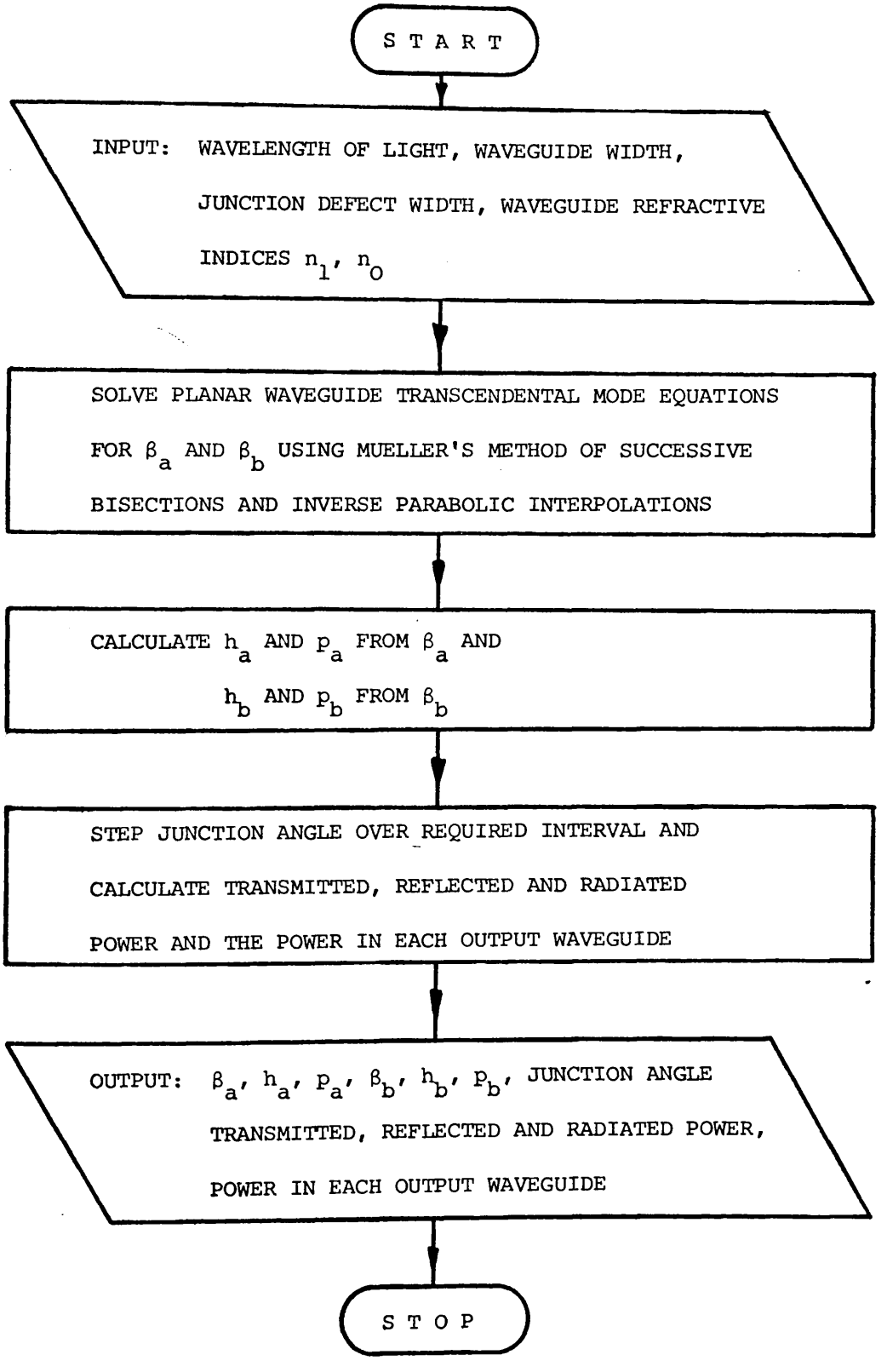

APPENDIX A10. COMPUTER FLOW DIAGRAM OF PROGRAM FOR CALCULATING THE POWER TRANSMISSION OF A STRIPE WAVEGUIDE POWER SPLITTER WITH A BLUNT WEDGE.

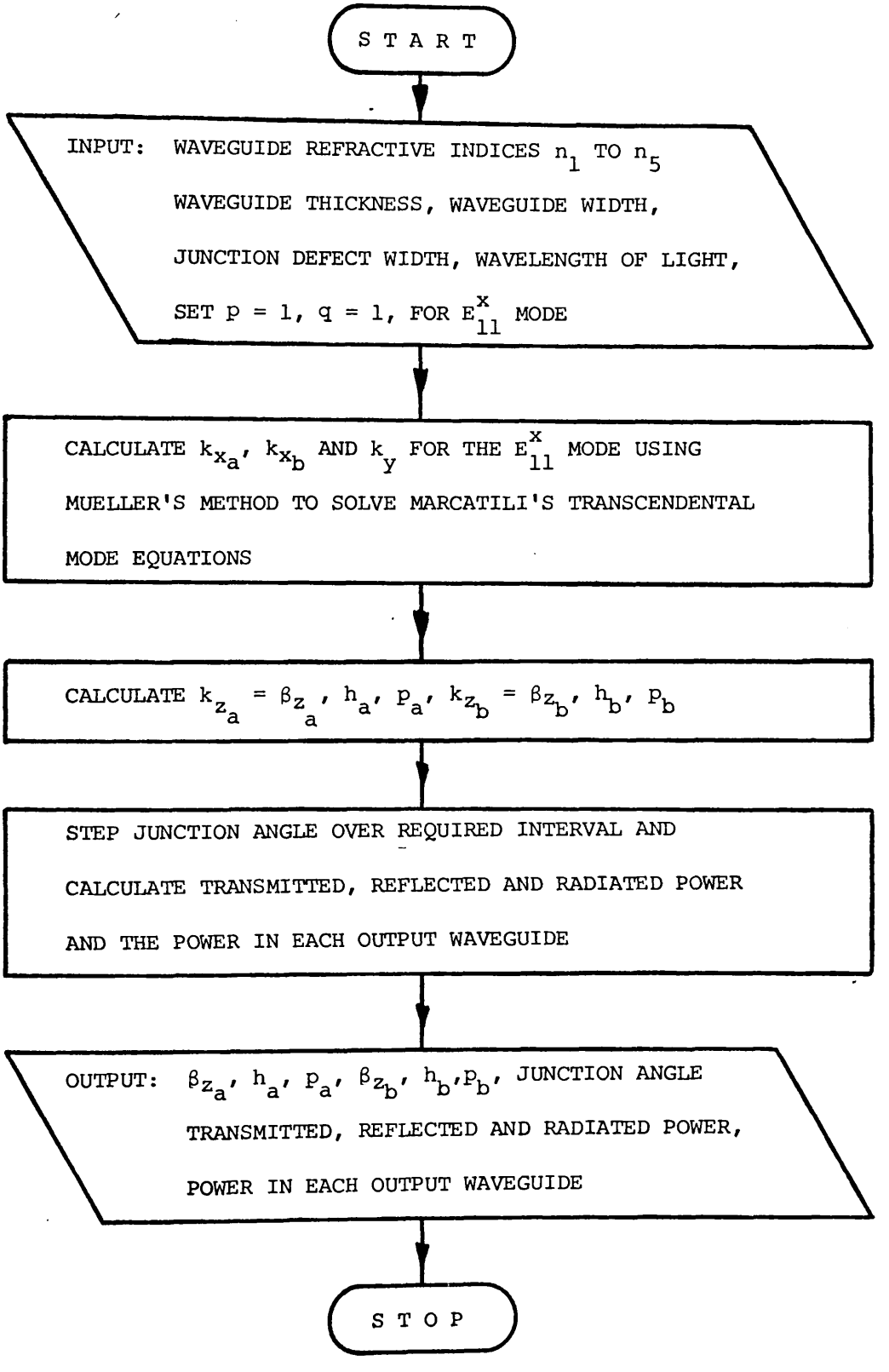

APPENDIX A11. COMPUTER FLOW DIAGRAM OF PROGRAM FOR CALCULATING THE LAUNCHING EFFICIENCY OF A TE_o SURFACE WAVE ON A GROUNDED DIELECTRIC SLAB WAVEGUIDE.

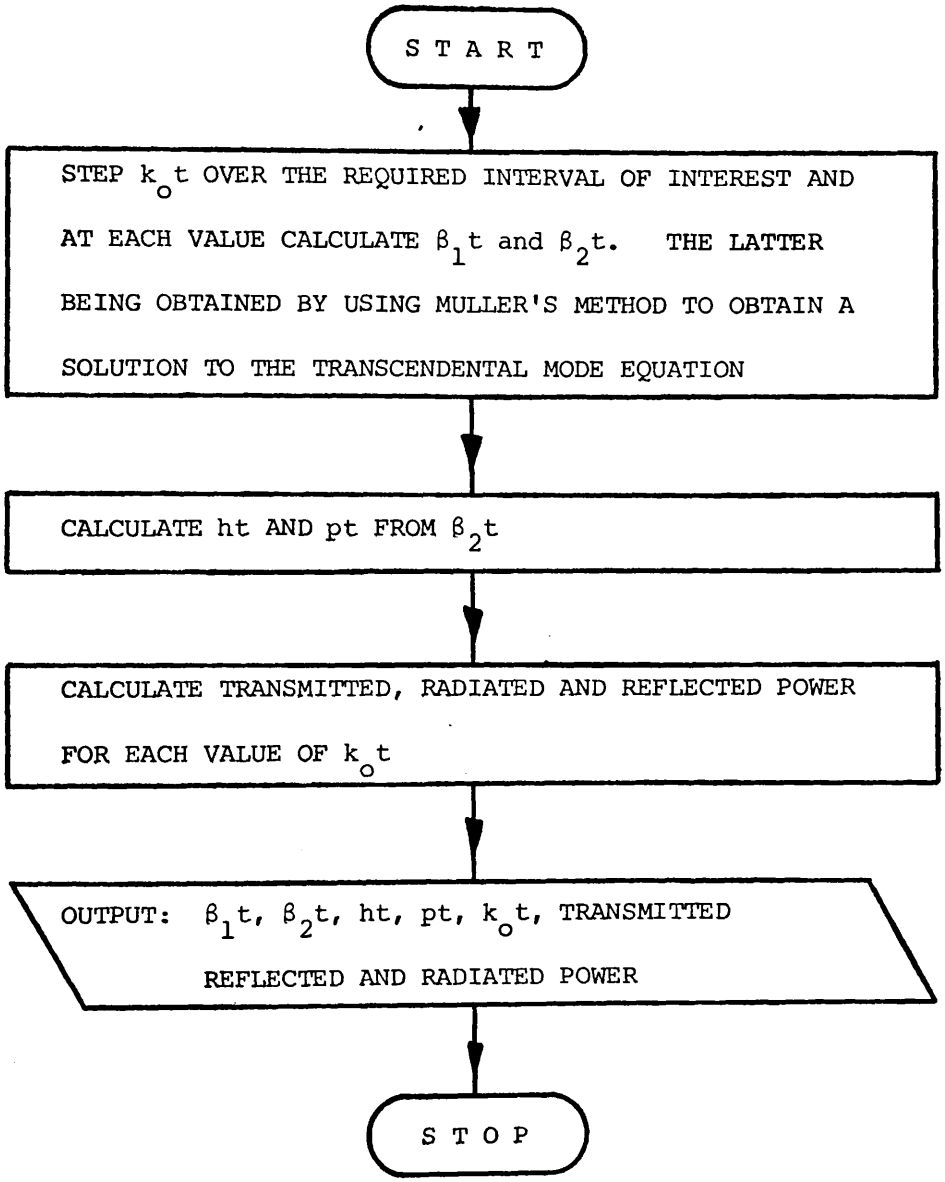

APPENDIX A12. COMPUTER FLOW DIAGRAM OF PROGRAM FOR CALCULATING THE TWO DIMENSIONAL WAVEGUIDE EFFECTIVE WIDTH.

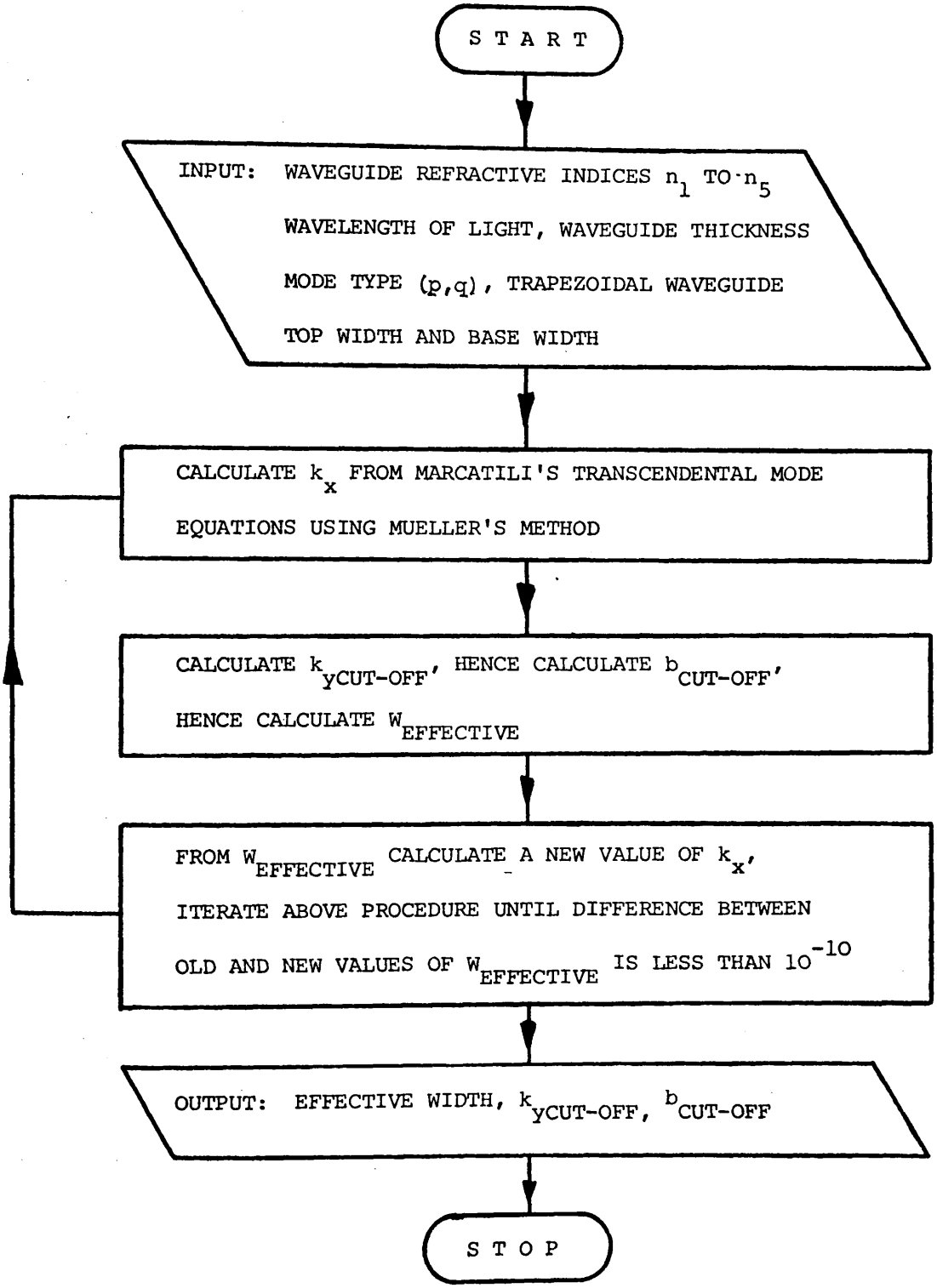

APPENDIX B1. TWO DIMENSIONAL RECTANGULAR DIELECTRIC WAVEGUIDE ANALYSIS.

The analysis presented here results in a solution identical to that found by Marcatili (56). The method adopted in this analysis, however, is different in that it employs a separation of variables technique to obtain approximate solutions for the waveguide fields. This technique permits a much simpler analysis than that presented by Marcatili (56).

B1.1. Rectangular Dielectric Waveguide Analysis.

We consider the rectangular waveguide structure of Figure B1.1 with the various waveguide refractive indices and dimensions as shown. For any guided mode, the transverse field component $\underline{E}^t$ can be expressed in terms of x and y components.

We consider the case with $\underline{E}^t = E_x$, i.e. the electric field is predominantly in the x direction, corresponding to the E^x_{pq} modes of Marcatili.

From the wave equation we have:-

$$(\underline{\nabla}^2 + k_\nu^2)\, E_x = 0 \qquad \nu = 1, \ldots .5 \tag{B1.1}$$

Assuming that the E_x field of the guided mode may be written as,

$$E_x(x,y,z) = E_x(x,y)\, e^{-j\beta_z . z} \tag{B1.2}$$

which by use of equation (B1.1) gives

$$\frac{\partial^2 E_x(x,y)}{\partial x^2} + \frac{\partial^2 E_x(x,y)}{\partial y^2} + (k_\nu^2 - \beta_z^2)\, E_x(x,y) = 0 \tag{B1.3}$$

We assume that the fields in the x and the y directions may be obtained by a separation of variables technique (99), accordingly,

$$E_x(x,y) = E_x(x) . E_x(y) \tag{B1.4}$$

allowing (B1.3) to be written as

$$\frac{1}{E_x(x)} \frac{\partial^2 E_x(x)}{\partial x^2} + \frac{1}{E_x(y)} \cdot \frac{\partial^2 E_x(y)}{\partial y^2} + (k_\nu^2 - \beta_z^2) = 0 \tag{B1.5}$$

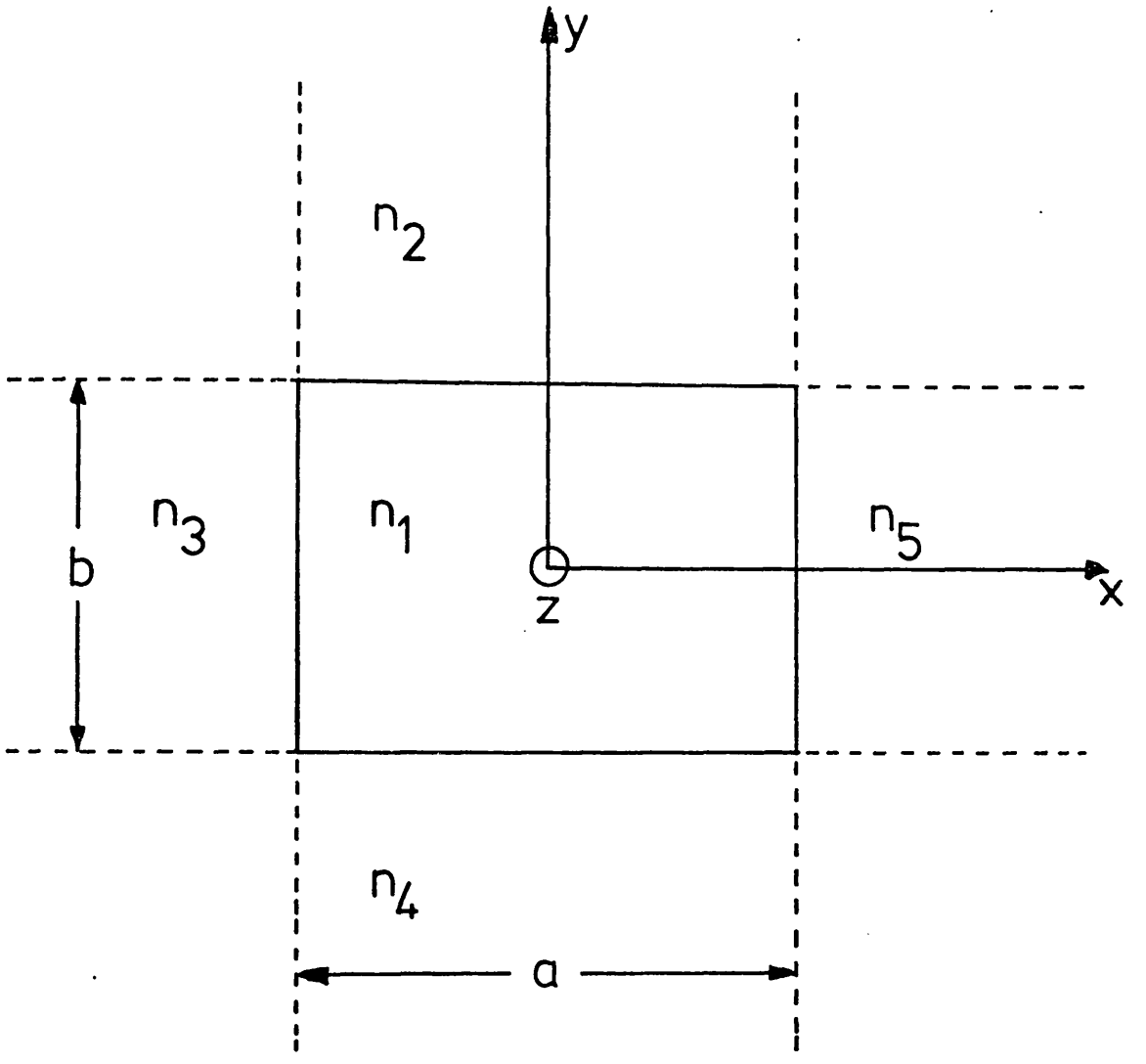

Fig. B1.1 Rectangular waveguide geometry

We let

$$\frac{1}{E_x(x)} \cdot \frac{\partial^2 E_x(x)}{\partial x^2} = - k_x^2 \qquad \text{(B1.6)}$$

$$\frac{1}{E_x(y)} \cdot \frac{\partial^2 E_x(y)}{\partial y^2} = - k_y^2 \qquad \text{(B1.7)}$$

For the fields inside the guide we have

$$k_1^2 - k_x^2 - k_y^2 - \beta_z^2 = 0 \qquad \text{(B1.8)}$$

Equation (B1.6,7) may be rewritten as

$$\frac{\partial^2 E_x(x)}{\partial x^2} + k_x^2 E_x(x) = 0 \qquad \text{(B1.9)}$$

$$\frac{\partial^2 E_x(y)}{\partial y^2} + k_y^2 E_x(y) = 0 \qquad \text{(B1.10)}$$

Equation (B1.9) is independent of y and corresponds to that of a T.M. mode propagating in a planar waveguide of width a (see Figure B1.2). Similarly equation (B1.10) is independent of x and corresponds to a T.E. mode propagating in a planar waveguide of width b (see Figure B1.3).

We choose the refractive indices of the guide and the surrounding media such that $n_1 > n_2, n_3, n_4, n_5$. The rays of the guided modes in the TE and TM planar waveguides impinge on the interfaces at grazing angles. Consequently the largest field components are perpendicular to the axis of propagation. Thus the predominant field components in a rectangular dielectric waveguide supporting an E^x mode are E^x and H^y, with small field components in the z direction.

Equations (B1.9) and (B1.10) are solved by applying the relevant boundary conditions along the waveguide/surrounding media interfaces, considering equation (B1.9), viz,

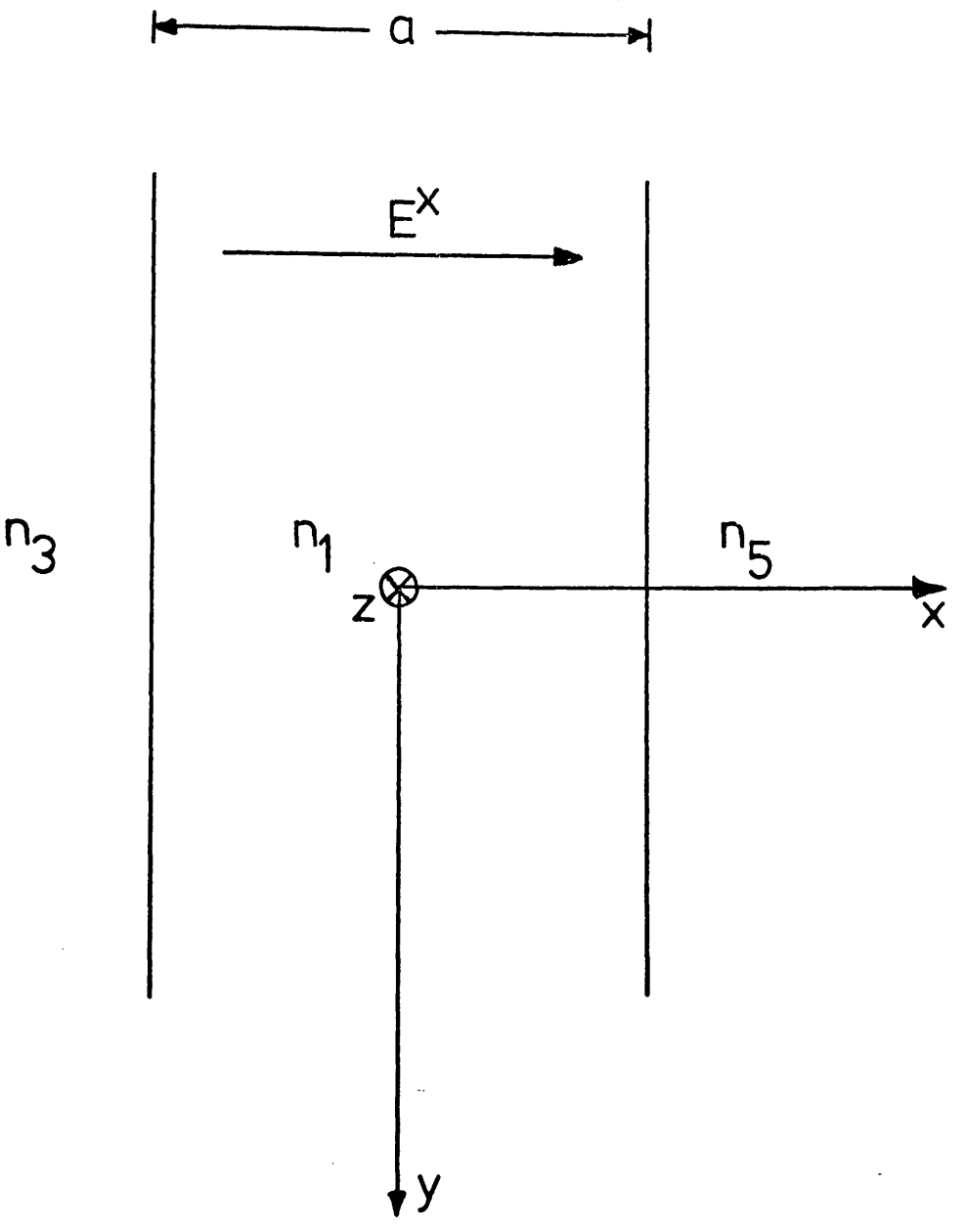

Fig. B1.2 Planar waveguide of width a propagating a TM mode

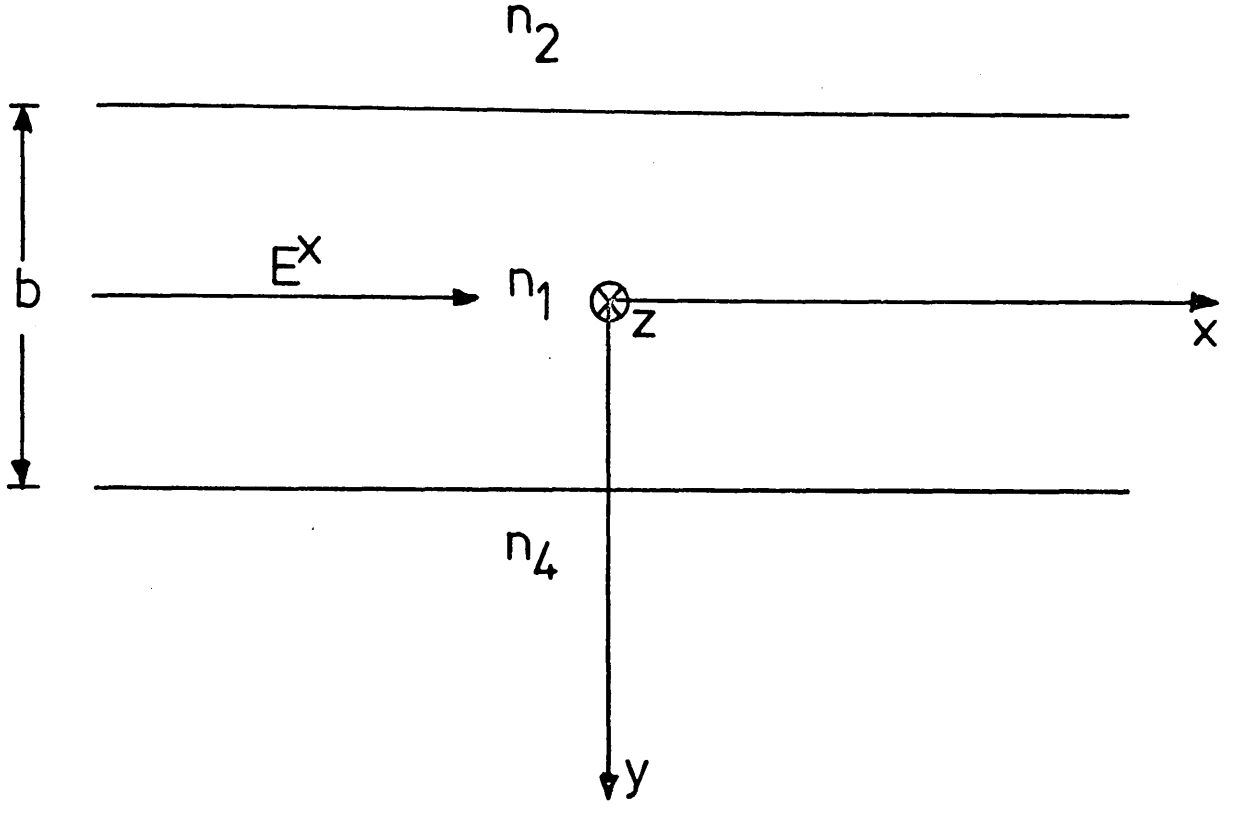

Fig. B1.3 Planar waveguide of width b propagating a TE mode

$$\frac{\partial^2 E_x(x)}{\partial x^2} + k_x^2 E_x(x) = 0 \qquad \text{(B1.9)}$$

As this is the same equation which describes a T.M. mode in a planar waveguide, we have H_y only, thus for region (1) we have a general solution of the form:-

$$E_x = \left[Ae^{+jk_x.x} + Be^{-jk_x.x} \right] e^{-j\beta_{TM}z} \qquad \text{(B1.11)}$$

with β_{TM} the guided mode propagation coefficient of the TM mode of equation (B1.9) and A and B are constants. From Maxwell's equations we have,

$$H_y = \frac{\omega n_1^2 \varepsilon_o}{\beta_{TM}} \left[Ae^{+jk_x.x} + Be^{-jk_x.x} \right] e^{-j\beta_{TM}.z} \qquad \text{(B1.12)}$$

$$E_z = \frac{k_x}{\beta_{TM}} \left[Ae^{+jk_x.x} + Be^{-jk_x.x} \right] e^{-j\beta_{TM}.z} \qquad \text{(B1.13)}$$

with the time dependence factor $e^{j\omega t}$ suppressed. Each of these field components must satisfy the wave equation,

$$\underline{\nabla}^2 \underline{E} = -k_x^2 \underline{E} \qquad \text{(B1.14)}$$

i.e.
$$k_x^2 + \beta_{TM}^2 = k_1^2 = (n_1 k_o)^2 \qquad \text{(B1.15)}$$

with β_{TM} the propagation coefficient associated with the planar waveguide of Figure B1.2 and equation (B1.9). We next consider the fields in the external regions (3) and (5). For $x > a/2$ we have,

$$H_y = \frac{\omega n_5^2 \varepsilon_o}{\beta_{TM}} Ce^{-p_5.x} e^{-j\beta_{TM}.z} \qquad \text{(B1.16)}$$

$$E_x = Ce^{-p_5.x} e^{-j\beta_{TM}.z} \qquad \text{(B1.17)}$$

$$E_z = \frac{-p_5}{j\beta_{TM}} Ce^{-p_5.x} e^{-j\beta_{TM}.z} \qquad \text{(B1.18)}$$

and similarly for $x < a/2$ we have,

$$H_y = \frac{\omega n_3^2 \varepsilon_o}{\beta_{TM}} \; De^{+p_3 x} \; e^{-j\beta_{TM} z} \tag{B1.19}$$

$$E_x = De^{+p_3 x} \; e^{-j\beta_{TM} z} \tag{B1.20}$$

$$E_z = \frac{-p_3}{j\beta_{TM}} \; De^{+p_3 x} \; e^{-j\beta_{TM} z} \tag{B1.21}$$

with C and D both constants. Again the above wave vectors must satisfy the wave equation, i.e.

$$\beta_{TM}^2 - p_5^2 = k_5^2 = (n_5 k_o)^2 \tag{B1.22}$$

$$\beta_{TM}^2 - p_3^2 = k_3^2 = (n_3 k_o)^2 \tag{B1.23}$$

The matching of the tangential electric and magnetic fields along the boundaries at $x = \pm a/2$ leads (after some algebraic manipulation) to,

$$e^{-jk_x a} \; e^{-2j\phi_{15}} = e^{+jk_x a} \; e^{+2j\phi_{13}} \tag{B1.24}$$

with

$$\phi_{15} = \tan^{-1}\left[\frac{n_5^2}{n_1^2} \cdot \frac{k_x}{p_5} \right] \tag{B1.25}$$

$$\phi_{13} = \tan^{-1}\left[\frac{n_3^2}{n_1^2} \cdot \frac{k_x}{p_3} \right] \tag{B1.26}$$

Noting that the modulus of equation (B1.24) is unity we obtain the most general eigenvalue equation using the phases of the above equations,

$$k_x . a + \phi_{15} + \phi_{13} = P.\pi \qquad P = 1,2,3,..... \tag{B1.27}$$

and

$$\beta_{TM}^2 = k_1^2 - k_x^2 = k_5^2 + p_5^2 = k_3^2 + p_3^2 \tag{B1.28}$$

Thus we see that by adopting the general wave solution of equation (B1.11) we may obtain the transcendental mode equation of a T.M. guided mode in an asymmetrical planar waveguide of refractive index n_1 surrounded on each side by lower index media of indices n_3 and n_5.

By adopting a similar method of analysis we may solve equation (B1.10) which in the most general case reduces to,

$$k_y.b + \phi_{12} + \phi_{14} = Q.\pi \qquad Q = 1,2,3, \ldots\ldots \tag{B1.29}$$

with
$$\phi_{12} = \tan^{-1}\left[\frac{k_y}{p_2}\right] \tag{B1.30}$$

$$\phi_{14} = \tan^{-1}\left[\frac{k_y}{p_4}\right] \tag{B1.31}$$

with
$$\beta_{TE}^2 = k_1^2 - k_y^2 = k_2^2 + p_2^2 = k_4^2 + p_4^2 \tag{B1.32}$$

with β_{TE} the guided mode propagation coefficient of the TE mode of equation (B1.10). Again we find that by adopting a general wave solution, the transcendental mode equation of a TE guided mode in an asymmetrical planar waveguide of index n_1 and surrounding indices n_2 and n_4, may be found.

By adopting a similar argument we may solve for the electric field polarised in the y direction, i.e. E^y modes, in which case the main results are,

$$k_x.a + \phi_{15} + \phi_{13} = P.\pi \qquad P = 1,2,3,\ldots. \tag{B1.33}$$

$$\phi_{15} = \tan^{-1}\left[\frac{k_x}{p_5}\right] \tag{B1.34}$$

$$\phi_{13} = \tan^{-1}\left[\frac{k_x}{p_3}\right] \tag{B1.35}$$

with equation (B1.28) holding as before, and,

$$k_y.b + \phi_{12} + \phi_{14} = Q.\pi \qquad Q = 1,2,3,\ldots. \tag{B1.36}$$

$$\phi_{12} = \tan^{-1}\left[\frac{n_2^2}{n_1^2}.\frac{k_y}{p_2}\right] \tag{B1.37}$$

$$\phi_{14} = \tan^{-1}\left[\frac{n_4^2}{n_1^2}.\frac{k_y}{p_4}\right] \tag{B1.38}$$

with equation (B1.32) as before.

Referring back to equations (B1. 5,6,7,8) in the separation of variables, we find the modal propagation coefficient β_z of a two dimensional (rectangular) dielectric waveguide may be obtained from

$$\beta_z^2 = k_1^2 - k_x^2 - k_y^2 \qquad \text{(B1.39)}$$

which relates the planar waveguide modes of equations (B1.9,10) to those of a rectangular waveguide. Thus we see that the propagation coefficient β_z of the rectangular waveguide may be related to the refractive indices of the surrounding media in much the same way as a planar waveguide. In fact if one of the waveguide dimensions a or b, is allowed to become infinitely large then the values of k_x or k_y become zero and equation (B1.39) reduces to that of a planar waveguide. The rectangular waveguide mode types may be designated E^x_{PQ} and E^y_{PQ}, where P and Q indicate the number of field maxima in the x and y directions respectively. These mode types are identical to the E^x_{pq} and E^y_{pq} modes of Marcatili (56). We see, therefore, that the separation of variables technique allows an analysis of a rectangular dielectric waveguide to be undertaken which results in the same solution as found by Marcatili (56) but which is much simpler in nature. We may conclude that the solution will become more accurate for modes which are further away from "cut-off" due to the small corner sections of waveguide becoming less significant, as in Marcatili's case.

B1.2. Comparison of Marcatili and Separable Field Solutions.

A comparison of the above separable field solutions with those obtained by Marcatili (56), reveals that they are identical in every respect. For example, considering Marcatili's E^x_{pq} modes, the parameters k_x and k_y are solutions of the following

transcendental equations as shown in Chapter 4.

$$k_x.a = p\pi - \tan^{-1}\left[\frac{n_3^2}{n_1^2}\, k_x\, \xi_3\right] - \tan^{-1}\left[\frac{n_5^2}{n_1^2}\, k_x \xi_5\right] \qquad \text{(B1.40)}$$

$$k_y.b = q\pi - \tan^{-1}\left[k_y.\zeta_2\right] - \tan^{-1}\left[k_y.\,\zeta_4\right] \qquad \text{(B1.41)}$$

k_x and k_y are the same variables as defined in Section (B1.1) and Marcatili's parameters ξ and ζ are given by,

$$\frac{1}{\xi_{3,5}^2} = k_1^2 - k_x^2 - k_{3,5}^2 = p_{3,5}^2 \qquad \text{(B1.42)}$$

$$\frac{1}{\zeta_{2,4}^2} = k_1^2 - k_y^2 - k_{2,4}^2 = p_{2,4}^2 \qquad \text{(B1.43)}$$

These are identical to $p_{3,5}$ and $p_{2,4}$ derived in the separable field solution of Section (B1.1), (see equations (B1.28, 32)).

We may conclude that a relatively straightforward separation of variables technique provides a simpler means of analysing rectangular dielectric waveguides than that of Marcatili. Both methods give identical results and are accurate for guides reasonably far away from cut-off for which the fields in the neglected corner regions are very small and have little effect on the overall propagation coefficient.

Appendix B2 uses the above results to show that theoretical planar waveguide device analyses can be used to predict the transmission performance of its two dimensional counterpart.

APPENDIX B2. USE OF PLANAR WAVEGUIDE ANALYSIS IN THE PREDICTION OF TWO DIMENSIONAL WAVEGUIDE DEVICE TRANSMISSION PERFORMANCE.

As stated in Chapters 5 through 7, this method allows the transmission performance of two dimensional stripe waveguide devices, (e.g. ion-etched, R.F. sputtered 7059 glass) to be described in terms of a planar waveguide model. We restrict ourselves to E^x modes, and in particular to the fundamental E^x_{11} mode which was launched exclusively in all the waveguide devices tested, being the fundamental mode of the waveguide type under consideration (i.e. ion-etched 7059 glass waveguides with a large aspect ratio (a>>b)).

B2.1. The Use of Two Dimensional Waveguide Parameters in Planar Waveguide Models.

From the analysis of Appendix B1, and referring to Figure B1.1, the fields in the ν^{th} regions of the waveguide are;

$$E_x(x,y) = K_1 \cos(k_x.x+\delta) \cos(k_y.y+\gamma) \quad \text{for } \nu = 1 \qquad \text{(B2.1)}$$

$$E_x(x,y) = K_2 \cos(k_x.x+\delta) \exp(p_2(b/2-y)) \quad \text{for } \nu = 2 \qquad \text{(B2.2)}$$

$$E_x(x,y) = K_3 \cos(k_y.y+\gamma) \exp(p_3(x+a/2)) \quad \text{for } \nu = 3 \qquad \text{(B2.3)}$$

$$E_x(x,y) = K_4 \cos(k_x.x+\delta) \exp(p_4(y+b/2)) \quad \text{for } \nu = 4 \qquad \text{(B2.4)}$$

$$E_x(x,y) = K_5 \cos(k_y.y+\gamma) \exp(p_5(a/2-x)) \quad \text{for } \nu = 5 \qquad \text{(B2.5)}$$

with the term $\exp(-j\beta_z.z + j\omega t)$ suppressed. The amplitude constant K_ν determines the amplitude of the field in the ν^{th} medium, and δ and γ locate the field maxima and minima in region 1. Application of the wave equation to (B2.1) through (B2.5) gives the following relationships,

$$k_x^2 + k_y^2 + \beta_z^2 = k_1^2 \qquad \text{(B2.6)}$$

$$k_x^2 - p_2^2 + \beta_z^2 = k_2^2 \qquad \text{(B2.7)}$$

$$k_y^2 - p_3^2 + \beta_z^2 = k_3^2 \qquad \text{(B2.8)}$$

$$k_x^2 - p_4^2 + \beta_z^2 = k_4^2 \qquad \text{(B2.9)}$$

$$k_y^2 - p_5^2 + \beta_z^2 = k_5^2 \qquad \text{(B2.10)}$$

Recalling that the analysis of Appendix B1 shows that the modal propagation coefficient of a rectangular dielectric waveguide may be obtained from two uncoupled mutually othogonal planar waveguides, we may use the above rectangular waveguide parameters to relate to those of the planar waveguides used in the device analyses of Chapters 5 through 7. Thus we have from equations (B1.9) and (B1.10),

$$k_x^2 + \beta_{TM}^2 = k_1^2 \qquad \text{(B2.11)}$$

$$\beta_{TM}^2 = k_3^2 + p_3^2 = k_5^2 + p_5^2 \qquad \text{(B2.12)}$$

$$k_y^2 + \beta_{TE}^2 = k_1^2 \qquad \text{(B2.13)}$$

$$\beta_{TE}^2 = k_2^2 + p_2^2 = k_4^2 + p_4^2 \qquad \text{(B2.14)}$$

We may now argue that, as the waveguide devices (e.g. Y-junction) considered in Chapters 5 through 7 have no variation in the y direction and since the transverse fields are othogonal, we may regard the equations which describe the field variation of the stripe waveguide device in the y direction as being independent of x and vice versa. Hence since the stripe waveguide devices considered have no variation in the y direction the transmission in this direction may be regarded as unvarying and only transmission in the x direction need be calculated. This may also be shown mathematically and is deduced as a direct result of the separable field solutions of Appendix B1.

In all the planar waveguide device analyses the incident and transmitted mode power is normalised to unity, (per unit length in the y direction). This may be readily extended to the case of two dimensional (stripe) waveguides where the incident and transmitted mode power may again be normalised to unity, e.g. for the incident mode we have

$$\frac{1}{2}\,\mathrm{Re}\int_{-\infty}^{\infty}\int_{-\infty}^{\infty}E_x^i(x,y).H_y^{i*}(x,y).dx.dy = 1 \qquad \text{(B2.15)}$$

which by use of the separable field solutions may be simplified to two independent integrals in x and y viz,

$$\frac{1}{2}\,\mathrm{Re}\int_{-\infty}^{\infty}E_x^i(x).H_y^{i*}(x).dx\int_{-\infty}^{\infty}E_x^i(y).H_y^{i*}(y).dy = 1 \qquad \text{(B2.16)}$$

which may be readily calculated. By a similar argument the transmitted mode power may also be normalised to unity viz,

$$\frac{1}{2}\,\mathrm{Re}\int_{-\infty}^{\infty}E_x^t(x).H_y^{t*}(x).dx\int_{-\infty}^{\infty}E_x^t(y).H_y^{t*}(y).dy = 1 \qquad \text{(B2.17)}$$

The same argument may also be used when calculating the transmission coefficient T which achieved by matching the tangential electric and magnetic fields of the stripe waveguide device along the z = 0 plane. This leads generally to an integral over all x and y involving both the incident and transmitted modes viz,

$$T = \frac{\beta_{za}\beta_{zb}}{\beta_{za}+\beta_{zb}}\cdot\frac{1}{\omega\mu_o}\int_{-\infty}^{\infty}\int_{-\infty}^{\infty}E_x^i(x,y).E_x^{t*}(x,y).dx.dy \qquad \text{(B2.18)}$$

except for the waveguide tilt case where $\beta_{za} = \beta_{zb}$ and equation (B2.18) simplifies accordingly. Using the separation of variables solution of Appendix B1 equation (B2.18) further reduces to two independent integrals in x and y viz,

$$T = \frac{\beta_{za}\,\beta_{zb}}{\beta_{za}+\beta_{zb}} \cdot \frac{1}{\omega\mu_o} \int_{-\infty}^{\infty} E_x^i(x).E_x^{t*}(x).dx \int_{-\infty}^{\infty} E_x^i(y).E_x^{t*}(y).dy \qquad \text{(B2.19)}$$

This expression further simplifies to a one dimensional problem in x, since, as there is no device variation in the y direction, the integral

$$\int_{-\infty}^{\infty} E_x^i(y).E_x^{t*}(y).dy = C \qquad \text{(B2.20)}$$

remains constant. Equation (B2.19) simplifies to

$$T = C.\ \frac{\beta_{za}\,\beta_{zb}}{\beta_{za}+\beta_{zb}} \cdot \frac{1}{\omega\mu_o} \int_{-\infty}^{\infty} E_x^i(x).E_x^{t*}(x).dx \qquad \text{(B2.21)}$$

which is identical to the expression found for the transmission coefficient of the planar waveguide devices of Chapters 5 through 7 but with the planar waveguide propagation coefficients (β_a, β_b) replaced with the stripe waveguide propagation coefficients (β_{za}, β_{zb}). Thus the above analysis shows that the transmission coefficient of a stripe waveguide device may be obtained from a planar waveguide device analysis. This greatly simplifies the analysis of stripe waveguide devices.

As all the experimental stripe waveguide devices considered in this thesis have air in regions 2, 3, and 5, the decay constants p_3 and p_5 are equal i.e. $p_3 = p_5 = p_o$. Thus we may relate the planar waveguide analysis parameters of Chapters 5 through 7, commonly denoted by β_a, β_b, h_a, h_b, p_a, p_b, to those of a stripe

waveguide device using the following substitutions.

$$\beta_a \equiv \beta_{za} \tag{B2.22}$$

$$\beta_b \equiv \beta_{zb} \tag{B2.23}$$

$$h_a \equiv k_{xa} \tag{B2.24}$$

$$h_b \equiv k_{xb} \tag{B2.25}$$

$$p_a \equiv p_{oa} = 1/\xi_{3,5a} \tag{B2.26}$$

$$p_b \equiv p_{ob} = 1/\xi_{3,5b} \tag{B2.27}$$

The above Marcatili defined stripe waveguide parameters allow the transmission performance of stripe waveguide devices to be predicted by using an equivalent planar waveguide device analysis.

APPENDIX C. COMPUTER PROGRAM FOR DETERMINING THE MODAL PROPAGATION CHARACTERISTICS OF ION-ETCHED 7059 GLASS WAVEGUIDES.

This program was primarily intended for the characterisation of two dimensional (stripe) silver ion exchange waveguides formed in soda-lime glass microscope slides using a method similar to that of Taylor's (105); a fuller description of this solution will be found in (104, 105). Again I wish to thank Dr. C.D.W.Wilkinson and Mr. R.G. Walker for extensively modifying the computer program and carrying out the computations; without their work no estimate of the accuracy of the effective width theory (see Section 4.3) for this type of waveguide could have been carried out. A brief summary of the computer method is given below.

The method proceeds as follows:-

A computer program called "WAVE" solves the scalar wave equation,

$$\left[\frac{\partial^2}{\partial x^2} + \frac{\partial^2}{\partial y^2} + k^2(x,y)\right] E = \beta^2 E$$

for E^x_{pq} modes (quasi T.E. modes) using a variational technique with Rayleigh-Ritz minimisation of a variational expression for the total field energy. The electric field E is modelled by a series of parabolic cylinder functions in each of the x and y directions assuming that $E(x,y) = E(x).E(y)$. The coefficients of the series are adjusted to minimise the variational expression which then gives the value of β^2, the eigenvalue, for each mode of the waveguide.

The accuracy (and computational time), increases with the number of trial functions used. The y-direction field function being asymmetric requires 10 trial functions to obtain sufficient accuracy; all the transverse modes (single depth mode) have the same y-direction field error.

The x-direction field is either symmetric or anti-symmetric, as are the trial functions, so fewer are needed. However, the error increases with the mode order for a given number of x-direction trial functions. This is more marked with ridge guides (i.e. ion etched waveguides), whose edges are defined by a very high refractive index difference, than with ion exchanged waveguides which have a smaller index difference.

13(y) and 7(x) trial functions were used for the over etched and second depth mode calculations while 10(y) and 6(x) trial functions were used for the single depth mode guides which were ion-etched to the surface of the substrate only. For further details of these numerical calculations see Figures 4.22, 4.23 and 4.24 respectively.

We may conclude that the above computer orientated numerical solution verifies the accuracy of the approximate effective waveguide width theory of Chapter 4, and returns values within the estimated error of the measurement of the normalised modal propagation coefficients.

APPENDIX D1. COMPARISON OF APPROXIMATE AND EXACT SOLUTIONS FOR THE LAUNCHING EFFICIENCY OF A T.E. SURFACE WAVE ON A GROUNDED DIELECTRIC SLAB WAVEGUIDE.

One of the major assumptions in the analysis of the waveguide devices considered in Chapters 5,6 and 7 is that of neglecting radiation in the backward direction from the device region. This assumption allows an analytical solution to be obtained for a problem which otherwise could only be solved with the use of a numerical technique. The validity of this approximation has been established in the analysis of a step discontinuity in a dielectric planar waveguide (71,72). As far as is known, however, no attempt has been made to compare an exact analytic solution with an approximate one which ignores radiation in the backward direction. One problem which does allow such a comparison is the launching of a surface wave on a grounded dielectric sheet.

D1.1. Approximate and Exact Solution Comparison.

Bates and Mittra (78) and Angulo and Chang (79) have carried out several analyses on the launching of surface waves from parallel plate waveguides. Exact solutions to the problems were obtained by the Wiener-Hopf boundary value factorisation technique. These exact solutions for the open structure problem can be directly compared with an approximate theory, which neglects radiation in the backward direction (80, 108). One system considered by Bates and Mittra is a surface wave launched on a grounded dielectric sheet, (see Figure D1.1.).

D1.1.1. Approximate Solution.

Referring to Figure D1.1 which shows a planar dielectric waveguide of permittivity ε_r resting on a perfectly conducting

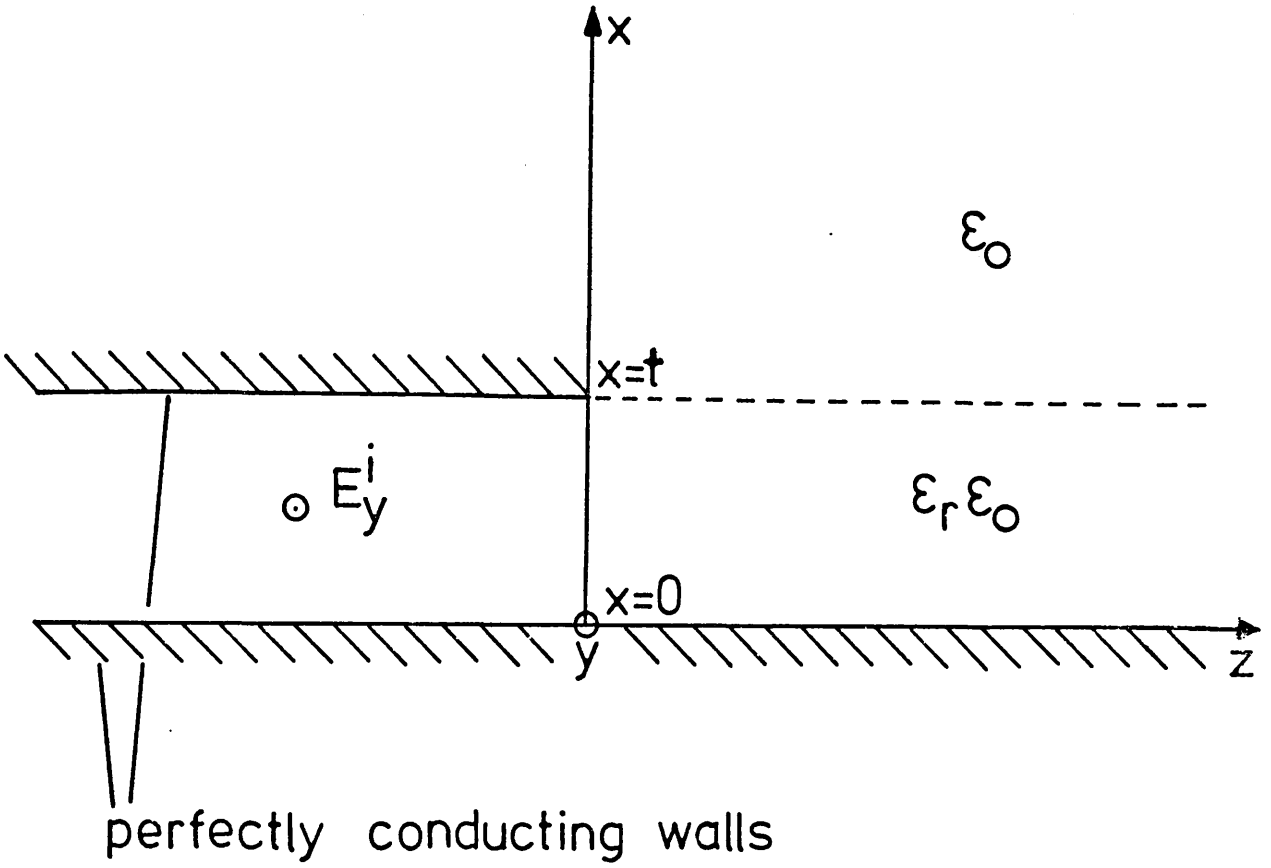

Fig. D1.1 Schematic diagram of waveguide structure

grounded sheet, we consider only the lowest order TE_o mode incident on the boundary. For $z<0$ the incident electric field in the y direction is

$$E_y^i = A \sin\left[\frac{\pi x}{t}\right] \exp(-j\beta_1 z) \tag{D1.1}$$

From Maxwell's equations, the corresponding magnetic field component is

$$H_x^i = \frac{-\beta_1}{\omega\mu_o} E_y^i \tag{D1.2}$$

with

$$\beta_1 = \left[k^2 - (\pi/t)^2\right]^{\frac{1}{2}}, \quad k = \sqrt{\varepsilon_r} k_o, \quad k_o = 2\pi/\lambda \tag{D1.3}$$

The coefficient A is now selected such that the incident mode power is unity (per unit length in the y direction), i.e.

$$\frac{1}{2} \mathrm{Re} \int_o^t E_y^i . H_x^{i*} . dx = 1 \tag{D1.4}$$

(D1.1) and (D1.2) give

$$A = 2\left[\frac{\omega\mu_o}{\beta_1 t}\right]^{\frac{1}{2}} \tag{D1.5}$$

Considering the region $z > 0$, the transmitted fields of the fundamental TE_o mode are,

$$\begin{aligned} E_y^t &= B \sin(ht) \exp(-p(x-t) - j\beta_2 z), \quad x \geq t \\ E_y^t &= B \sin(hx) \exp(-j\beta_2 z), \quad x \leq t \end{aligned} \tag{D1.6}$$

with

$$p = -h \cot(ht) \tag{D1.7}$$

and

$$\beta_2^2 = k_o^2 + p^2 = \varepsilon_r k_o^2 - h^2 \tag{D1.8}$$

From Maxwell's equations the corresponding magnetic field component is

$$H_x^t = \frac{-\beta_2}{\omega\mu_o} E_y^t \tag{D1.9}$$

The coefficient B is now selected such that the transmitted mode power is unity, i.e.

$$\frac{1}{2}\mathrm{Re}\int_0^\infty E_y^t . H_x^{t*}\,dx = 1 \qquad \text{(D1.10)}$$

which after some algebraic manipulation gives

$$B = 2\left[\frac{\omega\mu_o}{\beta_2(t+1/p)}\right]^{\frac{1}{2}} \qquad \text{(D1.11)}$$

Matching the tangential electric and magnetic fields on the $z = 0$ plane gives

$$(1+\rho)E_y^i + E_y^- = TE_y^t + E_y^+ \qquad \text{(D1.12)}$$

$$(1-\rho)H_x^i + H_x^- = TH_x^t + H_x^+ \qquad \text{(D1.13)}$$

where E_y^+, H_x^+ and E_y^-, H_x^- are the radiation components of the electric and magnetic fields in the forward and backward directions respectively. Due to the change in waveguide impedance at the $x = 0$ plane there is a reflected wave ρE_y^i and $-\rho H_x^i$ for the incident electric and magnetic fields. By neglecting E_y^- and H_x^- and multiplying (D1.12) by E_y^{t*} and (D1.13) by H_x^{t*} we obtain

$$(1+\rho)\int_0^\infty E_y^i . E_y^{t*}\,dx = T\int_0^\infty |E_y^t|^2\,dx + \int_0^\infty E_y^+ . E_y^{t*}\,dx \qquad \text{(D1.14)}$$

$$(1-\rho)\int_0^\infty H_x^i . H_x^{t*}\,dx = T\int_0^\infty |H_x^t|^2\,dx + \int_0^\infty H_x^+ . H_x^{t*}\,dx \qquad \text{(D1.15)}$$

From modal orthogonality we have

$$\int_0^\infty E_y^+ . E_y^{t*}\,dx = \int_0^\infty H_x^+ . H_x^{t*}\,dx = 0 \qquad \text{(D1.16)}$$

which allows an analytical solution to be obtained for T. Omitting details, (D1.14) and (D1.15) give

$$\rho = \frac{\beta_1 - \beta_2}{\beta_1 + \beta_2} \qquad \text{(D1.17)}$$

$$T = \frac{\beta_1\beta_2}{\beta_1+\beta_2}\frac{1}{\omega\mu_o}\int_o^t E_y^i . E_y^{t*}\,dx \qquad (D1.18)$$

After integration we obtain

$$T = \frac{4\pi}{\beta_1+\beta_2}\cdot\left[\frac{\beta_1\beta_2}{1+1/pt}\right]^{\frac{1}{2}}\cdot\frac{\sin(ht)}{\pi^2-(ht)^2} \qquad (D1.19)$$

The fractions of incident power transmitted to the output waveguide and reflected in the input waveguide are

$$T = |T|^2 \text{ and } R = |\rho|^2 \qquad (D1.20)$$

respectively. By conservation of power the fraction scattered into the surrounding medium is

$$S = 1 - R - T \qquad (D1.21)$$

A flow diagram of the computer program used to calculate R,S and T is given in Appendix All. A comparison of the above approximate solution with Bates and Mittra's exact solution is given in the next section.

D1.1.2. Comparison of Exact and Approximate Solutions.

Bates and Mittra used the Wiener-Hopf factorisation technique to obtain an exact solution for waveguide excitation of dielectric and plasma slabs. One particular structure they looked at was that of Figure D1.1. A TE_o mode in $z<0$ excites a TE_o mode in $z>0$ with a dielectric slab of dielectric constant $\varepsilon_r = 1.12$. A comparison of these results with those of the approximate theory of Section D1.1.1 is presented in Figure D1.2. As can be seen there is excellent agreement between the theory of Bates and Mittra and the approximate theory. Since the exact solution points were obtained directly from the graphs in the original publication, some error may be present due to the small size of

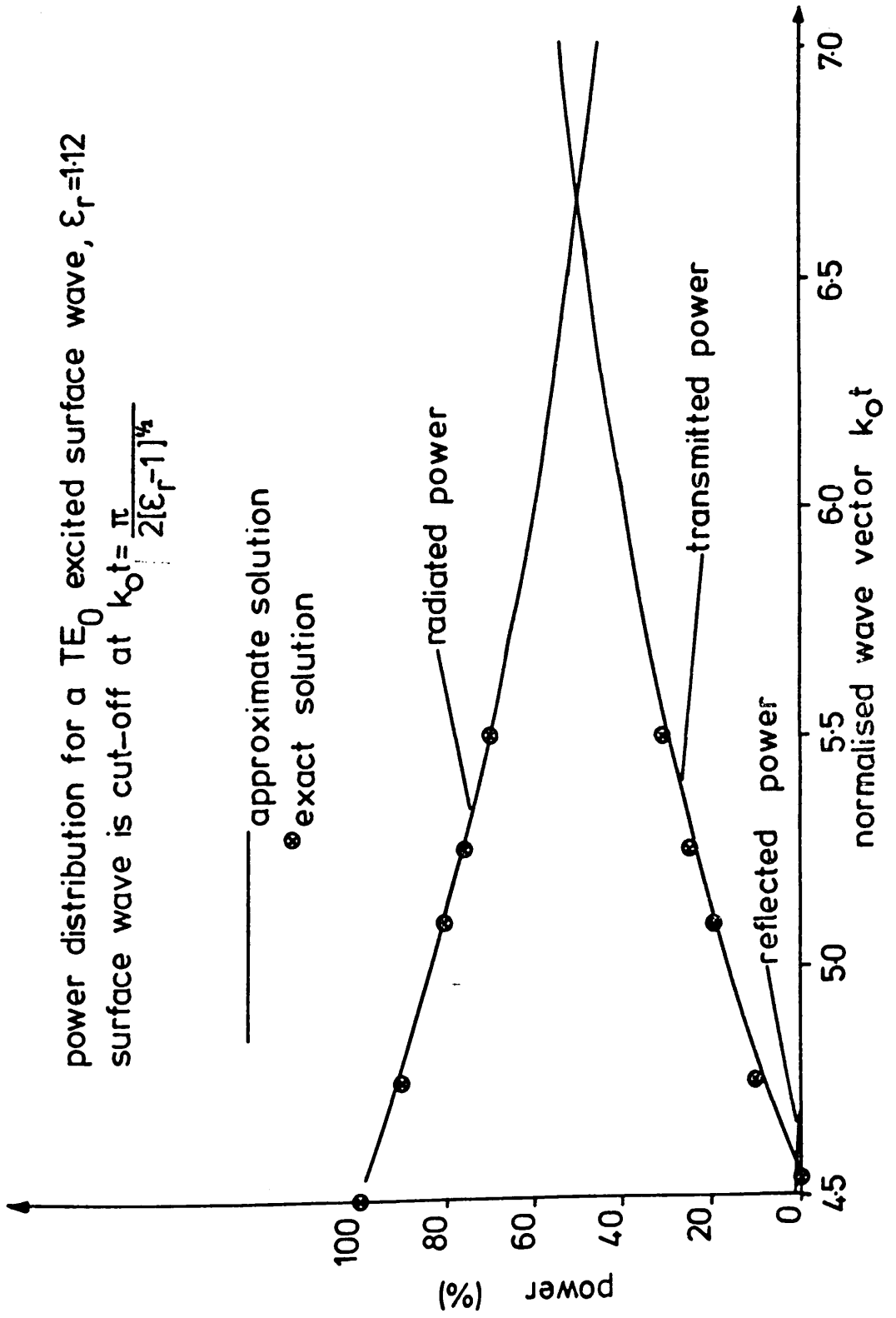

Fig. D1.2 Comparison of approximate and exact solutions

these graphs. However, the maximum error must be no more than a few percent. We may reasonably conclude that the approximate and exact solutions give identical results, at least for this particular case. There is no reason to suppose that this should be any different for other values of dielectric constant (ε_r). Unfortunately this could not be tested as this was the only TE_o dielectric surface wave considered by Bates and Mittra.

The above results show that neglect of radiation in the backward direction is a valid assumption and we may reasonably deduce that this condition should also hold for dielectric waveguide devices, e.g. Tilts, Y-Junctions, Power Splitters etc. By using this result it is possible to obtain an analytical solution for the aforementioned waveguide devices (see Chapters 5,6 and 7), which otherwise could only be solved using numerical techniques. The experimental results of these chapters also indicate that this is a valid assumption, as no radiation in the backward direction from the device area has ever been observed. This should be true for all waveguide devices which are large compared to the wavelength (λ); it may not be so valid for devices which are of size comparable with the wavelength, e.g. gratings, in which case large amounts of power in the reverse direction may be obtained (71).

D1.2. Conclusions.

A comparison of an approximate solution which neglects radiation in the backward direction and an exact solution for the launching efficiency of a TE_o surface wave on a grounded dielectric sheet has been undertaken. The methods are seen to give almost identical results justifying the neglect of backward radiation from the discontinuity. This allows analytical solutions to problems

which otherwise could only be solved numerically and provides a useful tool for the design of many dielectric waveguide devices. It has already been used in the analysis of waveguide tilts, Y-junctions and power splitters and a close correlation between theory and experiment has been obtained.

APPENDIX E. DESIGN OF A 3dB DIRECTIONAL COUPLER BASED ON TWO TANGENTIALLY TOUCHING CURVED ION ETCHED 7059 GLASS WAVEGUIDES.

The large refractive index difference between the waveguide and the surrounding media present in ion etched 7059 glass waveguides precludes the fabrication of evanescent field directional couplers due to the very small coupling gap required (0.1 μm for a reasonable coupling length). One way to avoid this problem is to decrease the refractive index difference between the waveguides and the surrounding media (see Section 8.2); the other is for the two waveguides to touch for a short distance, thus allowing some of the power in one to be transferred to the other.

The device considered here is based on the coupling of degenerate modes in two tangentially touching dielectric waveguides and is a special case of the problem considered by Anderson (77). It was originally hoped to test this device experimentally and to compare the measured transmitted power with that predicted from the theory; however, problems in cutting the waveguide mask pattern meant that no device could be tested. This appendix presents a brief design study of the waveguide dimensions necessary to fabricate a single mode (E^x_{11}) 3dB coupler in ion etched 7059 glass stripe waveguide. The notation of Anderson (77) is used throughout and frequent reference to his analysis in (77) is made.

We have already shown in Appendix B2 and in Chapters 5 through 7 that a planar waveguide device analysis may be used to describe the transmission performance of the stripe waveguide counterpart. Here we consider a coupler based on two tangentially touching curved ion etched 7059 glass stripe waveguides. Referring to

the analysis of Anderson (77) we choose the dimensions of the waveguides such that they support only the fundamental E^x_{11} mode. A suitable choice of waveguide dimensions and refractive indices that fulfil these conditions is given below.

Guide Index $n_g = n_1 = 1.56068$

Substrate Index $n_s = n_4 = 1.51272$

Waveguide Effective Width $a = 3.0\ \mu m$

Waveguide Thickness $b = 0.45\ \mu m$

From the analysis of Marcatili (56) we obtain the following stripe waveguide parameters

$$\beta_z = 15.0414, \quad k_x = 1.0236, \quad p_x = 1/\xi_{3,5} = 11.8532$$

Using these parameters in Andersons equation (10), viz

$$C_o = \frac{2h^2 p}{\beta_o} \left[(w + 2/p)(h^2 + p^2) \right]^{-1} \qquad \text{(E1.1)}$$

with $\beta_o \equiv \beta_z$, $h \equiv k_x$, $p \equiv p_x$, (see Appendices B1, B2), we obtain the coupling coefficient for two touching single mode waveguides

$$C_o = 3.682 \times 10^{-3}$$

Using equation 24 of Anderson, viz,

$$|E_1(z)| \sim |E_o| \quad \cos\left[C(d_o)\sqrt{\frac{\pi R}{p}} \right] \qquad \text{(E1.2)}$$

we let $|E_1(z)| \,/\, |E_o| = 1/\sqrt{2}$ for a 3dB coupler, i.e. half the incident power coupled into the touching adjacent waveguide. From equation E1.2 we obtain a radius of curvature R of the two tangentially touching waveguides necessary to ensure the equal division of the incoming mode power,

$$R = \frac{p\pi}{16 C_o^2} \qquad \text{(E1.3)}$$

By substituting the values of p and C_o obtained above into (E1.3) we obtain a value of R = 17.171cm and a value of coupling length $L_c = 4\sqrt{R/p}$ equal to 0.481 mm. Figure E1.1 shows a diagram of the 3dB stripe waveguide coupler.

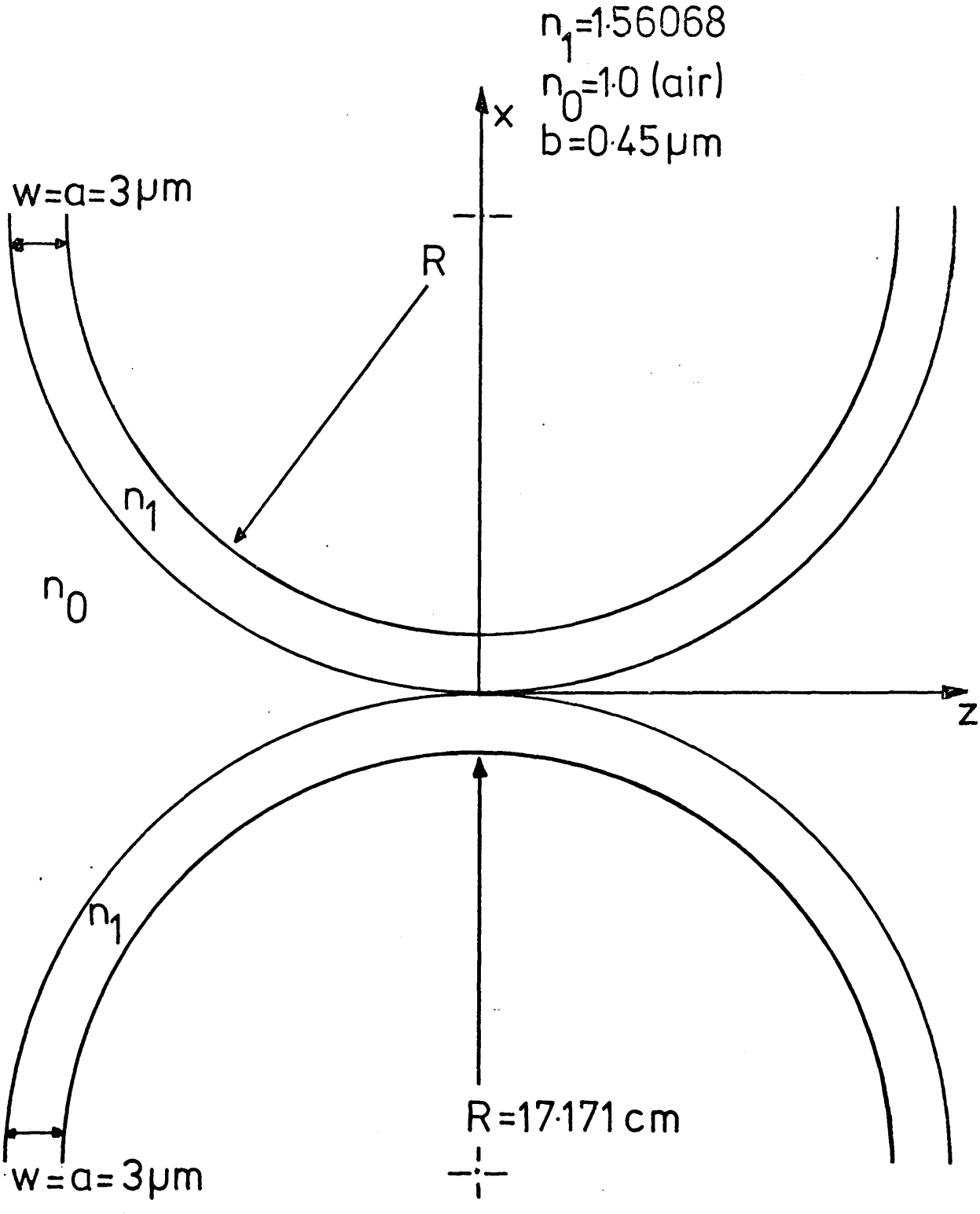

Fig. E1·1 3dB coupler formed from two tangentially touching stripe 7059 glass waveguides

A waveguide mask design with the above dimensions was submitted to the lithographic technicians. Unfortunately it proved impossible to cut the mask pattern with a radius of 17.171cm due to the large radius size at the initial cutting stage (approximately 14 metres).

CONCLUSION

A 3dB directional coupler has been designed in trapezoidal ion-etched 7059 glass waveguide. Due to difficulties in fabricating the mask no device was tested. As the device relies on the coupling of rather than the splitting of the incoming guided mode, the coupler should have smaller junction losses than the Y-junction of Chapter 6.

REFERENCES

REFERENCES

1. MILLER, S.E.
Integrated Optics - An Introduction.
Bell System Technical Journal, 48, 7, pp. 2059-2069, (1969).

2. MAIMAN, T.H.
Stimulated Optical Radiation in Ruby.
Nature, 187, pp.493, (1960).

3. OSTERBERG, H., SMITH, L.W.
Transmission of Optical Energy Along Surfaces: Part I and Part II.
Journal of the Optical Society of America, 54, pp.1073-1084, (1964).

4. TIEN, P.K. et al.
Modes of Propagating Light Waves in Thin Deposited Semiconductor Films.
Applied Physics Letters, 14, 9, pp.291-294, (1969).

5. KAMINOW, I.P. et al.
Thin Film $LiNbO_3$ Electro-optic Light Modulator.
Applied Physics Letters, 22, 10, pp.540-542, (1973).

6. SASAKI, H., De La RUE, R.M.
Electro-optic Y-junction Modulator/Switch.
Electronics Letters, 12, pp.459-460;
Also, Errata,
Electronics Letters, 12, pp.636, (1976).

7. RANANGATH, T.R., WANG, S.
Ti diffused $LiNbO_3$ Branched Waveguide Modulators: Performance and Design.
I.E.E.E. Trans., QE 13, pp. 290-295, (1977).

8. CHO, A.Y., ARTHUR, J.R.
Molecular Beam Epitaxy.
Progress in Solid State Chemistry, 10, 3, pp.157-191, (1975).

9. UMEBU, I. et al.
In — GaAsP/InP D.H. L.E.D.'S for Fibre-Optical Communications.
Electronics Letters, 14, 16, pp.499-500, (August 1978).

10. PAYNE, D., GAMBLING, W.A.
Zero Material Dispersion in Optical Fibres.
Electronics Letters, 11, 8, pp. 176-178, (1975).

11. ITO, T. et al.
Non-Repeatered 50 Km Transmission Experiment Using Low-Loss Optical Fibres.
Electronics Letters, 14, 16, pp.520-521, (August 1978).

12. GOELL, J.E., STANDLEY, R.D.
Sputtered Glass Waveguide for Integrated Optical Circuits.
Bell System Technical Journal, 48, pp.3445-3448, (1969).

13. TIEN, P.K. et al.
Thin Organosilicon Films for Integrated Optics.
Applied Optics, 11, pp.637-642, (1972).

14. GEDEON, A.
Spectaral Properties of TE_o and TM_o Modes in Dielectric Thin Film Waveguides Excited with a Prism Light Coupler.
Optica Acta, 19, 9, pp.765-779, (1972).

15. PITT, C.W. et al.
R.F. Sputtered Thin Films for Integrated Optical Components.
Thin Solid Films, 26, 1, pp. 25-51, (1975).

16. GIALLORENZI, T. G. et al.
Optical Waveguides Formed by Thermal Migration of Ions in Glass.
Applied Optics, 12, 6, pp.1240-1245, (1973).

17. VALETTE, S. et al.
Optical Waveguides in Ion Implanted ZnTe.
Journal of Applied Physics, 46, 6, pp.2731-2732, (1975).

18. KAMINOW, I.P. et al.
Optical Waveguiding Layers in $LiNbO_3$ and $LiTaO_3$.
Applied Physics Letters, 22, 7, pp.326-328, (1973).

19. TAYLOR, H.F. et al.
Fabrication of Single Crystal Semiconductor Optical Waveguides by Solid State Diffusion.
Applied Physics Letters, 21, 3, pp.95-98, (1972).

20. BLUM, F.A. et al.
Monolithic GaAs Circuit Elements for Integrated Optics.
Topical Meeting on Integrated Optics, (MA4), (1976).

21. GOELL, J.E.
Rib Waveguide for Integrated Optical Circuits.
Applied Optics, 12, 12, pp.2797-2798, (1973).

22. GALLAGHER, J.G., De La RUE, R.M.
Single Mode Stripe Optical Waveguides Formed by Silver Ion Exchange.
Electronics Letters, 12, 16, pp.397-398, (1976).

23. PAPUCHON, M. et al.
Electrically Switched Optical Directional Coupler: Cobra.
Applied Physics Letters, 27, pp.289-291, (1975).

24. TIEN, P.K.
Integrated Optics and New Wave Phenomena in Optical Waveguides.
Review of Modern Physics, 49, pp.361-420, (1977).

25. TOPICS IN APPLIED PHYSICS.
Volume 7. 'Integrated Optics'. Tamir, T. (Ed.),
Springer -Verlay, Heidelberg, (1975).

26. ANDREWS, R.A.
Optical Waveguides and Integrated Optics Technology.
Naval Research Laboratory, Washington, D.C., U.S.A.
Report 7291, (1971).

27. YARIV, A.
Guided-Wave Optics.
Scientific American, 240, 1, pp.54-62, (1979).

28. McMURRY, J.A.
Electro-optic Modulation of Infrared Radiation in Planar Cadmium Sulphide Waveguides.
Ph.D. Thesis, University of Glasgow, (1976).

29. JACKSON, G.N.
R.F. Sputtering.
Thin Solid Films, 5, pp.209-246, (1970).

30. MAISSEL, L.I., FRANCOMBE, M.H.
An Introduction to Thin Films.
Gordon and Breach, New York, (1973).

31. YI YAN, A.
Private Communication.

32. PITT,C.W.
Sputtered Glass Optical Waveguides.
Electronics Letters, 9, 17, pp.401-403, (1973).

33. TIEN, P.K.
Light Waves in Thin Films and Integrated Optics.
Applied Optics, 10, 11, pp.2395-2413, (1971).

34. LOTSCH, H.K.V.
Reflection and Refraction of a Beam of Light at a Plane Interface.
Journal of the Optical Society of America, 58, 4, pp.551-561, (1968).

35. SCHUBERT, R. et al.
Optical Surface Waves on Thin Films and Their Applications to Integrated Data Processors.
I.E.E.E. Trans. M.T.T., 16, 12, pp.1048-1054, (1968).

36. TIEN, P.K. et al.
Experiments on Light Waves in a Thin Tapered Film and a New Light Wave Coupler.
Applied Physics Letters, 18, 9, pp.398-401, (1971).

37. TIEN, P.K. et al.
Radiation Fields of a Tapered Film and a Novel Film to Fibre Coupler.
I.E.E.E. Trans. M.T.T., 23, 1, pp. 79-85, (1975).

38. KOGELNIK, H. et al.
Holographic Thin Film Coupler.
Bell System Technical Journal, 49, 7, pp.1602-1608, (1970).

39. DAKSS, M.L. et al.
Grating Coupler for Efficient Excitation of Optical Guided Waves in Thin Films.
Applied Physics Letters, 16, 12, pp. 523-525, (1970).

40. TIEN, P.K. et al.
Theory of Prism-Film Coupler and Thin Film Light Guides.
Journal of the Optical Society of America, 60, 10, pp.1325-1337, (1970).

41. KERSTEN, R.Th.
Numerical Solution of the Mode Equation of Planar Dielectric Waveguides to Determine Their Refractive Index and Thickness by Means of a Prism Film Coupler.
Optics Communications, 9, 4, pp.427-431, (1973).

42. ULRICH, R., TORGE, R.
Measurement of Thin Film Parameters with a Prism Coupler.
Applied Optics, 12, 12, pp.2901-2908, (1973).

43. CORNING GLASS INTERNATIONAL S.A. PRODUCT INFORMATION,
7059 Ground and Polished Photomask Substrates,
15th February 1972.

44. GOELL, J.E.
Barium Silicate Films for Integrated Optical Circuits.
Applied Optics, 12, 4, pp.737-742, (1973).

45. RAMASWAMY, V.
Strip Loaded Film Waveguide.
Bell System Technical Journal, 53, 4, pp.697-704, (1974).

46. FULHAM CORP., Schonectady, New York.

47. HUTCHINS, R.H., STANLEY, C.R.
Department of Electronics and Electrical Engineering Internal Report.
Glasgow University, (1973).

48. HUTCHINS, R.H., STANLEY, C.R.
Thin Film Thickness Monitor.
Dept. of Electronics and Electrical Engineering Internal Report,
Glasgow University, (1973).

49. YI YAN, A.
Ph.D. Thesis, Glasgow University, (1978).

50. U.D.T., Laser Power Meter, Model 122A,
United Detector Technology Inc., Santa Monica, California, U.S.A.

51. McMURRY, J.A., STANLEY, C.R.
Taper Coupling Between 7059-glass and CdS Films and Phase Modulation in the Composite Waveguide Structure.
Applied Physics Letters, 28, 3, pp.126-128, (1976).

52. WILSON, M.G.F., TEH, G.A.
Tapered Optical Directional Coupler.
I.E.E.E. Trans., MTT 23, 1, pp.85-92, (1975).

53. SASAKI, H., ANDERSON, I.
Theoretical and Experimental Studies on Active Y-Junctions in Optical Waveguides.
I.E.E.E. Journal of Quantum Electronics, QE14, 11, pp.883-892, (1978).

54. PAYNE, D.N., GAMBLING, W.A.
New Silica-Based Low-Loss Optical Fibre.
Electronics Letters, 10, 15, pp.289-290, (July 1974).

55. GOELL, J.E.
A Circular-Harmonic Computer Analysis of Rectangular Dielectric Waveguides.
Bell System Technical Journal, 48, pp.2133-2160, (1969).

56. MARCATILI, E.A.J.
Dielectric Rectangular Waveguide and Directional Coupler for Integrated Optics.
Bell System Technical Journal, 48, pp.2071-2102, (1969).

57. KNOX, R.M., TOULIOS, P.P.
Integrated Circuits for the Millimeter Through Optical Frequency Range.
Proceedings of Symposium on Submillimeter Waves, Fox, J. (Ed.) Polytechnic Press, Brooklyn, New York, pp.497-516, (1970).

58. YEH, C., DONG, S.B., OLIVER, W.
Arbitrarily Shaped Inhomogeneous Optical Fibre or Integrated Optical Waveguides.
Journal of Applied Physics, 46, 5, pp.2125-2129, (1975).

59. HOCKER, G.B., BURNS, W.K.
Mode Dispersion in Diffused Channel Waveguides by the Effective Index Method.
Applied Optics, 16, 1, pp.113-118, (1977).

60. PELOSI, P.M. et al.
Propagation Characteristics of Trapezoidal -Cross-Section Waveguides: an Experimental and Theoretical Investigation.
Applied Optics, 17, pp.1187-1193, (1978).

61. GALLAGHER, J.G.,
Ph.D. Thesis, Glasgow University, (1977).

62. MILLAR, C.A.
Ph.D. Thesis, Glasgow University, (1976).

63. SPENCER, E.G. et al.
Ion Beam Techniques for Device Fabrication.
Journal of Vacuum Science and Technology, 8, 5, pp.S52-S70, (1971).

64. GARVIN, H.L. et al.
Ion Beam Micromachining of Integrated Optics Components.
Applied Optics, 12, 3, pp.455-459, (1973).

65. HAWKINS, D.T.
Ion Milling (ion beam etching), 1954-1975: A Bibliography.
Journal of Vacuum Science and Technology, 12, 6, pp.1389-1398, (1975).

66. SHIPLEY EUROPE LIMITED, COVENTRY, U.K.

67. GLOERSEN, Per.G.
Masking for Ion Beam Etching.
Solid State Technology, 4, pp.68-73, (1976).

68. MARCUSE, D.
Radiation Losses of Dielectric Waveguides in Terms of the Power Spectrum of the Wall Distortion Function.
Bell System Technical Journal, 48, pp.3233-3242, (1969).

69. TAYLOR, H.F.
Power Loss at Directional Change in Dielectric Waveguides.
Applied Optics, 13, 3, pp.642-647, (1974).

70. ANDERSON, I.
Transmission Performance of Y-Junctions in Planar Dielectric Waveguide.
Microwaves, Optics and Acoustics, 2, 1, pp.7-12, (1978).

71. MARCUSE, D.
Radiation Losses of Tapered Dielectric Slab Waveguides.
Bell System Technical Journal, 49, pp.273-290, (1970).

72. BROOKE, G.H., KHARADLY, M.M.Z.
Step Discontinuities on Dielectric Waveguides.
Electronics Letters, 12, 18, pp.473-475, (1976).

73. GALLAGHER, J.G., et al.
Optical Guiding Structures by Ion Exchange.
Presented at the European Microwave Conference, Copenhagen, Denmark, 1977.

74. YAJIMA, H.
Theory and Applications of Dielectric Branching Waveguides.
Proceedings of the Symposium, Optical and Acoustical Micro-Electronics, New York, April 1974.

75. BURNS, W.K., MILTON, A.F.
Mode Conversion in Planar Dielectric Separating Waveguides.
I.E.E.E. Journal of Quantum Electronics, 11, pp.32-39, (1975).

76. YAJIMA, H.
Dielectric Thin Film Optical Branching Waveguide.
Applied Physics Letters, 22, 12, pp.647-649, (1973).

77. ANDERSON, I.
On the Coupling of Degenerate Modes on Non-Parallel Dielectric Waveguides.
Microwaves, Optics and Acoustics, 3, 2, pp.56-58, (March 1979).

78. BATES, C.P., MITTRA, R.
Waveguide Excitation of Dielectric and Plasma Slabs.
Radio Science, Vol. 3 (New Series), 3, pp.251-266, (1968).

79. ANGULO, C.M., CHANG, W.S.C.
The Launching of Surface Waves by a Parallel Plate Waveguide.
I.R.E. Trans. on Antennas and Propagation, AP7, 4, pp.359-368, (1959).

80. CLARRICOATS, P.J.B., SHARPE, A.B.
Modal Matching Applied to a Discontinuity in a Planar Surface Waveguide.
Electronics Letters, 8, 2, pp.28-29, (1972).

81. ANDERSON, D.B. et al.
Dielectric Waveguide Phase Matching of Infrared Parametric Interactions.
Proceedings of the Polytechnic Institute of Brooklyn, Symposium on Submillimeter Waves, March 1970, pp.191-209.

82. DALGOUTTE, D.G.
Ph.D. Thesis, University of Glasgow (1973).

83. STEWART, G. et al.
Planar Optical Waveguides Formed by Silver-Ion Migration in Glass.
I.E.E.E. Journal of Quantum Electronics, QE13, 4, pp.192-200, (1977).

84. BELLINGHAM and STANLEY, Abbé Refractometer, Type 60lED.

85. YAMAMOTO, Y. et al.
Propagation Characteristics of a Partially Metal Clad Optical Stripline.
Applied Optics, 14, 2, pp.322-326, (1975).

86. KAMINOW, I.P. et al.
Lithium Niobate Ridge Waveguide Modulator.
Applied Physics Letters, 24, 12, pp.622-626, (1974).

87. HOCKER, G.B.
Strip-loaded Diffused Optical Waveguides.
I.E.E.E. Journal of Quantum Electronics, QE12, 4, pp.232-236, (1976).

88. SMITH, H.I., et al.
A High-Yield Phololithographic Technique for Surface Wave Devices.
J. Electrochem. Soc., Electrochemical Technology, 118, 5, pp.821-825, (1971).

89. Headway Research Inc., 3713 Forest Lane, Garland, Texas, U.S.A.

90. G.V. Planar, Custom Built, Ion-Beam Etcher.

91. Tegal Corporation, Richmond, California, U.S.A.

92. G.V. Planar, Surfometer, Type SF100.

93. See for example, STEEL, W.H.
Interferometry, Cambridge University Press, London (1967).
pp. 7-8, pp.176-177, etc.

94. Spectra Physics Type "120", He - Ne Laser.

95. ESDAILE, R.
Private Communication.

96. HUTCHINS, R.H.
Private Communication.

97. MARCATILI, E.A.J.
Slab Coupled Waveguides.
Bell System Technical Journal, 53, 4, pp.645-674, (1974).

98. MILLER, S.E.
Coupled Wave Theory and Waveguide Applications.
Bell System Technical Journal, 33, 5, pp.661-719, (1954).

99. RAMO, S., WHINNERY, J.R., VAN DUZER, T.
Fields and Waves in Communication Electronics.
Wiley, New York, (1965).

100. MARCUSE, D.
Theory of Dielectric Optical Waveguides.
Academic Press, New York, (1974).

101. MARCUSE, D.
Light Transmission Optics.
Van Nostrand Reinhold Company, New York (1972).

102. 1979 Veeco Catalog, Veeco Instruments Inc., Terminal Drive,
Plainview, New York, 11803, pp.T17-T24.

103. CANTAGREL, M.
Considerations on High Resolution Patterns Engraved by Ion Etching.
I.E.E.E. Transactions on Electron Devices, ED22, 7, pp.483-486, (1975).

104. WILKINSON, C.D.W., WALKER, R.G.
The Diffusion Profile of Stripe Optical Waveguides Formed by Ion Exchange.
Electronics Letters, 14, 18, pp.599-600, (1978).

105. TAYLOR, H.F.
Dispersion Characteristics of Diffused Channel Waveguides.
I.E.E.E. Journal of Quantum Electronics, QE-12, 12, pp.748-752, (1976).

106. COLLIN, R.E.
Field Theory of Guided Waves.
McGraw-Hill, New York, (1960).

107. DUNSMUIR, R.
Private Communication.

108. BARLOW, H.M., BROWN, J.
Radio Surface Waves.
Oxford, (1962).

109. MILLAR, C.A., HUTCHINS, R.H.
As_2S_3 - p.e.s. Sandwich Ribbon Fibre for Coupling High-Refractive-Index Integrated Optics.
Electronics Letters, 15, 2, pp.60-61, (January 1979).

LIBRARY